UNIVERSITY OF CALIFORNIA, SAN DIEGO

Temperature Equilibration and Many-Particle Adiabatic Invariants

A dissertation submitted in partial satisfaction of the

requirements for the degree Doctor of Philosophy

in Physics

by

Shi-Jie Chen

Committee in charge:

Professor Daniel H.E. Dubin, Chairman
Professor Thomas M. O'Neil
Professor Daniel P. Arovas
Professor David R. Miller
Professor John H. Weare

1994

The dissertation of Shi-Jie Chen is approved, and it is acceptable in quality and form for publication on microfilm:

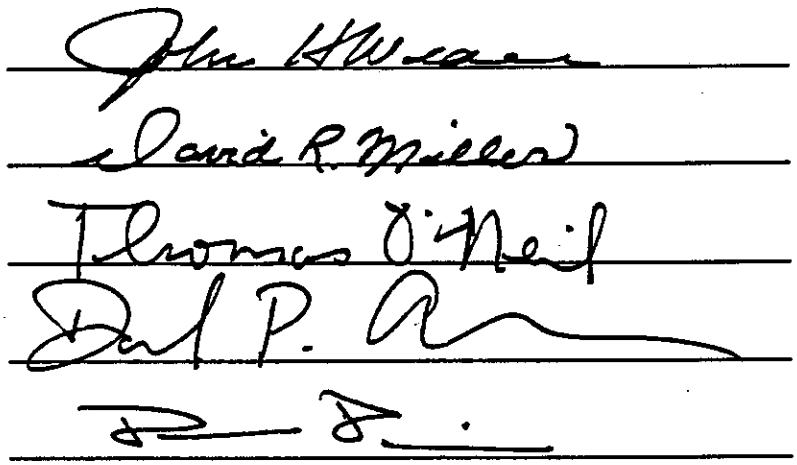

Chairman

University of California, San Diego

1994

To My Parents

Contents

List of Figures

Acknowledgments

I wish to thank my advisor, Professor Dan Dubin, who taught me how to grasp the spirit of the simple physics of a complicated system. During all these years, I benefited a great deal from his wisdom and patience as well as his encouragement of my creativity and independence. His uncanny intuition, rigorous research style, and dedication to science provided a model which has had a strong influence on my personal development in ways which go well beyond this thesis.

I am also greatly indebted to Professor Tom O'Neil for many insightful comments about my work and for showing me the formalism connecting the breaking of the adiabatic invariant to the temperature equilibration rate. During these years, I was always inspired by Tom's elegant scientific research style. I wish to thank Professor Dan Arovas for his strong encouragement and interest in my work and for his excellent notes on the Quantum Bosonic Bogoliubov Formalism, on which the classical canonical transformations in Chapter 4 is based. The other members of my committee, Professor David Miller and Professor John Weare are thankfully acknowledged for their interest and support. I would also like to thank Dr. Fred Driscoll for his help during all these years, Professor William Thompson for stimulating discussions and for his advice and assistance when I was looking for a postdoc position, and Professor Patrick Diamond for his help and his excellent lectures on Electrodynamics and Plasma Physics.

I am grateful for the invaluable friendship and help from my fellow gradu-

ate students and postdocs. Special thanks should go to Franscois Anderegg, Ann Cass, Brian Cluggish, Steve Crooks, Kevin Fine, Mike Glinsky, Andrie Gruzinov, Dirk Hartmann, Xiao-Pei Huang, Misha Kremliovsky, Vladmire Lebedev, Yiming Liang, Travis Mitchell, Gene Sandler and Wenli Zhang. Here, Steve deserves special mention, through our countless discussions, his active mind and physical intuitions helped to deepen my understanding of Plasma Physics. Jo Ann Christina's efficiency is also greatly appreciated.

In addition, I would like to thank Mr.and Mrs. Lauren and Joan Stayton for their hospitality and encouragement. My deepest thanks and appreciations go to my family: to my parents and sisters, without whose constant strong support my life of pursuing a Ph.D. in Physics would be more difficult; second, to my wife, whose love and steady encouragement inspired me through all these years; and finally, to my parents-in-law for their care and inspiration.

This work was supported by NSF PHY91-20240 and ONR N00014-89-J-1714.

Vita

Dec 18, 1965	Born in Hangzhou, Zhejiang, China
1987	B.S. in Physics, Zhejiang University
1988 –1994	Research/Teaching Assistant, University of California, San Diego
1990	M.S. in Physics, University of California, San Diego
1994	Ph.D. in Physics, University of California, San Diego

Publications

1. Shi-Jie Chen and Daniel H. E. Dubin, *Temperature Equilibration of a 1-D Coulomb Chain and a Many-Particle Adiabatic Invariant*, Phys. Rev. Lett. **71**, 2721 (1993)

2. Shi-Jie Chen and Daniel H. E. Dubin, *Equilibration Rate of Spin Temperature in a Strongly Magnetized Pure Electron Plasma*, Phys. Fluids B **5**, 691-710(1993)

3. Shi-Jie Chen and Daniel H. E. Dubin, *Temperature Equilibration of a 1-D Coulomb Chain and a Many-Particle Adiabatic Invariant* Bull. Am. Phys. Soc. **38**, 1972 (1993)

4. Shi-Jie Chen and Daniel H. E. Dubin, *Temperature Relaxation in a Strongly Magnetized Single Species Plasma*, Bull. Am. Phys. Soc. **37**,1415 (1992)

5. Shi-Jie Chen and Daniel H. E. Dubin, *Equilibration Rate of Spin Temperature in a Strongly Magnetized Pure Electron Plasma*, Bull. Am. Phys. Soc. **36**,2330 (1991)

Abstract of the Dissertation

Temperature Equilibration and Many-Particle Adiabatic Invariants

by

Shi-Jie Chen

Doctor of Philosophy in Physics

University of California, San Diego, 1994

Professor Daniel H.E. Dubin, Chairman

The temperature equilibration of single-species plasmas is investigated in both weakly and strongly correlated limits. The correlation strength of a plasma is determined by the correlation parameter $\Gamma = q^2/akT$, where q is the charge, T is the temperature and a is the inter-particle spacing. Strong correlation corresponds to $\Gamma \geq 1$ and weak correlation corresponds to $\Gamma \ll 1$.

For each equilibration process that is investigated, a many-particle adiabatic invariant limits the equilibration. The first process examined is the equilibration of spin temperature with kinetic temperature in a weakly correlated pure electron plasma in the strongly magnetized limit, where the distance of closest approach is large compared to the Larmor radius. In this limit, the spin precession frequency is large so the component of spin along the magnetic field is an adiabatic invariant which is broken only by resonant magnetic fluctuations at the spin precession frequency. In this case, we find that the most important spin flip mechanism stems from electron-electron collisions in a spatially inhomogeneous magnetic field. Such collisions cause

an exchange of spin and cyclotron quanta, and consequently the conventional many electron adiabatic invariant (i.e. the total number of cyclotron quanta) is broken and is replaced by a new adiabatic invariant, equal to the sum of the spin and cyclotron actions. A quantum Boltzmann equation is derived to describe the equilibration process.

The second process studied is the temperature equilibration of an ordered Coulomb chain of ions, where the charges have been cooled into the regime of strong correlation $\Gamma \gg 1$. We calculate the rate of irreversible energy transfer between the transverse and parallel degrees of freedom in the strong transverse confinement limit. In this limit, the transverse motions are much higher frequency than the parallel motion, and so the total action of the high frequency transverse motion is approximately a many-particle adiabatic invariant. Only when this adiabatic invariant is broken can thermal equilibration occur. We find that Coulomb collisions can couple the perpendicular to the parallel degrees of freedom and cause a breaking of this invariant,leading to an exponentially small equilibration rate.

The third process calculated is the equipartition rate between parallel and perpendicular motion of a single species plasma which is not only strongly magnetized, but also strongly correlated so that the plasma is crystallized. In this case, we classify the crystal's collective modes into three branches: a cyclotron mode, a plasma mode and a $\mathbf{E} \times \mathbf{B}$ drift mode. We find that the total action of the cyclotron modes is an adiabatic invariant, which can be broken via the resonant coupling between a single (high frequency) cyclotron mode and many (low frequency) plasma modes, leading to the equilibration between the parallel and perpendicular temperatures. We calculate the rate for this process and find that the rate is exponentially small and is an oscillatory function of the magnetic field orientation with respect to the crystal structure.

Chapter 1

General Introduction

1.1 Overview

This thesis addresses the role of many particle adiabatic invariants in the temperature equilibration of single-species plasmas. Three specific examples are studied. Chapter 2 presents the calculation of the rate of spin temperature equilibration in a strongly magnetized and weakly correlated pure electron plasma, Chapter 3 presents the calculation of the rate of the temperature equilibration of a one-dimensional Coulomb chain and Chapter 4 presents the calculation of the temperature equilibration in a strongly magnetized single species crystallized plasma.

These calculations have several features in common. First, in all three calculations, the plasmas consist of a single charge species, i.e., they are nonneutral plasmas. In experiments confinement times of several hours to several days have been achieved [1] for nonneutral plasmas, so states of confined thermal equilibrium are possible. This unique property of nonneutral plasmas provides an experimental opportunity to test our temperature equilibration calculations. Another significant difference between neutral and nonneutral plasmas is that nonneutral plasmas can be cooled to very low temperature without the occurrence of recombination. When kT drops below q^2/a, where q is the charge and a is the distance between neighboring charges, the plasma becomes strongly correlated and as the temperature is

reduced, one expects the plasma to become a liquid and then a crystal. This second property of a nonneutral plasma makes the experimental test of our calculations for the strongly correlated plasma possible.

Second, our three calculations have an essential feature in common, that is, the temperature equilibration is limited by the existence of an adiabatic invariant. Generally, an action J which is canonically conjugate to an angle variable θ, where θ varies on a timescale faster than any other timescales in the system, is an "almost constant of motion" and this approximate constant is called an adiabatic invariant. If J is an adiabatic invariant, then on a short timescale during which J is well conserved, the (partial) equilibrium distribution of the system has the form

$$D = Z^{-1} e^{-\beta H + \alpha J} \tag{1.1}$$

where H is the total energy of the system and Z, α, β are constants related to the temperature and the total number of particles. In order for the system to approach the thermal equilibrium state, which is described by the distribution $D = Z_0^{-1} e^{-\beta_0 H}$ with $\beta_0 \equiv 1/kT$ and T is the equilibrium temperature, the adiabatic invariant J must be broken. However, as a general characteristic of the breaking of the adiabatic invariant, dJ/dt is exponentially small and scales as $exp[-\Phi/\varepsilon]$, where Φ is an algebraic factor determined by the dynamics, and where the adiabaticity parameter ε, which equals the ratio between the fast timescale and the slow timescale of the dynamics, is small compared with unity. As a result of the exponentially small rate for the breaking of the adiabatic invariant, the time for the temperature equilibration is expected to be exponentially long as a function of ε. Here we see two very different timescales during the temperature equilibration process : on a short timescale, J is well conserved and the partial equilibrium with the distribution function described by Eq. (1.1) is established; on a exponentially long timescale, the breaking of J occurs,

causing the system to equilibrate toward the final thermal equilibrium. Obviously the overall temperature equilibration time is mainly determined by the second process. In Chapter 2, Chapter 3 and Chapter 4, we calculate this exponentially small rate of temperature equilibration for three specific processes.

In Chapter 2, we present a calculation of the equilibration rate of spin temperature in a pure electron plasma, where the plasma is assumed to be weakly correlated, i.e., $\Gamma \equiv q^2/akT \ll 1$. Furthermore, the plasma is in the strong magnetization regime where the cyclotron radius r_L is small compared with the distance of the closest approach $\bar{b} = 2q^2/kT$. Supposing that initially the plasma has a temperature T_s associated with the distribution of electron spins, which is different from the perpendicular kinetic temperature $T_\perp$ and parallel kinetic temperature $T_{||}$, we determine the rate at which T_s, $T_{||}$ and $T_\perp$ should relax to a common value.

The spin temperature T_s is defined by $\frac{1}{T_s} = \frac{1}{\hbar\Omega_p} \ln \frac{x_-}{x_+}$, where $\Omega_p = \frac{geB}{2mc}$, $g = 2.002\cdots$ is the Landé g factor, x_+ and x_- are the concentrations of electrons with spin up and spin down respectively. Spin up and spin down are defined in terms of the electron spin vector $\mathbf{s}$: $s_z = \mathbf{s}\cdot\mathbf{B}/|\mathbf{B}| = \pm\hbar/2$. where $\mathbf{B}$ is the magnetic field vector. In order for the spin temperature to equilibrate, processes which flip the electron spins must occur. In order to understand the spin-flip process intuitively, it is useful to consider a classical model of the spin dynamics in which the quantum spin is regarded as a classical magnetic moment. In a magnetic field, the direction of the magnetic moment precesses around the magnetic field line at the spin precession frequency $\Omega_p = \frac{g}{2}\Omega_c$, where $\Omega_c = \frac{eB}{mc}$ is the electron cyclotron frequency. In the regime of strong correlation, Ω_p is large and hence s_z is an adiabatic invariant. In order to flip the spin, this adiabatic invariant must be broken. We found that, except for collisions with neutrals, which are negligible in cryogenic experiments, the only way to break the adiabatic invariant is through the coupling with a fluctuating

magnetic field $\delta\mathbf{B}(t)$. Furthermore, it is the Fourier component of $\delta\mathbf{B}(t)$ at frequency equal to the spin precession frequency Ω_p that causes a spin flip.

The spin flip Hamiltonian can be written as $\delta H_{sf} = \frac{eg}{2mc}\mathbf{s}\cdot\delta\mathbf{B}(t)$. When $\delta\mathbf{B}(t)$ is associated with an electron's orbital motion, the coupling between spin and $\delta\mathbf{B}(t)$ leads to an energy exchange between spin and orbital degrees of freedom, causing energy equipartition for the system. After examining several mechanisms that couple the spin and kinetic degrees of freedom, we found that the dominant spin flip process is an electron-electron collision in a spatially nonuniform $\mathbf{B}$ field. The basic idea for this collisional depolarization is the following. As an electron moves in a nonuniform magnetic field, in its rest frame the electron sees a time varying perturbing magnetic field $\delta\mathbf{B}$, which to the lowest order of the inhomogeneity, has the form $\delta\mathbf{B}(t) \sim \mathbf{r}(t)\cdot\nabla\mathbf{B}$, where $\mathbf{r}(t)$ is the position of the electron. Therefore, the spin flip is driven by the resonant component of $\mathbf{r}(t)$ at frequency Ω_p. Notice that the electron's g factor is almost equal to 2 and so the electron's cyclotron motion has almost the right frequency to cause resonance. However, $\Omega_p - \Omega_c = (\frac{g}{2} - 1)\Omega_c \simeq 0.001\Omega_c$ is still a large frequency for a strong magnetic field, and thus a perturbation of the cyclotron motion must occur to make up the frequency difference and cause a resonance. In the regime of strong magnetization, we found that such a high frequency can be introduced in an electron-electron collision.

An electron-electron collision in a strongly magnetized plasma is quite different from conventional Rutherford scattering. The cyclotron radii for the two colliding electrons are small compared to distance between the electrons, and the electrons spiral toward and away from each another along tight helical orbits that follow field lines. During each collision, the cyclotron motion suffers a small time varying phase shift $\delta\theta(t)$[2], which varies at a characteristic frequency $O(v_{\|}/b)$, and the cyclotron orbit is thus of the form $r_L e^{i(\Omega_c t + \delta\theta(t))} \simeq r_L e^{i\Omega_c t} + i r_L \delta\theta(t) e^{i\Omega_c t}$. Here, $v_{\|}$ is the initial

parallel velocity between two electrons and b is the distance of the closest approach. Here, we may see that the term $r_L\delta\theta(t)e^{i\Omega_c t}$, which has a characteristic frequency $\Omega_c + O(v_{||}/b)$, can be in resonance with the spin precession frequency, causing a kick in the spin direction during each collision. Over many uncorrelated collisions the spin direction gradually diffuse in a random walk, leading to spin depolarization.

Based on this physical picture, for $|\Omega_p - \Omega_c| \leq O(v_{||}/\bar{b})$, we estimated that the spin flip probability amplitude $|\Delta c|$ scales as

$$|\Delta c| \sim \frac{\rho_L \Delta\theta}{L} \frac{\Omega_c}{\Omega_p - \Omega_c} \tag{1.2}$$

where $\bar{v}_{||}$, $\bar{b}$, $\bar{r}_L$ are the averaged values, L is the scale length of the magnetic field inhomogeneity, and $\Delta\theta$ is the change of the $\delta\theta(t)$ during a collision, which is roughly on the order of the small parameter $\bar{\varepsilon} \equiv \bar{v}_{||}/\bar{b}\Omega_c$. After many collisions, the spin depolarization rate is given by $\nu_{spin} \sim \nu_c|\Delta c|^2$, where $\nu_c = \pi n \bar{v} \bar{b}^2$ is the collision frequency. For $|\Omega_p - \Omega_c| \geq O(v_{||}/\bar{b})$, we will see that the rate becomes exponentially small.

The problem of spin relaxation in plasmas has not received much attention. It was only recently that this problem was considered for fusion plasmas[3]. The motivation there was that the cross-section for D-T reactions is enhanced when the reacting nuclei's spins are aligned, and so an increase of the fusion power output is achieved if the plasma ions are spin polarized. It was found that, except for the effect of plasma waves, collisional depolarization in an inhomogeneous magnetic field is also the dominant depolarization effect in fusion plasmas. However, the collisional depolarization effect in fusion plasmas is quite different from that for a strongly magnetized pure electron plasma. For collisions in a fusion plasma, the timescale on which the orbit changes, or the effective duration time of collision, is much shorter than the gyroperiod. So the detailed dynamics of an individual collision, which

may be termed an "impulsive" random kick, is expected to be unimportant and consequently it suffices to take $\Delta\theta \sim 2\pi$ in Eq.(1.2). On the other hand, in a strongly magnetized plasma, $\Omega_c^{-1} \ll \bar{b}/\bar{v}_{||}$ and thus during the effective duration time of collision $\bar{b}/\bar{v}_{||}$, the electron gyrates over many cycles and $\Delta\theta$ is small. Evidently, the detailed collisional gyrodynamics is important for the determination of this change during a given collision.

In Chapter 2, we first calculate the spin temperature equilibration rate ν_{spin} in the classical limit $kT \gg \hbar\Omega_c$. We find that for $\bar{\varepsilon} \geq 0.001$, $\nu_{spin} \simeq 1.5 \times 10^4 \nu_c (\bar{\varepsilon}\bar{r}_L/L)^2$. For a typical plasma density of $10^8 cm^{-3}$ and $B = 10kG$, this implies that the magnetic field inhomogeneity must satisfy $L(cm) \leq 7.15T^{5/4}(K)$ in order for ν_{spin}^{-1} to be less than the plasma confinement time, which is typically on the order of $10^5 sec$.

However, we must point out that in the classical limit, the kinetic energy is assumed to be large compared with the spin energy $\hbar\Omega_p$ and so the kinetic energy behaves like an infinite heat reservoir supplying energy to flip spin. In this case, the orbital state of the electron is not affected by the spin flip and thus the spin flip transition from $|+>$ to $|->$ and from $|->$ to $|+>$ have an equal probability. This implies that a thermal equilibrium state is reached only when the number of electrons with spin up equals the number of electrons with spin down, which corresponds to an infinite spin temperature. Therefore, we can not rely on the classical process to reach thermal equilibrium and we must treat the orbital motion quantum mechanically.

In fact, the parameter regime of strong magnetization is quite unusual. For $T_\perp \sim T_{||} \sim T$ the condition for strong magnetization $\bar{r}_L \ll \bar{b}$, can be written as $T(K) \ll 100B^{2/3}(Tesla)$, which requires a strong magnetic field and a low temperature. When $\mathbf{B}$ is sufficiently strong and $T_\perp$ is sufficiently low such that $kT \ll \hbar\Omega_c$, a quantum mechanical treatment is necessary. In this case, not only the cyclotron energy is quantized as $E_{\perp n} = (n + 1/2)\hbar\Omega_c$, where the non-negative integer n is the

quantum number of the Landau levels, but also spin flip would cause an appreciable change in the orbital state. Specifically, when spin is excited from $|- >$ to $|+ >$ state, the spin energy is increased by an energy quanta $\hbar\Omega_p$ and this amount of energy is supplied by the cyclotron energy ($\hbar\Omega_c$) and the parallel energy ($\hbar(\Omega_p - \Omega_c)$). Consequently, n is decreased by unity while s_z is increased from $-\hbar/2$ to $\hbar/2$. Similarly, for the opposite process, n is decreased by unity while s_z is flipped from $\hbar/2$ to $-\hbar/2$. This type of energy exchange between the spin the kinetic degrees of freedom is crucial to cause spin temperature equilibration.

The result of the quantum analysis shows the equilibration rate $\dot{T}_s/T_s$ is proportional to

$$[1 - e^{-\frac{\hbar\Omega_p}{kT_s} + \frac{\hbar\Omega_c}{kT_\perp} + \frac{\hbar(\Omega_p - \Omega_c)}{kT_{pa}}}] \cdot [\frac{\hbar\Omega_c/2kT_\perp}{\sinh(\hbar\Omega_c/2kT_\perp)}].$$

Here we note two important quantum effects. First, the term $[\frac{\hbar\Omega_c/2kT_\perp}{\sinh(\hbar\Omega_c/2kT_\perp)}]$ introduces a notable suppression in the rate when $kT \ll \hbar\Omega_c$. This is because almost all the electrons stay at the ground state of the Landau level in this case and they are forbidden to further give up energy to excite the spin flip. Second, in the thermal equilibrium state, $\dot{T}_s/T_s = 0$, we have

$$\frac{\hbar\Omega_p}{kT_s} = \frac{\hbar\Omega_c}{kT_\perp} + \frac{\hbar(\Omega_p - \Omega_c)}{kT_\parallel} \tag{1.3}$$

Certainly we can not conclude that $T_s = T_\perp = T_\parallel$ from Eq. (1.3). This implies that the spin flip collisions which we calculated can not drive the system toward a common equilibrium temperature, rather, it only drives the system toward partial equilibrium with temperature satisfying Eq. (1.3). The physical reason for this can be understood as follows. When spin and and orbital dynamics are decoupled, both s_z and cyclotron quantum number n are adiabatic invariants. However, when spin is coupled to the orbital dynamics, the invariants s_z and n both are broken. In the

mean time, the exchange between spin and cyclotron quanta leads to a new adiabatic invariant, which equals to the total action of spin and cyclotron motion: $s_z + n\hbar$. Furthermore, one can generalize this new adiabatic invariant to a many electron adiabatic invariant $\mu^{(N)} = \sum_i (s_{zi} + n_i\hbar)$, where the sum is over all the electrons. Substituting $J = \mu^{(N)}$ into Eq. (1.1), one may easily obtain Eq. (1.3) by rearranging the terms in the exponent.

In order for the complete equilibration to occur, the invariant $\mu^{(N)}$ must be broken. One of the most important collisional $\mu^{(N)}$ - breaking processes is that involving collisional perpendicular and parallel energy exchange without spin flip, which has been discussed in another paper[4]. For a weakly inhomogeneous field, this kind of $\mu^{(N)}$ -breaking collision is the dominant mechanism and these $\mu^{(N)}$-breaking collisions cause equilibration between $T_\perp$ and $T_{||}$ on a relatively fast timescale. If one assumes that $T_\perp = T_{||}$ during the spin-kinetic temperature equilibration process the condition $T_\perp = T_{||} = T_s$ follows directly from Eq. (1.3).

The spin temperature equilibration is an important fundamental transport process in nonneutral plasmas. Besides the intrinsic interest of this problem, it also has several important practical applications. For example, according to our calculation, the temperature equilibration rate depends on the scale length L of the magnetic field inhomogeneity through L^{-2}. In the experiments, L ranging from $10cm$ to $10^3 cm$ can be easily achieved by confining the plasma at different distances from the end of the solenoid which produces the confining magnetic field. This suggests that the rate at which the electron spin temperature approaches the kinetic temperature can be relatively easily controlled. If this rate is reasonably fast, it might be possible to use a measurement of the plasma spin polarization as a thermometer for the kinetic degrees of freedom. Since the electron spin distribution becomes polarized as kT falls below $\hbar\Omega_c$, measurement of the degree of polarization of the electron spins

could indirectly provide the kinetic temperature in a range of temperature on the order of $\hbar\Omega_c/k$. For $B \sim 10 - 60kG$, this temperature is on the order of $1K$, which is over an order of magnitude below the minimum temperature which have been measured using current techniques.

On the other hand, if the temperature equilibration rate is slow, one may use the spin of an electron as a tag in order to perform various test-particle measurements. For example, one might place a small sub-population of the plasma in the opposite spin state from the bulk of the plasma, and follow this population's subsequent dynamics in order to evaluate test-particle spatial and velocity diffusion coefficients.

We now turn to the problems discussed in Chapter 3 and Chapter 4. First of all, we note that the plasmas discussed in Chapter 3 and Chapter 4 are completely different from that discussed in Chapter 2, which is weakly correlated. In Chapter 3 and Chapter 4, the plasmas are in the strongly correlated regime, where the correlation parameter $\Gamma \equiv q^2/akT$, is much larger than unity, where q is the charge, a is the inter-particle spacing and T is the temperature. Compared with a weakly correlated plasma, there are some rather distinctive properties for a strongly correlated plasma. For example, as Γ increases, the plasma undergoes a transition from a gas-like state in the weakly correlated regime to a liquid and even crystallized state in the strongly correlated regime[5]. Furthermore, as the condensed state is formed, the particles interact with each other collectively rather than via binary collisions. These features determine that the dynamical process causing the temperature equilibration is very different from that for a weakly correlated plasma.

We first discuss the problem studied in Chapter 3— temperature equilibration of a one- dimensional Coulomb chain. The one-dimensional Coulomb chain is a 1D form of condensed matter, consisting of charges of a single species trapped in a linear

configuration through the application of strong external magnetic and/or electric fields. In at least two of the recent experiments, where the technique of laser cooling or electron cooling was applied to the trapped ions, the formation of one dimensional Coulomb chains has been observed[6],[7]. In one of the experiments[6] ions are trapped in a linear Paul trap, where ions are held together against their Coulomb repulsion by an external radiofrequency field, while in the other experiment[7], a Paul trap in ring configuration has been used to trap a toroidal cloud of ions. In addition, it was predicted that an ordered Coulomb chain may also be realized in a storage ring[8], where ions are confined by a external magnetic quadrupole field. For all these experiments, ions are attracted to the chain axis by an external potential of the form $\frac{1}{2}m\omega_r^2 r^2$, where r is the distance from the axis and ω_r is the (large) radial oscillation frequency.

The motivation of our investigation of the temperature equilibration of the 1D Coulomb chain is the effort to obtain a cold, quiescent chain and a low emittance ion source, which is highly desirable for high precision atomic physics and high energy physics experiments. In the experiments, when laser cooling or electron cooling is applied along the chain axis, $T_{||}$, the temperature associated with the longitudinal motion is cooled, but the temperature associated with the transverse motion, $T_\perp$, is not cooled. $T_\perp$ can only be cooled through Coulomb collisions[9], where the perpendicular energy is scattered into the parallel energy, which is removed by laser cooling or electron cooling. In this case, the overall cooling rate depends on the rate at which $T_\perp$ equilibrates with $T_{||}$.

We calculate the rate ν at which $T_\perp$ and $T_{||}$ relax to thermal equilibrium in the strong focusing limit, where parameter $\varepsilon = \omega_0/\omega_r$ is much smaller than unity. Here $\omega_0 \equiv \sqrt{q^2/ma^3}$ is the characteristic frequency of the longitudinal plasma oscillation. For large Γ, the collective interactions between ions can be well described by the

emission and absorption of phonons. In the ideal phonon limit, the ion's motion can be described by N longitudinal eigenmodes at frequency of order ω_0 and $2N$ transverse modes at frequency approximately equal to ω_r. In this case, the inequality $\varepsilon \ll 1$ implies that the transverse motion of ions is of much higher frequency than the longitudinal motion. Therefore, one may expect that the total action, or, the total quanta, of the transverse phonons is an adiabatic invariant. In order for the temperature equilibration to occur, this adiabatic invariant must be broken.

We find that the adiabatic invariant is broken by the anharmonic terms in the ion-ion interactions, which cause phonon-phonon collisions. The basic idea is as follows. According to the law of the conservation of energy, $\sum_m \omega_m^{(i)} = \sum_n \omega_n^{(f)}$, where $\omega_m^{(i)}$ is the frequency of the mth initial phonon and $\omega_n^{(f)}$ is that of the nth final phonon. We may then classify the phonon collisions into two types. The first type of phonon collisions conserve the adiabatic invariant while the second type of phonon collisions break the adiabatic invariant. For the first type of collisions, the number of (high frequency) transverse phonons are conserved. This type of phonon collision may involve only a small number of phonons and thus is a low-order process, which has a large rate. On the other hand, during the second type of phonon collision, the number of (high frequency) transverse phonons is changed before and after collision. In this case, since $\omega_0 \ll \omega_r$, annihilation (creation) of one transverse phonon requires creation (annihilation) of $M \sim O(1/\varepsilon) \gg 1$ parallel phonons and thus the collision is of high-order, which has an exponentially small rate. Due to these two types of collision, the overall temperature equilibration can be thought to evolve in two stages. On a short timescale, the first type of collisions dominate and the energy equipartition occurs between parallel phonons and between transverse phonons, causing the distribution of parallel and transverse energy to relax to Maxwellian distributions described by unequal temperature $T_{||}$ and $T_{\perp}$ separately.

However, the evolution does not stop at this stage. On a long timescale, the adiabatic invariant is broken due to the second type of collisions, which cause the temperature equilibration between transverse and parallel degrees of freedom.

In Chapter 3 in order to obtain the rate of the breaking of the adiabatic invariant, we calculate the rate for the lowest-order process of the second type of phonon collisions, that is, two high frequency transverse phonons decay into many low frequency parallel phonons. The transverse phonons are destroyed in pairs because of the symmetry of the Hamiltonian. Our result shows that for sufficiently small ε and sufficiently large Γ, the rate $\nu(\varepsilon,\Gamma)$ scales as $exp[-2(\tau_0-1)/\varepsilon-\sqrt{2\Gamma_{\|}\alpha_0}]$, where $\alpha_0=(7/8+1/\eta\varepsilon)^2/\Gamma_{\|}, \eta\equiv\sqrt{7\zeta(3)}, \Gamma_{\|}=q^2/akT_{\|}$ and $\tau_0\simeq\gamma+(\ln\gamma)/2\eta, \gamma\equiv\ln[\sqrt{\pi\eta\ln 2}/\varepsilon\alpha_0]$. Here we see that $\nu(\varepsilon,\Gamma)$ is exponentially small as we expected. Our calculation also shows that in order for the harmonic approximation to be valid, we must require $\varepsilon\Gamma_{\|}\gg 1$. To understand this condition, we notice that large parallel displacements are desirable in order to obtain a large adiabatic invariant breaking rate because large displacements yield large anharmonic interactions. However, such large displacements are improbable for low temperature and the competition between these two effects causes the rate to be dominated by parallel displacements with a peak at $a/\sqrt{\varepsilon\Gamma_{\|}}$. To ensure the harmonic phonon approximation is valid, we must require $a/\sqrt{\varepsilon\Gamma_{\|}}\ll a$, i.e., $\varepsilon\Gamma_{\|}\gg 1$. Another important validity condition for the harmonic approximation is $\Gamma_{\perp}\gg\varepsilon^2\sqrt{\Gamma_{\|}}$, where $\Gamma_{\perp}=q^2/akT_{\perp}$. This condition guarantees that the parallel force induced by the transverse motion, which is proportional to the square of the transverse displacements, is small compared to the linear restoring force.

A striking feature of the equilibration rate $\nu(\varepsilon,\Gamma)$ is the abrupt steps at integer ratios between frequencies $2\omega_r$ and the maximum parallel phonon frequency $\omega_m=\eta\omega_0$. This is because a phonon-phonon interaction which creates or annihilates

two transverse phonons and M parallel phonons can only occur if $M\omega_m > 2\omega_r$, or $2/\eta\varepsilon < M$. When $2/\eta\varepsilon$ exceeds this value the process no longer contributes and the rate decreases abruptly. For very large ε^{-1} these steps are smoothed out and finally disappear because the rate is then determined by many high order processes, each of which has a small effect when taken individually.

In fact, the temperature equilibration rate of a 1D Coulomb chain has been examined via numerical simulations[10]. However, the validity conditions for the harmonic approximation are not fully satisfied in that work. In particular, the condition $\Gamma_\perp \gg \varepsilon^2\sqrt{\Gamma_\parallel}$ is not satisfied and the transverse displacement is not small, which causes a nonperturbative driving force of the parallel motion. This makes a detailed comparison between that calculation and the present analysis not possible. Nevertheless, Ref[10] does document a decrease in the rate as ε decreases. We also note that in the actual experiments, other mechanisms, such as scattering with gas molecules or heating due to the r.f. micromotion in the trap, may contribute to the equilibration process in a real Paul trap or storage ring.

In addition, when the ion chain is confined in a ring configuration, it will be bent and in this case, the symmetry of the Hamiltonian is changed, causing a process where one (instead of two) transverse phonon decays into $M/2$ (instead of M) parallel phonons. Therefore, the rate ν' for this process is expected to be on the order of $\frac{a}{R}\nu(2\varepsilon, \Gamma)$, where R is the curvature radius. When $\frac{a}{R}$ is not sufficiently small, the curvature effect may play an important role. For example, the circular Paul trap experiments[6] $a \sim 5\mu m$ and $R \sim 1cm$ so $\frac{a}{R} \sim 5 \times 10^{-4}$. In storage ring experiments[8], typically $a \sim 1\mu m$, $R \sim 1m$ and $\frac{a}{R} \sim 10^{-6}$ is so small that ν' is negligible compared with ν, and in linear Paul trap experiments[7] $\frac{a}{R} = 0$.

We now turn our attention to the problem discussed in Chapter 4 — the perpendicular to parallel temperature equilibration of a crystallized single species plasma

in the strong magnetization limit, where the cyclotron frequency Ω_c is large compared to the plasma frequency ω_p. As we have mentioned, when a plasma is cooled to an extremely low temperature at sufficiently high density, the plasma becomes strongly correlated and furthermore, the strong correlation causes the formation of liquid and even crystallized structures. Theoretical calculation has predicted that a first-order phase transition should occur from a liquid to a body-centered-cubic (bcc) crystal at $\Gamma \simeq 172$ for an infinite homogeneous one component plasma. Moreover, recent experiments have trapped a cloud of $10^2 - 10^4$ ions at a sufficiently low temperature so that the correlation parameter Γ is large[11]. In this regime the system becomes strongly correlated and the transition to spatially ordered states has been observed.

However, it is important to note that in the actual experiments, the number of ions are relatively small so that surface effects may play an important role. Simulations involving these relatively small number of ions predict that the ion cloud will separate into concentric spheroidal shells[12]. This prediction has been verified in experiments[11]. In this case, instead of a sharp phase transition, the system is expected to evolve gradually from a liquid state characterized by short-range order and diffusion in all directions, to a state where there is diffusion within a shell but no diffusion between shells (liquid within a shell, solidlike in the radial direction), and ultimately to an overall solidlike state. Therefore, the temperature equilibration for the system can not in general be predicted by that for a perfect bcc crystal. However, in order to gain a physical insight for the temperature equilibration process, we chose a simplified model where the plasma consists of randomly oriented local bcc lattice structures[13]. As one may expect, the temperature equilibration process is dominated by the nearest neighbor interactions. This fact allows us to evaluate the temperature equilibration rate for the system by averaging the equilibration rate of a local crystal over randomly varying crystal orientations, or, equivalently, averag-

ing over the randomly varying magnetic field directions with respect to the crystal structure.

Specifically, the problem proposed in Chapter 4 is as follows: Suppose initially the plasma is characterized by unequal temperature $T_\perp$ and $T_\parallel$, where $T_\perp$ and $T_\parallel$ are the temperature associated with the motions perpendicular and parallel to the magnetic field respectively. We calculate the rate at which $T_\perp$ and $T_\parallel$ should relax to a common value.

This equilibration rate has been investigated by O'Neil and Hjorth[4] for a weakly correlated and strongly magnetized plasma where the equilibration is driven by binary collisions. In that case, the cyclotron frequency is larger than the characteristic frequency $\omega_\parallel$ of the collisional dynamics, which is on the order of $v_\parallel/b$, where $v_\parallel$ is the relative parallel velocity and b is distance of the closest approach. This large frequency separation implies that the sum of each individual cyclotron action is an adiabatic invariant. Due to the existence of this adiabatic invariant, the equilibration rate is an exponentially small function of $1/\varepsilon_1$, where $\varepsilon_1 = \omega_\parallel/\Omega_c \ll 1$ is the small adiabaticity parameter. Specifically, the exchange of perpendicular cyclotron energy and parallel energy that occurs during a single collision was found to be on the order of $e^{-\pi/2\varepsilon_1}$, and after many uncorrelated collisions, an average of $e^{-\pi/2\varepsilon_1}$ over a Maxwellian distribution yields the equilibration rate $\nu_1 \sim exp(-2.04/\bar{\varepsilon}_1^{2/5})$, where $\bar{\varepsilon}_1$ is the average of ε_1. However, in the strongly correlated regime, particles interact collectively with each other and $1/\omega_\parallel$ is characterized by the collective time scale associated with the slow parallel oscillation, which is on the order of ω_p^{-1}. Correspondingly, ε_1 is replaced by $\varepsilon \equiv \omega_p/\Omega_c \ll 1$. In this case, we find that for $\varepsilon\Gamma_\parallel \gg 1$ the equilibration rate $\nu \sim exp[-(1 + ln\varepsilon\Gamma_\parallel)/\varepsilon]$. Here, $\Gamma_\parallel \equiv q^2/akT_\parallel \gg 1$ and thus $\varepsilon = \Gamma_\parallel\sqrt{6\Gamma_\parallel}\bar{\varepsilon}_1 \gg \bar{\varepsilon}_1$, which implies that $\nu \gg \nu_1$. Therefore, in the regime of strong correlation, the rate due to collective interactions that we calculate here is much

larger than that predicted by the binary collisional equilibration rate.

In the regime of strong correlation, particles interact with one another collectively. In this case, the eigenmodes for the crystallized plasma can be classified into three branches with very different frequency regimes, namely, N perpendicular cyclotron modes with frequency on the order of Ω_c, N parallel plasma oscillation modes with frequency on the order of ω_p and N $\mathbf{E} \times \mathbf{B}$ drift modes with frequency on the order of ω_p^2/Ω_c. The condition of strong magnetization implies the ordering $\Omega_c \gg \omega_p \gg \omega_p^2/\Omega_c$. Furthermore, since the $\mathbf{E} \times \mathbf{B}$ drift modes have much smaller frequencies than the other modes and the amplitude of the drift modes are small compared with the inter-particle distance, we may neglect the contributions from these modes to the temperature equilibration. We can now easily see the strong similarity between this 3D magnetized problem and the 1D Coulomb chain problem, where ω_r assumes the role of Ω_c in the present problem. By analogy with the 1D Coulomb chain problem, we expect that the total action (quanta) of the cyclotron modes (phonons) is an adiabatic invariant and the breaking of this adiabatic invariant leads to an exponentially small equilibration rate as a function of the small adiabaticity parameter $\epsilon \equiv \omega_p/\Omega_c$. However, despite the similarities between the 1D and 3D problems, in what follows, we emphasize that there are distinctive features of the 3D problem.

One of the most distinctive features is that the abrupt steps in the equilibration rate of a 1D chain now disappears for the 3D plasma. This can be understood as follows. As we have mentioned, the rate is dominated by the processes involving large frequency parallel phonon modes. For a 1D chain, the largest parallel frequency ω_m occurs at the shortest wavelength mode with $k = \pi/a$, which has a divergent density of states proportional to $1/|k - \pi/a| \to \infty$, causing the abrupt steps in the rate. On the other hand, for a 3D plasma the maximum parallel frequency ω_p occurs at

the long wavelength modes with $k \to 0$, which has a density of states proportional to $k \to 0$. According to energy conservation, a phonon collision which creates or annihilates one cyclotron phonon and $M \sim O(1/\varepsilon)$ plasma phonons can only occur if $M > \Omega_c/\omega_p$. However, as $M \to \Omega_c/\omega_p$, $k \to 0$, and the number of the plasma modes $\to 0$, causing the abrupt steps to be smoothed out.

Another distinctive feature of the 3D problem is the dependence of the rate ν on the orientation of the magnetic field with respect to the crystal structure. This dependence can be understood from the following physical picture. In the guiding center limit, one may think of particle's motion as fast cyclotron motion in the perpendicular plane and relatively slow oscillation in the parallel direction. In this case, as a particle l oscillates slowly along the field line, it produces a slowly varying perturbing electrostatic force $\delta\mathbf{f}$ on another particle n. The perpendicular component of $\delta\mathbf{f}$, $\delta f_\perp \sim |\delta\mathbf{f}| \sin\theta_{ln}$, where θ_{ln} is the angle between the magnetic field and the relative position for l and n, would modify particle n's cyclotron motion causing a change of the cyclotron action, and leads to an energy equipartition at rate ν_{ln}. This type of interaction between different pairs of particles acts cumulatively and leads to the breaking of the adiabatic invariant at a rate $\nu = \sum_{n \neq l} \nu_{ln}$. The rate ν_{ln} can be obtained by expanding the interaction Hamiltonian, keeping only the lowest-order process, which corresponds to the annihilation of one cyclotron phonon into $M \sim O(1/\varepsilon) \gg 1$ parallel phonons. In the $\varepsilon \ll 1$ and $\varepsilon\Gamma_\parallel \gg 1$ limit, we find that ν_{ln} depends on ε and θ_{ln} as

$$e^{-\Phi/\epsilon}[(\cos\theta_{ln})^{1/\epsilon} P^{-1}_{1+1/\epsilon}(\cos\theta_{ln})]^2 \tag{1.4}$$

where $P^{-1}_{1+1/\epsilon}(x)$ is the associated Legendre function of the first kind,

$$\Phi \equiv \ln[\frac{\pi^2}{\sqrt{2\pi}}(\frac{\pi}{3})^{2/3} c_0^{5/2} \epsilon\Gamma_\parallel] + 1,$$

where c_0 is a positive constant weakly dependent of the magnetic field direction. As for the 1D case, here we see that the rate is exponentially small and in order to make the result sensible, we must require the validity condition for the harmonic approximation $\varepsilon\Gamma_{||} \gg 1$ to be satisfied. Furthermore, as a unique property of the 3D problem, ν is an oscillatory function of θ_{ln} shown by the Legendre function. Also, ν decays exponentially as θ_{ln} increases due to the factor $(\cos\theta_{ln})^{2/\epsilon}$. Notice that $P^{-1}_{1+1/\epsilon}(\cos\theta_{ln}) = 0$ at $\theta_{ln} = 0$. We therefore expect that the largest rate occurs at small but nonzero θ_{ln}. Physically, this is easy to understand. In order to obtain a large rate, a large parallel relative ion displacement is desirable. Furthermore, the rate is dominated by the largest frequency plasma modes, which, as we will see, are the long wavelength modes with wavevector $\mathbf{k} \parallel \mathbf{B}$. In this case, the largest parallel relative ion displacement obviously occurs at $\theta_{ln} = 0$. As an extreme case, the relative ion displacement would vanish for $\theta_{ln} = \pi/2$. However, when $\theta_{ln} \to 0$, $\delta f_\perp \sim |\delta\mathbf{f}|\sin\theta_{ln} \to 0$. Therefore, we expect that the competition between the tendencies of small and large θ_{ln} yield a peak in ν at small but nonzero θ_{ln} for large $1/\varepsilon$.

Finally, as a caveat, we must point out that in both Chapter 3 and Chapter 4, when calculating the rate of the breaking of the adiabatic invariant, we assume that the particle's exact trajectory can be approximated by the unperturbed trajectory determined by the harmonic Hamiltonian. The approximation of integration along the unperturbed trajectory works well for a weakly correlated plasma. However, its validity in the strong correlation regime needs to be tested. In fact, when the anharmonic terms become important, J can no longer be approximated by the total action associated with the high frequency (perpendicular) harmonic motion. Consequently, the constants α and β in Eq.(1.1) are not simply related to the perpendicular and parallel kinetic energies. Moreover, the particle's orbit is perturbed

by the anharmonic interactions and in this case, the perpendicular and parallel motion can be thought of as nonlinearly coupled harmonic oscillators. This nonlinear coupling will introduce a frequency shift which will effectively change the adiabaticity parameter ϵ, causing a change in the exponential of the rate for the breaking of the adiabatic invariant. Also, this nonlinear coupling, if sufficiently strong, may cause the parallel and perpendicular dynamics to become chaotic. This could produce high frequencies in the parallel motion (due to, say, close collisions), and low frequencies in the perpendicular motion (due to nonlinear resonances) which leads to strong coupling between the parallel and perpendicular degrees of freedom. Presumably, such effects are responsible for the relatively rapid equilibration rates observed in the previous simulations[10], where the amplitude of the perpendicular motion is large ($\Gamma_\perp < \epsilon^2\sqrt{\Gamma_\parallel}$). However, in the regime of nearly harmonic phonons discussed in this thesis, we believe that the use of harmonic orbits, while not rigorously justifiable, is a useful first approximation.

Chapter 2 of this thesis has been published in *The Physics of Fluids*[14]. Chapter 3 of this thesis has been published in *Physical Review Letters*[15].

1.2 References

1. J. H. Malmberg, T. M. O'Neil, A. W. Hyatt, and C. F. Driscoll, "The cryogenic Pure Electron Plasma" Proc. 1984 Sendai Symposium on Plasma Nonlinear Phenomena, 31 (1984)

2. T. M. O'Neil, Phys. Fluids **26**, 2128 (1983)

3. R. M. Kulsrud, E. J. Valeo, and S. C. Cowley, Nucl. Fusion **26**, 1443 (1986)

4. T. M. O'Neil and P. Hjorth, Phys. Fluids **28**, 3241 (1985)

After examining several mechanisms which couple the spin and kinetic degrees of freedom, we conclude that the dominant spin-flip process is an electron-electron collision in a spatially inhomogeneous magnetic field. In the experiments, the confining magnetic field is inhomogeneous due, among other things, to the finite length of the solenoid. The degree of field nonuniformity can be controlled by confining the plasma at different distances from the end of the solenoid. The ability to control the rate of spin temperature relaxation may be useful in future experiments which rely on measurements of the degree of electron spin polarization. Two such experiments are briefly discussed in the conclusion of the paper.

In order to understand the spin-flip process intuitively, it is useful to consider a classical model of the spin dynamics in which the spin is regarded as a classical magnetic moment. (It is well-known that this classical picture is rigorously correct if one considers the dynamics of the quantum expectation value of the spin operator.) The direction of the moment precesses around the magnetic field at the spin precession frequency $\Omega_p = g\Omega_c/2$, where g is the Lande g-factor, equal to 2.002... for electrons. In the regime of strong magnetization Ω_p is large and hence the component of the magnetic moment along the magnetic field is an adiabatic invariant. In order to flip the spin this adiabatic invariant must be broken. If collisions with neutrals are neglected (and we will see that this effect is unimportant in Section 2.2), the only way to break the invariant is through a resonant fluctuation in the magnetic field (that is, a fluctuation at frequency Ω_p in the electrons' rest frame. Electron cyclotron motion in a spatially nonuniform (but time-independent) magnetic field is almost of the right frequency to cause such a fluctuation in the electron's rest frame since the electron g factor is nearly equal to 2. However, $\Omega_p - \Omega_c \simeq 0.001\Omega_c$ is still a large frequency and so cyclotron motion by itself is not enough to break the invariant, and a perturbation of the cyclotron motion must occur which is of sufficiently high

5. E. Pollock and J. Hansen, Phys. Rev. A **8**, 3110 (1973)

6. G. Birkl, S. Kassner and H. Walther, Nature **357**, 310 (1992)

7. M.G. Raizen et al., Phys. Rev. A **45**, 6493 (1992)

8. J.P. Schiffer, Proc. Workshop on Crystalline Ion Beams 1988, edited by R.W. Hasse, I. Hofmann and D. Liesen (GSI, Darmstadt, 1989), p. 2.

9. J.P. Schiffer and P. Kienle, Z. Phys. A. **321**, 181 (1985)

10. R.W. Hasse, Phys. Rev. A **45**, 5189 (1992)

11. S. Gilbert, J. Bollinger and D. Wineland, Phys. Rev. Lett. **60**, 2022 (1988)

12. D. Dubin and T. M. O'Neil, Phys. Rev. Lett. **60**, 511 (1988)

13. S. Ichimaru, Rev. Mod. Phys. **54**, 1017 (1982)

14. Shi-Jie Chen and Daniel H. E. Dubin, Phys. Fluids B **5**, 691-710(1993)

15. Shi-Jie Chen and Daniel H. E. Dubin, Phys. Rev. Lett. **71**, 2721 (1993)

Chapter 2

Equilibration Rate of Spin Temperature in a Strongly Magnetized Pure Electron Plasma

2.1 Introduction

Recent experiments have confined and cooled a pure electron plasma to cryogenic temperatures, $T \sim 1 - 10^2 K$, in a strong solenoidal magnetic field, $B \sim 10 - 60 kG$[1]. This range of temperatures and magnetic fields places the plasma in the novel regime of strong magnetization, in which the average distance of closest approach $\bar{b} \equiv 2e^2/kT_{\|}$ is large compared to the average Larmor radius $\bar{r}_L = \sqrt{kT_\perp/m}/\Omega_c$ (where e is the electron charge, $T_{\|}$ and $T_\perp$ is the kinetic temperature associated with the distributions of velocities parallel and perpendicular to the magnetic field, m the electron mass and $\Omega_c = eB/mc$ is the electron cyclotron frequency).

In this paper we consider a strongly magnetized pure electron plasma which initially has a temperature associated with the distribution of electron spins, T_s, which is different from the kinetic temperatures $T_{\|}$ and $T_\perp$. We calculate the rate at which T_s, $T_{\|}$ and $T_\perp$ should relax to a common value. We assume throughout that the plasma is weakly correlated (i.e. that $n\lambda_D^3 \gg 1$ where n is the density and $\lambda_D = \sqrt{kT/4\pi e^2 n}$ is the Debye length).

After examining several mechanisms which couple the spin and kinetic degrees of freedom, we conclude that the dominant spin-flip process is an electron-electron collision in a spatially inhomogeneous magnetic field. In the experiments, the confining magnetic field is inhomogeneous due, among other things, to the finite length of the solenoid. The degree of field nonuniformity can be controlled by confining the plasma at different distances from the end of the solenoid. The ability to control the rate of spin temperature relaxation may be useful in future experiments which rely on measurements of the degree of electron spin polarization. Two such experiments are briefly discussed in the conclusion of the paper.

In order to understand the spin-flip process intuitively, it is useful to consider a classical model of the spin dynamics in which the spin is regarded as a classical magnetic moment. (It is well-known that this classical picture is rigorously correct if one considers the dynamics of the quantum expectation value of the spin operator.) The direction of the moment precesses around the magnetic field at the spin precession frequency $\Omega_p = g\Omega_c/2$, where g is the Lande g-factor, equal to 2.002... for electrons. In the regime of strong magnetization Ω_p is large and hence the component of the magnetic moment along the magnetic field is an adiabatic invariant. In order to flip the spin this adiabatic invariant must be broken. If collisions with neutrals are neglected (and we will see that this effect is unimportant in Section 2.2), the only way to break the invariant is through a resonant fluctuation in the magnetic field (that is, a fluctuation at frequency Ω_p in the electrons' rest frame. Electron cyclotron motion in a spatially nonuniform (but time-independent) magnetic field is almost of the right frequency to cause such a fluctuation in the electron's rest frame since the electron g factor is nearly equal to 2. However, $\Omega_p - \Omega_c \simeq 0.001\Omega_c$ is still a large frequency and so cyclotron motion by itself is not enough to break the invariant, and a perturbation of the cyclotron motion must occur which is of sufficiently high

frequency to make up the difference and cause a resonance between the spin and orbital dynamics. In the regime of strong magnetization the only perturbation of such high frequency is an electron-electron collision, which induces orbital perturbations with frequencies of order $\bar{v}/b$, where $\bar{v}$ is the thermal speed.

In order to estimate the magnitude of the spin depolarization rate due to electron-electron collisions in a spatially nonuniform **B**-field, consider a strong static magnetic field $B\hat{z}$ along with a small time varying magnetic field $\delta\mathbf{B}(t)$ in the electron's rest frame. This time dependent field is due to electron motion through the spatially inhomogeneous but time-independent external magnetic field. We will estimate $\delta\mathbf{B}$ presently, but for now all we need to assume is that for a time $\Delta t \sim \bar{b}/\bar{v}$, the timescale of an electron-electron collision, $\delta\mathbf{B}(t)$ has a right-circularly polarized component rotating at frequency $\omega = \Omega_p$. This component resonates with the spin precession and drives a spin flip. The magnitude of this resonant component, δB_R, will be given approximately by a sum over all temporal Fourier components of the right-polarized part of $\delta\mathbf{B}(t)$ with frequencies ω satisfying $|\omega - \Omega_p| \leq 2\pi/\Delta t$:

$$\delta B_R \sim \int_{|\omega-\Omega_p|<2\pi/\Delta t} d\omega \frac{(\hat{x}+i\hat{y})}{\sqrt{2}} \cdot \delta\tilde{B}(\omega)$$

where $\delta\tilde{B}(\omega)$ is the Fourier transform of $\delta B(t)$. The probability amplitude ΔC of the spin flip is then given, in perturbation theory, by the angle through which the spin precesses in time Δt due to this resonant field:

$$|\Delta C| \sim \frac{eg}{2mc}|\delta B_R|\Delta t.$$

Now, $\delta\mathbf{B}(t)$ can be estimated for an electron executing cyclotron motion in a slightly nonuniform magnetic field: $\delta\mathbf{B}(t) \sim \rho(t) \cdot \nabla\mathbf{B}$ where ρ is a vector describing the cyclotron motion: $\rho(t) = \bar{r}_L(\cos(\Omega_c t + \theta)\hat{x} + \sin(\Omega_c t + \theta)\hat{y})$, where θ is the constant gyrophase. If one further assumes that the electron suffers a collision for which the

impact parameter is large compared to the Larmor radius, we will see in Sec.(2.3) that the most important effect is that θ becomes a function of time, adding Fourier components which bring $\delta\mathbf{B}(t)$ into resonance with the spin precession: $\theta = \theta_0 + \delta\theta(t)$. Since $\delta\theta(t)$ is small in such a collision, one can expand to first order in $\delta\theta$ to find that the resonant magnetic field approximately

$$\delta B_R \sim B\frac{\bar{r}_L}{L}\int_{|\omega-\Omega_p|<2\pi/\Delta t}\frac{d\omega}{2\pi}\delta\tilde{\theta}(\omega-\Omega_c)$$

where $\tilde{\theta}$ is the Fourier transform of $\delta\theta(t)$ and L is the scale length of variation of B. Since $\delta\theta(t)$ varies on a time scale of order $\Delta t = \bar{b}/\bar{v}$, if one assumes that $(\Omega_p - \Omega_c)\Delta t \leq 1$ this integral can be estimated as approximately

$$\delta B_R \sim B\frac{\bar{r}_L}{\Delta t L}\delta\tilde{\theta}(\Omega_p - \Omega_c).$$

Furthermore, the magnitude of $\delta\tilde{\theta}(\Omega_p - \Omega_c)$ can be estimated using dimensional analysis of the integral expression for the Fourier transform:

$$|\delta\tilde{\theta}(\Omega_p - \Omega_c)| = |\int_{-\infty}^{\infty} dt\delta\theta(t)e^{-i(\Omega_p-\Omega_c)t}| \sim \Delta\theta/(\Omega_p - \Omega_c)$$

where $\Delta\theta$ is the total change in $\delta\theta(t)$ during the collision, and again we have assumed $(\Omega_p - \Omega_c)\Delta t \leq 1$. In this regime we show in Section 2.2 that $\Delta\theta$ is roughly on order of the small parameter $\bar{\epsilon} \equiv \bar{v}_z/\bar{b}\Omega_{c0}$, where $\bar{v}_z$ is the parallel relative thermal speed. This parameter is the ratio of the frequency associated with a collision compared to the cyclotron frequency. When $\bar{\epsilon} \ll 1$ the plasma is in the strongly magnetized regime. Using this estimate for $\Delta\theta$, the spin flip amplitude is approximately

$$|\Delta C| \sim \frac{\bar{r}_L\Delta\theta}{L}\frac{\Omega_c}{\Omega_p - \Omega_c} \sim \frac{\bar{\epsilon}\bar{r}_L}{L}\frac{\Omega_c}{\Omega_p - \Omega_c}. \tag{2.1}$$

Finally, over many uncorrelated collisions the spin direction gradually diffuses in a random walk and the rate of spin depolarization is given by $\nu_{spin} \sim \nu_c|\Delta C|^2$, where

$\nu_c = \pi n \bar{v} \bar{b}^2$ is the electron-electron collision frequency.

This estimate for the depolarization rate gives the proper scaling of the spin depolarization rate provided that $|\Omega_p - \Omega_c| \leq \bar{v}/\bar{b}$, or $\bar{\epsilon} \geq g/2 - 1 = .001$. For $\bar{\epsilon} < .001$ we will see that ν_{spin} becomes exponentially small. This is because $(\Omega_p - \Omega_c)\Delta t$ becomes greater than unity in this regime, so that $\Delta\theta$ becomes exponentially small.

Although there has been considerable previous work, both theoretical and experimental, on the spin relaxation in neutral gases and solids, spin relaxation in plasmas has not received as much attention. However, the problem has been considered theoretically for plasma parameters of fusion interest. In this interesting work[2] it was noted that the fusion cross-section for D-T reactions is enhanced when the reacting nuclei's spins are aligned, and so an increase of the fusion power output is achieved if the plasma ions are spin polarized. A calculation of the rate at which the nuclear spins are depolarized by various effects was then carried out.

It was found that, except for the effect of plasma waves, collisional depolarization in an inhomogeneous magnetic field is also the dominant depolarization effect in fusion plasmas. However, although collisions give rise to spin relaxation effects for both fusion plasmas and pure electron plasmas, the relaxation rates are quite different in the two cases. For collisions in a fusion plasma, the time scale on which the orbit changes, or the effective duration time of collision, is much shorter than the gyroperiod and so the detailed dynamics of an individual collision, which may be termed an "impulsive" random kick, is expected to be unimportant. In this case it suffices to take $\Delta\theta \sim 2\pi$ in Eq.(2.1), and then the relaxation rate given by Eq.(36) of Ref.[2] is recovered. On the other hand, during the effective duration time of collision in a strongly magnetized plasma, the electron gyrates over many cycles. In this case, there is only a small change of the gyrophase due to the Coulomb interaction. Evidently, the detailed collisional gyrodynamics is important for the determination

of this change during a given collision.

The collisional process considered here causes an exchange of spin and cyclotron energy, and consequently the many electron adiabatic invariant of O'Neil and Hjorth[3] equal to the sum of the perpendicular kinetic energies $\sum_i E_{\perp i}$, is broken. However, as we will see this adiabatic invariant is replaced by a new N-electron invariant equal to the sum of the spin and cyclotron actions:

$$\mu^{(N)} = \sum_i [s_{iz} + \frac{E_{\perp i}}{\Omega_c(\mathbf{x}_i)}] = const. \tag{2.2}$$

where s_{iz} is the component of the spin along the magnetic field for electron i and $E_{\perp i}/\Omega_c(\mathbf{x}_i)$ is the cyclotron action. The conservation of $\mu^{(N)}$ implies that this collisional process cannot by itself drive the system to complete thermal equilibrium and in general $T_s = T_\perp = T_{||}$ will be the result. Rather, in Section 2.5 we obtain the relation

$$\frac{1}{T_\perp} + \frac{(g/2-1)}{T_{||}} - \frac{g/2}{T_s} = 0 \tag{2.3}$$

which holds for the state of partial thermal equilibrium which is achieved after many collisions which conserve $\mu^{(N)}$. Of course, since $\mu^{(N)}$ is not an exact invariant, electron-electron collisions occur which cause exponentially small changes in its value. Because the spatial variation of the magnetic field is slow compared to the Larmor radius of the strongly-magnetized electrons, almost all of these collisions are of the type described by O'Neil and Hjorth in which the spin plays no role, and these collisions cause $T_\perp$ to approach $T_{||}$ according to the equations described in Ref.[3]. In turn, collisions considered in this paper which conserve $\mu^{(N)}$ cause T_s to approach the common value of $T_\perp$ and $T_{||}$ [see Eq.(2.3) for $T_\perp = T_{||}$], and hence a state of complete thermal equilibrium is achieved. This is the qualitative picture of spin relaxation which emerges from our analysis.

In Section 2.2 we make order-of-magnitude estimates of various spin flip processes, including spin flip due to the mutually generated magnetic field, radiative transitions and interactions with background waves, Thomas precession, electron-neutral collisions, and single particle electron motion through the inhomogeneous **B**-field. We find that all processes except for electron-electron collisions in an inhomogeneous **B**-field produce depolarization time scales which are longer than the plasma confinement time of approximately 10^5 seconds, provided that neutrals with partially-filled valence shells, such as N_2, are kept at pressures below $\sim 10^{-14}$ Torr (this is a reasonable upper bound in the cryogenic environment of the present experiments). In the regime $\hbar\Omega_c < kT_\perp$ and $\bar{\epsilon} > .001$, we find that spin depolarization rate is $\nu_{spin} = 1.5 \times 10^4 \nu_c (\bar{\epsilon}\bar{r}_L/L)^2$. For a typical plasma density of $10^8 cm^{-3}$ and $B = 10kG$, this implies that the **B**-field inhomogeneity scale length L must satisfy $L(cm) < 7.15T^{5/4}(K)$ in order for ν_{spin}^{-1} to be less than the plasma confinement time. In Section 2.3 we present a calculation of the spin flip transition rate due to electron electron collisions in a weakly inhomogeneous magnetic field assuming that the orbital motion can be treated classically (that is, assuming that the electron's kinetic energy is large compared to $\hbar\Omega_c$). This calculation improves the estimate for ν_{spin} given by Eq.(2.1), extending it to cover the range $\bar{\epsilon} \leq 0.1$. In Section 2.4 the calculation is repeated using a quantum description of the orbital motion, since in fact $T_\perp$ and $T_{||}$ can be of order $\hbar\Omega_c$ in the experiments. In the classical limit this rate agrees with that calculated in Section 2.3. In Section 2.5 we present a derivation of a Boltzmann collision operator for spin relaxation which conserves $\mu^{(N)}$ and drives the system to a partial thermal equilibrium described by Eq.(2.3). We summarize our results in the conclusion and discuss two possible experiments which rely on measurements of spin polarization.

2.2 Order of Magnitude Estimates for Spin Depolarization Processes

As pointed out in our discussion, spin depolarization is caused by a resonant perturbing magnetic field of frequency Ω_p due to an electron-electron collision in a nonuniform magnetic field. Such resonant fields can also be induced by other mechanisms. We will consider four such processes, as well as a fifth process due to spin exchange in electron-neutral collisions. In order to simplify results we assume that $T_\perp$ and $T_{||}$ are of the same order of magnitude.

2.2.1 Spin flip due to mutually generated magnetic field

Consider two electrons, 1 and 2, immersed in a uniform external field $\mathbf{B}$, separated by relative distance $\mathbf{r}$ and passing by one another with impact parameter ρ on the order of $\bar{b} \gg \bar{r}_L$ (see Fig.(2.1)). Then electron 1 sees a time varying magnetic field induced by the relative motion of electron 2 as well as electron 2's intrinsic magnetic moment. In the former case the field is $\mathbf{B} = (e/c)(\dot{\mathbf{r}} \times \mathbf{r})/r^3$, and the component of this field which is resonant with the spin precession is approximately $\delta B_R \sim (e/c)v_\perp z/r^3$, to lowest order in $\bar{r}_L/\bar{b}$. Taking $v_\perp$ equal to the thermal velocity $\bar{v} \equiv \sqrt{kT/m}$ and the effective interaction time of the electrons equal to $\bar{b}/\bar{v}$, we find the change in direction of spin is $\Delta C \sim eg\delta B_R/2mc \cdot \bar{b}/\bar{v} \sim (\bar{v}/c)^2 \sim 10^{-10}\bar{T}$, where $\bar{T}$ is the temperature in K. This gives rise to an extremely small depolarization rate $\nu_c(\Delta C)^2 \sim 10^{-12}T^{1/2}\bar{n}(sec^{-1})$, where $\nu_c \simeq \pi\bar{b}^2 n\bar{v}$ is the electron-electron collision frequency and $\bar{n}$ is the electron density (n) in units of $10^7 cm^{-3}$.

The intrinsic magnetic dipole moment of electron 2 also induces a time varying magnetic field at electron 1. However, this magnetic field is so weak that the spin depolarization effect is negligible, even compared to the above estimate.

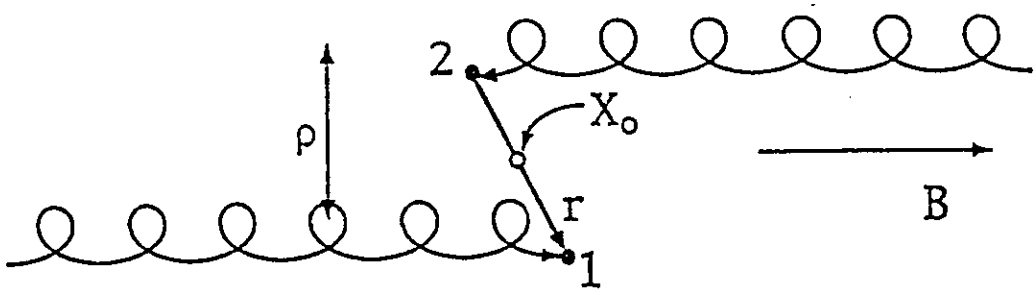

Figure 2.1: Schematic picture for an electron-electron collision in a uniform magnetic field in the strongly magnetized limit.

2.2.2 Radiative transitions and interactions with background waves

As an electron's spin precesses, its related intrinsic magnetic moment will radiate spontaneously through magnetic dipole transition. The rate for the spontaneous radiation is [4] $\frac{2}{3}(\frac{g}{2})^2\frac{e^2\hbar}{m^2c^5}\Omega_c^3 \simeq 7\times 10^{-11}\bar{B}^3(sec^{-1})$, where **B** is the magnitude of the magnetic field in Tesla.

In addition, as pointed out by, for example, R.M. Kulsrud et al.[2] in a uniform magnetic field, the right circularly polarized component of an electromagnetic wave with harmonics near Ω_p will cause an electron spin depolarization. It is easy to show that a thermal level of electromagnetic waves produces negligible depolarization provided that the plasma is optically thin. When the plasma is optically thick, the problem is more complicated due to the dielectric behavior of the magnetized plasma, but we believe that for a thermal equilibrium plasma at cryogenic temperature, the electric current fluctuation is negligibly small and there aren't appreciable excitation

of magnetic fluctuations. However, waves which are unstable in the range of electron spin precession frequency could cause appreciable spin depolarization. Although electromagnetic instabilities could be driven when $T_\perp$ and $T_{||}$ differ, if the temperature difference $|T_\perp - T_{||}|$ is not too large and no external heating is assumed, then, unlike the spin polarized fusion plasma, the presence of strong cyclotron damping should make the existence of unstable waves at the spin precession frequency unlikely (since the electron spin precession frequency $\Omega_p = \frac{g}{2}\Omega_c$ is close to the cyclotron frequency Ω_c).

Another possible depolarization effect is due to the electron position shift driven by electrostatic waves at the spin precession frequency Ω_p. In a spatially nonuniform magnetic field the magnetic field seen in the electron's rest frame is perturbed at frequency Ω_p and the electron spin is flipped by the resonant magnetic field perturbation. However, one may show that compared with the collisional effect, this effect is also negligible for a thermal level of waves in the strongly magnetized cryogenic plasma. Physically this is due to the relatively few degrees of freedom involved in these collective electrostatic modes compared with the perturbing electrostatic field due to collisions.

2.2.3 Thomas precession

Due to this pure relativistic effect, the electron sees an additional perturbing magnetic field corresponding to a precession frequency $\omega_T(t) \simeq \dot{\bar{\mathbf{v}}} \times \bar{\mathbf{v}}/2c^2$. The magnitude of this frequency does not equal Ω_p except during an electron-electron collision. During the collision, a component of the Thomas precession frequency given by $\omega_T(t) \simeq \dot{\bar{\mathbf{v}}}_\perp \times \bar{\mathbf{v}}_{||}/2c^2$ varies at the resonant frequency and so leads to a spin direction change $\Delta C \sim (\Omega_c \bar{v}_\perp \bar{v}_{||}/2c^2) \cdot (\bar{b}/\bar{v}_{||}) \sim (\frac{\bar{b}}{\bar{r}_L}) \cdot (\frac{\bar{v}_\perp}{c})^2$. Here we have again kept only the lowest order component of ω_T in an expansion in $\bar{r}_L/\bar{b}$. The

depolarization rate is then $\nu_c(\Delta C)^2 \sim 10^{-7}\bar{n}\bar{B}^2\sqrt{T_\perp}T_{||}^{-3}(sec^{-1})$. As before, $\bar{B}$ is in units of Tesla and $\bar{n}$, $T_\perp$, $T_{||}$ are again in units as defined in section (2.2.1).

2.2.4 Electron-neutral collisions

In the cryogenic environment of the experiment it is likely that the residual neutrals are almost entirely helium since most of the neutral gas freezes on the wall. Nevertheless there may be traces of other gases, and here we also consider collisions with nitrogen molecules as a representative example. To calculate the spin depolarization rate due to electron-neutral collision, we note that the spin flip cross section due to spin exchange between the free electron and atomic electron is several orders of magnitude larger than that due to other effects[5] such as the spin-orbit interaction. For electron-helium collisions the spin exchange is inhibited by the Pauli exclusive principle and so the depolarization effect is effectively negligible for them. For an electron-nitrogen collision, the spin flip cross section is $\sigma_{spin\ flip} \simeq \sigma_{spin\ exchange} \leq \sigma_{kinetic} \simeq 3\mathring{A}^2$ and thus the depolarization rate is approximately $\sigma_{spin\ flip} \cdot \bar{n}_{N_2}\bar{v}_e \leq 10^{-5}T^{-1/2}\bar{n}_{N_2}(sec^{-1})$ where $\bar{n}_{N_2}$ is the density of nitrogen molecules in units of $10^4/cm^3$ and T is again the temperature in units of Kelvin.

In addition, electron-neutral collisions change electron's orbit randomly resulting in a fluctuating magnetic field in the electron's rest frame due to the non-uniform external magnetic field. This perturbing field causes a spin flip at rate [2] $\nu_{spin} \simeq 9.57 \times 10^{-13}T^{3/2}B^{-2}L^{-2}\bar{n}_N$, where the scale length of magnetic field inhomogeneity L is in units of cm and $\bar{n}_N$ is the neutral density in units of $10^4/cm^3$.

2.2.5 Single particle motion

Single particle motion consists of cyclotron motion together with a slow $\mathbf{E}\times\mathbf{B}$ rotation of the plasma column and parallel streaming along the slightly curved mag-

netic field lines. Neither of these drifts cause sufficiently high frequency perturbations to the magnetic field observed in the electron rest frame and so these effects cause negligible spin depolarization. However, as an electron approaches the end of the plasma along a field line, the electron feels an electric potential with a scale length of gradient of order of λ_D, the Debye length. Due to the electric potential, the electron gyro-orbit is disturbed and thus, in the slightly nonuniform B-field, as in an electron-electron collision, a secular spin depolarization results. However, since $\lambda_D \gg b$, the "collision" with the end of the plasma is much slower than an electron-electron collision, and the resonant field δB_R is much smaller. The size of this effect can be estimated by substitution of λ_D for b in Eq.(2.1) and use of the axial bounce frequency $\nu_b = \bar{v}/L_p$ rather than ν_c, where L_p is the length of the plasma. This implies a depolarization rate smaller than that given by Eq.(2.1) by the factor $(\frac{\nu_b}{\nu_c}) \cdot (\frac{\bar{b}}{\lambda_D})^2 \sim 10^{-3}/T\bar{L}_p$, where $\bar{L}_p$ are lengths in units of centimeters. This result is further reduced if the electron mean free path is less than L_p, and so should be regarded as an upper bound.

The depolarization rate ν_{spin} for various spin relaxation processes are plotted as a function of small parameter $\bar{\epsilon} = \bar{r}_L/\bar{b} = 10^{-3}\bar{T}^{3/2}/\bar{B}$ in Fig.(2.2), where the other parameters $\bar{B}$, $\bar{n}$, $\bar{n}_{N_2}$, and $\bar{n}_N$ are set to be unity and $\bar{L}$ is set to be $10cm$. The conclusion we draw from the figure is that the spin relaxation time ν_{spin}^{-1} due to all effects considered other than that of collisional depolarization in a nonuniform magnetic field is longer than the maximum plasma confinement time of approximately $10^5 sec$ provided that $\bar{n}_{N_2} \leq 1$. Therefore, we conclude that the dominant depolarization effect is due to collisional depolarization in an inhomogeneous magnetic field.

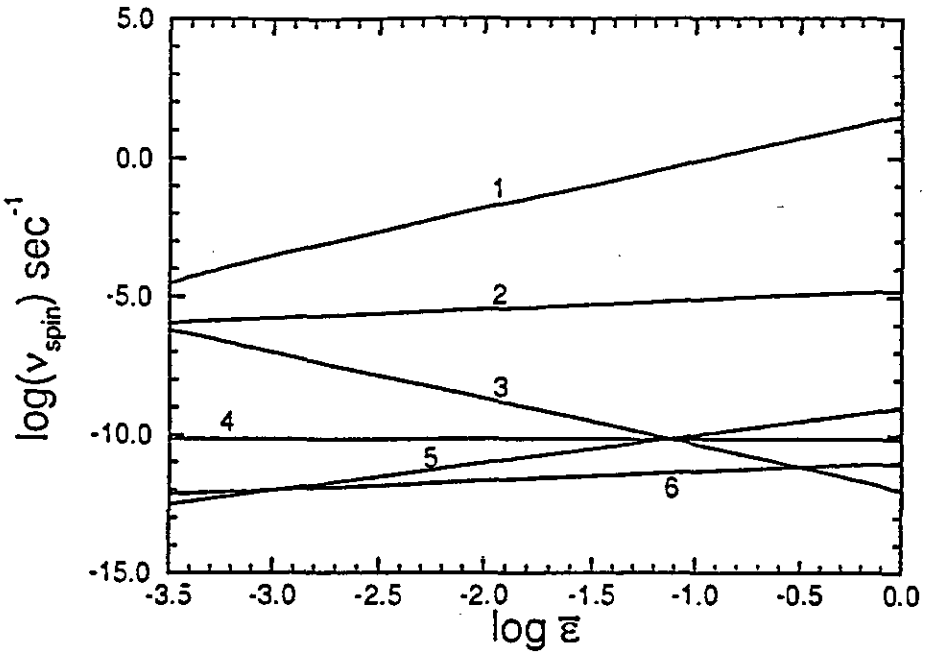

Figure 2.2: Plot of the spin depolarization rate as a function of $\bar{\epsilon} = \bar{r}_L/\bar{b} = 10^{-3}\bar{T}^{3/2}/\bar{B}$ for different processes. Curve 1: collisional depolarization in a nonuniform magnetic field. Curve 2: spin exchange effect during electron-neutral collisions. Curve 3: Thomas precession. Curve 4: spontaneous magnetic dipole radiation. Curve 5: spin flip due to mutually generated magnetic field. Curve 6: spin flip due to electron-neutral collision in a nonuniform magnetic field. The electron density n_e is assumed to be $10^7 cm^{-3}$, the neutral density is taken to be $10^4 cm^{-3}$, the magnetic field is $1 Tesla$ and the scale length of magnetic field inhomogeneity is taken to be $10 cm$.

2.3 Collisional Spin Depolarization in an Inhomogeneous Magnetic Field

In this section we consider in detail the problem of spin depolarization due to electron-electron collisions in a weakly inhomogeneous magnetic field. The velocities of the colliding electrons are taken to be sufficiently large so that we can treat the orbital dynamics classically. We will eventually expand in the small parameters r_L/b and r_L/L, but in order to set up the problem we consider the spin dynamics of a spin $\frac{1}{2}$ particle moving on a general classical trajectory through an inhomogeneous magnetic field[2] In a fixed laboratory frame of reference the spin part of the wavefunction $|\psi>$

evolves according to

$$i\hbar\frac{\partial}{\partial t}|\psi>=\mathbf{s}\cdot\mathbf{\Omega}_p|\psi> \tag{2.4}$$

where $\mathbf{\Omega}_p(t)=\frac{g}{2}\frac{eB}{mc}(\mathbf{x}(t))$, $\mathbf{x}(t)$ is the position of the electron, $\mathbf{s}=\frac{\hbar}{2}(\sigma_x,\sigma_y,\sigma_z)$ is the spin operator for spin $\frac{1}{2}$ particles and $\sigma_x,\sigma_y,\sigma_z$ are the Pauli matrices, with respect to some fixed coordinate axes. The classical approximation employed throughout this section implies that $\mathbf{x}(t)$ is unaffected by the spin state and so is a given function of time.

Now, because the spin component along the field is an adiabatic invariant we consider the evolution of the spin in a noninertial frame of reference which follows the electron and which keeps the z axis directed along the magnetic field. Since these coordinate axes rotate in time as the field varies in direction in the electrons' rest frame, the spin Hamiltonian $\mathbf{s}\cdot\mathbf{\Omega}_p$ transforms into the noninertial frame according to the usual relation $\hat{H}'=\mathbf{s}\cdot\mathbf{\Omega}_p-\mathbf{s}\cdot\omega$, where $\omega=\hat{b}\times\frac{d\hat{b}}{dt}-\omega_z\hat{b}$ is the rate of rotation of the coordinate frame, ω_z represents an arbitrary rotation of the coordinates around $\mathbf{B}$, and $\hat{b}=\mathbf{B}/B$. Thus, in the rotating frame, Eq. (2.4) become[2])

$$i\hbar\frac{\partial|\psi>}{dt}=(\Omega_p-\omega)\cdot\mathbf{s}|\psi>.$$

Writing $|\psi>$ as $|\psi>=C_+(t)|+>+C_-(t)|->$, where $|+>$ and $|->$ are states polarized parallel and antiparallel to $\hat{b}$ (i.e. they are eigenstates of σ_z in the coordinates moving with the electron), linearized solutions can be found for the transition amplitudes as a function of time assuming that at the initial time $t=t_1$ the spin is in either the $+$ or $-$ state only, so that $C_\pm(t_1)=1$. The probability amplitude of transition to the opposite state follows after some simple algebra:

$$C_\mp\simeq\frac{i}{2}\int_{t_1}^{t}dt'\omega_\pm(t')e^{\mp i\int_{t_1}^{t'}[\Omega_p(t'')-\omega_z(t'')]dt''}$$

where $\omega_\pm = \omega_x \pm i\omega_y$. This expression clearly shows that $|C_+|^2 = |C_-|^2$, so we consider only C_+ from now on.

In order to make further progress we choose to set $\omega_z = 0$ and further specialize to the regime of strong magnetization in which one may write $\omega(t)$ in a guiding center expansion:

$$\omega(t) = \sum_n \omega^{(n)}(t) e^{in\int_{t_1}^t \Omega_c(t')dt'} \tag{2.5}$$

where the $\omega^{(n)}$ś are relatively slowly varying functions compared to the oscillatory factor; $\omega^{(0)}$ is the term stemming from guiding-center motion, and the other terms in the series are associated with harmonics of the cyclotron motion. The largest terms are $\omega^{(0)}$ and $\omega^{(\pm 1)}$. These are of magnitude v/L, as can be seem from the expression $\omega = \hat{b} \times \mathbf{v} \cdot \nabla \hat{b}$. Before we evaluate the $\omega^{(n)}$'s explicitly in terms of the strongly-magnetized electron trajectory, it proves useful to integrate by parts in order to separate out a small oscillatory contribution due to the limits of integration:

$$C_+(t) = \frac{i}{2}\sum_n \left[\frac{\omega_{(n)}(t')}{i(n+g/2)\Omega_c(t')} e^{i\int_{t_1}^{t'}[n+g/2]\Omega_c(t'')dt''} \right|_{t'=t}^{t'=t_1} - \int_{t_1}^t dt' \frac{\frac{d}{dt'}\omega_{(n)}(t')}{i[n+g/2]\Omega_c(t')} e^{i\int_{t_1}^{t'}[n+g/2]\Omega_c(t'')dt''} \Bigg] \tag{2.6}$$

We neglect the first term because it is small and nonsecular. By this we mean that even after many collisions, the velocity of the electron remains on the order of the thermal speed and so $\omega^{(n)}/\Omega_c$ also remains small. Furthermore, although there is a nearly resonant denominator for the $n = -1$ term in the series, the term is still only of order $r_L/(g-2)L \ll 1$. It is also true that after any single collision the change of the second term of Eq. (2.6) is small (in fact it is smaller than the first term by $O(\bar{\epsilon})$, as we will see). However, over the course of many collisions this second

term grows secularly in a random walk and hence dominates the expression for C_+ over time. Physically, the first term represents the effect of fast spin precession in a slowly varying magnetic field, which causes small oscillations in the z-component of the spin as $\mathbf{B}$ changes direction in the electron rest frame. To make an analogy with the classical theory of adiabatic invariants, the exact adiabatic invariant is not s_z, but is instead an infinite asymptotic expansion with s_z as the lowest order term. The small oscillations in s_z represented by the first term of Eq. (2.6) are due to higher order non-secular terms in the invariant, and are not important in determining the secular change of the invariant.

We further simplify the expression for C_+ by neglecting terms of order $(r_L/L)^2$ and higher. Since ω is already of $O(r_L/L)$ we can therefore neglect the magnetic field gradient in the dynamics of the electron orbits and evaluate the collisional dynamics in a constant field $\mathbf{B}_0 = \mathbf{B}(\mathbf{x}_0)$, where we choose $\mathbf{x}_0$ as the center of mass position at the instant of closest approach of the colliding electrons (see Fig.(2.1)). Furthermore, to lowest order in r_L/L, ω itself can be written as

$$\omega = \hat{b}_0 \times \mathbf{v} \cdot (\nabla \hat{b})_0$$

where $\hat{b}_0 = \hat{b}(\mathbf{x}_0)$ and $(\nabla \hat{b})_0 = \nabla \hat{b}(\mathbf{x}_0)$ are constant, and the velocity $\mathbf{v}$ has a guiding center expansion of the same form as Eq. (2.6). Then keeping only the near-resonant $n = -1$ term in the series over n in Eq. (2.6), the expression becomes

$$C_+(t) = \frac{-1}{(g-2)\Omega_{c0}} \int_{t_1}^{t} \left[\hat{b}_0 \times \frac{d}{dt'} \mathbf{v}^{(-1)} \cdot (\nabla \hat{b})_0 \right] e^{i(t'-t_1)(g/2-1)\Omega_{c0}} dt'$$

$$+ O\left(\left(\frac{r_L}{L} \right)^2 \right), \qquad (2.7)$$

where $\Omega_{c0} = \Omega_c(\mathbf{x}_0)$. All other terms in the series give contributions which are exponentially small because of the fast variation of the phase factor in the integrand.

Finally, $\frac{d\mathbf{v}^{(-1)}}{dt}(t)$ is evaluated in a guiding center expansion in the small parameter $\epsilon \equiv v_z(t_1)/b\Omega_0$ where $b = 2e^2/\mu v_z^2(t_1)$ is the distance of closest approach, $v_z(t_1)$ is the initial relative parallel velocity, and $\mu = m/2$ is the reduced mass. We again consider two electrons, labeled 1 and 2, colliding in a uniform magnetic field $\mathbf{B}$. In the strongly magnetized regime the collision may be pictured schematically as shown in Fig.(2.1). The electrons spiral in tight Larmor orbits toward one another along the magnetic field lines, and their mutual Coulomb repulsion perturbs the orbits. This perturbation shifts the cyclotron frequency, bringing it into resonance with the spin precession, and inducing a spin flip transition. We will determine the trajectories of the electrons and use them to calculate C_+ for electron 1. The equations of motion for two electrons are

$$m\dot{\mathbf{x}}_{1,2} = e\frac{\partial}{\partial \mathbf{x}_{1,2}}\phi(\mathbf{x}_1 - \mathbf{x}_2) - \frac{e}{c}\dot{\mathbf{x}}_{1,2} \times \mathbf{B}_0$$

where $\phi = -e/|\mathbf{x}_1 - \mathbf{x}_2|$ is the interaction potential. The center of mass motion can be separated out by transforming to center of mass coordinates through $\mathbf{R} = (\mathbf{x}_1 + \mathbf{x}_2)/2$, $\mathbf{r} = \mathbf{x}_1 - \mathbf{x}_2$, leading to

$$m\dot{\mathbf{R}} = -\frac{e}{c}\dot{\mathbf{R}} \times \mathbf{B}_0, \tag{2.8}$$

$$m\dot{\mathbf{r}} = 2e\frac{\partial}{\partial \mathbf{r}}\phi(r) - \frac{e}{c}\dot{\mathbf{r}} \times \mathbf{B}_0 \tag{2.9}$$

Equation (2.8) describes center of mass motion which is just a combination of constant amplitude Larmor gyrations and parallel streaming. Since $d\mathbf{v}^{(-1)}/dt$ is zero for this motion, the center of mass motion makes no contribution to C_+.

Turning to the equation for relative motion, we solve for $\dot{\mathbf{r}}$ by expanding in ϵ

using standard asymptotic techniques. To $O(\epsilon)$ the result is[6]

$$\dot{\mathbf{r}} = \mathbf{v}_g(t) + v_{\perp 0} + Re\left\{e^{i[\Omega_{c0}(t-t_1)+\theta_0+\delta\theta(t)]}[\hat{x}-i\hat{y}]\right\} + O(\epsilon^2) \qquad (2.10)$$

where θ_0 is the initial relative gyrophase, $\mathbf{v}_{g(t)}$ is the slowly-varying guiding center relative velocity, $v_{\perp 0} = v_\perp(t_1)$ is the initial perpendicular relative velocity, and $\delta\theta$ is a $O(\epsilon)$ slow variation of the relative gyrophase given by[6]

$$\delta\theta(t) = \frac{e^2}{\mu\Omega_{c0}}\int_{t_1}^{t} dt' \frac{z^2(t') - \frac{1}{2}\rho_0^2}{(z^2(t')+\rho_0^2)^{5/2}} \qquad (2.11)$$

where the function $z(t)$ is the lowest order z position of the guiding center, determined by solution of the equation

$$\dot{z} = \frac{e^2}{\mu}\frac{z}{(z^2+\rho_0^2)^{3/2}} \qquad (2.12)$$

and $\rho_0 = \sqrt{x(t_1)^2 + y(t_1)^2}$ is the initial impact parameter. The time t_1 is chosen so that the electrons are initially far apart, i.e. $|z_0(t=0)| \gg \rho_0$.

A further simplification can be made by noting that $\frac{d\mathbf{v}^{(-1)}}{dt}$ appears in Eq.(2.7) only in the combination

$$\frac{d\omega_-^{(-1)}}{dt} = \left[\hat{b}_0 \times \frac{d\mathbf{v}^{(-1)}}{dt}\cdot\nabla\hat{b}_0\right]_- .$$

Using the fact that $\nabla\cdot\mathbf{B} = \nabla\times\mathbf{B} = 0$, this expression can be rewritten as

$$\frac{d\omega_-^{(-1)}}{dt} = \frac{i}{2B_0}\left[\frac{\partial B_z}{\partial z_0}\frac{dv_-^{(-1)}}{dt} + \left(\frac{\partial B_y}{\partial y_0} - \frac{\partial B_x}{\partial x_0} + 2i\frac{\partial B_x}{\partial y_0}\right)\frac{dv_+^{(-1)}}{dt}\right.$$

$$\left. -2\left(\frac{\partial B_z}{\partial x_0} - i\frac{\partial B_z}{\partial y_0}\right)\frac{dv_z^{(-1)}}{dt}\right],$$

where $v_\pm = v_x \pm iv_y$. However, Eq. (2.10) implies that only the term involving

$dv_-^{(-1)}/dt$ provides a resonant contribution at $O(\epsilon)$, so to this order we find

$$\frac{d\omega_-^{(-1)}}{dt} = \frac{1}{4B_0}\frac{\partial B_z}{\partial z_0}\cdot v_{\perp 0}\frac{d\delta\theta}{dt}e^{i\theta_0} + O(\epsilon^2).$$

Here an extra factor of $1/2$ appears because electron 1's velocity equals $\dot{\mathbf{R}} + \frac{1}{2}\dot{\mathbf{r}}$. Thus, to $O(\epsilon)$ only the slow time variation of the gyrophase contributes to C_+.

Substitution of this expression into Eq.(2.7), together with Eq.(2.8), leads to a simple form for the secular change in C_+ during a single collision

$$\Delta C_+ = \frac{1}{4(g-2)}\frac{r_L}{B_0}\frac{\partial B_z}{\partial z_0}\frac{e^{-i\theta'}}{\Omega_{c0}}\frac{e^2}{\mu}\int_{-\infty}^{\infty}\frac{z^2(t') - \frac{1}{2}\rho_0^2}{(z^2(t')+\rho_0^2)^{5/2}}e^{i\Omega_{c0}(g/2-1)t'}dt'$$

$$+O(\epsilon^2) + O\left((\frac{r_L}{L})^2\right) \tag{2.13}$$

where $\theta' = \theta_0 + \Omega_{c0}(\frac{g}{2}-1)t_1$, and $r_L = v_{\perp 0}/\Omega_{c0}$ is the initial relative Larmor radius. Here we have taken the limits of integration to $\pm\infty$ in order to determine the total change in C_+ after a single collision. Of course, this assumes that the plasma is weakly correlated so that two particle collisions are well-separated in time.

It is also useful to work with dimensionless distances and times, defining $\bar{t} = tv_z(t_1)/b$, $\bar{\rho} = \rho_0/b$ and $\bar{z} = z_0/b$. Then Eq.(2.13) becomes, after some simple algebra,

$$\Delta C_+ = \frac{1}{8(g-2)}\frac{r_L}{B_0}\frac{\partial B_z}{\partial z_0}e^{-i\theta'}\epsilon I[(\frac{g}{2}-1)/\epsilon, \bar{\rho}] \tag{2.14}$$

where the function $I(x,\bar{\rho})$ is defined by

$$I(x,\bar{\rho}) = \int_{-\infty}^{\infty}d\bar{t}e^{-ix\bar{t}}\frac{\bar{z}^2 - \bar{\rho}^2/2}{(\bar{\rho}^2+\bar{z}^2)^{5/2}} \tag{2.15}$$

and $\bar{z}(t)$ satisfies the differential equation [see Eq. (2.12)]

$$\dot{\bar{z}}^2 + \frac{1}{\sqrt{\bar{\rho}^2+\bar{z}^2}} = 1 \tag{2.16}$$

with initial conditions $z(t=-\infty)=-\infty$, $\dot{\bar{z}}(t=-\infty)=1$. We note that Eq.(2.16) can be analytically integrated and $\bar{t}$ can be expressed in terms of $\bar{z}$ through elliptic integrals (see Appendix 2B).

In a few special cases analytical forms for I can be obtained: For example,

$$I(x,\bar{\rho}) = -x^2 K_0(x\bar{\rho}) \quad \text{for} \bar{\rho} \gg 1$$

$$I(x,\bar{\rho}) = h(x,\bar{\rho}) e^{-xg(\bar{\rho})} \quad \text{for} x \gg 1 \tag{2.17}$$

where

$$g(\bar{\rho}) \equiv |\int_{\bar{\rho}}^{1} d\bar{x} \frac{\bar{x}^3/2}{\sqrt{\bar{x}^2-\bar{\rho}^2}\sqrt{1-\bar{x}}}|$$

and $h(x,\bar{\rho})$ is a function which is neither exponentially small nor exponentially large. For head-on collisions,

$$I(x,0) \simeq \frac{8\pi}{9} x e^{-\frac{\pi}{2}x} \quad \text{for} x \gg 1 \tag{2.18}$$

$$I(x,0) = \frac{8}{3} + x^2 \ln x + O(x^2) \text{for} x \ll 1 \tag{2.19}$$

However, for general values of x and $\bar{\rho}$, $I(x,\bar{\rho})$ must be determined numerically. The integral over $\bar{t}$ in the definition of I was performed by transformation of the integration variable from $\bar{t}$ to $\bar{z}$ via elliptic integral expressions of the guiding center orbit $\bar{t}(\bar{z})$ derived in Appendix 2B, and then the $\bar{z}$-integral was calculated using the SLATEC [7] subroutine DQAGSE.

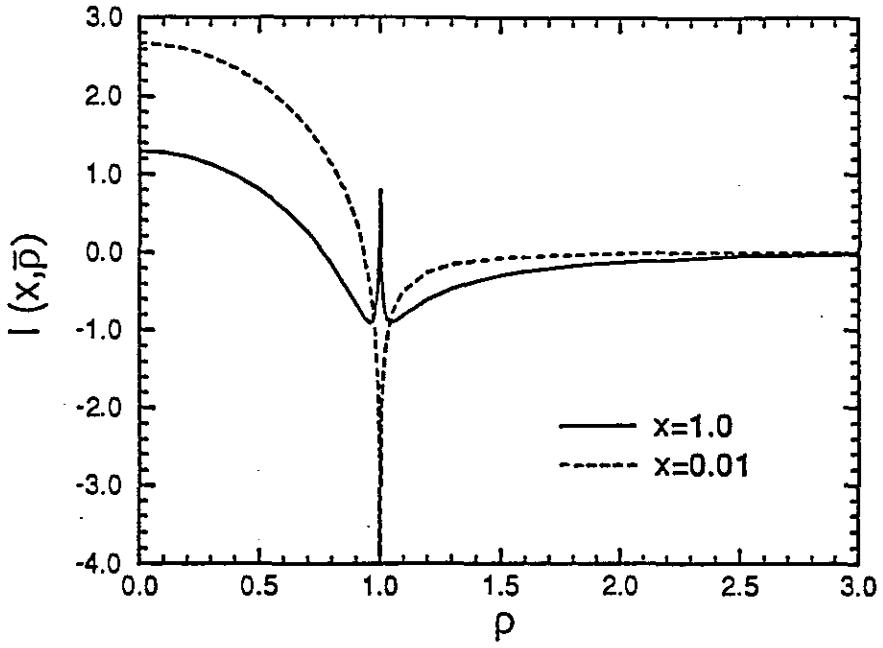

Figure 2.3: Plot of $I(x, \bar{\rho})$ as a function of $\bar{\rho}$ for different values of x. The behavior of $I(x, \bar{\rho})$ becomes singular at $\bar{\rho} = 1$, the separatrix point between passage and reflection of the two electrons. For $x = 0.01$, $I(x, 0) \simeq 8/3$ coincides with Eq.(2.19).

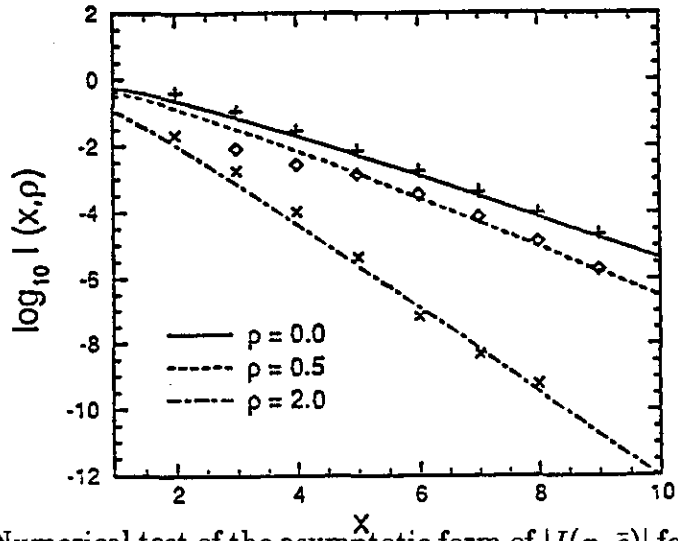

Figure 2.4: Numerical test of the asymptotic form of $|I(x, \bar{\rho})|$ for large x. The curves represent asymptotic values given by Eq.(2.17) and Eq.(2.18), where the function $h(x, \bar{\rho})$ is approximated by $h(x, 0) = \frac{8\pi}{9}x$.[3] This form works reasonably well even for values of ρ where I is negative. This is because the exponential dependence of I on x dominates the behavior for large x. The numerical results are denoted by $+$: $\bar{\rho} = 0$; $\diamond$: $\bar{\rho} = 0.5$ and $\times$: $\bar{\rho} = 2$.

The function $I(x, \bar{\rho})$ is plotted in Fig.(2.3) as a function of $\bar{\rho}$ for $x = 0.01$ and $x = 1$. The singular behavior at $\bar{\rho} = 1$ is due to the effectively infinite collision time at the separatrix for the electrons to pass by or reflect from each other. The behavior of $I(x, \bar{\rho})$ for large x is also plotted as a function of x for different impact parameters $\bar{\rho}$ in Fig.(2.4), where the numerical results are compared to the analytic expressions.

Equation (2.14) gives the probability amplitude for spin flip due to the classical electrostatic collision of two strongly-magnetized electrons in a weakly inhomogeneous magnetic field. By averaging over a Maxwellian distribution of electrons the average rate of spin flip can be obtained. This calculation is carried out in Section 2.5.

2.4 Quantum Analysis

In this section, the previous assumption of classical orbital motion is relaxed. For the strong magnetic fields and low temperatures of the experiments on cryogenic electron plasmas, the perpendicular mean thermal energy $kT_\perp$ can be as low as the spacing of the Landau levels $\hbar\Omega_c$, so quantum mechanics is necessary to describe the orbital motion. Moreover, since $kT_\perp$ is then also comparable with the energy difference $\hbar\Omega_p$ between spin up and down, a spin flip changes the orbital state of the electron appreciably. This spin-orbit energy exchange process is important for the plasma thermal equilibration, as will be seen in Section 2.5. Since the electron thermal de Broglie wavelength is small compared to the classical distance of closest approach, the antisymmetry of the two-electron wavefunction will be ignored as this approximation will only cause an exponentially small relative correction.

As in Section 2.3, we calculate the probability amplitude of a spin flip transition during the collision of two electrons in a spatially inhomogeneous magnetic

field. The collision is described by the two electron Hamiltonian

$$\hat{H} = \frac{(\mathbf{p}_1 + \frac{e}{c}\mathbf{A}_1)^2}{2m} + \mathbf{s}_1 \cdot \mathbf{\Omega}_p(\mathbf{x}_1) + \frac{(\mathbf{p}_2 + \frac{e}{c}\mathbf{A}_2)^2}{2m} + \mathbf{s}_2 \cdot \mathbf{\Omega}_p(\mathbf{x}_2) + \frac{e^2}{|\mathbf{x}_1 - \mathbf{x}_2|}.$$

We also follow Section 2.3 in assuming that $\mathbf{B}(\mathbf{x})$ varies slowly compared to the scale lengths associated with the electron-electron collision, and so we expand $\mathbf{B}$ to linear order about an arbitrary point: $\mathbf{B} = B_0\hat{z} + \mathbf{x} \cdot \nabla\mathbf{B}$, where $\mathbf{x}$ is measured with respect to this point. Although the eigenfunctions of $\hat{H}$ are not localized, through a judicious choice of the initial states of the colliding electrons, this arbitrary point will become the collision center $\mathbf{x}_0$ in the classical limit, so this expansion is justified on physical grounds. We will see that the expansion is justified mathematically by the convergence of the overlap integrals which couple the initial and final states through the magnetic perturbation.

In terms of the center of mass position $\mathbf{R} = \frac{1}{2}(\mathbf{x}_1 + \mathbf{x}_2)$ and the relative position $\mathbf{r} = \mathbf{x}_1 - \mathbf{x}_2$, to the first order in ∇B, the Hamiltonian expands out to the form $\hat{H} = \hat{H}_{cm} + \hat{H}_{rel} + \hat{H}_{spin} + \delta\hat{H}_{orbit} + \hat{H}_{sf}$ where

$$\hat{H}_{cm} = \frac{1}{2}m(\mathbf{P}_R - \frac{e}{c}\mathbf{R} \times \mathbf{B}_0)^2$$

$$\hat{H}_{rel} = \frac{1}{2\mu}(\mathbf{p} - \frac{e}{c}\mathbf{r} \times \mathbf{B}_0)^2 + \frac{e^2}{r}$$

$$\hat{H}_{spin} = (\mathbf{s}_1 + \mathbf{s}_2) \cdot \mathbf{\Omega}_{p0}$$

$$\delta\hat{H}_{orbit} = \frac{e}{mc}\delta\mathbf{A}(\mathbf{x}_1) \cdot (\mathbf{p}_1 - \frac{e}{2c}\mathbf{x}_1 \times \mathbf{B}_0) + \frac{e}{mc}\delta\mathbf{A}(\mathbf{x}_2) \cdot (\mathbf{p}_2 - \frac{e}{2c}\mathbf{x}_2 \times \mathbf{B}_0)$$

and

$$\hat{H}_{sf} = (\mathbf{s}_1 + \mathbf{s}_2) \cdot (\mathbf{R} \cdot \nabla)\mathbf{\Omega}_{p0} + \frac{1}{2}(\mathbf{s}_1 - \mathbf{s}_2) \cdot (\mathbf{r} \cdot \nabla)\mathbf{\Omega}_{p0}.$$

Here, $\mathbf{\Omega}_{p0} \equiv \frac{g}{2}\Omega_{c0} = \frac{g}{2}\frac{eB_0}{mc}$, $\mathbf{P}_R = -i\hbar\frac{\partial}{\partial \mathbf{R}}$, and $\mathbf{p} = -i\hbar\frac{\partial}{\partial \mathbf{r}}$ are the momentum operators of the center of mass and relative motion respectively. The function $\delta\mathbf{A}(\mathbf{x}) = \mathbf{A}(\mathbf{x}) - \frac{1}{2}\mathbf{B}_0 \times \mathbf{x}$ is the correction to the vector potential due to the spatial variation in $\mathbf{B}(\mathbf{x})$.

Since the spin and orbital dynamics decouple in $\hat{H}_{cm}$, $\hat{H}_{rel}$, $\hat{H}_{spin}$ and $\delta\hat{H}_{orbit}$, these Hamiltonians are not responsible for the spin flip transition. The spin flip transition is due only to $\hat{H}_{sf}$. According to Fermi's "golden rule", the probability per unit time of a transition from state $|i>$ to state $|f>$ is given by

$$a_i^f = \frac{2\pi}{\hbar}\rho_f |< f|H_{sf}|i >|^2. \tag{2.20}$$

Here, $|i>$ and $|f>$ are the eigenstates of $\hat{H}_{cm} + \hat{H}_{rel} + \hat{H}_{spin} + \delta\hat{H}_{orbit}$, ρ_f is the density of the final states and the transition conserves the total spin and orbital energy.

Before beginning the calculation of the transition rate, we note that the spin flip Hamiltonian $\hat{H}_{sf}$ can be rewritten as

$$\begin{aligned}\hat{H}_{sf} &= X\partial_x\mathbf{\Omega}_{p0}\cdot(\mathbf{s}_1+\mathbf{s}_2) + Y\partial_y\mathbf{\Omega}_{p0}\cdot(\mathbf{s}_1+\mathbf{s}_2) + Z\partial_z\mathbf{\Omega}_{p0}\cdot(\mathbf{s}_1+\mathbf{s}_2) \\ &+ \frac{x}{2}\partial_x\mathbf{\Omega}_{p0}\cdot(\mathbf{s}_1-\mathbf{s}_2) + \frac{y}{2}\partial_y\mathbf{\Omega}_{p0}\cdot(\mathbf{s}_1-\mathbf{s}_2) + \frac{z}{2}\partial_z\mathbf{\Omega}_{p0}\cdot(\mathbf{s}_1-\mathbf{s}_2)\end{aligned}$$

where (X, Y, Z) and (x, y, z) are center of mass and relative coordinates respectively. To calculate the transition rate to the leading order of ∇B, we use for the states $|i>$ and $|f>$ the states of colliding electrons in a uniform field $\mathbf{B}_0$, i.e. the eigenstates of $\hat{H}_{cm} + \hat{H}_{rel} + \hat{H}_{spin}$ (in the absence of $\delta\hat{H}_{orbit}$), since $\delta\hat{H}_{orbit}$ is of order ∇B.

Several simplifications of H_{sf} can now be made. First we note that the operators $\hat{s}_1$ and $\hat{s}_2$ are linearly combined in $\hat{H}_{sf}$, so only one spin can be flipped in the transition. This implies that a spin flip transition always involves a spin energy

change of magnitude $\hbar\Omega_{p0}$. Now, the first two terms of $\hat{H}_{sf}$ couple the spin and the center of mass motion. However, this motion is described by $\hat{H}_{cm}$, which has well-known harmonic-oscillator eigenstates with energies separated by $\hbar\Omega_{c0}$ for the $X-Y$ motion, and free streaming for the z motion. Since $\hbar\Omega_{p0} = \hbar\Omega_{c0}$ and the parallel electron states are unchanged, energy conservation forbids a spin flip transition so the first two terms of $\hat{H}_{sf}$ may be neglected.

The third and sixth terms in $\hat{H}_{sf}$ can be neglected for a similar reason. These terms couple the spin and parallel dynamics, so during a spin-flip transition energy conservation requires a parallel energy change of magnitude $\hbar\Omega_{p0}$. However, in the strongly-magnetized regime this is a large change; the initial and final parallel states would have extremely disparate wavenumbers, leading to an exponentially small contribution to the overlap integrals appearing in the golden rule, Eq. (2.20). There then remains only the resonant interaction between the relative (x, y) dynamics and the spin, which involves the fourth and fifth terms in $\hat{H}_{sf}$:

$$
\begin{aligned}
& [\frac{x}{2}\partial_x \mathbf{\Omega}_{p0} + \frac{y}{2}\partial_y \mathbf{\Omega}_{p0}] \cdot (\mathbf{s}_1 - \mathbf{s}_2) \\
= \; & \frac{eg}{2mc}\frac{\rho}{8}\left\{\left[-\frac{\partial B_z}{\partial z_0}e^{-i\theta} + (\frac{\partial B_x}{\partial x_0} - \frac{\partial B_y}{\partial y_0} - 2i\frac{\partial B_y}{\partial x_0}) \cdot e^{i\theta}\right]\hat{s}^{(+)}\right. \\
+ \; & \left. 2(\frac{\partial B_z}{\partial x_0} - i\frac{\partial B_z}{\partial y_0})(\hat{s}_{1z} - \hat{s}_{2z})\right\} + (\text{hermitian conjugate})
\end{aligned}
$$

On the right hand side we have written (x, y) in terms of polar coordinates (ρ, θ) and we have introduced the spin creation and annihilation operators $\hat{s}^+$ and $\hat{s}^-$, where $s^{(\pm)} = \hat{s}_{1x} - \hat{s}_{2x} \pm i(\hat{s}_{1y} - \hat{s}_{2y})$. The term involving $\hat{s}_{1z} - \hat{s}_{2z}$ cannot induce transitions between different spin states and so can be neglected. Thus, the effective spin flip

Hamiltonian is

$$\hat{H}_{sf} = \frac{eg}{2mc}\frac{\rho}{8}\left\{-\frac{\partial B_z}{\partial z_0}e^{-i\theta} + (\frac{\partial B_x}{\partial x_0} - \frac{\partial B_y}{\partial y_0} - 2i\frac{\partial B_y}{\partial x_0})e^{i\theta}\right\}\hat{s}^{(+)}$$

$$+ \text{ hermitian conjugate} \qquad (2.21)$$

It can easily be verified that the term proportional to $\partial B_z/\partial z_0$ commutes with the operator $\hat{s}_z - i\hbar\partial/\partial\theta$, so this term conserves total angular momentum in the z-direction. However, the other term is proportional to field gradients expressing the cylindrical asymmetry of the external field and so it is not surprising that this term does not conserve total angular momentum. This difference will have important ramifications when we employ Eq. (2.21) in the calculation of Fermi's "golden rule," Eq. (2.20).

However, before we can apply the golden rule to Eq. (2.21) we will require expressions for the initial and final states which are the eigenstates of $\hat{H}_{cm} + \hat{H}_{rel} + \hat{H}_{spin}$. These states can be expressed as the product $\psi_{cm}(\mathbf{R})\psi_{rel}(\mathbf{r})|s_{1z}, s_{2z}>$, where $\psi_{cm}(\mathbf{R})$, $\psi_{rel}(\mathbf{r})$, and $|s_{1z}, s_{2z}>$ are eigenstates of $\hat{H}_{cm}$, $\hat{H}_{rel}$, and $\hat{H}_{spin}$ respectively. Since the center of mass dynamics does not appear and the spin eigenstates are trivial, it remains only to find ψ_{rel}. We therefore calculate ψ_{rel} for two colliding electrons using a quantum version of the classical guiding-center expansion[3] The expansion is most easily derived by first expressing the relative Hamiltonian in terms of cylindrical coordinates:

$$\hat{H}_{rel} = \frac{-\hbar^2}{2\mu}\left(\frac{1}{\rho}\frac{\partial}{\partial\rho}(\rho\frac{\partial}{\partial\rho}) + \frac{1}{\rho^2}\frac{\partial^2}{\partial\theta^2} + \frac{\partial^2}{\partial z^2}\right) + \frac{\hbar\Omega_{c0}}{2i}\frac{\partial}{\partial\theta} + \frac{\mu\Omega_{c0}}{8}\rho^2 + \frac{e^2}{\sqrt{\rho^2+z^2}}.$$

Since $\hat{H}_{rel}$ is θ-independent, the z component of the angular momentum $L_z = l\hbar$ is conserved and we look for eigenstates of the form $\frac{e^{il\theta}}{\sqrt{2\pi}}\psi_{l\alpha}(\rho, z)/\sqrt{\rho}$, where α denotes the two quantum numbers associated with dynamics in ρ and z. Replacing $\frac{\partial}{\partial\theta}$ by il

in $\hat{H}_{rel}$ yields the reduced Hamiltonian for $\psi_{l\alpha}(\rho, z)$:

$$\hat{H}_{rel} = \frac{-\hbar^2}{2\mu}\frac{\partial^2}{\partial z^2} - \frac{\hbar^2}{2\mu}\frac{\partial^2}{\partial \rho^2} + \frac{\mu {\Omega_{c0}}^2}{8\rho^2}(\rho^2 - \rho_l^2)^2 - \frac{\hbar^2}{8\mu}\frac{1}{\rho^2} + \frac{e^2}{\sqrt{\rho^2 + z^2}}$$

where $\rho_l^2 = -2\hbar l/\mu\Omega_{c0}$.

We will see that the main contribution to the integral expression for the spin flip rate comes from wavefunctions with ρ_l such that $r_{qL} \ll \rho_l \leq b$, where $r_{qL} \equiv \sqrt{2\nu\hbar/\mu\Omega_{c0}}$ is the quantum Larmor radius, ν is the quantum number of cyclotron motion, and b is the classical distance of closest approach. Physically, $\rho = \rho_l$ corresponds to the impact parameter of the guiding center of a reduced mass electron incident on the force center. The wavefunction $\psi_{l\alpha}(\rho, z)$ is peaked near $\rho \simeq \rho_l$, at the minimum point of the centrifugal potential of $\hat{H}_{rel,l}$, and $\psi_{l\alpha}(\rho, z)$ falls off rapidly in a distance of order the cyclotron radius $r_{qL} \ll \rho_l$. It is therefore useful to introduce the variable $x_l \equiv \rho - \rho_l$ in the relative Hamiltonian. Expansion of $\hat{H}_{rel}$ to second order in r_{qL}/ρ_l then yields

$$\hat{H}_{rel} = H_l^{(0)} + \hat{H}^{(1)} + \hat{H}^{(2)} + O\left(\frac{r_{qL}}{\rho_l}\right)^3, \tag{2.22}$$

where

$$\hat{H}_l^{(0)}(x_l, z) = \frac{-\hbar^2}{2\mu}\frac{\partial^2}{\partial z^2} + \frac{e^2}{\sqrt{\rho_l^2 + z^2}} - \frac{\hbar^2}{2\mu}\frac{\partial^2}{\partial x_l^2} + \frac{1}{2}\mu {\Omega_{c0}}^2 x_l^2,$$

$$\hat{H}^{(1)}(x_l, z) = -\frac{1}{2}\mu\Omega_{c_0}^2\frac{x_l^3}{\rho_l} + g(z)x_l,$$

$$\hat{H}^{(2)}(x_l, z) = \frac{5}{8}\mu\Omega_{c_0}^2 x_l^2(\frac{x_l}{\rho_l})^2 + f(z)x_l^2 - \frac{\hbar^2}{8\mu\rho_l^2},$$

and the functions f and g arise from Taylor expansion of the Coulomb potential,

and are defined by

$$f(z) \equiv \frac{e^2(\rho_l^2 - z^2/2)}{(\rho_l^2 + z^2)^{5/2}},$$

and

$$g(z) \equiv -\frac{e^2\rho_l}{(\rho_l^2 + z^2)^{3/2}}.$$

Each term $\hat{H}^{(n)}$ in this expansion has magnitude of order $\hbar\Omega_{c0}(\frac{r_{qL}}{\rho_l})^n$ since x_l is of order r_{qL}. Furthermore, it is clear that eigenfunctions of $\hat{H}_{rel}$ are, in the position representation, functions of ρ through the variable x_l:

$$\psi_{l\alpha}(\rho, z) = \bar{\psi}_{l\alpha}(x_l, z), \tag{2.23}$$

where $\psi bar_{l\alpha}$ is the eigenfunction of the Hamiltonian of Eq. (2.22), and α denotes the two quantum numbers which, along with l, parametrize the state. In this form, $\hat{H}_{rel}$ is a perturbed harmonic oscillator Hamiltonian in the variable x_l, so $\bar{\psi}_{l\alpha}(x, z)$ is highly peaked around $x = 0$.

The unperturbed Hamiltonian $H_l^{(0)}(x_l, z)$ has eigenstates $|l, \alpha > (0)$ which we write in the position representation as $|l, \alpha > (0) = G_\nu(x_l)F_{l\kappa}(z)$. Here, $G_\nu(x)$ is a harmonic oscillator eigenfunction with eigenenergy $(\nu + \frac{1}{2})\hbar\Omega_{c0}$, and $F_{l\kappa}(z)$ is the eigenfunction of the parallel dynamics, with energy κ. Thus, α can be represented by the values of ν and κ. The total energy of an eigenstate of $H_l^{(0)}$ is denoted by E_α and is given by $E_\alpha = (\nu + \frac{1}{2})\hbar\Omega_{c0} + \kappa$. (Although E_α is also a function of l through the dependence of κ on l, we drop this subscript in order to save space.)

Taking $|l, \alpha > (0)$ as the base vector and using second order perturbation theory, we obtain a perturbation expansion for $|l, \alpha >$:

$$|l, \alpha >= (1 - \frac{d_\alpha}{2})|l, \alpha >^{(0)} + \sum_{\alpha'}(a_{\alpha\alpha'} + b_{\alpha\alpha'} + c_{\alpha\alpha'})|l, \alpha >^{(0)} + O(\frac{r_{qL}}{\rho_l})^3 \tag{2.24}$$

where

$$a_{\alpha\alpha'} = H^{(1)}_{\alpha\alpha'}/(E_\alpha - E_{\alpha'})$$

$$b_{\alpha\alpha'} = H^{(2)}_{\alpha\alpha'}/(E_\alpha - E_{\alpha'})$$

$$c_{\alpha\alpha'} = \sum_{\alpha_1} H^{(1)}_{\alpha'\alpha_1} H^{(1)}_{\alpha_1\alpha}/(E_\alpha - E_{\alpha'})(E_\alpha - E_{\alpha_1})$$

$$d_\alpha = \sum_{\alpha_1} |H^{(1)}_{\alpha\alpha_1}|^2/(E_\alpha - E_{\alpha_1})$$

and where we employ the notation $H_{\alpha\alpha'}$ to denote the matrix element $^{(0)} < l\alpha|H|l\alpha >^{(0)}$.

However, to calculate the transition matrix element of Eq. (2.20), we will also require an expression for $|l \pm 1, \alpha >$. Although this expression can in principle be obtained from Eq.(2.23) by substitution of $l \pm 1$ for l, it is more convenient to determine $|l \pm 1, \alpha >$ in terms of $|l, \alpha >^{(0)}$ rather than $|l \pm 1, \alpha >^{(0)}$. The ket $|l \pm 1, \alpha >^{(0)}$ is the eigenstate of $\hat{H}^{(0)}_{l\pm1}$, which is related to $\hat{H}^{(0)}_l$ through a Taylor expansion of ρ_l:

$$\hat{H}^{(0)}_{l\pm1}(x,z) = \hat{H}^{(0)}_l(x,z) \mp \frac{\hbar}{\mu\Omega_{c0}} \frac{e^2}{(\rho_l^2 + z^2)^{3/2}} + O(\frac{r_{qL}}{\rho_l})^3$$

Taking the term $\mp \frac{\hbar}{\mu\Omega_{c0}} \frac{e^2}{(\rho_l^2 + z^2)^{3/2}}$ as the perturbation, we find that in the position representation the kets are related by

$$\bar{\psi}^{(0)}_{l\pm1,\alpha}(x,z) = \bar{\psi}^{(0)}_{l,\alpha}(x,z) \mp \sum_{\alpha'} h_{\alpha\alpha'} \bar{\psi}^{(0)}_{l,\alpha'}(x,z) \tag{2.25}$$

where

$$h_{\alpha\alpha'} = \left(\frac{-\hbar}{\mu\Omega_{c0}} \frac{e^2}{(\rho_l^2 + z^2)^{3/2}} \right)_{\alpha\alpha'} /(E_\alpha - E_{\alpha'}). \tag{2.26}$$

Substituting Eq. (2.25) in Eq. (2.24) with l replaced by $l \pm 1$ yields

$$\bar{\psi}_{l\pm1,\alpha}(x,z) = \bar{\psi}_{l\alpha}(x,z) \mp \sum_{\alpha'} h_{\alpha\alpha'} \bar{\psi}^{(0)}_{l,\alpha'}(x,z) + O(\frac{r_{qL}}{\rho_l})^3. \tag{2.27}$$

We now evaluate the transition matrix element $< f|H_{sf}|i >$. Without loss of generality, we take the initial state to be

$$|i >= \frac{e^{il\theta}}{\sqrt{2\pi}} \frac{1}{\sqrt{\rho}} \bar{\psi}_{l,\alpha}(x_l, z)|-\frac{\hbar}{2}, \frac{\hbar}{2}>, \tag{2.28}$$

and the final state to be

$$|f >= \frac{e^{il_f\theta}}{\sqrt{2\pi}} \frac{1}{\sqrt{\rho}} \bar{\psi}_{l_f\alpha_f}(x_{l_f}, z)|\frac{\hbar}{2}, \frac{\hbar}{2}>, \tag{2.29}$$

so that during the transition spin 1 is flipped from down to up. Energy conservation at zeroth order in r_{qL}/ρ_l requires that

$$(\nu + \frac{1}{2})\hbar\Omega_{c0} - \frac{\hbar}{2}\Omega_{p0} + \kappa = (\nu_f + \frac{1}{2})\hbar\Omega_{c0} + \frac{\hbar}{2}\Omega_{p0} + \kappa_f.$$

Then the zeroth order parallel energy change is $\kappa_f - \kappa = (\nu - \nu_f)\hbar\Omega_{c0} - \hbar\Omega_{p0} = (\nu - \nu_f - \frac{g}{2})\hbar\Omega_{c0}$. As discussed at the beginning of this section, since the z motion is very slow compared with spin precession at frequency Ω_{p0}, by far the largest contribution to the transition comes from $\nu_f = \nu - 1$; then $|(\kappa_f - \kappa)/\hbar| = \Omega_{p0} - \Omega_{c0} = (\frac{g}{2} - 1)\Omega_{c0} \ll \Omega_{p0}$. That is, while the spin is excited from down to up, the orbital perpendicular motion provides one quantum of energy $\hbar\Omega_{c0}$ to the spin, and since $\hbar\Omega_{p0} = \hbar\Omega_{c0}$ the spin also absorbs energy $\hbar(\Omega_{p0} - \Omega_{c0})$ from the parallel motion. Thus, the orbital state jumps to a lower energy state with new quantum numbers (ν_f, κ_f, l_f). Since a spin flip from down to up is induced by the spin creation operator $\hat{s}^{(+)}$ in $\hat{H}_{sf}$, from Eq. (2.21) we have

$$< f|\hat{H}_{sf}|i >= \frac{\hbar}{8}\frac{eg}{2mc}\left\{-\frac{\partial B_z}{\partial z_0}\int_{-\infty}^{+\infty} dz \int_0^{\infty} d\rho \psi^*_{l-1,\alpha_f}(\rho, z)\rho\psi_{l\alpha}(\rho, z)\right.$$

$$+ \quad (\frac{\partial B_x}{\partial x_0} - \frac{\partial B_y}{\partial y_0} - 2i\frac{\partial B_y}{\partial x_0}) \int_{-\infty}^{+\infty} dz \int_0^{\infty} d\rho \psi^*_{l+1,\alpha_f}(\rho, z)\rho\psi_{l\alpha}(\rho, z)\Big\} \qquad (2.30)$$

where $l_f = l \pm 1$ is a result of the integral over θ, and the matrix element $< \frac{\hbar}{2}, \frac{\hbar}{2}|\hat{s}^{(+)}|- \frac{\hbar}{2}, \frac{\hbar}{2} >= \hbar$ has been used.

The inner products appearing here can be evaluated in the quantum guiding center approximation by changing integration variables from ρ to x_l. The required integrals are

$$\begin{aligned} M_\pm &= \int_{-\infty}^{+\infty} dz \int_0^{\infty} d\rho \psi^*_{l\pm1,\alpha_f}(\rho, z)\rho\psi_{l\alpha}(\rho, z) \\ &= \int_{-\infty}^{+\infty} dz \int_{-\infty}^{+\infty} dx_l \bar{\psi}^*_{l\pm1,\alpha_f}(x_{l\pm1}, z)(\rho_l + x_l)\bar{\psi}_{l\alpha}(x_l, z), \end{aligned}$$

where the integration range in x_l is extended to $\pm\infty$ because $\bar{\psi}_{l\alpha}(x, z)$ is highly peaked around $x = 0$. The first argument of the barred wavefunctions appearing in $M_\pm$ are evaluated at different positions, $x_{l\pm1}$ and x_l. However, these positions are related through the equation

$$x_{l\pm1} - x_l = \rho_l - \rho_{l\pm1} = \pm\frac{\hbar}{\mu\Omega_{c0}\rho_l}.$$

In order to simplify the evaluation of the integrals we then Taylor expand $\psi_{l\pm1,\alpha_f}(x_{l\pm1}, z)$ around x_l:

$$\bar{\psi}_{l\pm1,\alpha_f}(x_{l\pm1}, z) = \left(1 \pm \frac{i\hat{P}_l}{\mu\Omega_{c0}\rho_l} - \frac{\hat{P}_l^2}{2(\mu\Omega_{c0}\rho_l)^2} + O(\frac{r_{qL}}{\rho_l})^3\right) \bar{\psi}_{l\pm1,\alpha_f}(x_l, z)$$

where $\hat{P}_l = -i\hbar\partial/\partial x_l$ is the momentum operator. Then to second order in r_{qL}/ρ_l, $M_\pm$ is given by

$$M_\pm = \rho_l < l \pm 1, \alpha_f|1 - \frac{\hat{P}_l^2}{2(\mu\Omega_{c0}\rho_l)^2}|l\alpha >$$

$$+ \quad < l \pm 1, \alpha_f | x_l \pm \frac{i\hat{P}_l}{\mu\Omega_{c0}} | l\alpha > + O(\frac{r_{qL}}{\rho_l})^3, \tag{2.31}$$

where the inner products denote integrals with respect to z and x_l of barred wavefunctions evaluated at the same point; for example,

$$< l'\alpha' | l\alpha > \equiv \int_{-\infty}^{\infty} dz dx \bar{\psi}_{l'\alpha'}(x,z) \bar{\psi}_{l\alpha}(x,z).$$

Equation (2.31) can be further simplified since some of the terms are negligible. For example,

$$\begin{aligned} < l-1, \alpha_f | l\alpha > &= < l\alpha_f | l\alpha > + \sum_{\alpha'} h_{\alpha_f \alpha'} < l\alpha' | l\alpha > + O(\frac{r_{qL}}{\rho_l})^3 \\ &= h_{\alpha_f \alpha} + O(\frac{r_{qL}}{\rho_l})^3 \end{aligned}$$

Where Eq. (2.25) has been employed, and in the second line we have used the orthogonality of $|l\alpha>$ and $|l\alpha'>$ together with the selection rule $\nu_f = \nu - 1$. However, Eq. (2.26) implies that $h_{\alpha\alpha'}$ is proportional to $\delta_{\nu\nu'}$ so $< l-1, \alpha_f | l\alpha > \sim O(r_{qL}/\rho_l)^3$ and may be neglected. Similarly, one can also show that

$$< l-1, \alpha_f | \frac{\hat{P}_l^2}{2(\mu\Omega_{c0}\rho_l)^2} | l\alpha > O(\frac{r_{qL}}{\rho_l})^3$$

so we neglect this term's contribution to Eq. (2.31) as well. Combining Eq. (2.30) and Eq. (2.31) then yields a simple result for the spin-flip transition matrix element:

$$< f | H_{sf} | i > = -\frac{\hbar r_{qL}}{8\sqrt{\nu}} \frac{eg}{2mc} \cdot$$

$$\cdot \begin{cases} \frac{\partial B_x}{\partial z_0} < l_f \alpha_f | \hat{a} | l\alpha >, & l_f = l-1 \\ (\frac{\partial B_x}{\partial x_0} - \frac{\partial B_y}{\partial y_0} - 2i\frac{\partial B_y}{\partial x_0}) < l_f \alpha_f | \hat{a}^+ | l\alpha >, & l_f = l+1 \end{cases} \tag{2.32}$$

where $\hat{a}^+$ and $\hat{a}$ are the creation and annihilation operators for cyclotron quanta:

$\hat{a} \equiv \sqrt{\mu\Omega_{c0}/2\hbar}(x_l + i\hat{P}_l/\mu\Omega_{c0})$. This form for $< f|H_{sf}|i >$ has a clear physical interpretation. The case $l_f = l - 1$ corresponds to the transition dynamics we have already described. As one of the electron spin flips from down to up, a relative cyclotron quantum is annihilated by $\hat{a}$ and the z-component of the relative orbital angular momentum, $\hbar l$, is reduced by one unit, conserving the sum of the spin and orbital angular momentum. However, in the second case, $l_f = l + 1$, and the sum of the spin and orbital angular momentum is increased by two units because the transition occurs in a nonuniform external magnetic field with a cylindrical asymmetry described by the combination of gradients preceding the matrix element. In this case a quantum of cyclotron action is created by $\hat{a}^+$, but does not go into cyclotron dynamics, since ν_f must equal $\nu - 1$ in order to conserve energy. Instead, two cyclotron quanta are distributed into energy and canonical angular momentum associated with a change in the relative radial guiding center position, so that the final state still has one fewer quantum in the cyclotron motion. This interpretation follows from the fact that the radial guiding center position, i.e., the position of the peak of $\psi_{l\alpha}$ in ρ, is characterized by the combination $\nu - l$[8] so the guiding centers end up farther apart by a distance of order r_{qL}. However, since the guiding center motion is relatively slowly varying compared to the cyclotron dynamics, we would expect that such a process is off-resonance and so it should give a negligible contribution to the transition probability.

The guiding center expansion for $\bar{\psi}_{l\alpha}(x, z)$, Eq. (2.24), can now be employed in order to explicitly calculate the matrix elements up to $O(r_{qL}/\rho_l)^2$. This lengthy algebraic exercise is left to Appendix 2A. We find that the case $l_f = l + 1$ does not contribute, as expected. The other case, $l_f = l - 1$, is given by Eq. (2.54), and leads

to a relatively simple form for the transition matrix element:

$$< f|H_{sf}|i >= \frac{\partial B_z}{\partial z_0}\frac{e^3\hbar r_{qL}}{8\mu^2 c\Omega_{c_0}^2(g-2)}\left(\int dz \frac{F_{\kappa_f}^{(l)*}(z)(z^2-\rho_l^2/2)F_{\kappa}^{(l)}(z)}{(\rho_l^2+z^2)^{5/2}}\right). \qquad (2.33)$$

As discussed in Appendix 2A, this expression neglects terms of order $(r_{qL}/\rho_l)^3$ and higher.

Equation (2.33) is the transition matrix element for the spin of electron 1 to flip from down to up, which upon substitution into Eq. (2.20) yields the transition probability per unit time a_i^f. However, in the Boltzmann analysis of the next section, rather than a_i^f we need P_i^f, the transition probability per collision given by $a_i^f J_\kappa^{-1}$, where J_κ is the incident flux associated with the initial relative wavefunction of parallel energy κ. To calculate J_κ and the density of final states ρ_f of Eq. (2.20), we impose periodic boundary conditions at $z = \pm L (L \gg \rho_l)$[3] One finds that $\rho_f = \frac{L}{\pi\hbar v_z(\kappa_f)}$ and $J_\kappa = \frac{v_z(\kappa)}{2L}$, where $\frac{\mu}{2}v_z^2(\kappa) \equiv \kappa$, and the incident (initial) state and outgoing (final) state are taken to be $|i>$ of Eq. (2.28) and $|f>$ of Eq. (2.29). Finally, we have $P_i^f = |\Delta C_+|^2$, where

$$|\Delta C_+| = \frac{|\partial B_z/\partial z_0|}{\Omega_{c_0}^2}\frac{e^3 r_{qL}}{8\mu^2 c(g-2)}\frac{2L}{\sqrt{v_z(\kappa)v_z(\kappa_f)}}$$

$$\left| \int dz \frac{F_{\kappa_f}^{(l)*}(z)(z^2-\rho_l^2/2)F_{\kappa}^{(l)}(z)}{(\rho_l^2+z^2)^{5/2}}\right| \qquad (2.34)$$

Since the parallel thermal de Broglie wavelength is much smaller than the distance of closest approach a WKB solution for $F_\kappa^{(l)}(z)$ is valid. Then if we further assume that $\kappa \sim kT_{||} \gg (\frac{g}{2}-1)\hbar\Omega_{c0} = 10^{-3}\hbar\Omega_{c0}$, a quasi-classical expansion of the WKB wavefunction can be carried out, and the z integral can be transformed into a

time-history integral over the classical orbit[3]

$$\frac{2L}{\sqrt{v_z(\kappa)v_z(\kappa_f)}}\int_{-L}^{L}dz\frac{F_{\kappa_f}^{(l)^*}(z)(z^2-\rho_l^2/2)F_{\kappa}^{(f)}(z)}{(\rho_l^2+z^2)^{5/2}}$$

$$=\int dt\frac{z^2-\rho_l^2/2}{(\rho_l^2+z^2)^{5/2}}e^{-i(g/2-1)\Omega_{c0}t}. \tag{2.35}$$

In Eq. (2.35) the limit $\pm L$ has been extended to $\pm\infty$ since $L \gg \rho_l$, and $z(t)$ is given by Eq. (2.16).

Substitution of Eq. (2.35) into Eq. (2.34) then yields the final form for the transition amplitude in the quantum regime:

$$|\Delta C_+| = \frac{|\partial B_z/\partial z_0|}{\Omega_{c_0}^2}\frac{e^3 r_{qL}}{8\mu^2 c(g-2)}\left|\int dt e^{-i(g/2-1)\Omega_{c0}t}\frac{z^2-\rho_l^2/2}{(\rho_l^2+z^2)^{5/2}}\right|. \tag{2.36}$$

For large quantum number ν, Eq. (2.36) returns to the classical result of Eq. (2.13) because r_{qL} approaches the classical Larmor radius r_L, as may be seen by the energy correspondence

$$\frac{1}{2}\mu r_L^2\Omega_{c0}^2 = (\nu+\frac{1}{2})\hbar\Omega_{c0} \simeq \nu\hbar\Omega_{c0}.$$

2.5 Boltzmann Analysis for the Spin Temperature Equilibration Rate

In this section a collision operator is derived for spin relaxation due to electron-electron collisions in an inhomogeneous magnetic field. The plasma is assumed to be weakly correlated and the effective spin flip interaction only occurs over a short range of order b, so only two-particle interactions are important and these collisions can be regarded as point collisions. We therefore use the Boltzmann equation to describe the spin relaxation process. Since the electron de Broglie wavelength

is small compared to the average interparticle distance, classical Boltzmann statistics rather than the quantum Fermi statistics will be used throughout the calculation.

We first focus on the spin temperature relaxation problem for the classical electron motion discussed in Chapter (2.3). In this case, the kinetic temperatures $T_\perp$ and $T_\parallel$ are large compared to $\hbar\Omega_p$, and so the kinetic energy of the electrons behaves like an infinite temperature heat reservoir supplying energy to excite the spin motion. For this classical case the orbital state of the electron is not affected by the spin flip though the spin flip probability is determined by the orbital motion, so the spin flip transitions from $|+>$ to $|->$ and from $|->$ to $|+>$ have equal probability. Therefore, we may immediately write down the time rate of change of the spin population due to collisions:

$$\left(\frac{d}{dt}x_-\right)_{coll} = \nu_{spin}(\mathbf{x})(x_+ - x_-) \tag{2.37}$$

where $x_\pm$ is the concentration of electrons with spin state $|+>$ or $|->$ in a volume element at position $\mathbf{x}$, where the size of the mathematically infinitesimal volume is physically large compared with the average inter-particle distance but small compared with the scale length of the magnetic field inhomogeneity. The spin depolarization rate is given by

$$\nu_{spin} = \int d^3\mathbf{v} f(v_\perp, v_z) \int 2\pi\rho_0 d\rho_0 n|v_z||\Delta C|^2 \tag{2.38}$$

Here $|\Delta C|$ is given by Eq. (2.14) and $f(v_\perp, v_z)$ is the two-temperature Maxwellian distribution function. A two-temperature Maxwellian distribution is employed since the perpendicular kinetic energy is an adiabatic invariant and so electron-electron collisions drive the velocity distribution to the two-temperature Maxwellian form on a fast time scale on the order of the electron-electron collision frequency[6]

Directly substituting Eq. (2.14) for $|\Delta C|$ in Eq. (2.38) and performing the

integrals over $\mathbf{v}_\perp$, one obtains

$$\nu_{spin}(\mathbf{x}) = \left(\frac{\bar{r}_L(\mathbf{x})}{8(g-2)L(\mathbf{x})}\right)^2 n\sqrt{\frac{\mu}{2\pi kT_{||}}} \cdot \int dv_z exp\left(\frac{-\mu v_z^2}{2kT_{||}}\right)|v_z| \cdot$$

$$\epsilon^2 \cdot \int 2\pi\rho_0 d\rho_0 |I((\frac{g}{2}-1)\epsilon^{-1}, \bar{\rho})|^2$$

where I is the integral given by Eq. (2.15), and where $\bar{r}_L(\mathbf{x}) = \sqrt{2kT_\perp/\mu}/\Omega_{c0}(\mathbf{x})$ is the Larmor radius and $L(\mathbf{x}) = (\frac{1}{B_0}\frac{\partial B_z}{\partial z_0})^{-1}$ is the scale length of the magnetic field inhomogeneity.

Furthermore, Eq. (2.37) implies a simple form for the time evolution equation for the local spin temperature $T_s(\mathbf{x})$, which is defined by $\frac{1}{T_s} = (\frac{\partial S}{\partial E})_N = \frac{1}{\hbar\Omega_{p0}} \ln\frac{x_-}{x_+}$, where S, E are the entropy and energy of the spin system:

$$\frac{\dot{T}_s(\mathbf{x})}{T_s} = \frac{2kT_s}{\hbar\Omega_{p0}} \sinh(\frac{\hbar\Omega_{p0}}{kT_s})\nu_{spin} \tag{2.39}$$

where

$$\nu_{spin} = 2.5 \times 10^2 \nu_c \left(\frac{\bar{\epsilon}\bar{r}_L}{L}\right)^2 \eta(\bar{\epsilon}) \tag{2.40}$$

Here $\nu_c = \pi\bar{b}^2 n\bar{v}_z$ is the electron-electron collision frequency, $(g-2)$ is taken to be approximately 0.0023 and $\eta(\bar{\epsilon})$ is given by

$$\eta(\bar{\epsilon}) = \int_0^\infty du u^{1/3} exp(-\frac{1}{2}u^2/3) \int_0^\infty d\bar{\rho} 2\pi\bar{\rho} |I((\frac{g}{2}-1)(u\bar{\epsilon})^{-1}, \bar{\rho})|^2, \tag{2.41}$$

where we have transformed the integral over velocities by introducing the parameter $u \equiv \epsilon/\bar{\epsilon} = (v_z/\bar{v}_z)^3$ where $\bar{\epsilon} = \bar{v}_z/\bar{b}\Omega_{c0}$ is the mean adiabaticity parameter, $\bar{v}_z = \sqrt{kT_{||}/\mu}$ is the relative thermal speed and $\bar{b} = e^2/\frac{1}{2}\mu\bar{v}_z^2 = 2e^2/kT_{||}$ is the mean distance of closest approach.

To evaluate the numerical value of $\eta(\bar{\epsilon})$, two integrals over $\bar{\rho}$ and u respectively were performed after the numerical integration of I. The $\bar{\rho}$-integral was calculated

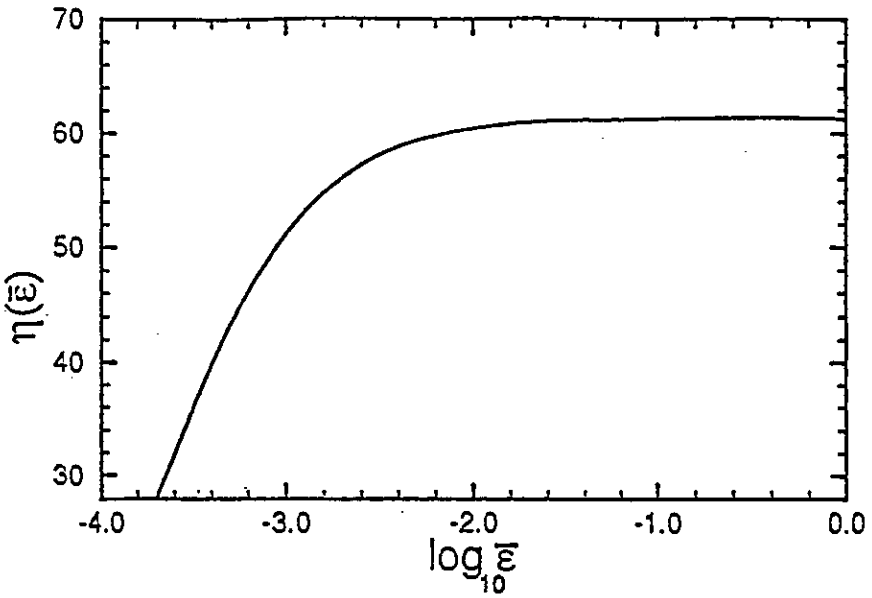

Figure 2.5: Plot of $\eta(\bar{\epsilon})$. For $\bar{\epsilon} \geq 0.01$, $\eta(\bar{\epsilon})$ is almost a constant [see Eq.(2.42)]. For $\bar{\epsilon} < 0.01$, $\eta(\bar{\epsilon})$ decreases exponentially since spin and orbital motion are out of resonance as $\bar{\epsilon}$ decreases. This $\eta(\bar{\epsilon})$ curve is valid only for $\bar{\epsilon} \leq 0.1$ due to our assumption of guiding center dynamics during the electron-electron collision.

numerically using the IMSL[9] subroutine DQDAGP with the upper integration limit cut off at $\bar{\rho} = 8$, which introduces an error of less than $\pm 0.6\%$. For the u-integral, the integrand is a smoothly varying function of u, and so a cubic spline interpolation method was then applied by using subroutines SPLINE and SPLINT in Ref.[10] to obtain the interpolated integrand. Finally the u-integration was completed by IMSL subroutine DQAGS. A careful estimate of the errors involved in the cubic spline interpolation along with the cut off in the $\bar{\rho}$-integral imply an error of less than $\pm 2\%$ for the value of $\eta(\bar{\epsilon})$.

It is useful to note that for $\bar{\epsilon} \gg (\frac{g}{2} - 1) \simeq 0.001, I(\frac{g/2-1}{\epsilon u}, \bar{\rho})$ can be approximated by $I(0, \bar{\rho})$ since the distribution $u^{1/3} exp(-\frac{1}{2}u^{2/3})$ is peaked near $u = 1$. In this case a numerical integration yields

$$\eta(\bar{\epsilon}) \simeq \int_0^\infty du u^{1/3} exp(-\frac{1}{2}u^{2/3}) \int_0^\infty d\bar{\rho} 2\pi\bar{\rho} |I(0,\bar{\rho})|^2 \simeq 61, \bar{\epsilon} \gg .001. \qquad (2.42)$$

We then recover the simple scaling of Eq. (2.1); the numerical coefficients of the two results are within an order of magnitude of one another. The function $\eta(\bar{\epsilon})$ is plotted in Fig.(2.5).

The spin depolarization effect is appreciable in a large variety of parameter regimes. As an example, we take $T_\perp \sim T_\parallel \sim 20K$, $\bar{n} \sim 10^2$, $B \sim 10kG$ and $L \sim 10cm$. In this case $\bar{\epsilon} \sim 8.4 \times 10^{-2}$ and $\nu_{spin} \sim 9.1 \times 10^{-2}(sec^{-1})$, corresponding relaxation time $\nu_{spin}^{-1} \sim 11sec$. However, if B is sufficiently uniform or strong so that spins are tightly bound to the magnetic field line the depolarization effect is negligible.

Now, the spin temperature equilibration determined by Eq.(2.39) implies that a thermal equilibrium state is reached only when $n_+ = n_-$, i.e. $T_s \to \infty$. Physically, this conclusion is the direct result of the assumption of classical orbital motion. The kinetic energy of the orbital dynamics is assumed large compared to $\hbar\Omega_p$, and serves as an infinite heat reservoir for the spin motion. In order to observe true thermal equilibrium one must therefore treat the orbital motion quantum mechanically.

Denote the occupation number of state $|s, \Gamma>$ in a volume element at position $\mathbf{x}$ by $\tilde{f}(s, \Gamma, \mathbf{x}) = x_s(\mathbf{x}) f(\Gamma, \mathbf{x})$, where s represents the spin state and Γ stands for the local single-particle orbital state with respect to the local magnetic field $\mathbf{B}(\mathbf{x})$ which is virtually constant inside the volume element. The orbital distribution function $f(\Gamma)$ is normalized by $\sum_\Gamma f(\Gamma) = N$, where N is the total number of electrons in the volume element. Obviously, x_s, the concentration of electrons with spin state $s(= \pm)$ in the volume element, is normalized by $\sum_s x_s = x_+ + x_- = 1$.

The rate of change of $\tilde{f}$ due to collisions is governed by the following master equation:

$$\left(\frac{d}{dt}\tilde{f}_i\right)_{coll} = \sum_{jkl}(a_{kl}^{ij}\tilde{f}_k\tilde{f}_l - a_{ij}^{kl}\tilde{f}_i\tilde{f}_j) \tag{2.43}$$

where $\tilde{f}_i \equiv \tilde{f}(s_i, \Gamma_i, \mathbf{x})$, etc. and a_{kl}^{ij} is the transition rate for electron 1 scattered from state $|s_k\Gamma_k>$ to state $|s_i\Gamma_i>$ and electron 2 scattered from $|s_l\Gamma_l>$ to $|s_j\Gamma_j>$. In Eq. (2.43), the time derivative is a partial derivative at a fixed position $\mathbf{x}$; it denotes the rate of change of the distribution function due to collisions.

Making use of the normalization condition $\sum_{\Gamma_i} \tilde{f}_i = N x_i$ together with the "detailed balance" symmetry relation [11] $\sum_{kl} a_{kl}^{ij} = \sum_{kl} a_{ij}^{kl}$ in Eq. (2.43), we find a general expression for the rate of change of the spin distribution due to collisions:

$$\left[\frac{d}{dt}x_i\right]_{coll} = \frac{1}{N}\sum_{\Gamma_i}\frac{d}{dt}\tilde{f}_i$$

$$= \frac{1}{N}\sum_{\Gamma_i}[\sum_{jkl} a_{kl}^{ij}(\tilde{f}_k\tilde{f}_l - \tilde{f}_i\tilde{f}_j)]$$

$$= \frac{1}{N}\sum_{\Gamma_i}[\sum_{jkl} a_{kl}^{ij}(x_k x_l f(\Gamma_k)f(\Gamma_l) - x_i x_j f(\Gamma_i)f(\Gamma_j))].$$

We now assume that $s_i = +$ and consider the form of this rate equation when the Golden Rule, Eq. (2.20), is used to determine the a's. As noted previously, the form of H_{sf} implies that in any given two-particle interaction at most one spin can be flipped, so transition rates like $a_{-\Gamma_k,+\Gamma_l}^{+\Gamma_i,-\Gamma_j}$ vanish. Furthermore, the form of $\hat{H}_{sf}$ also implies that the transition rate for electron 1 is independent of the spin state of electron 2. Also, if neither spin is flipped in the interaction another detailed balance symmetry relation holds for transitions involving only orbital changes: $\sum_{\Gamma_k,\Gamma_l} a_{s_i\Gamma_i,s_j\Gamma_j}^{s_i\Gamma_k,s_j\Gamma_l} = \sum_{\Gamma_k,\Gamma_l} a_{s_i\Gamma_k,s_j\Gamma_l}^{s_i\Gamma_i,s_j\Gamma_j}$. This follows from the fact that the wavefunctions of the initial and final states separate into a product of a spin wavefunction and an orbital wavefunction, both of which are members of complete sets over the spin and orbital Hilbert spaces.

Using these relations in the rate equation, several cancellations occur and we

are left with

$$\left[\frac{d}{dt}x_+\right]_{coll} = \frac{1}{N}\sum_{\Gamma_i\Gamma_j\Gamma_k\Gamma_l} a^{+\Gamma_i,\Gamma_j}_{-\Gamma_k,\Gamma_l}[x_- f(\Gamma_k)f(\Gamma_l) - x_+ f(\Gamma_i)f(\Gamma_j)] \tag{2.44}$$

where $a^{+\Gamma_i,\Gamma_j}_{-\Gamma_k,\Gamma_l} \equiv a^{+\Gamma_i,+\Gamma_j}_{-\Gamma_k,+\Gamma_l} = a^{+\Gamma_i,-\Gamma_j}_{-\Gamma_k,-\Gamma_l}$.

If, as before, we assume that $f(\Gamma)$ is an anisotropic Maxwellian distribution function of form $exp(-\frac{E_\perp(\Gamma)}{T_\perp} - \frac{E_\parallel(\Gamma)}{T_\parallel})$, then we may rewrite the two particle distribution function $f(\Gamma_k)f(\Gamma_l)$ as the product of center of mass (C) and relative (R) distribution function $f_c(\Gamma^C_{kl})f_R(\Gamma^R_{kl})$ with normalization condition $\sum_{\Gamma^C_{kl}} f_C(\Gamma^C_{kl}) = N$ and $\sum_{\Gamma^R_{kl}} f_R(\Gamma^R_{kl}) = N$. As we discussed in Section 2.4, the center of mass variables do not participate in the spin flip transition. In other words, the transition rate is only a function of Γ^R_{ij} and Γ^R_{kl}. Then summing over the CM states in Eq. (2.44) and applying the normalization condition we have

$$\left[\frac{d}{dt}x_+\right]_{coll} = \sum_{\Gamma^R_{kl}\Gamma^R_{ji}} a^{+\Gamma^R_{ij}}_{-\Gamma^R_{kl}}[x_- f_R(\Gamma^R_{kl}) - x_+ f_R(\Gamma^R_{ij})]$$

Further taking Γ^R_{kl} to be the quantum numbers (l,ν,κ) associated with state $|i>$ of Eq. (2.28) and Γ^R_{ij} to be the quantum numbers of state $|f>$ of Eq. (2.29) with values $(l_f,\nu_f,\kappa_f) = (l-1,\nu-1,\kappa-\hbar(g/2-1)\Omega_{c0})$, we obtain

$$\begin{aligned}
\frac{d}{dt}x_+ &= \sum_{\nu\kappa l} a^{+l-1,\nu-1,\kappa-\hbar(g/2-1)\Omega_{c0}}_{-l\nu\kappa} \\
&\quad [x_- f_R(l,\nu,\kappa) - x_+ f_R(l-1,\nu-1,\kappa-\hbar(g/2-1)\Omega_{c0})] \\
&= \frac{1}{2L}\sum_{l=-\infty}^{0}\sum_{\nu=1}^{\infty}\sum_{\kappa=\hbar(g/2-1)\Omega_{c0}}^{\infty} |\Delta C|^2 v_z(\kappa)\cdot \\
&\quad [x_- f_R(l,\nu,\kappa) - x_+ f_R(l-1,\nu-1,\kappa-\hbar(g/2-1)\Omega_{c0})]
\end{aligned} \tag{2.45}$$

where the equation $a_{-l\nu\kappa}^{+l-1,\nu-1,\kappa-\hbar(g/2-1)\Omega_{c0}} = |\Delta C|^2 \frac{v_z(\kappa)}{2L}$ has been used [see Eq. (2.34)]. The sum over ν begins at one rather than zero because $|\Delta C|^2 = 0$ for $\nu = 0$. Furthermore, the sum over κ begins at $\hbar(g/2-1)\Omega_{c0}$ rather than zero because, in a transition from $-$ to $+$, this is the minimum relative parallel energy required to conserve energy in the transition. Finally, the sum over l is cut off at 0 rather than ν because we consider only guiding center dynamics for which $\rho_l \gg r_{qL}$. This introduces a negligible relative error of order $(r_{qL}/\bar{b})^2$ to the total transition probability.

The sums can be performed when the explicit form for the relative Maxwellian distribution is employed:

$$f_R(l,\nu,\kappa) = A exp(\frac{-(\nu+\frac{1}{2})\hbar\Omega_{c0}}{kT_\perp} - \frac{\kappa}{kT_{||}})$$

where the constant A is determined by normalization condition

$$\sum_{l=-\infty}^{0}\sum_{\nu=0}^{\infty}\sum_{\kappa=0}^{\infty} f_R(l,\nu,\kappa) = N$$

. Making the substitutions

$$\sum_l \rightarrow \int_0^\infty 2\pi\rho_l d\rho_l / \frac{\hbar}{\mu\Omega_{c0}}; \sum_\kappa \rightarrow \int_0^\infty \rho(\kappa)d\kappa,$$

where $\rho(\kappa) = \frac{L}{\pi\hbar v_z(\kappa)}$ is the density of states, and $\kappa = \frac{1}{2}\mu v_z^2(\kappa)$, we find that

$$A = \frac{2Nh^2 \sinh(\hbar\Omega_{c0}/2kT_\perp)}{\mu\Omega_{c0}V\sqrt{2\pi\mu kT_{||}}},$$

where $V \equiv 2L\int 2\pi\rho_l d\rho_l$ is the volume of the volume element. Substituting this expression for $f_R(l,\nu,\kappa)$ in Eq. (2.45) yields

$$\left[\frac{d}{dt}x_+\right]_{coll} = \sum_{\nu=1}^{\infty}\int_0^\infty 2\pi\rho_l d\rho_l \int_{\kappa\geq\hbar(g/2-1)\Omega_{c0}} dv_z(\kappa)|\Delta C|^2 \cdot \frac{\mu^2\Omega_{c0}f_R(l,\nu,\kappa)}{h^2}$$

$$(x_- - x_+ e^{\frac{\hbar\Omega_{c0}}{kT_\perp} + \frac{\hbar(g/2-1)\Omega_{c0}}{kT_\parallel}}) \tag{2.46}$$

where $n \equiv \frac{N}{V}$ is the electron number density. Finally, the sum over ν can also be performed, and with the aid of Eq. (2.36) for $|\Delta C|$ Eq. (2.46) can be rewritten in terms of the spin temperature as

$$\frac{1}{kT_s}\frac{d}{dt}kT_s(\mathrm{x}) = \frac{kT_s}{\hbar\Omega_{p0}}(1+e^{\hbar\Omega_{p0}/kT_s})(1-e^{\frac{\hbar\Omega_{c0}}{kT_\perp} + \frac{\hbar(g/2-1)\Omega_{c0}}{kT_\parallel}} - \frac{\hbar\Omega_{p0}}{kT_s})\nu_{spin}^{(Q)} \tag{2.47}$$

where the quantum spin depolarization rate $\nu_{spin}^{(Q)}$ is given by

$$\nu_{spin}^{(Q)} = \left(\frac{\sqrt{2\hbar/\mu\Omega_{c0}}}{8(g-2)L}\right)^2 n\sqrt{\frac{\mu}{2\pi kT_\parallel}}\frac{1}{2sinh(\frac{\hbar\Omega_{c0}}{2kT_\perp})}\cdot$$

$$\int_{\frac{1}{2}\mu v_z^2 \geq \hbar(g/2-1)\Omega_{c0}} dv_z|v_z|\cdot exp(\frac{-\mu v_z^2}{2kT_\parallel})\cdot\epsilon^2\int 2\pi\rho_l d\rho_l |I((\frac{g}{2}-1)\epsilon^{-1},\bar{\rho})|^2. \tag{2.48}$$

When we again normalize the integrals as in Eq. (2.40) we obtain

$$\nu_{spin}^{(Q)} = 2.5\times 10^2\nu_c\left(\frac{\bar{\epsilon}\bar{r}_\perp}{L}\right)^2\cdot\left(\frac{\hbar\Omega_{c0}/2kT_\perp}{sinh(\hbar\Omega_{c0}/2kT_\perp)}\right)\cdot\eta^{(Q)}(\bar{\epsilon},\Omega_{c0}) \tag{2.49}$$

where $\eta^{(Q)}(\bar{\epsilon},\Omega_{c0})$ is

$$\eta^{(Q)}(\bar{\epsilon},\Omega_{c0}) = \int_{u_m}^{\infty} duu^{1/3}exp(-\frac{1}{2}u^{2/3})\int_0^\infty 2\pi\bar{\rho}d\bar{\rho}|I((\frac{g}{2}-1)(u\bar{\epsilon})^{-1},\bar{\rho})|^2$$

and the lower cutoff u_m is

$$u_m = (\frac{g}{2}-1)^{3/2}(r_{qL}\Omega_c/\bar{v}_z)^3$$

Note that $u_m \ll 1$ provided that $kT_\parallel \gg (g/2-1)\hbar\Omega_c$, a condition well-satisfied in the experiments. In this case $\eta^{(Q)}(\bar{\epsilon},\Omega_{c0})$ approaches the classical result $\eta(\bar{\epsilon})$. However, even when $u_m \ll 1$ Eq. (2.49) implies that the spin relaxation rate is notably suppressed by quantum effects when $kT_\perp \ll \hbar\Omega_c$. This is because almost

all of the electrons will stay at the ground Landau level in this case and they are forbidden to further give up energies to excite the spin flip. Aside from the quantum suppression factor in Eq. (2.49), the equilibration rate is also strongly modified by the factor

$$(1 - e^{\frac{\hbar\Omega_{c0}}{kT_\perp} + \frac{\hbar(\frac{g}{2}-1)\Omega_{c0}}{kT_\parallel} - \frac{\hbar\Omega_{p0}}{kT_s}})$$

in Eq. (2.47), which arises from the self-consistent consideration for the energy transfer between spin and kinetic degrees of freedom. However, if $kT_\perp \gg \hbar\Omega_c$ and $kT_\parallel \gg (g/2-1)\hbar\Omega_c$ one may verify that the spin temperature equilibration equation (2.47) returns to the form of the classical equation, Eq. (2.39).

As discussed in connection with Eq. (2.3), we see from Eq. (2.47) that the spin flip collisions just calculated cannot drive T_s, $T_\perp$ and $T_\parallel$ toward a common equilibrium temperature. Instead, they can only drive the plasma to a partial equilibrium between T_s, $T_\perp$ and $T_\parallel$ such that

$$\frac{\hbar\Omega_{c0}}{T_\perp} + \frac{\hbar(g/2-1)\Omega_{c0}}{T_\parallel} - \frac{\hbar\Omega_{p0}}{T_s} = 0, \tag{2.50}$$

from which Eq. (2.3) immediately follows. This is a consequence of the fact that these collisions conserve an N-particle adiabatic invariant which equals the sum of the cyclotron action and the spin component along the magnetic field for each particle. For each binary collision, this invariant reduces to the two-particle invariant $\mu^{(2)} = s_{1z} + s_{2z} + \frac{E_\perp^R}{\Omega_c} + \frac{E_\perp^c}{\Omega_c}$, where $E_\perp^R$ and $E_\perp^c$ are the relative and center of mass perpendicular (cyclotron) energies. The invariance of $\mu^{(2)}$ is evident because for the spin flip collisions discussed in this paper, $E_\perp^c$ and one of the two spins, say, s_{2z}, are not changed before and after collision, and the remaining part in the invariant, $s_{1z} + \frac{E_\perp^R}{\Omega_c} = s_{1z} + (\nu + 1/2)\hbar$, is also conserved since $\Delta\nu = -\frac{\Delta s_{1z}}{\hbar}$. For a weakly correlated plasma in which the collisions are predominantly binary, one may generalize

$\mu^{(2)}$ to a many electron adiabatic invariant $\mu^{(N)}$:

$$\mu^{(N)} = \sum_i (s_{iz} + \frac{E_i^\perp}{\Omega_c}) \tag{2.51}$$

where the sum is over all the particles. This expression is an extension of the many-electron adiabatic invariant $\sum_i E_i^\perp/\Omega_c$ derived previously for a system in which the spin orbital dynamics are decoupled[3] In such a system the spin and cyclotron actions are conserved separately. However, an inhomogeneous magnetic field couples the spin and cyclotron dynamics causing an exchange of spin and cyclotron quanta, which leads to the generalized many electron invariant of Eq. (2.51).

Equation (2.3) follows directly from the statistical mechanics of $\mu^{(N)}$-conserving collisions. As a consequence of the invariance of μ, the equilibrium distribution has the form $\rho = Z^{-1}exp(-\beta H + \alpha\mu^{(N)})$, where $H = \sum_i (s_{iz}\Omega_p + E_i^\perp + E_{i\|})$ is the total energy and Z, α, β are constants. By rearranging terms, ρ can be put in the form

$$\rho = Z^{-1}exp\sum_i (-\frac{s_{iz}\Omega_p}{kT_s} - \frac{E_{i\perp}}{kT_\perp} - \frac{E_{ipar}}{kT_\|})$$

where $T_\|$, $T_\perp$ and T_s are related to α and β through the equations

$$\beta = \frac{1}{kT_\|}; \beta - \frac{\alpha}{\Omega_p} = \frac{1}{kT_s}; \beta - \frac{\alpha}{\Omega_c} = \frac{1}{kT_\perp}$$

. These relations are equivalent to Eq. (2.3).

Equation (2.3) leads us to conclude that T_s will approach $T_\perp$ in this partial equilibrium if $T_\| \gg (g/2-1)T_\perp \simeq 10^{-3}T_\perp$. The fact that Eq. (2.3) does not result in the thermal equilibrium condition $T_\perp = T_\| = T_s$ implies that we cannot rely on these spin flip collisions to drive the system to complete thermal equilibrium. Complete thermal equilibrium requires that action invariants such as $\mu^{(N)}$ must be broken. One of the most important $\mu^{(N)}$-breaking collisions is that involving collisional perpendicular and parallel energy exchange without spin flip, which

has been discussed by another paper[3] For a weakly inhomogeneous field, this kind of $\mu^{(N)}$-breaking collision is the dominant mechanism and these $\mu^{(N)}$-breaking collisions cause equilibration between $T_\perp$ and $T_\parallel$ on a relatively fast time scale. If one assumes that $T_\perp = T_\parallel$ during the spin-kinetic temperature equilibration process the condition $T_\perp = T_\parallel = T_s$ follows directly from Eq. (2.50).

2.6 Discussion

We have seen that in a cryogenic strongly-magnetized pure electron plasma the equilibration rate between the spin temperature and the kinetic temperature is dominated by a single process—electron-electron collisions in a nonuniform magnetic field. We have calculated this rate for the case of a weakly-correlated plasma in which the collisions are uncorrelated binary events, taking into account the possibility that the cyclotron motion may be quantized. Although many other processes can also cause spin flip transitions, we have estimated the rates for these processes to be longer than the typical loss rate of the plasma, which is on the order of $10^{-5} sec^{-1}$.

We find that the equilibration rate is proportional to L^{-2}, where L is the scale length of the magnetic field inhomogeneity. In the experiments the uniformity of the magnetic field can be varied over several orders of magnitude simply by confining the plasma at different distances from the end of the solenoid which produces the magnetic field. Inhomogeneity scale lengths from $L \sim 10cm$ to $L \sim 10^3 cm$ can easily be achieved through this technique. This suggests that the rate at which the electron spin temperature approaches the kinetic temperature can be relatively easily controlled. If this rate is reasonably fast, it might be possible to use a measurement of the plasma spin polarization as a thermometer for the kinetic degrees of freedom. Since the electron spin distribution becomes polarized as kT_s falls below $\hbar\Omega_c$, measurement of the degree of polarization of the electron spins could indirectly

provide the kinetic temperature in a range of temperatures on the order of $\hbar\Omega_c/k$. For $B \sim 10 - 60kG$, this temperature is on the order of $1K$, which is over an order of magnitude below the minimum temperatures which have been measured using current techniques[12]

On the other hand, if the plasma is confined in the central region of the solenoid where the field is very uniform, the electron spin distribution is effectively time-independent. This suggests a second experiment, in which one uses the spin of an electron as a tag in order to perform various test-particle measurements. For example, one might place a small subpopulation of the plasma in the opposite spin state from the bulk of the plasma, and follow this population's subsequent dynamics in order to evaluate test-particle spatial and velocity diffusion coefficients.

Of course, both of these experiments rely on some scheme for detection of the polarization state of the electrons, and in the test particle experiment a technique to set up an initial spin distribution is also required. Fortunately, several methods for manipulation and measurement of electron spins have been perfected. For example, the phenomenon known as Mott-scattering[13] has been employed for many years in order to both produce polarized electrons and accurately measure their spin state. A novel technique has also recently been propose[12] in order to produce large quantities of cryogenic spin polarized electrons by using the magnetic inhomogeneity due to finite solenoid length in a trap of the type discussed in this paper. The proposed technique makes use of the idea that the spin Hamiltonian $\mathbf{s} \cdot \mathbf{\Omega}_p(\mathbf{x})$ acts as an effective potential in the orbital energy, and this potential is of opposite sign for electrons of opposite spin. As the spatial distribution of electrons thermalizes along each magnetic field line, the $-$ spins collect in regions of large $\Omega_p(\mathbf{x})$ and $+$ spins collect in the regions of low $\Omega_p(\mathbf{x})$, provided that the parallel kinetic temperature $kT_{\|}$ is less than $\hbar|\Delta\Omega_p|$ where $\Delta\Omega_p$ is the difference between the spin precession

frequency in the strong field and weak field regions. This proposed technique could be used to provide copious quantities of cryogenic spin polarized electrons for the spin tagging experiment, as well as other experiments involving polarized electrons.

Finally, we briefly discuss the effect of plasma rotation on the spin depolarization rate. The plasma is confined against radial expansion by the $\mathbf{v} \times \mathbf{B}$ force induced by rotation through the strong applied magnetic field. Throughout the paper we have assumed that the plasma rotation frequency ω_r is small compared to $\Omega_p - \Omega_c$, so that we may neglect the effect of rotation on the dynamics. This is the usual operating regime for the experiments, which generally involve low density plasmas. For a uniform density plasma column the density is related to the rotation frequency through the expression $\omega_p^2 = 2\omega_r(\Omega_c - \omega_r)$[14] However, the rotation frequency can at least theoretically be as large as Ω_c (although this can be difficult to achieve in practice), so it is useful to consider this situation.

In a frame rotating with the plasma the coriolis force, which acts like a magnetic field, shifts the cyclotron frequency to the vortex frequency $\Omega_c - 2\omega_r$[15] Furthermore, the spin precession frequency is Doppler shifted to $\Omega_p - \omega_r$. Thus, if ω_r is not too close to Ω_p or to $\Omega_c/2$ our results remain valid provided that one substitutes for $\Omega_p - \Omega_c$ the expression $\Omega_p - \Omega_c + \omega_r$, and substitutes for $\bar{r}_L$ the effective Larmor radius in the rotating frame, $\bar{r}_L\Omega_c/(\Omega_c - 2\omega_r)$. For ω_r near $\Omega_c/2$ the guiding center approximation for the orbital dynamics breaks down, although s_z remains an adiabatic invariant. For ω_r near Ω_p the spin precession frequency is no longer large and s_z is no longer an adiabatic invariant. This introduces a rather novel density dependence in the spin depolarization rate, which can be summarized as follows. Starting at low densities, as the density increases the collision frequency increases and the rate of spin relaxation increases linearly with density. As density increases further, ω_r increases to $O(\Omega_p - \Omega_c)$ and the electron spin precession (as seen in

the rotating frame) goes out of resonance with the cyclotron motion, exponentially reducing the rate of spin relaxation. However, as ω_r approaches Ω_c, the effective spin precession frequency in the rotating frame, $\Omega_p - \omega_r$, can become as small as $(g/2-1)\Omega_c$. Thus, for a narrow range of rotation frequencies near Ω_c the rate of spin relaxation should increase dramatically due to resonances between the spin precession and any orbital motions having frequencies on the order of $(g/2-1)\Omega_c$, such as collisional dynamics parallel to **B**.

2.7 Appendix 2A: Calculation of the Transition Matrix Elements

In this appendix we calculate the transition matrix elements in Eq. (2.32) for a spin flip from down to up. We will evaluate $< l-1, \alpha_f|\hat{a}|l\alpha >$ first. The initial value of α is defined by quantum numbers (ν, κ) describing the cyclotron quantum state and the parallel energy respectively. The final value $\alpha_f = (\nu-1, \kappa-\hbar(g/2-1))$ is in accordance with energy conservation in a resonant transition from spin down to spin up. According to Eq.(2.23),(2.24), and (2.27), we have, to the second order of r_L/ρ_l,

$$< l-1, \alpha_f|\hat{a}|l\alpha >= M_1 + M_2 + M_3 + M_4 \tag{2.52}$$

where

$$M_1 = {}^{(0)} < l\alpha_f|\hat{a}|l\alpha >^{(0)} (1 - d_\alpha - d_\alpha^*),$$

$$M_2 = \sum_{\alpha'} (a^*_{\alpha_f\alpha'} + b^*_{\alpha_f\alpha'} + c^*_{\alpha_f\alpha'} + h^*_{\alpha_f\alpha'})^{(0)} < l\alpha'|\hat{a}|l\alpha >^{(0)},$$

$$M_3 = \sum_{\alpha'} (a_{\alpha\alpha'} + b_{\alpha\alpha'} + c_{\alpha\alpha'})^{(0)} < l\alpha_f|\hat{a}|l\alpha' >^{(0)},$$

$$M_4 = \sum_{\alpha'\alpha''} a^*_{\alpha_f\alpha'} a^{(0)}_{\alpha\alpha''} < l\alpha'|\hat{a}|l\alpha'' >^{(0)} .$$

We now compute M_1, M_2, M_3 and M_4. Since $\kappa_f \neq \kappa$, the orthogonality of kets $|l\alpha >^{(0)}$ and $|l\alpha_f >^{(0)}$ implies that $M_1 = 0$. In order to calculate M_2, we note that $^{(0)} < l\alpha'|\hat{a}|l\alpha >^{(0)} = \sqrt{\nu}\delta_{\nu',\nu-1}\delta_{\kappa'\kappa}$ for $\alpha' = (\nu'\kappa')$ and therefore we only need to calculate the perturbation coefficients $a_{\alpha_f\alpha'}$, $b_{\alpha_f\alpha'}$, $c_{\alpha_f\alpha'}$, $h_{\alpha_f\alpha'}$ for $\alpha' = (\nu-1,\kappa)$. However, Eq. (2.22) and (2.23) imply that in this case $a_{\alpha_f\alpha'} = 0$ because $< \nu_f|x^3|\nu-1 >=< \nu_f|x|\nu-1 >= 0$ for $\nu_f = \nu - 1$. Furthermore,

$$b_{\alpha_f\alpha'} = \frac{5}{8}\frac{\mu\Omega^2_{c_0}}{\rho_l^2}\frac{^{(0)} < \nu_f\kappa_f|x^4|\nu-1,\kappa >^{(0)}}{\kappa_f - \kappa}$$

$$+ \frac{^{(0)} < \kappa_f|f(z)|\kappa >^{(0)(0)} < \nu_f|x^2|\nu-1 >^{(0)}}{\kappa_f - \kappa}$$

$$= (2 - \frac{1}{\nu})(\frac{r_{qL}}{2})^2 f_{\kappa_f\kappa}/(\kappa_f - \kappa)$$

where $f_{\kappa_f\kappa} = ^{(0)} < \kappa_f|f(z)|\kappa >^{(0)}$ and we have made use of the matrix elements $^{(0)} < \nu_f|x^2|\nu-1 >^{(0)}= (2-1/\nu)r^2_{qL}/4$ and $^{(0)} < \nu_f\kappa_f|x^4|\nu-1,\kappa >^{(0)} = 0$ since $\kappa_f \neq \kappa$. Continuing on to the next term in M_2, we have

$$c_{\alpha_f\alpha'} \equiv \sum_{\alpha_1} \frac{< \alpha_f|\frac{-\mu\Omega^2_{c_0}}{2\rho_l}x^3 + g(z)x|\alpha_1 >< \alpha_1|\frac{-\mu\Omega^2_{c_0}}{2\rho_l}x^3 + g(z)x|\alpha' >}{(\kappa_f - \kappa)[(\nu_f - \nu_1)\hbar\Omega_{c0} + \kappa_f - \kappa_1]} .$$

We observe that the numerator of each term vanishes unless $\nu_1 = \nu_f \pm 1$ or $\nu_f \pm 3$ for $\alpha_1 = (\nu_1,\kappa_1)$. But $\nu_1 = \nu_f \pm 3$ can be excluded since then the numerator equals

$$< \nu_f\kappa_f|\frac{-\mu\Omega^2_{c_0}}{2\rho_l}x^3|\nu_f \pm 3,\kappa_1 >< \nu_f \pm 3,\kappa_1|\frac{-\mu\Omega^2_{c_0}}{2\rho_l}x^3|\nu_f,\kappa >$$

which is zero for $\kappa_f \neq \kappa$. Then, using the matrix elements $< \nu|x^3|\nu-1 >= \frac{3}{8}r_{qL}^3$ and $< \nu|x|\nu-1 >= \frac{1}{2}r_{qL}$, we find that the numerator equals

$$\frac{-3\mu}{32\rho_l}(\nu\Omega_{c0}r_{qL}^2)^2 g_{\kappa_f\kappa}(\delta_{\kappa\kappa_1}+\delta_{\kappa_f\kappa_1}) + \frac{1}{4}r_{qL}^2 g_{\kappa_f\kappa_1}g_{\kappa_1\kappa}$$

for $\nu_1 = \nu_f + 1$. The result is identical for $\nu_1 = \nu_f - 1$ except that ν is replaced by $\nu - 1$. Adding the expressions for $\nu = \nu_f \pm 1$ together, we obtain

$$c_{\alpha_f\alpha'} = \frac{-3\mu(\Omega_{c0}r_{qL}^2)^2 g_{\kappa_f\kappa}}{32\rho_l(\kappa_f-\kappa)\nu^2}\left[\frac{\nu^2}{-\hbar\Omega_{c0}+\kappa_f-\kappa} - \frac{\nu^2}{\hbar\Omega_{c0}} + \frac{(\nu-1)^2}{\hbar\Omega_{c0}+\kappa_f-\kappa} + \frac{(\nu-1)^2}{\hbar\Omega_{c0}}\right]$$

$$+ \frac{r_{qL}^2}{4(\kappa_f-\kappa)\nu}\sum_{\kappa_1} g_{\kappa_f\kappa_1}g_{\kappa_1\kappa}\left[\frac{\nu}{-\hbar\Omega_{c0}+\kappa_f-\kappa_1} + \frac{\nu-1}{\hbar\Omega_{c0}+\kappa_f-\kappa_1}\right].$$

Finally, $h_{\alpha_f\alpha'} = \dfrac{r_{qL}^2 g_{\kappa_f\kappa}}{2\rho_l(\kappa_f-\kappa)\nu}$ by definition. Now combining the above results, we obtain the following expression for M_2:

$$M_2 = \frac{r_{qL}^2}{4(\kappa_f-\kappa)\sqrt{\nu}}(2\nu-1)f_{\kappa_f\kappa} + \frac{2g_{\kappa_f\kappa}}{\rho_l}\left\{1 - \frac{3}{8\nu}\mu(\Omega_{c0}r_{qL})^2\right.$$

$$\left.\left[\frac{(\nu-1)^2}{\hbar\Omega_{c0}} - \frac{\nu^2}{\hbar\Omega_{c0}} + \frac{\nu^2}{-\hbar\Omega_{c0}+\kappa_f-\kappa} + \frac{(\nu-1)^2}{\hbar\Omega_{c0}+\kappa_f-\kappa}\right]\right\}$$

$$+ 4\sum_{\kappa_1} g_{\kappa_f\kappa_1}g_{\kappa_1\kappa}\left[\frac{\nu}{-\hbar\Omega_{c0}+\kappa_f-\kappa_1} + \frac{\nu-1}{\hbar\Omega_{c0}+\kappa_f-\kappa_1}\right]$$

where $\kappa_f - \kappa = -\hbar(\Omega_p - \Omega_c)$. Turning to M_3, a similar calculation yields

$$M_3 = \frac{\sqrt{\nu}r_{qL}^2}{4(\kappa-\kappa_f)\sqrt{\nu}}\left\{(2\nu+1)f_{\kappa_f\kappa} - \frac{3}{8}\frac{g_{\kappa_f\kappa}}{\rho_l\nu}\mu(\Omega_{c0}r_{qL})^2\cdot\right.$$

$$\left.\left[\frac{(\nu+1)^2}{-\hbar\Omega_{c0}+\kappa-\kappa_f}\frac{(\nu+1)^2}{\hbar\Omega_{c0}} + \frac{\nu^2}{\hbar\Omega_{c0}+\kappa-\kappa_f} + \frac{\nu^2}{\hbar\Omega_{c0}}\right]\right.$$

$$+4\sum_{\kappa_1} g_{\kappa\kappa_1} g_{\kappa_1\kappa_f}\left[\frac{\nu+1}{-\hbar\Omega_{c0}+\kappa-\kappa_1}+\frac{\nu}{\hbar\Omega_{c0}+\kappa-\kappa_1}\right]\Bigg\}$$

Turning to M_4, we notice that $< l\alpha'|\hat{a}|l\alpha'' >= \sqrt{\nu'+1}\delta_{\nu'',(\nu'+1)}\delta_{\kappa''\kappa'}$. Then

$$M_4 = \sum_{\alpha'} \sqrt{\nu'+1} a^*_{\alpha_f\alpha'} a_{\alpha,(\nu'+1)\kappa'}$$

$$= \sum_{\alpha'} \sqrt{\nu'+1} \frac{< \alpha'|H^{(1)}|\alpha_f >< \alpha|H^{(1)}|\nu'+1,\kappa' >}{[(\nu_f-\nu')\hbar\Omega_{c0}+\kappa_f-\kappa'][(\nu-\nu'-1)\hbar\Omega_{c0}+\kappa-\kappa']}.$$

From Eq. (2.22) the numerator is nonzero only when $\nu'-\nu_f = \pm 1$ or ± 3. In these cases, the denominator is of order $O(\hbar\Omega_{c0})^2$ because $|\kappa_f-\kappa'|$ and $|\kappa-\kappa'|$ must be much smaller than $\hbar\Omega_{c0}$; otherwise the inner products involving the dynamics in z would result in exponentially small results. Recalling that $H^{(1)}$ is of order $O(\frac{r_{qL}}{\rho_l})$, we see that M_4 is of order $O(\frac{r_{qL}}{\rho_l})^4$, which is negligible compared with M_2 and M_3.

Finally, combining these results we have

$$< l-1,\alpha_f|\hat{a}|l\alpha >= M_2 + M_3 + O(\frac{r_{qL}}{\rho_l})^3$$

$$= \frac{r_{qL}^2}{4(\kappa_f-\kappa)\sqrt{\nu}}\left\{-2f_{\kappa_f\kappa}+\frac{2g_{\kappa_f\kappa}}{\rho_l}-\frac{3g_{\kappa_f\kappa}}{2\rho_l}\cdot\left[1+\frac{\hbar\Omega_{c0}-(2\nu^2+1)(\kappa_f-\kappa)}{\hbar\Omega_{c0}-(\kappa_f-\kappa)^2/\hbar\Omega_{c0}}\right]\right.$$

$$+4\sum_{\kappa_1} g_{\kappa_f\kappa_1} g_{\kappa_1\kappa}\left[\frac{\hbar\Omega_{c0}+(2\nu-1)(\kappa_f-\kappa_1)}{(\hbar\Omega_{c0})^2-(\kappa_f-\kappa_1)^2}\right.$$

$$\left.\left.-\frac{\hbar\Omega_{c0}+(2\nu+1)(\kappa-\kappa_1)}{(\hbar\Omega_{c0})^2-(\kappa-\kappa_1)^2}\right]\right\} \qquad (2.53)$$

This expression may be further simplified as follows. As shown in the Appendix of Ref.[3], the matrix element $g_{\kappa_f\kappa}$ can be evaluated to the lowest order in $(\kappa_f-\kappa)/\kappa$ $=(\frac{g}{2}-1)\hbar\Omega_{c0}/\kappa$ by integration along the classical $\bar{z}(t)$ orbit: $g_{\kappa_f\kappa} = \int dt g(\bar{z}(t))$ $e^{-i(\kappa_f-\kappa)t/\hbar}$ [see Eq. (2.35)]. In order to avoid an exponentially small result, we

require that $\frac{\hbar}{\kappa_f - \kappa} \geq O(\frac{\rho_l}{v})$, where ρ_l/v is the time scale during which the function $g(\bar{z}(t))$ changes and $v = \sqrt{2\kappa/\mu}$. Then we obtain the ordering $\frac{\kappa_f - \kappa}{\hbar\Omega_{c0}} \leq O(\frac{r_{qL}}{\rho_l})\sqrt{\frac{\kappa}{\nu\hbar\Omega_{c0}}}$ and therefore

$$\frac{\hbar\Omega_{c0} - (2\nu^2+1)(\kappa_f - \kappa)}{\hbar\Omega_{c0} - (\kappa_f - \kappa)^2/\hbar\Omega_{c0}} = 1 + O(\frac{r_{qL}}{\rho_l}).$$

Using the same argument, we find that

$$\frac{\hbar\Omega_{c0} + (2\nu - 1)(\kappa_f - \kappa_1)}{(\hbar\Omega_{c0})^2 - (\kappa_f - \kappa_1)^2} = \frac{1}{\hbar\Omega_{c0}}(1 + O(\frac{r_{qL}}{\rho_l})),$$

and

$$\frac{\hbar\Omega_{c0} + (2\nu + 1)(\kappa - \kappa_1)}{(\hbar\Omega_{c0})^2 - (\kappa - \kappa_1)^2} = \frac{1}{\hbar\Omega_{c0}}(1 + O(\frac{r_{qL}}{\rho_l})),$$

so the difference between these two expressions is of order $\frac{1}{\hbar\Omega_{c0}}O(\frac{r_{qL}}{\rho_l}))$. This implies that the term in Eq. (2.53) involving the sum over κ_1 is approximately equal to $\sum_{\kappa_1} g_{\kappa_f\kappa_1}(g_{\kappa_1\kappa}\hbar\Omega_{c0}) \cdot O(\frac{r_{qL}}{\rho_l})$ which is higher order in $\frac{r_{qL}}{\rho_l}$ than the other terms in Eq. (2.53). Combining the above results yields

$$\begin{aligned} < l-1, \alpha_f|\hat{a}|l, \alpha > \quad &= \frac{r_{qL}^2}{4(\kappa_f - \kappa)\sqrt{\nu}}(-2f_{\kappa_f\kappa} - \frac{g_{\kappa_f\kappa}}{\rho_l}) + O(\frac{r_{qL}}{\rho_l})^3 \\ &= \frac{r_{qL}e^2}{4\hbar(\Omega_p - \Omega_c)\sqrt{\nu}}\left(\frac{\rho_l^2 - 2z^2}{(\rho_l^2 + z^2)^{5/2}}\right)_{\kappa_f\kappa} \end{aligned} \tag{2.54}$$

We may easily calculate the other matrix element $< l+1, \alpha_f|\hat{a}^+|l, \alpha >$ following the same procedure as for $< l-1, \alpha_f|\hat{a}|l, \alpha >$. This matrix element can be written as $M_1' + M_2' + M_3' + M_4' + O(\frac{r_{qL}}{\rho_l})^3$ where M_1' to M_4' have the same form as M_1 to M_4 except that $\hat{a}$ is changed to $\hat{a}^+$ and $h^*_{\alpha_f\alpha'}$ is changed to $-h^*_{\alpha_f\alpha'}$. We determine the order of magnitude of the matrix elements M_1' to M_4' in order to show that they are negligible. First, $M_1' = 0$ since $\kappa_f \neq \kappa$. For M_2', the term

$< l\alpha'|\hat{a}^+|l\alpha >$ yields the selection rule: $\nu' = \nu + 1$, $\kappa' = \kappa$. Then $a_{\alpha_f\alpha'} = 0$ since $< \nu_f|x^3|\nu + 1 >=< \nu_f|x|\nu + 1 >= 0$ for $\nu_f = \nu - 1$, and

$$b_{\alpha_f\alpha'} = \frac{5}{8}\mu\Omega_{c_0}^2\rho_l^2\frac{< \nu_f\kappa_f|x^4|\nu + 1, \kappa >}{\kappa_f - \kappa - 2\hbar\Omega_{c0}} + \frac{f_{\kappa_f\kappa} < \nu_f|x^2|\nu + 1 >}{\kappa_f - \kappa - 2\hbar\Omega_{c0}} \sim O(\frac{r_{qL}}{\rho_l})^3$$

since $< \nu_f|x^2|\nu + 1 >\sim O(r_{qL}^2)$. Similarly, we have $c_{\alpha_f\alpha'} \sim h_{\alpha_f\alpha'} \sim O(\frac{r_{qL}}{\rho_l})^3$ and therefore $M_2' \sim O(\frac{r_{qL}}{\rho_l})^3$. One may also check that $M_3' \sim O(\frac{r_{qL}}{\rho_l})^3$. Turning to M_4', the term $< l\alpha'|\hat{a}^+|l\alpha'' >$ implies the selection rule $\nu' = \nu''+1$, $\kappa' = \kappa''$ and therefore in analogy to M_4 we have $M_4' \sim O(\frac{r_{qL}}{\rho_l})^4$. In conclusion, we find that the matrix element $< l+1, \alpha_f|\hat{a}^+|l, \alpha >$ is of $O(\frac{r_{qL}}{\rho_l})^3$, which is negligible compared to $< l-1, \alpha_f|\hat{a}|l, \alpha >$.

2.8 Appendix 2B: Evaluation of the Elliptic Integral Expression for $t(z, \rho)$

In this appendix we obtain a closed-form analytic expression in terms of elliptic integrals for the parallel guiding center motion $t(z, \rho)$ given by Eq. (2.16). This simplifies numerical evaluation of the function $I(x, \bar{\rho})$. Although alternative expressions for $t(z, \rho)$ are possible, the one derived in this appendix has the advantage that it avoids (removable) singularities and is then useful for numerical calculations. From Eq. (2.16), $\bar{t}$ can be expressed as

$$\bar{t}(\bar{z}, \bar{\rho}) = \int_{\bar{z}_m}^{\bar{z}} d\bar{z}/\sqrt{1 - (\frac{1}{\sqrt{\bar{z}^2 + \bar{\rho}^2}})} \tag{2.55}$$

where $\bar{z}_m$ is the $\bar{z}$ value at the distance of closest approach:

$$\bar{z}_m = \begin{cases} 0 & \text{for } \bar{\rho} \geq 1 \\ \sqrt{1 - \bar{\rho}^2} & \text{for } \bar{\rho} < 1 \end{cases}$$

For $\bar{\rho} = 0$, the integral in Eq. (2.55) can be easily calculated and the result is that $\bar{t}(\bar{z}, 0) = \sqrt{\bar{z}^2 - \bar{z}} + \ln(\sqrt{\bar{z} - 1} + \sqrt{\bar{z}})$.

For $\bar{\rho} \neq 0$, we introduce the new variable $u = \frac{1}{2}\arctan(\bar{z}/\bar{\rho})$; then Eq. (2.55) becomes

$$\bar{t}(u,\bar{\rho}) = 2\bar{\rho}\int_{u_m}^{u} \frac{du}{(1-2\sin^2 u)^2\sqrt{(1-\frac{1}{\bar{\rho}})+\frac{2}{\bar{\rho}}\sin^2 u}} \tag{2.56}$$

where

$$u_m \equiv \frac{1}{2}arctan(\bar{z}_m/\bar{\rho}).$$

We now proceed to evaluate $\bar{t}(u)$ separately for the $\rho \geq 1$ and $\rho < 1$ cases.

(A) $\rho > 1$ case. .br We rewrite $\bar{t}(u)$ as

$$\frac{\bar{\rho}\sqrt{\bar{\rho}}}{2\sqrt{\bar{\rho}-1}}[P_{-2}(u,\bar{\rho}) - P_{-2}(u_m,\bar{\rho})]$$

where we define

$$P_n(u,\bar{\rho}) \equiv \int_0^u du(-\frac{1}{2}+\sin^2 u)^n/\Delta_1,$$

$$\Delta_1 \equiv \sqrt{1+p^2\sin^2 u},$$

$$p \equiv 2/(\bar{\rho}-1).$$

Notice that P_{-2} can be expressed in terms of $P_{\pm 1}$ through the identity[16]

$$-p^2 P_1 = -\Delta_1 \tan 2u + \frac{p^2}{4}P_{-1} + \frac{1}{2}(1+\frac{p^2}{2})P_{-2}. \tag{2.57}$$

Now we relate $P_{\pm 1}$ to elliptic functions. First, we note that

$$\begin{aligned} P_1 &= \int \frac{-\frac{1}{2}+\sin^2 u}{\Delta_1}du = -(\frac{1}{2}+\frac{1}{p^2})\int \frac{du}{\Delta_1} + \frac{1}{p^2}\int \Delta_1 du \\ &= -(\frac{1}{2}+\frac{1}{p^2})\frac{1}{\sqrt{1+p^2}}F_1 + \frac{1}{p^2}[\sqrt{1+p^2}E_1 - p^2\sin u\cos u/\Delta_1], \end{aligned}$$

where E_1, F_1 denote the first and second kind elliptic integrals: $E_1 \equiv E(\beta, k_1)$; $F_1 \equiv F(\beta, k_1)$, and

$$\beta \equiv arcsin\left(\frac{\sqrt{1+p^2}\sin u}{\Delta_1}\right),$$

$$k_1 \equiv p/\sqrt{1+p^2}.$$

For P_{-1} we use identity

$$\frac{1}{(-\frac{1}{2}+\sin^2 u)\Delta_1} = \frac{-4}{p^2+2}\frac{\Delta_1}{1-2\sin^2 u} - \frac{2p^2}{(p^2+2)\Delta_1},$$

and obtain

$$P_{-1} = \frac{-4}{p^2+2}\frac{1}{\sqrt{1+p^2}}\Pi_1 + \frac{p^2}{p^2+2}\frac{1}{\sqrt{1+p^2}}F_1,$$

where Π_1 denotes the third kind elliptic integral:

$$\Pi_1 \equiv \Pi(\beta, \frac{2+p^2}{1+p^2}, k_1).$$

Finally, substituting the elliptic integral expression for $P_{\pm 1}$ in Eq. (2.57) yields

$$\begin{aligned} P_{-2}(u,\bar{\rho}) &= \frac{2\bar{z}(u)}{\bar{\rho}\Delta_1} + [1+\frac{p^4}{(2+p^2)^2}]\frac{2}{\sqrt{1+p^2}}F_1 \\ &- \frac{4\sqrt{1+p^2}}{2+p^2}E_1 + \frac{4p^2}{(2+p^2)^2}\frac{1}{\sqrt{1+p^2}}\Pi_1, \end{aligned} \tag{2.58}$$

where $\bar{z}(u) = \bar{\rho}\tan 2u$.

(B) $\rho < 1$ case. We rewrite Eq. (2.56) as

$$\bar{t}(v,\bar{\rho}) = \frac{\bar{\rho}\sqrt{\bar{\rho}}}{2\sqrt{\bar{\rho}+1}}(Q_{-2}(v_m,\bar{\rho}) - Q_{-2}(v,\bar{\rho}))$$

where

$$Q_n(v,\bar{\rho}) \equiv \int_0^v dv(-\frac{1}{2}+\sin^2 v)^n/\Delta_2$$

$$\Delta_2 \equiv \sqrt{1-k_2^2\sin^2 v}$$

$$k_2 \equiv \sqrt{\frac{2}{1+\bar{\rho}}}$$

$$v \equiv \frac{\pi}{2}-u,$$

$$v_m \equiv \frac{\pi}{2}-u_m = \frac{\pi}{2}-\frac{1}{2}arctan\sqrt{\frac{1}{\rho^2}-1}.$$

In analogy to Eq. (2.57), we have, for Q_n,

$$k_2^2 Q_1 = -\Delta_2 \tan 2v - \frac{k_2^2}{4}Q_{-1} + \frac{1}{2}(1-\frac{k_2^2}{2})Q_{-2} \qquad (2.59)$$

where

$$\begin{aligned} Q_1 &= \int \frac{-\frac{1}{2}+\sin^2 v}{\Delta_2}dv \\ &= -\frac{1}{k_2^2 E_2} + (\frac{1}{k_2^2}-\frac{1}{2})F_2. \end{aligned}$$

Here E_2 and F_2 denote elliptical integrals of the first and second kind: $E_2 \equiv E(v,k_2)$; $F_2 \equiv F(v,k_2)$. For

$$Q_{-1} = -2\int \frac{dv}{(1-2\sin^2 v)\Delta_2} = -2\Pi(v,2,k_2),$$

we have[17]

$$Q_{-1} = 2\Pi_2 - 2F_2 - \frac{1}{p_1}\ln|\frac{p_1\tan v+\Delta_2}{p_1\tan v-\Delta_2}|$$

where Π_2 denotes the elliptic integral of the third kind:

$$\Pi_2 \equiv \Pi(v, \frac{1}{1+\bar{\rho}}, k_2),$$

and

$$p_1 \equiv \sqrt{\frac{\bar{\rho}}{\bar{\rho}+1}}.$$

Finally, substituting the elliptic integral expression of $Q_{\pm 1}$ in Eq. (2.59) yields

$$\begin{aligned} Q_{-2}(v,\bar{\rho}) &= 2(1-\frac{1}{\bar{\rho}})F_2 - 2(1+\frac{1}{\bar{\rho}})E_2 + \frac{1}{\bar{\rho}}\Pi_2 \\ &- 2(1+\frac{1}{\bar{\rho}})\frac{\bar{z}}{\bar{\rho}}\Delta_2 - \frac{1}{\bar{\rho}p_1}\ln|\frac{p_1\tan v+\Delta_2}{p_1\tan v-\Delta_2}| \end{aligned} \tag{2.60}$$

where $\bar{z}(v) = -\bar{\rho}\tan 2v$.

This chapter has appeared as an article in *Phys.Fluids* B, **5**, 691-710(1993).

2.9 References

1. J.H. Malmberg, C.F. Driscoll, B. Beck, D.L. Eggleston, J. Fajans, K.S. Fine, X.-P. Huang, and A.W. Hyatt, in *Nonneutral Plasma Physics*, edited by C.W. Roberson and C.F. Driscoll (American Institute of Physics, New York, 1988), pp. 28-71.

2. R.M. Kulsrud, E.J. Valeo and S.C. Cowley, Nucl. Fusion **26**, 1443 (1986).

3. T.M. O'Neil and P. Hjorth, Phys. Fluids**28**, 3241 (1985).

4. J.D. Jackson, Rev. Mod. Physics **48**(3), 417 (1976).

5. W. Happer, Rev. Mod. Physics **44**(2), 169 (1972).

6. T.M. O'Neil, Phys. Fluids **26**, 2128 (1983).

7. SLATEC Mathematical Program Library, Revision 830701.

8. M.H. Johnson and B.A. Lippmann, Phys. Rev. **76**, 828 (1949).

9. IMS MATH/LIBRARY, Version 1.1, December 1989.

10. W.H. Press, B.P. Flannery, S.A. Teukolsky and W.T. Vetterling, *Numerical Recipes* (Cambridge Univ. Press, 1989).

11. E.M. Lifshitz and L. P. Pitaevski, *Physical Kinetics* (Pergamon, Oxford, 1981) p. 7.

12. 12. B.R. Beck, Private communication (1992).

13. 13. A. Rich and J.C. Wesley, Rev. Mod. Physics **44**, 250 (1972).

14. 14. R.C. Davidson, *Theory of Nonneutral Plasmas* (W.A. Benjamin, London, 1974), p. 22.

15. 15. Ibid, p. 8.

16. 16. I.S. Gradshteyn and I.M. Ryzhik, *Tables of Integrals, Series, and Products* (Academic Press, Inc., 1980) pp. 171-173.

17. 17. M. Abramowitz and I.A. Stegun, *Handbook of Mathematical Functions* (Dover, New York, 1970) p. 599.

Chapter 3

Temperature Equilibration of a 1-D Coulomb Chain and a Many-Particle Adiabatic Invariant

3.1 Temperature Equilibration of a 1-D Coulomb Chain and a Many Particle Adiabatic Invariant

The one dimensional Coulomb chain is a form of condensed matter consisting of charges of a single species trapped in a linear configuration through the application of strong external magnetic and/or electric fields. Recently, such chains have been realized in two experiments,[1],[2] in which the charges have been cooled into the regime of strong correlation where the correlation parameter $\Gamma \equiv q^2/aT$ is much larger than unity. (Here q is the ion charge, T is the temperature and a is the average intercharge spacing). The 1-D chain has been suggested as an advantageous configuration for a novel type of atomic clock based on trapped ions.[2],[3] It has also been predicted that such chains may form in heavy ion storage rings provided that sufficiently strong electron or laser cooling is applied.[4] Such cold 1-D chains would provide an attractive low emittance ion source.

Although the charges are strongly bound to the axis of the trap or the stor-

age ring by the applied forces, high frequency transverse motions still occur and the temperature $T_\perp$ associated with these motions need not be the same as that associated with the motions parallel to the axis, $T_\parallel$. For example, when laser cooling or electron cooling is applied along the chain axis, the transverse oscillations are not directly cooled and come to equilibrium with the parallel motion only indirectly through Coulomb collisions.[5] In this case the overall cooling rate depends on the rate at which collisions cause $T_\perp$ and $T_\parallel$ to equilibrate. This equilibration rate has been examined via numerical simulations.[6] However, the regime in which both parallel and transverse motions are of small amplitude (near harmonic) has not yet been explored, and it is often in this regime that the experiments operate.

In this paper we calculate the rate ν at which an anisotropic temperature distribution relaxes to thermal equilibrium in a strongly-correlated ($\Gamma \gg 1$) 1-D chain in the strong focusing limit, where the motions transverse to the axis are of high frequency compared to the parallel motions. Because of this timescale separation we find that a many particle adiabatic invariant exists, equal to the total action associated with the transverse motions. If this approximate invariant were exactly conserved, equilibration could not occur. However, we find that N body collisions cause small changes in the invariant, leading to a slow rate of equilibration, exponentially small in the ratio of transverse to parallel frequencies.

Our model for the trap consists of a harmonic radial confining potential of the form $m\omega_r^2(x^2+y^2)/2$ where $\mathrm{r} = (x,y,z)$ are Cartesian coordinates with z oriented along the beam axis. In the strong focusing limit of interest here, the parameter $\epsilon \equiv \omega_0/\omega_r$ is small, where $\omega_0 \equiv \sqrt{q^2/ma^3}$ is a plasma frequency associated with parallel oscillations. This radial potential is an excellent approximation for the linear[2] and circular[1] Paul trap experiments, and is a useful first approximation for the comoving frame of ions in a storage ring.[4] The Hamiltonian for the N-ion

system is then written as

$$H(\mathbf{r}_1, \mathbf{p}_1, ...\mathbf{r}_N, \mathbf{p}_N) = \sum_{n=1}^{N}(p_n^2/2m + m\omega_r^2[x_n^2 + y_n^2]/2)$$

$$\sum_{l>n} q^2/\sqrt{x_{ln}^2 + y_{ln}^2 + [z_{ln} + a(l-n)]^2}$$

where $\mathbf{r}_{ln} \equiv \mathbf{r}_l - \mathbf{r}_n$, and for each ion $\mathbf{r}_n$ is measured from its equilibrium position in the linear chain. For simplicity we assume here that in equilibrium the ions are equally spaced, as in the ring trap, and image charges and curvature effects, if any, are neglected.

When the ions are strongly correlated, the dynamics is dominated by N body processes rather than 2 body collisions. Here we assume that both $\Gamma_\perp \equiv q^2/aT_\perp$ and $\Gamma_{||} \equiv q^2/aT_{||}$ are sufficiently large so that we may describe the ion-ion interaction as emission and absorption of phonons. The ideal phonon limit is then attained by expansion of the Coulomb potential in $|\mathbf{r}_n|/a$ to second order in this small quantity. The resulting harmonic Hamiltonian H_0 then describes N eigenmodes with polarizations parallel to z and $2N$ transverse modes. The parallel and transverse mode frequencies are given by[6] $\omega_z(k) = \omega_0[8\sum_{n=1}^{\infty} sin^2(nk/2)/n^3]^{1/2}$, and $\omega_\perp(k) = \sqrt{\omega_r^2 - \omega_z^2(k)/2}$ respectively, where $k = 2\pi n/N (n = 0, 1, ..., N-1)$ is the parallel wavevector of the eigenmodes normalized to a.

Even at low temperatures, anharmonic terms neglected in H_0 but present in H couple the parallel (or transverse) phonons to one-another, e.g. through 3 phonon collisions. This low-order phonon-phonon coupling is expected to cause the distribution of parallel (or transverse) energy to relax to a Maxwellian described by a temperature $T_{||}(T_\perp)$. However, when $\epsilon \ll 1$ energy conservation does not allow these low order processes to create or destroy transverse phonons, because annihilation of a single transverse phonon requires creation of many parallel phonons.

The total number of quanta (i.e. the total action) associated with the high frequency transverse motions is then an adiabatic invariant. In order for the transverse and parallel temperatures to equilibrate this invariant must be broken: transverse phonons must be created or annihilated. In fact, the symmetry of H in x and y implies that transverse phonons must be created or destroyed in pairs. The rate ν for parallel to transverse equilibration can then be estimated using an order of magnitude estimate based on Fermi's golden rule: $\nu \sim \omega_0 < (\Delta H/H_0)^2 >$ where ΔH is the interaction energy for a process which annihilates two transverse phonons, and $< \cdots >$ denotes a statistical average. Recognizing that about M parallel phonons must be created in this process, where $M = 2\omega_r/\omega_m$ and $\omega_m = \eta\omega_0$ is the maximum parallel phonon frequency and $\eta \equiv \sqrt{7\zeta(3)}$. We crudely approximate ΔH as a Taylor expansion of H: $\Delta H/H_0 \sim z^M(x^2+y^2)/a^{M+2}$. We perform the average using a harmonic Einstein approximation for the distribution of displacements, proportional to $exp[-(\Gamma_{||}z^2 + \Gamma_\perp(x^2+y^2)/\epsilon^2)/a^2]$. Neglecting an unimportant multiplicative constant, the average yields

$$\nu \sim (\omega_0\epsilon^4/\Gamma_\perp^2)exp[-2\{1+\ln(\eta\epsilon\Gamma_{||}/2)\}/\eta\epsilon] \tag{3.1}$$

which is exponentially small, as expected. Note however that $\epsilon\Gamma_{||}$ must be greater than unity in order for the result to be sensible, because the average is dominated by z displacements with a peak at $z/a \sim 1/\sqrt{\epsilon\Gamma_{||}}$. That is, large displacements in z would make a large contribution to the rate, but when $\Gamma_{||} \gg 1$ such displacements are improbable. When $\epsilon\Gamma_{||} > 1$ small displacements make the main contribution to ν, consistent with the assumption of harmonic fluctuations.

To calculate the equipartition rate more rigorously, we perform a series of three canonical transformations in order to isolate the total transverse action variable

J_0. We first transform to phonon coordinates $(\tilde{\mathbf{r}}_k, \tilde{\mathbf{p}}_k)$, through the Fourier relations

$$(\tilde{\mathbf{r}}_k, \tilde{\mathbf{p}}_k) = N^{-1/2} \sum_{l=0}^{N-1} (\mathbf{r}_l e^{-ikl}, \mathbf{p}_l e^{ikl}). \tag{3.2}$$

In these coordinates H_0 has the form of $3N$ uncoupled harmonic oscillators of frequencies ω_j, where j refers to both wavenumber k and polarization direction ($\hat{x}, \hat{y}$, or $\hat{z}$): $H_0 = \sum_j [p_j^2/2m + m\omega_j^2 r_j^2/2]$. We next transform the $2N$ transverse phonon variables to $2N$ action angle pairs (ψ_j, I_j) via the transformation

$$(\tilde{r}_j, \tilde{p}_j) = \sqrt{2I_j/m\omega_j}(\sin\psi_j, m\omega_j \cos\psi_j). \tag{3.3}$$

The angle variables ψ_j evolve on a timescale of order ω_τ^{-1}. Finally, we apply the canonical transformation[7]

$$\theta_0 = \psi_0, \theta_j = \psi_j - \psi_0, (j \neq 0), J_0 = \sum_j I_j, J_j = I_j, (j \neq 0). \tag{3.4}$$

Now only θ_0 varies at ω_τ^{-1}; all other variables are slowly varying. The total transverse action J_0 is therefore an adiabatic invariant.

We are interested in the time rate of change of J_0 averaged over a suitably chosen statistical distribution D of systems: $d < J_0 > /dt = \int d\lambda D[J_0, H]_\lambda$ where λ is a point in the $6N$ dimensional phase space, and $[\cdot,\cdot]_\lambda$ is a Poisson bracket. At some time in the past, long compared to the relaxation time to a two-temperature Maxwellian but short compared to the $T_\perp \rightarrow T_\parallel$ relaxation time, we assume that D was a two-temperature Maxwellian, written as $D_0 = Z^{-1} exp[-\omega_\tau J_0/T_\perp - (H - \omega_\tau J_0)/T_\parallel]$. However, since J_0 is not an exact constant of the motion, a fluctuation D_1 develops which may be obtained through solution of Liouville's equation with D_0 as the initial condition: $D_1(\lambda, t) = -\int_{-\infty}^{t} dt' [D_0, H]_{\lambda(t')}$, where the Poisson bracket is evaluated along the phase-space trajectory $\lambda(t')$ for which $\lambda(t) = \lambda$, and where the slow time dependence of $T_\perp$ and $T_\parallel$ has been neglected. Substitution of D_1 into

$d < J_0 > /dt$ then yields

$$d < J_0 > /dt = \int d\Lambda D_0[J_0, H]_\lambda + (1/T_\perp - 1/T_\parallel)(2\epsilon)^{-1} \int_{-\infty}^{+\infty} d\tau C(\tau) \qquad (3.5)$$

where we introduce the correlation function $C(\tau) \equiv < \dot{J}_0(t)\dot{J}_0(0) >$, $\tau \equiv \omega_0 t$, $\dot{J}_0 = -\partial H/\partial\theta_0$, and where $< \cdots >$ represents an average over D_0. For a detailed derivation for Eq. (3.5), see Appendix 3A. The first term of Eq. (3.5) vanishes because D_0 depends on λ only through J_0 and H; and the time integral in the second term has been extended to $t = +\infty$ using the symmetry $C(\tau) = C(-\tau)$.

However, the time integral in Eq. (3.5) cannot be evaluated because it involves the exact trajectory $\lambda(t)$. We follow standard practice[8] by substituting approximate trajectories $\lambda^{(0)}(t)$, in this case determined by the harmonic Hamiltonian H_0, and we also replace $D_0(H, J_0)$ by $D_0(H_0, J_0)$. That is, we approximate the dynamics by that of an ideal phonon gas, so the system must be strongly correlated, i.e., $\Gamma_\parallel \gg 1$. We also assume here that the parallel force due to transverse displacements, of order $q^2 r_{ln}^2/a^4$, can be treated as a small perturbation of the parallel motion, which requires $\Gamma_\perp \gg \epsilon^2\sqrt{\Gamma_\parallel}$. The substitution of $\lambda(t)$ by $\lambda^{(0)}(t)$ is a major assumption of our calculation. Despite the fact that this type of assumption works well for a weakly correlated plasma[7], its validity needs to be tested for a strongly correlated plasma. Furthermore, we expect that processes involving creation and annihilation of only two transverse phonons will dominate the equilibration rate so we Taylor expand $\partial H/\partial\theta_0$ in x_{ln}^2 and y_{ln}^2 keeping only lowest order non-zero terms: $\dot{J}_0 = (q^2/2)\sum_{l>n} Z_{ln}^{-3}\partial r_{ln}^2/\partial\theta_0$ where $r_{ln}^2 \equiv x_{ln}^2 + y_{ln}^2$ and $Z_{ln} \equiv (l-n)a + z_{ln}$ is the z distance between ions l and n.

With these assumptions we find that the averages over transverse and parallel

phonons appearing in $C(\tau)$ decouple:

$$C(\tau) = T_\perp^2 \sum_{\mathbf{m}} C_{\mathbf{m}}^{\perp}(\tau,\epsilon) C_{\mathbf{m}}^{\parallel}(\tau,\Gamma_\parallel),$$

where $\mathbf{m} \equiv (l,n,\bar{l},\bar{n})$, and the sum runs over all $l > n$, $\bar{l} > \bar{n}$. The (dimensionless) parallel and transverse parts of $C(\tau)$ are $C_{\mathbf{m}}^{\parallel}(\tau,\Gamma_\parallel) \equiv 4a^6 < Z_{ln}^{-3}(\tau) Z_{\bar{l}\bar{n}}^{-3}(0) >$, and

$$C_{\mathbf{m}}^{\perp}(\tau,\epsilon) \equiv \Gamma_\perp^2 < \partial r_{ln}^2(\tau)/\partial\theta_0 \partial r_{\bar{l}\bar{n}}^2(0)/\partial\theta_0 > /16a^4$$

respectively. Employing harmonic phonon orbits $\lambda^{(0)}(t)$ to determine $r_{ln}^2(\tau)$, the average in $C_{\mathbf{m}}^{\perp}$ can be performed explicitly (see Appendix 3B):

$$C_{\mathbf{m}}^{\perp}(\tau,\epsilon) = 2\epsilon^4([S_{\mathbf{m}}^{+}(\epsilon\tau)]^2 - [S_{\mathbf{m}}^{-}(\epsilon\tau)]^2)\cos(2\tau/\epsilon) + 2S_{\mathbf{m}}^{+}(\epsilon\tau)S_{\mathbf{m}}^{-}(\epsilon\tau)\sin(2\tau/\epsilon) \quad (3.6)$$

where the functions $S_{\mathbf{m}}^{+}$ and $S_{\mathbf{m}}^{-}$ are defined as

$$S_{\mathbf{m}}^{+}(\tau) \equiv \int_0^\pi \frac{dk}{2\pi}[\cos k(l-\bar{l}) + \cos k(n-\bar{n}) - (l \leftrightarrow n)]\cos[\omega_\parallel^2(k)\tau/4\omega_0^2]. \quad (3.7)$$

$$S_{\mathbf{m}}^{-}(\tau) \equiv \int_0^\pi \frac{dk}{2\pi}[\cos k(l-\bar{l}) + \cos k(n-\bar{n}) - (l \leftrightarrow n)]\sin[\omega_\parallel^2(k)\tau/4\omega_0^2]. \quad (3.8)$$

We now turn to the parallel correlation function. The use of harmonic phonons in the parallel average implies

$$C_{\mathbf{m}}^{\parallel} = \int_0^\beta dx_1 dx_2 g_{\mathbf{m}}(x_1,x_2) h_{\mathbf{m}}(\tau, 2x_1x_2/\Gamma_\parallel)$$

where the functions $g_{\mathbf{m}}$ and $h_{\mathbf{m}}$ are given by

$$\begin{aligned} g_{\mathbf{m}}(x_1,x_2) &= (x_1x_2)^2 exp[-x_1(l-n) - x_2(\bar{l}-\bar{n}) \\ &\quad + 2[x_1^2 f_{l-n}(0) + x_2^2 f_{\bar{l}-\bar{n}}(0)]/\Gamma_\parallel], \end{aligned} \quad (3.9)$$

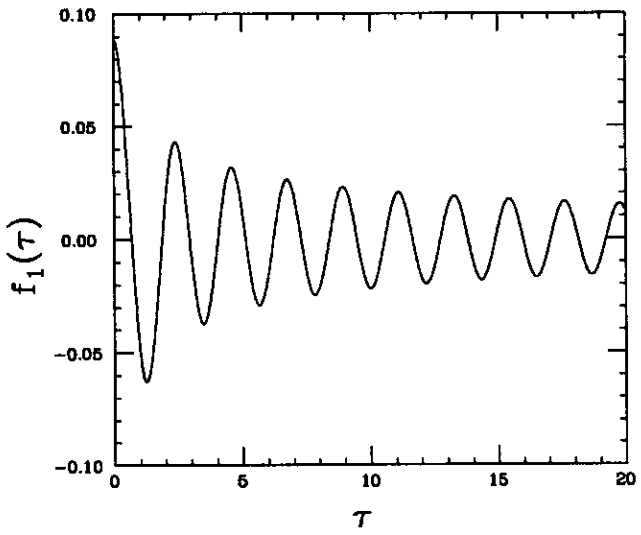

Figure 3.1: Plot of the parallel correlation function $f_1(\tau)$

$$h_{\mathbf{m}}(\tau,\alpha) \;=\; exp[-\alpha f_{l-l}(\tau) + f_{n-\bar{n}}(\tau) - (l \leftrightarrow n)], \tag{3.10}$$

and where the time dependence enters only through the correlation function $f_{l-n}(\tau) \equiv \Gamma_{\|} < z_{ln}(\tau) z_{ln}(0) > /4a^2$ which can be written in terms of the parallel phonon spectrum:

$$f_n(\tau) = \int_0^\pi dk \frac{1-\cos kn}{2\pi\omega_{\|}^2(k)/\omega_0^2} cos[\omega_{\|}(k)\tau/\omega_0].$$

As shown in Fig. 3.1, $f_n(\tau)$ is an oscillatory function. Furthermore, as we derived in Appendix 3D, when $\tau \to \infty$, the amplitude of this oscillation scales as $1/\sqrt{\tau} \to 0$.

In deriving this expression for $C_{\mathbf{m}}^{\|}$ we have employed the a technique discussed in Appendix 3C. We replace Z_{ln}^{-3} by a smoothed function dependent on a parameter β:

$$Z_{ln}^{-3} \simeq \int_0^\beta dx_1 x_1^2 exp(-x_1 Z_{ln}/a)/2a^3.$$

This is exact for $\beta \to \infty$, but for finite β it avoids the singularity in Z_{ln}^{-3} which

occurs for close collisions, i.e. when $Z_{ln} \to 0$. This singularity is disallowed under exact dynamics, but is allowed in the harmonic dynamics which we employ, and it would lead to a singular result for $C^{\|}_{\mathbf{m}}$ [this can be observed in $g_{\mathbf{m}}(x_1, x_2)$, which blows up as x_1 or x_2 approach ∞]. However, we will find that a range of large but finite β values exist for which $C^{\|}_{\mathbf{m}}$ is independent of β, provided that $\epsilon\Gamma_{\|} \gg 1$. Only then is $C^{\|}_{\mathbf{m}}$ dominated by small z displacements, just as in Eq. (3.1).

To evaluate Eq. (3.5) we first perform the time integral

$$I_{\mathbf{m}}(\epsilon, \alpha) \equiv \int_{-\infty}^{+\infty} d\tau C^{\perp}_{\mathbf{m}}(\tau, \epsilon) h_{\mathbf{m}}(\tau, \alpha).$$

The function $h_{\mathbf{m}}$, associated with parallel fluctuations, is slowly varying compared to the rapid oscillations of $C^{\perp}_{\mathbf{m}}$; this leads to an exponentially small result for $I_{\mathbf{m}}$. It is also important to note that $C^{\perp}_{\mathbf{m}} \to 0$ on a timescale of order $(\epsilon\omega_0)^{-1}$ due to phase mixing of the transverse phonons; that is, S^+ and $S^- \to 0$ on this time scale, so the integral is convergent. We evaluate $I_{\mathbf{m}}$ using the saddle point method in the complex τ plane. Since the integrand is an entire function of τ, we can deform the contour through the saddle points. Their positions depend on $\mathbf{m}$ but after examining $I_{\mathbf{m}}$ for different $\mathbf{m}$'s in Appendix 3E, we find that the integral obtained from nearest neighbor interactions, $\mathbf{m}^* = (l, l-1, l, l-1)$, dominates the final result for ν so we keep only this term.

In Fig.3.2 we show that the original integration path from $-\infty$ to ∞ is deformed to the new contour $\sum_{n=-\infty}^{\infty} L_n$, where L_n is the steepest decent path passing through the saddle point τ_n. The saddle point positions are then solutions of the saddle point equation $\dot{f}_1(\tau) = -i/\epsilon\alpha$. Because $f_1(Re[\tau])$ is oscillatory, as shown in Fig.3.2, there are an infinite number of solutions distributed symmetrically on each side of the imaginary τ axis, as well as one pure imaginary solution. However, for small ϵ only a few saddle points nearest $Re[\tau] = 0$ need to be kept, and in fact the

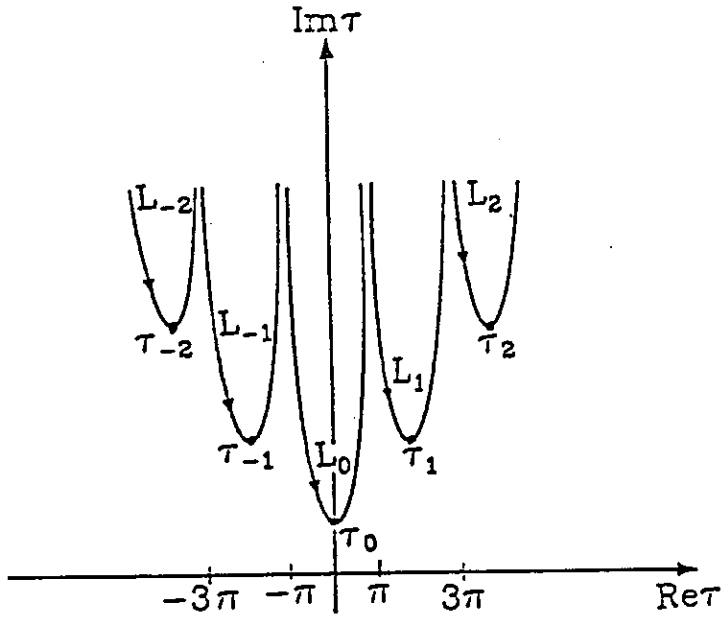

Figure 3.2: Plot of the steepest decent contour in the complex τ plane for the saddle point calculation of $I_{\mathbf{m}^*}(\epsilon, \alpha)$

pure imaginary saddle point gives the main trend of the integral. A comparison of the saddle point method and direct numerical integration is shown in Fig.3.3.

An important feature of Fig.3.3 is the abrupt steps in $I^*_{\mathbf{m}}$ at integer ratios between frequencies $2\omega_r$ and the maximum parallel phonon frequency $\omega_m = \eta\omega_0$. These steps are a consequence of the fact that the frequency spectrum of the harmonic parallel dynamics [described by $f_1(\tau)$] exhibits a sharp cut off at ω_m, as shown in Fig.3.4. This implies that a phonon-phonon interaction which creates or annihilates two transverse phonons and M parallel phonons can only occur if $M\omega_m > 2\omega_r$, or $\epsilon^{-1} < M\eta/2$. When ϵ^{-1} exceeds this value the process no longer contributes and the rate decreases abruptly. For very large ϵ^{-1} these steps are smoothed out and finally disappear because the rate is then determined by many high order processes, each of which has a small effect when taken individually.

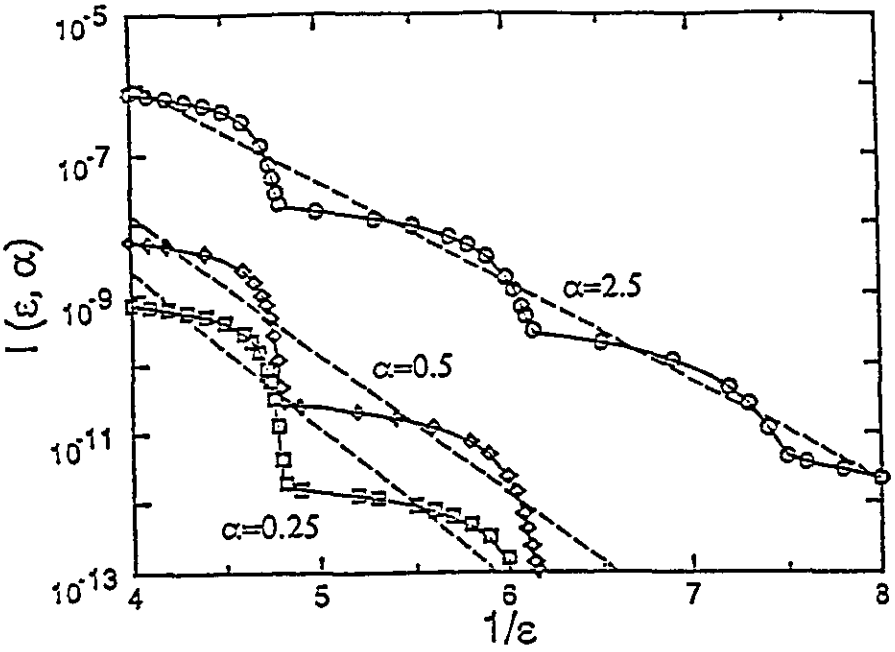

Figure 3.3: Plot of the time integral $I_{\mathbf{m}^*}(\epsilon, \alpha)$ for different α values. Solid lines: saddle point calculation keeping 11 saddle points on each side of the imaginary τ axis and the pure imaginary saddle point. Dashed lines: saddle point calculation keeping only the pure imaginary saddle point. Symbols: direct numerical integration; ◯: $\alpha = 2.5$; ◇: $\alpha = 0.5$ and □: $\alpha = 0.25$.

To complete the rate calculation we evaluate the integral

$$\bar{\nu}(\epsilon, \Gamma_{||}) \equiv (4\epsilon)^{-1} \int_0^\beta dx_1 dx_2 g_{\mathbf{m}^*}(x_1, x_2) I_{\mathbf{m}^*}(\epsilon, 2x_1 x_2/\Gamma_{||}). \tag{3.11}$$

The integral is performed by direct numerical integration. The equilibration rate $\nu \equiv \dot{T}_\perp/T_\perp$ can be written as $\nu = \omega_r(1 - T_\perp/T_{||})\bar{\nu}(\epsilon, \Gamma_{||})$ where the approximation $< J_0 > \simeq 2NkT_\perp/\omega_r$ has been employed. The integrand in Eq. (3.11) is sharply peaked near $x_1, x_2 \sim O(1/\epsilon)$, but begins to diverge at large x_1 and x_2 due to the aforementioned unphysical singularity in Z_{ln}^{-3} (see Fig.3.5). However, we find that the integral is independent of β provided that we choose $1/\epsilon \ll \beta \leq \Gamma_{||}$, which implies $\epsilon\Gamma_{||} \gg 1$. Only under this condition will the harmonic phonon approximation be valid.

The scaled equilibration rate $\bar{\nu}(\epsilon, \Gamma_{||})$ is shown in Fig.3.6. The rate is strongly

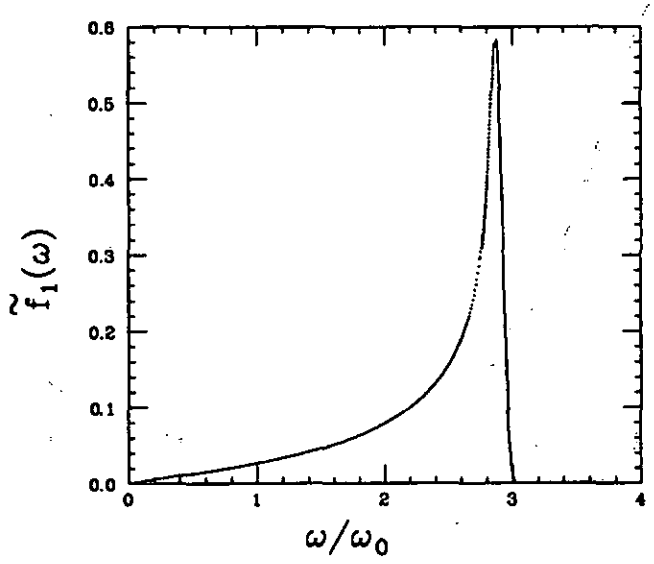

Figure 3.4: Plot of the Fourier transform of $f_1(\tau)$, which shows a sharp cutoff at the maximum parallel frequency $\omega_m = \sqrt{7\zeta(3)}\omega_0 \simeq 2.9\omega_0$.

reduced as ϵ decreases. As we have discussed, the rather striking steps in the rate stem from the existence of a maximum frequency in the parallel dynamics, and are a qualitative signature of the strongly correlated regime. Such steps do not occur in weakly correlated plasma where binary interactions dominate and no sharp frequency cutoff exists in the relative parallel dynamics. Indeed, Fig.3.6 shows that the steps decrease in magnitude as $\Gamma_{||}$ decreases.

The dashed line in Fig.3.6 is the result for $\bar{\nu}(\epsilon, \Gamma_{||})$ when only the single pure imaginary saddle point is kept in $I_{\mathbf{m}^*}$. In this case a saddle-point evaluation of the integrals in Eq. (3.11) yields

$$\bar{\nu}(\epsilon, \Gamma_{||}) = \sqrt{\pi^7\epsilon/8\eta^2}(\alpha_0\Gamma_{||})^{5/2}[S^+_{\mathbf{m}^*}(i\epsilon\tau_0) + S^-_{\mathbf{m}^*}(i\epsilon\tau_0)]^2 \cdot$$

$$exp[-2\tau_0/\epsilon + 2\alpha_0 f_1(i\tau_0) - \sqrt{2\Gamma_{||}\alpha_0}] \qquad (3.12)$$

where $\alpha_0 = (7/8 + 1/\eta\epsilon)^2/\Gamma_{||}$, $i\tau_0$ is the pure imaginary solution of the saddle point

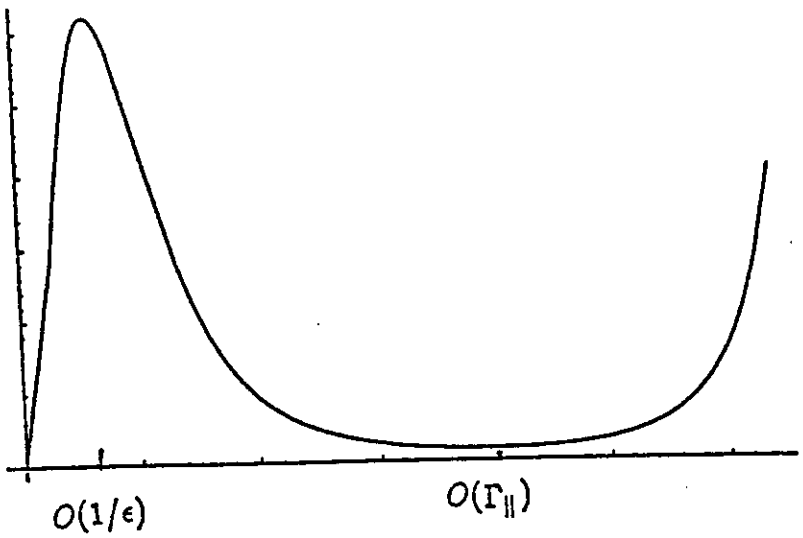

Figure 3.5: A schematic picture for the integrand in Eq.(3.10) along the $x_1 = x_2$ direction.

equation evaluated at $\alpha = \alpha_0$. When $\epsilon\Gamma_{||} \gg 1$, $\tau_0 \simeq \gamma + (\ln\gamma)/2\eta$, where $\gamma \equiv \ln[\sqrt{\pi\eta \ln 2}/\epsilon\alpha_0]/\eta$. Furthermore, for small $\epsilon\tau_0$,

$$S^+_{\mathbf{m}^*}(i\epsilon\tau_0) + S^-_{\mathbf{m}^*}(i\epsilon\tau_0) \simeq 1,$$

which simplifies Eq.(3.12). As either ϵ or $\Gamma_{||}$ decreases, Eq. (3.12) becomes a better approximation to $\bar{\nu}(\epsilon, \Gamma_{||})$ (see Fig.3.6). To lowest order in ϵ and $(\epsilon\Gamma_{||})^{-1}$ the exponential dependence in Eq. (3.12), $exp[-2\ln(\epsilon\Gamma_{||})/\eta\epsilon]$, is the same as the crude estimate of Eq. (3.1).

In order for our calculation to be valid, the aforementioned conditions $\epsilon \ll 1$, $\epsilon\Gamma_{||} \gg 1$ and $\Gamma_\perp \gg \epsilon^2\sqrt{\Gamma_{||}}$ must be satisfied. In fact, these conditions are not fully satisfied in the previous molecular dynamics calculation [6] (the last condition in particular) and therefore a detailed comparison between that calculation and the present analysis is not possible. However, Ref.[6] does document a decrease in the equilibration rate as ϵ decreases. New simulations are underway in order to test our

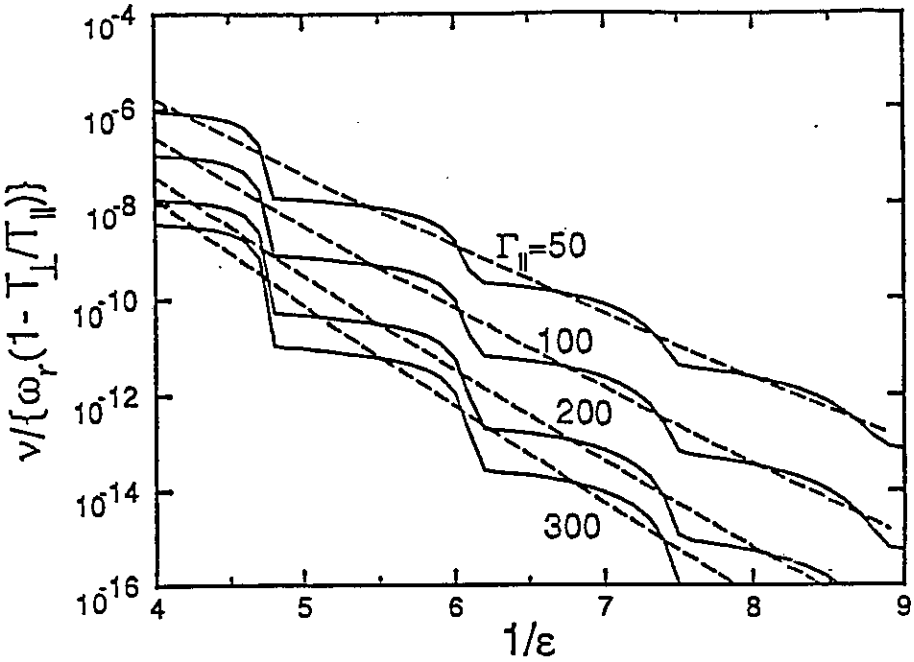

Figure 3.6: Plot of $\bar{\nu}(\epsilon, \Gamma_{||}) = \nu/\omega_r(1 - T_\perp/T_{||})$ for different values of $\Gamma_{||} \equiv q^2/aT_{||}$. Here ν is the equilibration rate, and $\epsilon \equiv \omega_0/\omega_r$. The dashed lines represent the results given by Eq.(3.11). Equation (3.5) becomes a better approximation for larger $1/\epsilon$ and smaller $\Gamma_{||}$.

results. We also note that other mechanisms, such as scattering with gas molecules or heating due to the r. f. micromotion in the trap, may contribute to the equilibration process in a real Paul trap or storage ring.

In addition, when the ion chain is confined in a ring configuration, it will be bent and in this case, between neighboring ions there exists a slowly time varying component of the transverse perturbing force:

$$\delta f_\perp = \frac{1}{2R}\frac{q^2}{|a + \delta z(t)|} + O\left(\frac{a}{R}\left(\frac{r(t)}{a}\right)^2\right) + O\left(\frac{a}{R}\right)^2,$$

where R is the curvature radius and $\delta z(t)$ is the relative parallel displacement and $r(t) = r_0 e^{i\omega_r t}$ is the relative transverse displacement. Furthermore $\delta f_\perp$ causes a change of the transverse kinetic energy given by

$$\frac{dE_\perp}{dt} \sim \delta f_\perp \cdot \dot{r}(t) \sim \frac{1}{2R}\frac{q^2 i\omega_r r_0}{|a + \delta z(t)|} e^{i\omega_r t},$$

which shows the coupling between one (rather than two) transverse mode and $M/2$ (rather than M) parallel modes. One may thus expect that the curvature effect causes a rate $\nu' \sim \frac{a}{R}\nu(2\epsilon, \Gamma)$. When $\frac{a}{R}$ is not sufficiently small , the curvature may play an important role. For example, the circular Paul trap experiments[1] $a \sim 5\mu m$ and $R \sim 1cm$ so $\frac{a}{R} \sim 5 \times 10^{-4}$. In storage ring experiments[6], typically $a \sim 1\mu m$, $R \sim 1m$ and $\frac{a}{R} \sim 10^{-6}$ is so small that ν' is negligible compared with ν, and in linear Paul trap experiments[2] $\frac{a}{R} = 0$.

Finally, it is worth noting that there is a strong similarity between the present problem and the perpendicular to parallel temperature equilibration of a crystallized single species plasma in the strong magnetization limit, where the cyclotron frequency is large compared with the plasma frequency; now the cyclotron frequency assumes the role of ω_r. This equilibration process has been examined by O'Neil and Hjorth for a weakly correlated plasma where the equilibration is driven by binary collisions.[7] However, a calculation analogous to that described here should also make it possible to extend our understanding of the equilibration process of a magnetized plasma into the strongly correlated regime. We discuss such a calculation in the next chapter.

3.2 Appendix 3A: Formalism for the Rate of the Breaking of an Adiabatic Invariant

In this appendix, we consider a Hamiltonian given by $H = H_0 + \delta H$, where H_0 and δH are the unperturbed and the perturbing Hamiltonian:

$$H_0 = \sum_{j=1}^{N} \frac{p_j^2}{2m} + \Phi_H$$

$$\delta H = \Phi - \Phi_H$$

Here Φ_H is the harmonic potential energy, which is a quadratic function of the particles' displacements and Φ is the total potential energy. In order to make connection to Chapter 3 and Chapter 4, where our formalism applies, we assume that H_0 describes $3N$ eigenmodes with large frequency separation, namely, one or two branches of the modes are high frequency modes and the rest of the modes are the low frequency modes. Therefore there must exist an adiabatic invariant associated with the high frequency modes. Supposing that there are n high frequency modes and $3N-n$ low frequency modes, then, as we derived in Chapter 3 and Chapter 4, through a series of canonical transformations, we can transform H_0 into the following general form in terms of the action-angle variables:

$$H_0 = \omega_0 J_0 + \sum_{j=1}^{n-1}(\omega_j - \omega_0)J_j + \sum_{l=1}^{3N-n}(\frac{P_l^2}{2m} + \frac{1}{2}m\omega_l^2 Q_l^2),$$

where J_0 is the sum of the actions of the n high frequency modes, and ω_j and $J_j (j \neq 0)$ are the frequency and action variable of the jth high frequency mode. ω_l and (Q_l, P_l) are the frequency and generalized (coordinate, momentum) pair of the lth low frequency mode. Since δH depends on all the angle variables θ_j conjugate to J_j, $\dot{J}_j = -\partial \delta H/\partial \theta_0 \neq 0$ and so J_0 is not exactly conserved. However, because $\omega_0 \gg |\omega_j - \omega_0|; \omega_l$, J_0 is an adiabatic invariant.

In this appendix we derive a formula for the rate of the change of the adiabatic invariant J_0 averaged over the statistical distribution D of the system:

$$< J_0 >= \int d\Lambda J_0 D(\Lambda)$$

where Λ is a point in the $6N$-dimensional phase space. We start with the Liouville Theorem:

$$\frac{dD}{dt} = \frac{\partial D}{\partial t} + [D, H] = 0$$

where $[\cdots]$ is the Poisson Bracket. Then

$$\frac{\partial D}{\partial t} = -[D, H]$$

and hence

$$\begin{aligned} \frac{d < J_0 >}{dt} &= \int d\mathbf{\Lambda} J_0 \frac{\partial D}{\partial t} \\ &= -\int d\mathbf{\Lambda} J_0 [D, H] \end{aligned}$$

Furthermore, we note that

$$J_0[D, H] = [J_0 D, H] - D[J_0, H]$$

which yields

$$\frac{d < J_0 >}{dt} = \int d\mathbf{\Lambda} D[J_0, H] \tag{3.13}$$

where we have used the fact that $\int d\mathbf{\Lambda}[J_0 D, H] = 0$.

In what follows, we perform a quasilinear calculation for $d < J_0 > /dt$. We assume that, on a short time scale, low order (phonon) collisions which do not break the adiabatic invariant keep the distribution function near a two temperature thermal equilibrium:

$$D_0(H, J_0) = Z^{-1} \exp[-\frac{\omega_0 J_0}{T_\perp} - \frac{H - \omega_0 J_0}{T_\parallel}]$$

However, on a long time scale, since J_0 is not an exact constant of motion, a fluctuation D_1 of the distribution function develops which may be obtained through the

solution of the Liouville's equation with D_0 as the initial condition:

$$\begin{aligned}\frac{dD}{dt} &= \frac{dD_0}{dt} + \frac{dD_1}{dt} \\ &= [D_0, H] + \frac{dD_1}{dt} \\ &= 0\end{aligned}$$

and so $D_1(t) = -\int_{-\infty}^{t}[D_0, H]_{\Lambda(t')}dt'$, where $[\cdots]_{\Lambda(t')}$ denotes the Poisson bracket evaluated at time t'. Substituting this expression for D_1 into Eq.(3.13) we obtain

$$\begin{aligned}\frac{d < J_0 >}{dt} &= \int d\Lambda(D_0(t) + D_1(t))[J_0, H]_{\Lambda(t)} \\ &= \int d\Lambda D_0(t)[J_0, H]_{\Lambda(t)} - \int d\Lambda[J_0, H]_{\Lambda(t)} \int_{-\infty}^{t}[D_0, H]_{\Lambda(t')}dt',\end{aligned}$$

where $d\Lambda$ means $d\Lambda(t)$. Furthermore, since

$$\begin{aligned}[D_0, H] &= \frac{\partial D_0}{\partial J_0}[J_0, H] \\ &= \omega_0(\frac{1}{T_{||}} - \frac{1}{T_\perp})D_0[J_0, H],\end{aligned}$$

we have

$$\int d\Lambda D_0(t)[J_0, H]_{\Lambda(t)} = \int d\Lambda \frac{[D_0, H]}{\omega_0(\frac{1}{T_{||}} - \frac{1}{T_\perp})} = 0.$$

Hence,

$$\begin{aligned}\int d\Lambda[J_0, H]_{\Lambda(t)} \int_{-\infty}^{t}[D_0, H]_{\Lambda(t')}dt' &= \int d\Lambda[J_0, H]_{\Lambda(t)} \\ &\int_{-\infty}^{t}\omega_0(\frac{1}{T_{||}} - \frac{1}{T_\perp})D_0(t')[J_0, H]_{\Lambda(t')}dt',\end{aligned}$$

which leads to

$$\frac{d < J_0 >}{dt} = \omega_0(\frac{1}{T_\perp} - \frac{1}{T_\parallel}) \int d\Lambda [J_0(t), H] \int_{-\infty}^{t} D_0(t')[J_0, H]_{\Lambda(t')} dt'$$

$$= \omega_0(\frac{1}{T_\perp} - \frac{1}{T_\parallel}) \int_{-\infty}^{t} dt' C(t - t'), \tag{3.14}$$

where

$$C(t - t') = \int d\Lambda D_0(t')[J_0, H]_{\Lambda(t)}[J_0, H]_{\Lambda(t')}$$

$$= < \frac{\partial H(t)}{\partial \theta_0} \frac{\partial H(t')}{\partial \theta_0} >$$

$$= < \dot{J}_0(t) \dot{J}_0(t') > .$$

Here <> denotes the statistical average $\int d\Lambda(t) D_0(t')$.

Since $\partial H_0 / \partial \theta_0 = 0$, we may write correlation function $C(t)$ as

$$\begin{aligned} C(t) &= < \frac{\partial \delta H(t)}{\partial \theta_0} \frac{\partial \delta H(0)}{\partial \theta_0} > \\ &= < \frac{\partial (\Phi(t) - \Phi_H(t))}{\partial \theta_0} \frac{\partial (\Phi(0) - \Phi_H(0))}{\partial \theta_0} > \\ &= < \frac{\partial \Phi(t)}{\partial \theta_0} \frac{\partial \Phi(0)}{\partial \theta_0} > - C_0(t) \end{aligned}$$

where

$$C_0(t) = < \frac{\partial \Phi_H(t)}{\partial \theta_0} \frac{\partial (\Phi(0) - \Phi_H(0))}{\partial \theta_0} > + < \frac{\partial \Phi(t)}{\partial \theta_0} \frac{\partial \Phi_H(0)}{\partial \theta_0} >$$

Since D_0 is (quasi) stationary, we have

$$< \frac{\partial \Phi(t)}{\partial \theta_0} \frac{\partial \Phi(0)}{\partial \theta_0} > \simeq < \frac{\partial \Phi(0)}{\partial \theta_0} \frac{\partial \Phi(-t)}{\partial \theta_0} > \tag{3.15}$$

and

$$< \frac{\partial\Phi(t)}{\partial\theta_0}\frac{\partial\Phi_H(0)}{\partial\theta_0} > \simeq < \frac{\partial\Phi(0)}{\partial\theta_0}\frac{\partial\Phi_H(-t)}{\partial\theta_0} >$$

We note that the time dependence of $C_0(t)$ is determined by $\frac{\partial\Phi_H(-t)}{\partial\theta_0}$, which is associated with the two phonon collisions due to the harmonic potential. In the diagrammatic picture of phonon collisions, such low order collisions do not contribute to the breaking of the adiabatic invariant, and we therefore neglect C_0. As a conclusion, we can effectively write the correlation function $C(t)$ as $< \frac{\partial\Phi(t)}{\partial\theta_0}\frac{\partial\Phi(0)}{\partial\theta_0} >$ and making use of Eq.(3.15) we may rewrite Eq.(3.14) as

$$\frac{d < J_0 >}{dt} = (\frac{1}{T_\perp} - \frac{1}{T_{||}})\frac{1}{2\varepsilon}\int_{-\infty}^{\infty} d\tau < \frac{\partial\Phi(t)}{\partial\theta_0}\frac{\partial\Phi(0)}{\partial\theta_0} > \tag{3.16}$$

where $\tau \equiv \omega_p t$.

3.3 Appendix 3B: Derivation of $C_{\mathbf{m}}^{\perp}(\tau,\epsilon)$

The perpendicular correlation $C_{\mathbf{m}}^{\perp}(\tau,\epsilon)$ of the 1D Coulomb chain is defined as

$$C_{\mathbf{m}}^{\perp}(\tau,\epsilon) \equiv \Gamma_\perp^2 < \partial r_{ln}^2(\tau)/\partial\theta_0 \partial r_{ln}^2(0)/\partial\theta_0 > /16a^4,$$

where $\tau = \omega_0 t$, ω_0 is the plasma frequency, and where the average is over an ideal phonon gas distribution. In this appendix we perform the statistical averaging to derive Eq. (3.6). All the notations in this appendix have the same meaning as that in Chapter 3.

We start with $r_{ln}^2 \equiv x_{ln}^2 + y_{ln}^2$ and then $\partial r_{ln}^2(\tau)/\partial\theta_0 = 2x_{ln}\partial x_{ln}/\partial\theta_0 + (x \leftrightarrow y)$. In order to calculate $\partial x_{ln}/\partial\theta_0$ and $\partial y_{ln}/\partial\theta_0$, we use the the inverse transformation

of Eq. (3.2):

$$(\mathbf{r}_l, \mathbf{p}_l) = N^{-1/2} \sum_k (\tilde{\mathbf{r}}_k e^{ikl}, \tilde{\mathbf{p}}_k e^{-ikl}).$$

and write x_{ln} as

$$x_{ln} = N^{-1/2} \sum_k \mu_{ln}(k) \tilde{x}_k \tag{3.17}$$

where

$$\mu_{ln}(k) = e^{ikl} - e^{ikn}$$

Furthermore, we transform $(\tilde{\mathbf{r}}_k, \tilde{\mathbf{p}}_k)$ to the action-angle variables through Eq. (3.3) and Eq. (3.4). We then find

$$\frac{\partial \tilde{x}_k}{\partial \theta_0} = \frac{\tilde{p}_{xk}}{m\omega_\perp(k)} \tag{3.18}$$

To calculate $C^\perp_{\mathbf{m}}(\tau, \epsilon)$ we write

$$C^\perp_{\mathbf{m}}(\tau, \epsilon) = < f_x(\tau) f_x(0) + f_y(\tau) f_y(0) > + < f_x(\tau) f_y(0) + f_y(\tau) f_x(0) > \tag{3.19}$$

where

$$f_x(\tau) \equiv \frac{\Gamma_\perp}{2a^2} x_{ln}(\tau) \frac{\partial x_{ln}(\tau)}{\partial \theta_0}$$

$$f_y(\tau) \equiv \frac{\Gamma_\perp}{2a^2} y_{ln}(\tau) \frac{\partial y_{ln}(\tau)}{\partial \theta_0}$$

Combining Eq. (3.17), Eq. (3.18) and using the equation of motion of the phonons:

$$\tilde{x}_k(t) = \tilde{x}_k \cos \omega_\perp(k) t + \frac{\tilde{p}_{xk}}{m\omega_\perp(k)} \sin \omega_\perp(k) t;$$

$$\tilde{p}_{xk}(t) = \tilde{p}_{xk} \cos \omega_\perp(k) t - m\omega_\perp(k) \tilde{x}_k \sin \omega_\perp(k) t,$$

we obtain

$$f_x(\tau) = \frac{\Gamma_\perp}{2Na^2}\sum_k\sum_{k'}\mu_{ln}(k)\mu_{ln}(k')[\tilde{x}_k\cos\omega_\perp(k)t+\frac{\tilde{p}_{xk}}{m\omega_\perp(k)}\sin\omega_\perp(k)t]\cdot$$

$$[\frac{\tilde{p}_{xk'}}{m\omega_\perp(k')}\cos\omega_\perp(k')t-\tilde{x}_{k'}\sin\omega_\perp(k')t]$$

$$= \frac{\Gamma_\perp}{2Na^2}\sum_k\sum_{k'}\mu_{ln}(k)\mu_{ln}(k')\tilde{x}_k\tilde{p}_{xk}\cos[\omega_\perp(k)+\omega_\perp(k')]t. \qquad (3.20)$$

In Eq. (3.20) the sum of the terms containing $\sin[\omega_\perp(k)+\omega_\perp(k')]t$ vanishes because these terms are antisymmetric under the exchange k and k'.

Furthermore, from Eq. (3.20) we have

$$< f_x(\tau)f_x(0) >$$

$$= \frac{{\Gamma_\perp}^2}{4a^4N^2}\sum_k\sum_{k'}\sum_{k''}\sum_{k'''}\mu_{ln}(k)\mu_{ln}(k')\mu_{\bar{l}\bar{n}}(k'')\mu_{\bar{l}\bar{n}}(k''')$$

$$= \cos[\omega_\perp(k)+\omega_\perp(k')]t\frac{<\tilde{x}_k\tilde{x}_{k''}><\tilde{p}_{xk'}\tilde{p}_{xk'''}>}{m\omega_\perp(k)\omega_\perp(k')}$$

$$= \frac{{\Gamma_\perp}^2{T_\perp}^2}{4a^4N^2m^2}\sum_k\sum_{k'}\mu_{ln}(k)\mu_{ln}(k')\mu_{\bar{l}\bar{n}}(k)\mu_{\bar{l}\bar{n}}(k)\frac{\cos[\omega_\perp(k)+\omega_\perp(k')]t}{\omega_\perp(k)^2\omega_\perp(k')^2}$$

$$= [\frac{\Gamma_\perp T_\perp}{2ma^2}]^2([\sum_k\mu_{ln}(k)\mu_{\bar{l}\bar{n}}(k)\frac{\cos\omega_\perp(k)t}{\omega_\perp(k)^2}]^2$$

$$-[\sum_k\mu_{ln}(k)\mu_{\bar{l}\bar{n}}(k)\frac{\sin\omega_\perp(k)t}{\omega_\perp(k)^2}]^2), \qquad (3.21)$$

where we have used

$$<\tilde{p}_{xk}\tilde{p}_{xk'}>=m\omega_\perp(k)\omega_\perp(k')<\tilde{x}_k\tilde{x}_{k'}>$$

$$= [m\omega_\perp(k)]^2 < \tilde{x}_k^2 > \delta_{kk'} = mT_\perp \delta_{kk'}.$$

We also find that $< f_x(\tau) f_x(0) > = < f_y(\tau) f_y(0) >$ and the cross terms $< f_x(\tau) f_y(0) >$ and $< f_y(\tau) f_x(0) >$ vanish because

$$< \tilde{x}_k \tilde{p}_{xk'} \tilde{y}_{k''} \tilde{p}_{yk'''} > = 0$$

for any k, k', k''' and k'''. Therefore we have $C_{\mathbf{m}}^{\perp}(\tau, \epsilon) = 2 < f_x(\tau) f_x(0) >$.

We next substitute the perpendicular dispersion relation

$$\omega_\perp(k) = \sqrt{\omega_\tau^2 - \omega_z^2(k)/2} \simeq \omega_\tau - \delta\omega,$$

where $\delta\omega \equiv \omega_z^2(k)/4\omega_\tau$, into Eq. (3.21) and obtain

$$< f_x(\tau) f_x(0) > \simeq [\frac{\Gamma_\perp T_\perp}{ma^2}]^2 \left([(S_{\mathbf{m}}^+)^2 - (S_{\mathbf{m}}^-)^2] \cos 2\omega_\tau t + 2 S_{\mathbf{m}}^+ S_{\mathbf{m}}^- \sin 2\omega_\tau t \right)$$

where

$$S_{\mathbf{m}}^+ = \frac{1}{2N} \sum_k \mu_{ln}(k) \mu_{\bar{l}\bar{n}}(k) \cos \delta\omega t$$

$$S_{\mathbf{m}}^- = \frac{1}{2N} \sum_k \mu_{ln}(k) \mu_{\bar{l}\bar{n}}(k) \sin \delta\omega t$$

One may easily check that $S_{\mathbf{m}}^+$ and $S_{\mathbf{m}}^-$ are equal to $S_{\mathbf{m}}^+(\varepsilon\tau)$ and $S_{\mathbf{m}}^-(\varepsilon\tau)$ defined by Eq. (3.7) and Eq. (3.8) by changing $\sum_k$ to $\frac{N}{\pi} \int_0^\pi dx$ with $x \equiv ka$. Furthermore, since $\Gamma_\perp \equiv q^2/kT_\perp$ and $\omega_0^2 = q^2/ma^3$, one may see that $[\Gamma_\perp T_\perp / ma^2]^2 = \varepsilon^4$, where $\varepsilon \equiv \omega_0/\omega_\tau$. Finally, noticing that $< f_x(\tau) f_x(0) > = < f_y(\tau) f_y(0) >$, Eq. (3.19) can be written as Eq. (3.6).

3.4 Appendix 3C: Calculation of the Parallel Correlation Function —— $< e^{-t_1 z_{ln}(t)} e^{-t_2 z_{l'n'}(0)} >$

In this appendix we calculate the correlation function $< e^{-t_1 z_{ln}(t)} e^{-t_2 z_{l'n'}(0)} >$, where t_1 and t_2 are parameters which can either be real or complex and z_{ln} and $z_{l'n'}$ are the relative displacement of particles in the $\hat{z}$ direction. This correlation function is important because it appears in the calculation for the rate of the breaking of the adiabatic invariant in both Chapter 3 and Chapter 4. In Chapter 3 the $\hat{z}$ is direction is along the chain axis while in Chapter 4, the $\hat{z}$ axis directed along the magnetic field. In both cases, the displacements are written in terms of the Fourier components through either Eq. (3.2) (complex form) or through Eq. (4.4) (real form). The result for this correlation function does not depend on which form we choose. In order to simplify the algebra, we here choose the real form :

$$z_{ln}(t) = \sqrt{\frac{2}{N}} \sum_{\mathbf{k}>0} \left([z_{\mathbf{k}}(0) \cos \omega_z(\mathbf{k}) t + \frac{\dot{z}_{\mathbf{k}}(0)}{\omega_z(\mathbf{k})} \sin \omega_z(\mathbf{k}) t] c_{ln} \right.$$

$$\left. [z_{-\mathbf{k}}(0) \cos \omega_z(\mathbf{k}) t + \frac{\dot{z}_{-\mathbf{k}}(0)}{\omega_z(\mathbf{k})} \sin \omega_z(\mathbf{k}) t] s_{ln} \right) \tag{3.22}$$

$$c_{ln} = \cos \mathbf{k} \cdot \mathbf{R}_n - \cos \mathbf{k} \cdot \mathbf{R}_l$$

$$s_{ln} = \sin \mathbf{k} \cdot \mathbf{R}_n - \sin \mathbf{k} \cdot \mathbf{R}_l$$

where $\mathbf{R}_l$'s are the equilibrium positions for the charges. In Eq.(3.22), $\sum_{\mathbf{k}>0}$ denotes the sum over half of the Brillouin zone. We note that when the total number of the particle N is an odd number, the sum over $\mathbf{k}$ may leave out a single point on the edge of the Brillouin zone. However for large N, this single point makes negligible contribution and is therefore ignorable.

In the harmonic approximation the phonon coordinates $(z_{\mathbf{k}}, \dot{z}_{\mathbf{k}})$ evolve along the trajectory of a simple harmonic oscillator with frequency $\omega_z(\mathbf{k})$:

$$z_{\mathbf{k}}(t) = z_{\mathbf{k}} \cos \omega_z(\mathbf{k})t + \frac{\dot{z}_{\mathbf{k}}}{\omega_z(\mathbf{k})} \sin \omega_z(\mathbf{k})t. \tag{3.23}$$

The statistical average is taken for the distribution of a ideal phonon gas:

$$D_0 = \prod_{\mathbf{k}} \frac{m\omega_z(\mathbf{k})}{2\pi T_{\|}} e^{-\frac{m[\dot{z}_{\mathbf{k}}^2 + \omega_z^2(\mathbf{k}) z_{\mathbf{k}}^2]}{2T_{\|}}},$$

which is normalized as

$$\int\int \cdots \int \prod_{\mathbf{k}} (dz_{\mathbf{k}} d\dot{z}_{\mathbf{k}}) D_0 = 1.$$

Then we can write $< e^{-t_1 z_{ln}(t)} e^{-t_2 z_{l'n'}(0)} >$ as the following integral

$$\int\int \cdots \int \prod_{\mathbf{k}} (dz_{\mathbf{k}} d\dot{z}_{\mathbf{k}}) D_0 e^{-t_1 z_{ln}(t)} e^{-t_2 z_{l'n'}(0)}.$$

To evaluate this integral, we substitute Eq. (3.22) and Eq. (3.23) for $z_{ln}(t)$ and $z_{l'n'}(0)$. By completing the squares in the exponent, we obtain

$$\begin{aligned} &< e^{-t_1 z_{ln}(t)} e^{-t_2 z_{l'n'}(0)} > \\ &= e^{\frac{2T_{\|}}{m\omega_0^2}\{t_1^2 f_{l-n}(0) + t_2^2 f_{l'-n'}(0)\}} \\ &\quad e^{-\frac{2T_{\|} t_1 t_2}{m\omega_0^2}\{[f_{l-l'}(\tau) + f_{n-n'}(\tau) - f_{l-n'}(\tau) - f_{l'-n}(\tau)]\}} \end{aligned} \tag{3.24}$$

where $\omega_0 \equiv \sqrt{q^2/ma^3}$ (a is the inter-particle distance) is the characteristic frequencies of the parallel plasma oscillation for a 1D chain, and $\tau \equiv \omega_0 t$. The function $f_{l-n}(\tau)$ is defined as

$$f_{l-n}(\tau) \equiv \frac{1}{N} \sum_{\mathbf{k}>0} \frac{1 - \cos \mathbf{k} \cdot (\mathbf{R}_l - \mathbf{R}_n)}{\bar{\omega}_z(\mathbf{k})^2} \cos \bar{\omega}_z(\mathbf{k})\tau, \tag{3.25}$$

where $\bar{\omega}_z(\mathbf{k}) \equiv \omega_z(\mathbf{k})/\omega_0$.

In order to uncover the physical meaning of the function $f_{l-n}(\tau)$, we let $t_1 = t_2 = 0$ after taking the derivative $\partial^2/\partial t_1 \partial t_2$ on both sides of Eq.(3.24) and we are left with

$$< z_{ln}(t) z_{l'n'}(0) >= \frac{2T_{\|}}{m\omega_0^2}[f_{l-n'}(\tau) + f_{l'-n}(\tau) - f_{l-l'}(\tau) - f_{n-n'}(\tau)]$$

In particular, for the diagonal case: $l = l', n = n'$, we obtain

$$f_{l-n}(\tau) = \frac{m\omega_0^2}{4T_{\|}} < z_{ln}(t) z_{ln}(0) > \tag{3.26}$$

which implies that, $f_{l-n}(\tau)$ is effectively the correlation function of the particles' relative parallel displacements.

To calculate the function $f_{l-n}(\tau)$ given by Eq. (3.25), we will convert the sum of the wavevector into an integral form. Specifically, we will replace $\sum_{\mathbf{k}>0}$ by

$$\int_0^{\pi/a} \frac{Nadk}{2\pi}.$$

We note that when applying Eq.(3.24), Eq.(3.25) and Eq.(3.26) to a crystallized 3D plasma, we will replace ω_0 by the plasma frequency $\omega_p \equiv \sqrt{\frac{4\pi ne^2}{m}}$ (n is the density). Also, for the 3D case, we transform $\sum_{\mathbf{k}>0}$ into an integral in the Brillouin zone:

$$\frac{1}{2}\int_{B.Z.} \frac{Nvd^3\mathbf{k}}{(2\pi)^3},$$

where v is the volume of the Brillouin zone which equals $4a_0^3$ for a body-centered cubic lattice. Here $a_0 = a/2$ is half of the lattice constant.

3.5 Appendix 3D: Asymptotic Expression for $f_l(i\bar{t})$ in the $|\bar{t}| \gg 1$ Limit

In this appendix, we derive an asymptotic formula for the correlation function $f_l(i\bar{t})$ in the $|\bar{t}| \gg 1$ limit, where $f_l(i\bar{t})$ is defined by equation (3.25) for a one-dimensional Coulomb chain.

For a 1-D system, $f_l(i\bar{t})$ can be written as

$$f_l(i\bar{t}) = \int_0^\pi \frac{dx}{2\pi} \frac{1-\cos lx}{\bar{\omega}_z^2} \cosh(\bar{\omega}_z \bar{t}) \tag{3.27}$$

where $x = ka$ is the wavenumber normalized by the inter-particle spacing a and the normalized longitudinal oscillation frequency $\bar{\omega}_z \equiv \omega_z/\omega_0$ is given by

$$\bar{\omega}_z = 2\sqrt{2\sum_{n=1}^{\infty} \sin^2(\frac{nx}{2})/n^3} \tag{3.28}$$

which is plotted in Fig.3.7 as a function of x. Furthermore, in terms of the special function $\Phi(z,s,v)$[9], $\bar{\omega}_z$ can be written as

$$\bar{\omega}_z = 2\sqrt{\Phi(1,3,1) - Re\Phi(e^{ix},3,1)}.$$

when $|\bar{t}| \gg 1$, $f_l(i\bar{t})$ is dominated by the contribution from the stationary phase point corresponding to the maximum value of $\omega_z(x)$, which occurs at $x = \pi$. In order to obtain an expression for ω_z near the maximum, we first calculate the derivatives:

$$\frac{d}{dx}(\bar{\omega_z}^2) = 4\sum_{n=1}^{\infty} \frac{\sin nx}{n^2}$$

$$\frac{d^2}{dx^2}(\bar{\omega_z}^2) = 4\sum_{n=1}^{\infty} \frac{\cos nx}{n^2} = -2\ln[2(1-\cos x)]$$

$$\frac{d^3}{dx^3}(\bar{\omega_z}^2) = -2\cot\frac{x}{2}$$

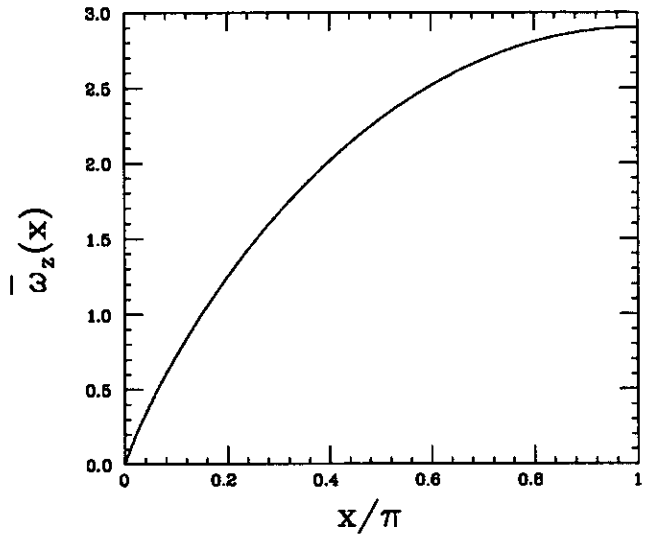

Figure 3.7: Plot of the parallel dispersion relation $\bar{\omega}_z(x)$ for a Coulomb chain, where $x \equiv ka$

$$\frac{d^4}{dx^4}(\bar{\omega_z}^2) \;=\; \csc^2(\frac{x}{2})$$

With these derivatives, we can expand $\bar{\omega_z}^2$ in terms of $\Delta = \pi - x \ll 1$ as

$$\bar{\omega_z}^2 \simeq \eta^2 - 2\eta b\Delta^2 + \frac{\Delta^4}{24}$$

and hence

$$\bar{\omega_z} \simeq \eta - b\Delta^2 + c\Delta^4$$

where

$$\eta = \sqrt{7\zeta(3)}; b = \frac{\ln 2}{\eta}; c = (\frac{1}{24} - b^2)/(2\eta).$$

Finally, we substitute the approximate expression for $\bar{\omega_z}$ into Eq.(3.27). By changing the integration variable from x to Δ and changing the upper integration

limit from π to ∞, we obtain

$$f_l(i\bar{t}) = \int_0^\infty \frac{d\Delta}{2\pi} \frac{1-\cos l(\pi-\Delta)}{\eta^2 - 2\eta b\Delta^2 + \frac{\Delta^4}{24}} \cosh[\bar{t}(\eta - b\Delta^2 + c\Delta^4)]$$

$$\simeq \frac{e^{\eta\bar{t}}}{4\pi}\int_0^\infty d\Delta[1-(-1)^l\cos(l\Delta)][1+\frac{2b}{\eta}\Delta^2+(\frac{3b^2}{\eta^2}-\frac{2c}{\eta})\Delta^4][1+c\bar{t}\Delta^4]e^{-b\bar{t}\Delta^2}$$

$$\simeq \frac{e^{\eta\bar{t}}}{4\pi\eta^2}\sqrt{\frac{\pi}{b\bar{t}}}[\frac{1-(-1)^l}{2}+\frac{\gamma_1}{\bar{t}}+O(\frac{1}{\bar{t}^2})] \tag{3.29}$$

where

$$\gamma_1 = [1-(-1)^l](\frac{1}{2\eta}+\frac{3c}{8b^2})+(-1)^l\frac{l^2}{8b}$$

In Fig.3.8 we plot both the asymptotic result given by Eq. (3.29) and the result of direct numerical integration for $f_1(i\bar{t})$. We see that two results approach each other for large $\bar{t}$.

3.6 Appendix 3E: Discussions of the time integral $I_{\mathbf{m}}(\epsilon,\alpha)$

In this appendix we discuss the function $I_{\mathbf{m}}(\epsilon,\alpha)$ defined in Chapter 3 as

$$I_{\mathbf{m}}(\epsilon,\alpha) \equiv \int_{-\infty}^{+\infty} d\tau C^{\perp}_{\mathbf{m}}(\tau,\epsilon)h_{\mathbf{m}}(\tau,\alpha) \tag{3.30}$$

for different $\mathbf{m} \equiv (l,n,\bar{l},\bar{n})$, where $C^{\perp}_{\mathbf{m}}(\tau,\epsilon)$ and $h_{\mathbf{m}}(\tau,\alpha)$ are defined by Eq. (3.6) and Eq. (3.10) respectively. We first perform an analytical saddle point analysis for $I_{\mathbf{m}}(\epsilon,\alpha)$ in the $\varepsilon \ll 1$ limit and then we present the result of the numerical integration. As a conclusion of our discussion, we find that $\mathbf{m} = \mathbf{m}^* \equiv (l,l-1,l,l-1)$ gives the largest result for $I_{\mathbf{m}}(\epsilon,\alpha)$.

In order to make the algebra simple, we replace τ by $i\bar{t}$ in Eq. (3.30) and we

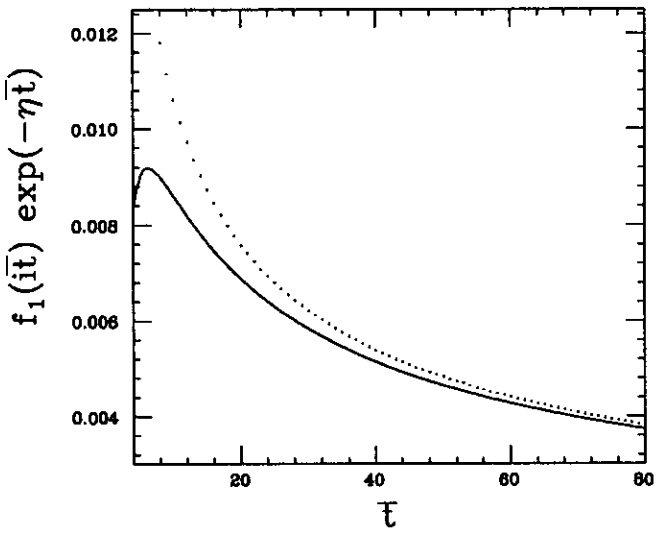

Figure 3.8: A comparison between the asymptotic expression and numerical integration result for $f_1(i\bar{t})$, where $\eta \equiv \sqrt{7\zeta(3)}$. The exponential factor in the asymptotic expression of $f_1(i\bar{t})$ (see Eq.(3.29)) has been pulled out by $e^{-\eta\bar{t}}$. In this figure, the solid line represents the asymptotic result and the dotted line represents the numerical result.

may then write the saddle point equation as

$$\frac{d}{d\bar{t}}[f_{l-\bar{n}}(i\bar{t}) + f_{n-\bar{l}}(i\bar{t}) - f_{l-\bar{l}}(i\bar{t}) - f_{n-\bar{n}}(i\bar{t})] = \frac{2}{\epsilon\alpha} \tag{3.31}$$

In the $\epsilon \ll 1$ limit, the solution for $\bar{t}$ is expected to be large and so we employ Eq. (3.29) for the asymptotic formula of $f_l(i\bar{t})$ (see Appendix 3D):

$$f_l(i\bar{t}) \simeq \frac{e^{\eta\bar{t}}}{4\pi\eta^2}\sqrt{\frac{\pi}{b\bar{t}}}[\frac{1-(-1)^l}{2} + \frac{\gamma_1}{\bar{t}} + O(\frac{1}{\bar{t}^2})], \tag{3.32}$$

where

$$\gamma_1 = [1-(-1)^l](\frac{1}{2\eta} + \frac{3c}{8b^2}) + (-1)^l\frac{l^2}{8b},$$

$$\eta \equiv \sqrt{7\zeta(3)}; b \equiv \frac{\ln 2}{\eta}; c \equiv (\frac{1}{24} - b^2)/(2\eta).$$

Taking the derivative for Eq. (3.32), we obtain, to the lowest order in $1/\bar{t}$,

$$\frac{\partial}{\partial \bar{t}} f_l(i\bar{t}) \simeq \frac{e^{\eta \bar{t}}}{4\pi\eta}\sqrt{\frac{\pi}{b\bar{t}}}[\frac{1-(-1)^l}{2} + \frac{1}{\bar{t}}(\gamma_1 - \frac{1-(-1)^l}{2\eta})].$$

Eq. (3.31) then becomes

$$\frac{e^{\eta \bar{t}}}{2\pi\eta}\sqrt{\frac{\pi}{b\bar{t}}}(\mu_{\mathbf{m}} + \frac{\beta_{\mathbf{m}}}{\bar{t}}) = \frac{2}{\epsilon\alpha} \tag{3.33}$$

where

$$\mu_{\mathbf{m}} \equiv \frac{1}{4}[(-1)^{l-\bar{l}} + (-1)^{n-\bar{n}} - (l \leftrightarrow n)]$$

$$\beta_{\mathbf{m}} \equiv (\frac{1}{2\eta} + \frac{3c}{8b^2})\mu_{\mathbf{m}} + \frac{1}{16b}[(-1)^{l-\bar{n}}(l-\bar{n})^2 + (-1)^{n-\bar{l}}(n-\bar{l})^2 - (l \leftrightarrow n)]$$

Since $\mu_{\mathbf{m}}$ can be either 0 or ± 1 for different $\mathbf{m}$'s. we discuss these three cases separately:

(1)For $\mu_{\mathbf{m}} = 1$, which occurs when both $l-n$ and $\bar{l}-\bar{n}$ are odd and $l-\bar{l}$ is even, an iterative solution for $\bar{t}$ is

$$\bar{t}_j \simeq \gamma_2 + \frac{i2\pi j}{\eta} + \frac{1}{2\eta}\ln(\gamma_2 + \frac{i2\pi j}{\eta}) - \frac{\beta_{\mathbf{m}}}{\eta \bar{t}_j} \tag{3.34}$$

where $j = 0, \pm 1, \pm 2, \cdots$, and

$$\gamma_2 \equiv \frac{1}{\eta}\ln\left(\frac{4\eta\sqrt{b\pi}}{\epsilon\alpha}\right).$$

According to the saddle point method, $I_{\mathbf{m}}(\epsilon, \alpha)$ is determined by the exponentially small factor $exp[-2Re(\bar{t})/\epsilon]$. From Eq.(3.34), we have

$$Re(\bar{t}_j) \simeq \gamma_2 + \frac{1}{2\eta}\ln\sqrt{\gamma_2^2 + \left(\frac{2\pi j}{\eta}\right)^2},$$

and

$$\frac{exp[-2Re(\bar{t}_j)/\epsilon]}{exp[-2Re(\bar{t}_0)/\epsilon]} \simeq \left[1+\left(\frac{2\pi j}{\gamma_2\eta}\right)^2\right]^{-1/2\eta\epsilon},$$

which is exponentially small for $j \neq 0$ and $\epsilon \ll 1$. Therefore, $I_{\mathrm{m}}(\epsilon,\alpha)$ is dominated by the $j=0$ saddle point, which has a real part

$$Re(\bar{t}_0) \simeq \gamma_2 + \frac{1}{2\eta}\ln\gamma_2 - \frac{\beta_{\mathrm{m}}}{\eta\bar{t}_0} \tag{3.35}$$

(2)For $\mu_{\mathrm{m}} = 0$, which occurs when $l-n$ is odd (even) and $\bar{l}-\bar{n}$ is even (odd), or both $l-n$ and $\bar{l}-\bar{n}$ are even, by the same argument used for the $\mu_{\mathrm{m}} = 1$ case, we find that $I_{\mathrm{m}}(\epsilon,\alpha)$ is dominated by the pure real saddle point which has the minimum real part given by:

$$Re(\bar{t}_0) \simeq \gamma_2 + \frac{1}{2\eta}\ln\gamma_2 - \frac{1}{\eta}Re[\ln\frac{\beta_{\mathrm{m}}}{\bar{t}_0}]. \tag{3.36}$$

(3)For $\mu_{\mathrm{m}} = -1$, which occurs when $l-n$, $\bar{l}-\bar{n}$ and $l-\bar{l}$ are all odd, by the same argument used for the $\mu_{\mathrm{m}} = 1$ case, we find that $I_{\mathrm{m}}(\epsilon,\alpha)$ is dominated by the pair of the saddle points closest to the real $\bar{t}$ axis. They have the (equal) minimum real parts given by:

$$Re(\bar{t}_0) \simeq \gamma_2 + \frac{1}{2\eta}\ln\sqrt{\gamma_2^2+\pi^2} + \frac{\beta_{\mathrm{m}}}{\eta\bar{t}_0} \tag{3.37}$$

By comparing Eq. (3.35), Eq. (3.36) and Eq. (3.37), we find that the $\mu_{\mathrm{m}} = 1$ case gives the smallest $Re(\bar{t}_0)$. Here we have assumed that $|\beta_{\mathrm{m}}/\bar{t}_j \ll 1|$, which is the condition that must be satisfied in order for the asymptotic expression given by Eq. (3.32) to be valid.

Furthermore, for the $\mu_{\mathrm{m}} = 1$ case, $Re(\bar{t}_0)$ reaches the minimum when β_{m},

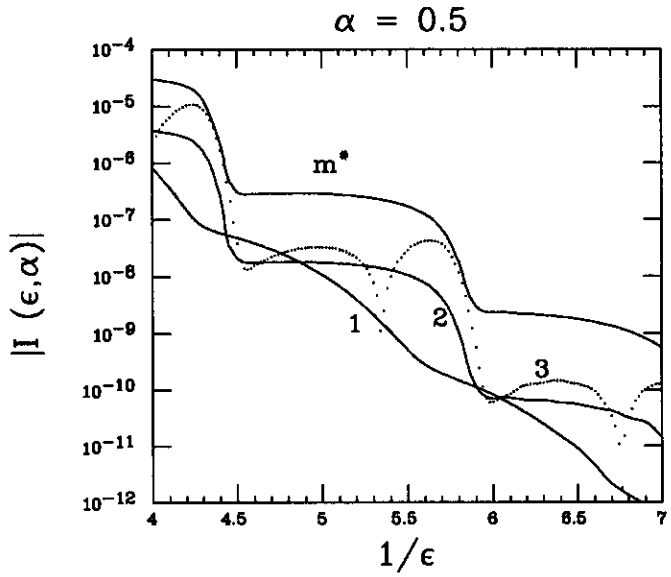

Figure 3.9: A comparison of $I_{\mathbf{m}}(\epsilon,\alpha)$ for different $\mathbf{m}$'s. Curve 1: $\mathbf{m} = (l, l-1, l, l-2), \mu_{\mathbf{m}} = 0$; Curve 2: $\mathbf{m} = (l, l-1, l, l-3), \mu_{\mathbf{m}} = 1$; Curve 3: $\mathbf{m} = (l, l-1, l-1, l-2), \mu_{\mathbf{m}} = -1$. Here we see that Curve 1, Curve 2 and Curve 3 are all below the Curve $\mathbf{m}^*$.

given by

$$\beta_{\mathbf{m}} = \frac{1}{2\eta} + \frac{3c}{8b^2} - \frac{1}{16b}[(l-\bar{n})^2 + (n-\bar{l})^2 + (l-\bar{l})^2 + (n-\bar{n})^2]$$

is the maximum, which occurs for $\mathbf{m} = \mathbf{m}^* = (l, l-1, l, l-1)$. This proves that in the $\epsilon \ll 1$ limit, $\mathbf{m} = \mathbf{m}^*$ gives the largest $I_{\mathbf{m}}(\epsilon,\alpha)$.

For a general case, Eq. (3.32) is no longer a good approximation for $f_l(i\bar{t})$ and we must check our conclusion numerically. The result of $|I_{\mathbf{m}}(\epsilon,\alpha)|$ for several typical $\mathbf{m}$'s are plotted in Fig.3.9 for $\alpha = 0.5$, where $|I_{\mathbf{m}}(\epsilon,\alpha)|$'s are calculated through direct numerical integrations. Here we take the absolute value of $I_{\mathbf{m}}(\epsilon,\alpha)$ because for $\mu_{\mathbf{m}} = -1$, $I_{\mathbf{m}}(\epsilon,\alpha)$ is oscillatory and could be negative for some values of the argument (ϵ,α). From the figure, we see that $\mathbf{m} = \mathbf{m}^*$ indeed gives the largest result for $I_{\mathbf{m}}(\epsilon,\alpha)$.

The saddle point calculation for $I_{\mathbf{m}^*}(\epsilon,\alpha)$ is straightforward. For $\epsilon \ll 1$, we

only need to keep the contribution from $\bar{t}_0$, by using the approximation $f_1''(i\bar{t}_0) \simeq f_1'(i\bar{t}_0)$ we obtain

$$I_{\mathbf{m}^*}(\epsilon,\alpha) \simeq \sqrt{\pi\epsilon}[S^+_{\mathbf{m}^*}(i\epsilon\bar{t}_0) + S^-_{\mathbf{m}^*}(i\epsilon\bar{t}_0)]^2 e^{\frac{-2\bar{t}_0}{\epsilon}} + \alpha f_1(i\bar{t}_0) \tag{3.38}$$

3.7 Appendix 3F: Derivation of the Equilibration Rate $\bar{\nu}(\varepsilon, \Gamma_\parallel)$

In this appendix, we derive the equilibration rate $\bar{\nu}(\varepsilon, \Gamma_\parallel)$ given by Eq. (3.12) in Chapter 3. We begin with equation Eq. (3.11):

$$\bar{\nu}(\epsilon,\Gamma_\parallel) \equiv (4\epsilon)^{-1} \int_0^\beta \int_0^\beta dx_1 dx_2 (x_1 x_2)^2 e^{-x_1 - x_2 + \frac{2f_1(0)}{\Gamma_\parallel}(x_1^2 + x_2^2)} I_{\mathbf{m}^*}(\epsilon, 2x_1x_2/\Gamma_\parallel). \tag{3.39}$$

By changing the integration variables to $(u,v) \equiv (x_1 + x_2, x_1 x_2)$, we rewrite $\bar{\nu}(\varepsilon, \Gamma_\parallel)$ as

$$\bar{\nu}(\epsilon,\Gamma_\parallel) = (4\epsilon)^{-1} \int_0^{\beta^2} dv v^2 e^{-\frac{4v}{\Gamma_\parallel} f_1(0)} I_{\mathbf{m}^*}(\epsilon, 2v/\Gamma_\parallel) \int_{\sqrt{4v}}^{\beta + v/\beta} \frac{du}{\sqrt{u^2 - 4v}} e^{-u + \frac{2}{\Gamma_\parallel} f_1(0) u^2}$$

We perform the u integral first. As shown in Fig.3.10, the integrand for the u integral goes to ∞ at $u = \sqrt{4v}$ due to the Jacobian $1/\sqrt{u^2 - 4v}$. It also starts to blow up at $u \simeq \Gamma_\parallel / 4f_1(0)$, corresponding to the contribution from the close collisions, which must be avoided in the harmonic approximation. We thus choose β such that

$$1 \ll \beta + v/\beta \ll \Gamma_\parallel / 4f_1(0) \tag{3.40}$$

In this case, we may neglect the small term $\frac{2}{\Gamma_\parallel} f_1(0) u^2$ and take $\beta + v/\beta \to \infty$. We then obtain

$$\int_{\sqrt{4v}}^{\beta + v/\beta} \frac{du}{\sqrt{u^2 - 4v}} e^{-u + \frac{2}{\Gamma_\parallel} f_1(0) u^2} \simeq K_0(2\sqrt{v}) \tag{3.41}$$

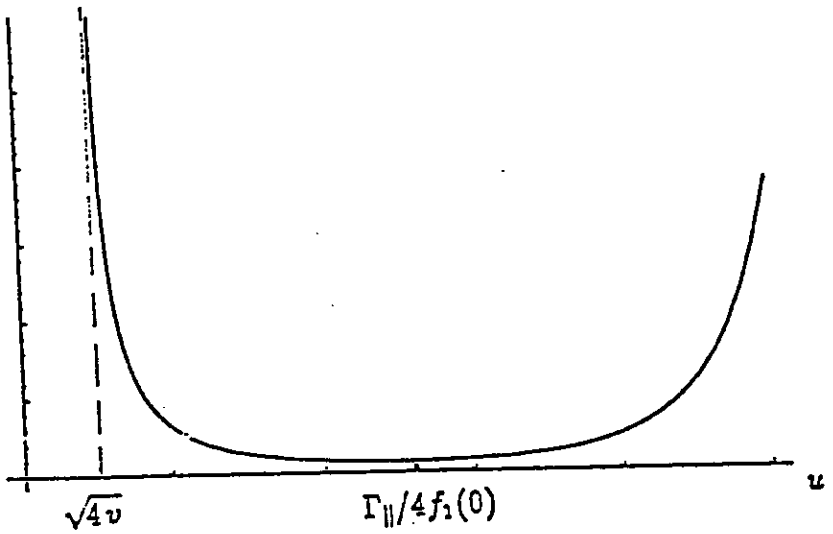

Figure 3.10: Plot of the integrand of the $u-$integral

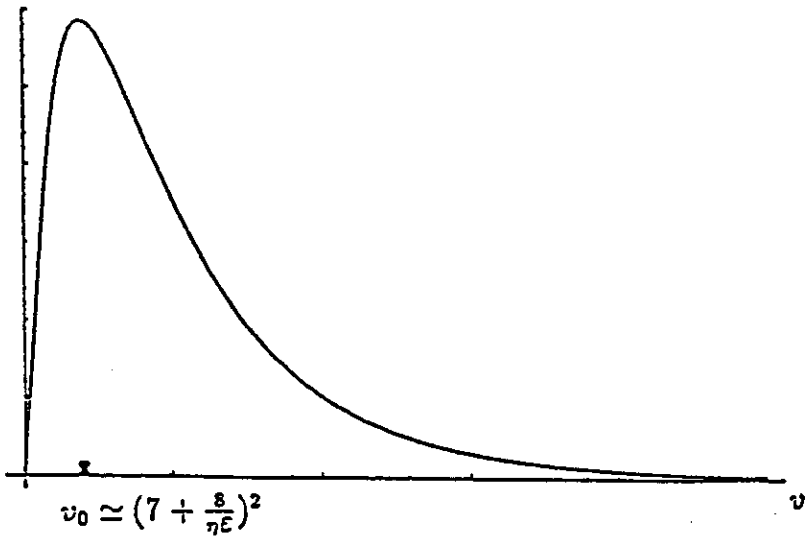

Figure 3.11: Plot of the integrand of the $v-$integral

We next complete the v integral:

$$\bar{\nu}(\epsilon,\Gamma_{\|}) \simeq (4\epsilon)^{-1}\int_0^{\beta^2} dv v^2 e^{-\frac{4v}{\Gamma_{\|}}f_1(0)} K_0(2\sqrt{v}) I_{\mathbf{m}^*}(\epsilon, 2v/\Gamma_{\|}) \qquad (3.42)$$

Using Eq. (3.38) for $I_{\mathbf{m}^*}(\epsilon, 2v/\Gamma_{\|})$ and the asymptotic formula for the $K_0(2\sqrt{v})$, $K_0(2\sqrt{v}) \simeq \sqrt{\frac{\pi}{4\sqrt{v}}}e^{-2\sqrt{v}}$, we have

$$\bar{\nu}(\epsilon,\Gamma_{\|}) \simeq \frac{\pi}{8}\varepsilon^{-1/2}\int_0^{\beta^2} dv v^{7/4} e^{-2\sqrt{v} - \frac{2\bar{t}_0}{\varepsilon} + \frac{4v}{\Gamma_{\|}}f_1(i\bar{t}_0)}.$$

Here we have neglected the small term $exp[-\frac{4v}{\Gamma_{\|}}f_1(0)]$ in the integrand of the v integral, and $\bar{t}_0$ is defined as the root of the saddle point equation:

$$\frac{d}{d\bar{t}}f_1(i\bar{t}) = \frac{\Gamma_{\|}}{2\varepsilon v}$$

As shown in Fig.3.11, the integrand of the v integral is peaked at $v = v_0$, where v_0 is the solution of the equation $\frac{\partial}{\partial v}[\frac{7}{4}\ln v - 2\sqrt{v} - \frac{2\bar{t}_0}{\varepsilon} + \frac{4v}{\Gamma_{\|}}f_1(i\bar{t}_0)] = 0$. By making use of the saddle point equation and the asymptotic formula of $f_1(i\bar{t})$, we find $v_0 \simeq (7 + \frac{8}{\eta\varepsilon})^2$, where $\eta \equiv \sqrt{7\zeta(3)}$.

In order for the result of $\bar{\nu}(\epsilon,\Gamma_{\|})$ to be independent of the choice of β, we must require $\beta^2 \gg v_0$, which, combined with inequality (3.40), yields

$$\Gamma_{\|} \gg 8f_1(0)(7 + \frac{8}{\eta\varepsilon}), \qquad (3.43)$$

which is the condition must be satisfied for the harmonic approximation to be valid. Notice that since $f_1(0) \simeq 8.82 \times 10^{-2}$ and $\varepsilon \ll 1$, inequality (3.43) can also be written as $\varepsilon\Gamma_{\|} \gg 1$.

Finally, by expanding the exponent $\frac{7}{4}\ln v - 2\sqrt{v} - \frac{2\bar{t}_0}{\varepsilon} + \frac{4v}{\Gamma_{\|}}f_1(i\bar{t}_0)$ near $v = v_0$ and performing the saddle point calculation for the v integral, we are left with $\bar{\nu}(\epsilon,\Gamma_{\|})$ given by Eq. (3.12).

This chapter has appeared, with only minor changes, as an article in *Phys.Rev.Lett.*,

71, 2721 (1993).

3.8 References

1. G. Birkl, S. Kassner and H. Walther, Nature **357**, 310 (1992)

2. M.G. Raizen et al., Phys. Rev. A **45**, 6493 (1992)

3. W.H. Itano and N.F. Ramsey, Scientific American, July, 56 (1993)

4. J.P. Schiffer, Proc. Workshop on Crystalline Ion Beams 1988, edited by R.W. Hasse, I. Hofmann and D. Liesen (GSI, Darmstadt, 1989), p. 2.

5. J.P. Schiffer and P. Kienle, Z. Phys. A. **321**, 181 (1985)

6. R.W. Hasse, Phys. Rev. A **45**, 5189 (1992)

7. T. M. O'Neil and P. Hjorth, Phys. Fluids **28**, 3241 (1985)

8. L.D. Landau and E.M. Lifshitz, Mechanics, (Pergamon Press, New York, 1988), p. 161

9. I.S. Gradshteyn and I.M. Ryzhik, *Tables of Integrals, Series, and Products* (Academic Press, Inc., 1980)

Chapter 4

Temperature Equilibration of a Strongly Magnetized Single Species Crystallized Plasma

4.1 Introduction

Recent experiments[1] have trapped a cloud of N ions ($N \sim 10^2 - 10^4$) at a sufficiently low temperature T so that the correlation parameter Γ , defined by $q^2/a_{ws}kT$, is much larger than unity. (Here q is the ion charge and a_{ws} is the Wigner-Seitz radius defined by $\frac{4\pi}{3}na_{ws}^3 = 1$). In this regime the system becomes strongly correlated and transitions to liquid and crystal states are observed. Theoretically, computer simulation and analytic theory for an infinite one component plasma predict that for $\Gamma \geq 2$ the system begins to exhibit local order characteristic of liquid, and for $\Gamma \geq 172$ there is a first order phase transition to a body centered cubic (bcc) crystal[2].

In experiments the plasma is confined in a Penning trap, which utilizes a strong magnetic field in order to confine the ions. Since the ions are laser cooled to low temperatures, the distance of the closest approach $b = q^2/kT$ can be much larger than the Larmor radius, and the cyclotron frequency Ω_c is the largest frequency of the dynamics. In other words, the plasma is in the strongly magnetized regime.

As for the case of the 1D chain discussed in the previous chapter, an adiabatic invariant then exists which greatly decreases the rate of equilibration of parallel and perpendicular temperatures, where now $T_{||}$ and $T_{\perp}$ are associated with motions parallel and perpendicular to the applied magnetic field. In this chapter we study the rate at which $T_{||}$ and $T_{\perp}$ equilibrate in a plasma that is both strongly magnetized and strongly correlated.

This equilibration rate has been investigated by O'Neil and Hjorth[3] and verified by Beck *etal.*[4] experimentally, for a weakly correlated and strongly magnetized plasma where the equilibration is driven by binary collisions. In that case, the cyclotron frequency is large compared with the characteristic frequency $\omega_{||}$ of the collisional dynamics, which is on the order of $v_{||}/b$. Here $v_{||}$ is the relative parallel velocity and b is distance of the closest approach. The large frequency separation implies that the total action of the cyclotron motion is an adiabatic invariant. Due to the existence of this adiabatic invariant, the equilibration rate is an exponentially small function of $1/\varepsilon_1$, where $\varepsilon_1 = \omega_{||}/\Omega_c \ll 1$ is the small adiabaticity parameter. Specifically, the exchange of the perpendicular cyclotron energy and the parallel energy that occurs during a single collision was found to be on the order of $e^{-\pi/2\varepsilon_1}$, and after many collisions, an average of $e^{-\pi/2\varepsilon_1}$ over the distribution yields the equilibration rate $\nu_1 \sim exp(-2.04/\bar{\varepsilon}_1^{2/5})$, where $\bar{\varepsilon}_1$ is the average of ε_1. However, in the strongly correlated regime, particles interact collectively with each other and $1/\omega_{||}$ is characterized by the collective time scale associated with the slow parallel oscillation, which is on the order of ω_p^{-1}. Correspondingly, ε_1 is replaced by $\varepsilon \equiv \omega_p/\Omega_c \ll 1$. In this case, we find that for $\varepsilon\Gamma_{||} \gg 1$ the equilibration rate scales as $\nu \sim exp[-(1 + ln\varepsilon\Gamma_{||})/\varepsilon]$, just as for the 1D chain. Here, $\Gamma_{||} \equiv q^2/akT_{||} \gg 1$ and thus $\varepsilon = \Gamma_{||}\sqrt{6\Gamma_{||}}\varepsilon_1 \gg \varepsilon_1$, which implies that $\nu \gg \nu_1$. Therefore, in the regime of strong correlation, the rate due to collective interactions that we calculate is much

larger than that predicted by the binary collisional equilibration rate.

For a strongly correlated plasma, we may describe the ion-ion collective interactions as emission and absorption of phonons. A conventional normal modes analysis shows that the $3N$ harmonic phonon modes can be classified into three branches of very different frequency regimes. The N highest frequency phonon modes are associated with cyclotron motion perpendicular to the magnetic field with frequency on the order of Ω_c. The next set of N phonon modes correspond to plasma compression along the magnetic field and the N lowest frequency phonon modes describe $\mathbf{E} \times \mathbf{B}$ drift motion of the guiding centers. The frequency of the latter two modes are on the order of ω_p and ω_p^2/Ω_c respectively.

However, the crystal is not perfectly harmonic and even for very large Γ, anharmonic interactions cause coupling between the normal modes. In other words, the anharmonic interactions cause phonon-phonon collisions. For example, one cyclotron phonon may decay into another cyclotron phonon with lower frequency and one plasma compression phonon. During the phonon collisions, the total phonon energy must be conserved: $\sum_m \omega_m^{(i)} = \sum_n \omega_n^{(f)}$, where $\omega_m^{(i)}$ is the frequency of the mth initial phonon and $\omega_n^{(f)}$ is that of the nth final phonon. The low order phonon-phonon collisions are expected to cause energy equipartition between the low frequency modes and between the cyclotron modes, causing the distribution of the low and high frequency modes to relax to a Maxwellian with different temperatures, $T_\perp$ and $T_\parallel$, in a short time scale on the order of ω_p^{-1}, where $T_\perp$ is the temperature associated with the cyclotron phonons and $T_\parallel$ is that associated with plasma frequency phonons. However, when $\varepsilon = \omega_p/\Omega_c$ is small, energy conservation does not allow these low order process to create or annihilate cyclotron phonons, because creation or annihilation of a single cyclotron phonon involves the annihilation or creation of many low frequency phonons. Therefore there is negligible energy exchange between

the cyclotron modes and the low frequency modes on a short time scale. In fact, the large frequency separation of the phonons implies a many particle adiabatic invariant equal to the total quanta (action) of the highest frequency phonons, namely, the cyclotron phonons. In order for temperature equilibration to occur between $T_\perp$ and $T_\parallel$ this invariant must be broken. As we will see, the rate of the breaking of the adiabatic invariant is exponentially small and so the time for the equilibration is exponentially long as a function of $1/\varepsilon$.

Based on the phonon collision picture, we can obtain a crude estimate for the rate of the equilibration ν. We first notice that the drift modes have small amplitude and have frequencies even smaller than the plasma compression modes by a factor $\varepsilon \equiv \omega_p/\Omega_c \ll 1$ and are therefore negligible for the temperature equilibration. We consider two ions l and n separated by a lattice constant a with equilibrium separations of Z_{ln} and ρ_{ln} parallel and perpendicular to the $\mathbf{B}$ field (see Fig.4.1). We write the ion-ion Coulomb interaction as $\Phi = q^2/\sqrt{(\rho_{ln}+\delta\rho_{ln})^2+(Z_{ln}+\delta z_{ln})^2}$, where $\delta\rho_{ln}$ and δz_{ln} are the relative displacements due to the cyclotron motion and the parallel plasma oscillation respectively. Furthermore, as an crude estimate, we assume that the cyclotron motion and the plasma oscillation are characterized by frequencies Ω_c and ω_p respectively. According to Fermi's golden rule the rate ν can be estimated as $\nu = \sum_{l,n}\nu_{lnn}$, where $\nu_{lnn} \sim \omega_p < (\delta H/H_0)^2 >$. Here the sum is over all the pairs of ions, H_0 and δH are the harmonic and anharmonic part of the total Hamiltonian, and $< >$ denotes a statistical average. In particular we take δH as the anharmonic Hamiltonian that annihilates a cyclotron phonon, which is the lowest order process to cause the change of the cyclotron quanta. Recognizing that $M \sim 1/\varepsilon$ low energy phonons must be created in this process, we can crudely write

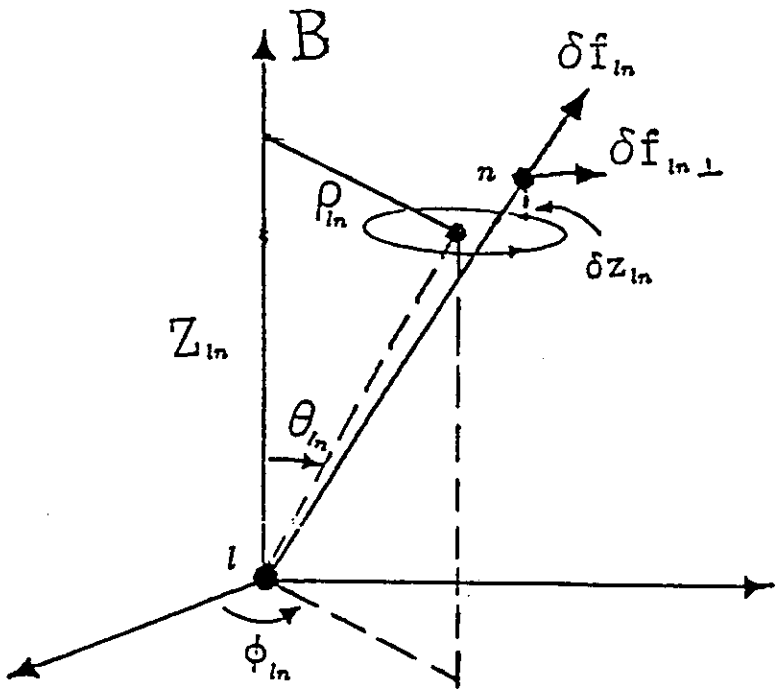

Figure 4.1: Schematic picture for the ion-ion interaction in a strong magnetic field **B**. In the strong **B** limit, each particle executes fast cyclotron motion as well as slow parallel plasma oscillation and extremely slow $\mathbf{E} \times \mathbf{B}$ drift motion, where the cyclotron motion causes the perpendicular relative displacement $\delta\rho_{ln}$ and the parallel oscillation causes the parallel relative displacement δz_{ln}. $\delta\rho_{ln}$ and δz_{ln} furthermore induce a perturbing Coulomb force $\delta\mathbf{f}$ and the perpendicular component of this force, $\delta\mathbf{f}_{ln\perp}$, modifies the cyclotron motion, causing the breaking of the adiabatic invariant. In the figure, ϕ_{ln} is the azimuthal angle of the relative equilibrium positions between l and n with respect to **B**.

$\delta H/H_0$ as

$$\delta H/H_0 \sim \delta\rho_{ln}(\delta z_{ln})^M \frac{1}{\Phi}\frac{\partial^M}{\partial Z_{ln}^M}\frac{\partial\Phi}{\partial\rho_{ln}} = \frac{\delta\rho_{ln}}{a_0}\left(\frac{\delta z_{ln}}{a_0}\right)^M C(\theta_{ln}, M) \tag{4.1}$$

$$C(\theta_{ln}, M) = \frac{a_0^{M+1}}{\Phi}\frac{\partial^M}{\partial Z_{ln}^M}\frac{\partial\Phi}{\partial\rho_{ln}}, \tag{4.2}$$

Here θ_{ln} is the angle between the magnetic field and the relative equilibrium positions between particle l and particle n.

To perform the statistical average, we employ a (two-temperature) Boltz-

mann distribution for H_0:

$$Z_{ln}^{-1} \exp[-\frac{3}{2}\Gamma_{||}(\delta z_{ln}/a_{ws})^2 - \frac{3}{2}\Gamma_{\perp}\varepsilon^{-2}(\delta\rho_{ln}/a_{ws})^2]$$

where $\Gamma_{\perp} = q^2/a_{ws}kT_{\perp}$. We then obtain

$$< (\delta\rho/a_{ws})^2 >= \frac{\varepsilon^2}{3\Gamma_{\perp}}$$

and

$$< (\delta z_{ln}/a_{ws})^{2M} >= \frac{\Gamma(M+1/2)}{\sqrt{\pi}}(\frac{2}{3\Gamma_{||}})^M \simeq \sqrt{2}exp[-M - M\,ln\frac{\Gamma_{||}}{M}]$$

where we have used the approximation $\Gamma(x) \simeq \sqrt{2\pi/x}\,exp[-x + xln(x)]$ for $x \gg 1$. Finally we obtain the rate ν_{lnn} given by

$$\nu_{lnn} \sim \omega_p(\varepsilon^2/{\Gamma_{\perp}}^2)e^{-(1+ln\varepsilon\Gamma_{||})/\varepsilon}|C(\theta_{ln}, M)|^2$$

which is exponentially small as we expected. Here we note several important features of the above expression of ν_{lnn}. We notice that in order for the result to be sensible ε $\Gamma_{||}$ must be greater than unity. Physically this is because a large displacement in δz_{ln} would make a large contribution to the rate, but such displacements are not probable. As a result, for small ε the statistical average is dominated by δz_{ln} displacements with a peak at $\delta z_{ln} \sim a_{ws}/\sqrt{\varepsilon\Gamma_{||}}$. In order for the harmonic approximation to be valid, we must require that the position of this peak to be small compared with the inter-particle spacing, i.e., $\varepsilon\Gamma_{||} \gg 1$. One may notice that the same condition is required for the one dimensional Coulomb chain (see Chapter 2).

A distinctive feature of the 3-dimensional plasma is that ν_{lnn} depends on the orientation of the magnetic field as shown by Eq.(4.1). First, we will see that $C(\theta_{ln}, M)$ is an oscillatory function of θ_{ln}, in other words, there is an oscillation in the rate ν_{lnn} as a function of the magnetic field direction with respect to the crystal

structure. Second, we will see that the maximum rate occurs when the magnetic field is so oriented that θ_{ln} is small but nonzero. Physically, this is easy to understand. From Eq.(4.1), we find that for $M \gg 1$, the maximum value of ν_{lnn} occurs when δz_{ln} is the largest. Furthermore, according to the phonon collision picture, ν_{lnn} is dominated by the contributions from the largest frequency plasma modes, which, as we will see, are long wavelength modes with $\mathbf{k} \parallel \mathbf{B}$. For one such mode, the relative displacement δz_{ln} between ions with given equilibrium separation Z_{ln} is $|\delta z_{ln}| \propto 1 - \cos kZ_{ln} \sim \frac{1}{2}k^2 Z_{ln}^2$, and therefore δz_{ln} reaches the maximum when Z_{ln} is the maximum, which occurs when $\theta_{ln} = 0$ assuming that we vary θ_{ln} keeping $\sqrt{Z_{ln}^2 + \rho_{ln}^2}$ fixed. However, for small θ_{ln}, $C(\theta_{ln}, M)$is proportional to θ_{ln}, corresponding to the vanishing of the perpendicular perturbing force $\delta \mathbf{f}_{ln\perp}$ (see Fig.4.1). As a result, for small θ_{ln}, ν_{lnn} goes like $Z_{ln}^{4M}\rho^2 = a_0^{4M+2}(\cos\theta_{ln})^{4M}(\sin\theta_{ln})^2$, which is peaked at $\theta_{ln} \sim 1/\sqrt{2M} \ll 1$.

It is important to note that the temperature equilibration rate calculated for a perfect crystal does not apply to the present experiments, because in present experiments the number of ions is relatively small ($N \leq 10^4$) so that surface effects are important[5]. For large Γ, rather than undergoing a simple first order transition from a liquid to a bcc crystal, the ion cloud separates into concentric spheroidal shells and it only exhibits a bcc-like structure through nearest neighbor coordination numbers. Moreover, for $\Gamma < 172$, rather than forming a crystalline structure, the strongly correlated plasma is in a liquid state, which consists of structures with only short-range order[6]. In this case, the temperature equilibration for this system can not be predicted by that for a perfect bcc crystal. However, in order to gain a physical insight for the temperature equilibration process, we chose a simplified model where the plasma is approximated by a bcc lattice structure, which is a limiting case of large Γ and large N. Furthermore, as one may expect, the temperature equilibration

process is dominated by the nearest neighbor interactions and this fact would allow us to evaluate the temperature equilibration rate for a less ordered system by averaging the equilibration rate of a local crystal over randomly varying crystal orientations, or, equivalently, averaging over the randomly varying magnetic field directions with respect to the crystal structure. We therefore expect that the general feature of the equilibration that is exponentially slow in the parameter $1/\epsilon$ will apply in disordered, possibly even liquid phases, provided that $\epsilon \ll 1$ and $\epsilon\Gamma_{\|} \gg 1$.

In this chapter, we first develop a formalism for the calculation of the temperature equilibration rate, where the equilibration rate is written in terms of the Fourier integral of a correlation function associated with the slow plasma compression motion. We then evaluate this integral, where, in order to simplify the physical picture, the guiding center limit is taken. Finally, based on the result of this integral, we discuss various important characteristics of the equilibration rate, for example, the dependence of the rate on the magnetic field orientation with respect to the crystal lattice. In section 4.2, by employing a series of canonical transformations, we obtain the harmonic phonon modes. In section 4.3, we derive an expression for the adiabatic invariant J, which equals the total action of the cyclotron phonon modes. This invariant is further shown to have the same form as the conventional cyclotron adiabatic invariant[3]. In section 4.4, we derive the formula for the rate of the breaking of the adiabatic invariant in terms of the time integral of the correlation function $< \dot{J}(t)\dot{J}(0) >$. In section 4.5, we evaluate the equilibration rate in the guiding center limit and the important features shown in the result is thereby discussed.

4.2 Normal Modes Analysis

In this section we derive the harmonic phonon modes by employing a series of canonical transformations for the harmonic part of the total Hamiltonian: $H = \sum_{l=1}^{N}(\frac{\mathbf{\Pi}_l^2}{2m}) + \Phi$, where Φ is the total potential energy given by

$$\Phi = \frac{1}{2}\sum_{l}\sum_{n\neq l} q^2/|\mathbf{r}_l - \mathbf{r}_n| \tag{4.3}$$

and where $\mathbf{\Pi}_l = \mathbf{p}_l - \frac{q}{c}\mathbf{A}_l$, $\mathbf{p}_l$ and $\mathbf{A}_l$ the canonical momentum and the vector potential of the lth particle. Following the conventional approach by assuming that charges are confined to small excursion $\mathbf{u}_n$ about the equilibrium positions $\mathbf{R}_n$, we expand Φ as $\Phi = \Phi_H + \Delta\Phi$ where Φ_H is the harmonic expansion of Φ and $\Delta\Phi$ is the anharmonic correction, writing

$$\begin{aligned} H &= H_0 + \Delta\Phi \\ H_0 &= \frac{1}{2}\sum_{l}\sum_{n\neq l}\frac{q^2}{|\mathbf{R}_l - \mathbf{R}_n|} + \sum_{l}(\frac{\mathbf{\Pi}_l^2}{2m}) + \Phi_H \\ \Phi_H &= \frac{1}{2}\sum_{l=1}^{N}\sum_{n\neq l}\mathbf{u}_l \cdot \mathbf{G}_{ln} \cdot \mathbf{u}_n \\ \Delta\Phi &= \Phi - \Phi_H \end{aligned}$$

where the matrix $\mathbf{G}_{ln}$ is given by: $\mathbf{G}_{ln} = \nabla_l\nabla_n(q^2/|\mathbf{R}_l - \mathbf{R}_n|)$, where ∇_l denotes $\partial/\partial\mathbf{R}_l$. In order to make further calculation simpler, we choose the coordinate system such that $\hat{z}$ is pointed along the magnetic field direction. The first term of H_0 is the Madlung energy of the crystal and will be ignored as having no effect to the dynamics.

To uncover the normal modes, we first introduce the phonon coordinates ($\mathbf{u}_\mathbf{k}$,

$\mathbf{\Pi_k}$) through the Fourier relations[7]:

$$(\mathbf{u}_l, \mathbf{p}_l) = \sqrt{\frac{2}{N}} \sum_{\mathbf{k}>0} [(\mathbf{u_k}, \mathbf{p_k}) \cos \mathbf{k} \cdot \mathbf{R}_l + (\mathbf{u}_{-\mathbf{k}}, \mathbf{p}_{-\mathbf{k}}) \sin \mathbf{k} \cdot \mathbf{R}_l] \tag{4.4}$$

where $\mathbf{k} = \frac{n_1}{N_1}\mathbf{b}_1 + \frac{n_2}{N_2}\mathbf{b}_2 + \frac{n_3}{N_3}\mathbf{b}_3 \, (0 \leq n_i \leq N_i - 1, i = 1, 2, 3)$ so that the periodic boundary condition: $\mathbf{u}(\mathbf{R}_l + N_i\mathbf{a_i}) = \mathbf{u}(\mathbf{R}_l)$ is satisfied for any lattice vector $\mathbf{R}_l = l_1\mathbf{a_1} + l_2\mathbf{a_2} + l_2\mathbf{a_3} \, (0 \leq l_i \leq N_i - 1, i = 1, 2, 3)$. Here $\mathbf{a}_i$ and $\mathbf{b}_i$ are the primitive vectors of the direct and reciprocal lattice, l_i and n_i are integers, and N_i are large integers satisfying $N = N_1 N_2 N_3$. In addition, the notation $\mathbf{k} > 0$ in Eq.(2.1) denotes the sum over half of the Brillouin zone. We note that when the total number of the particle N is an odd number, the sum over $\mathbf{k}$ may leave out a single point on the edge of the Brillouin zone. However for large N, this single point makes a negligible contribution and can thus be ignored.

In terms of the phonon coordinates H_0 becomes a sum of independent Hamiltonians for each $\mathbf{k}$:

$$H_0 = \sum_{\mathbf{k}} H_0(\mathbf{k})$$

$$H_0(\mathbf{k}) = \frac{\mathbf{\Pi}_\mathbf{k}^2}{2m} + \Phi_H(\mathbf{k}) \tag{4.5}$$

where the harmonic potential $\Phi_H(\mathbf{k})$ is given by

$$\Phi_H(\mathbf{k}) = \frac{1}{2}\mathbf{u_k} \cdot \mathbf{G}(\mathbf{k}) \cdot \mathbf{u_k} \tag{4.6}$$

where $\mathbf{G}(\mathbf{k}) = \sum_l \mathbf{G}_{ln} e^{i\mathbf{k}\cdot(\mathbf{R}_l - \mathbf{R}_n)}$.

After employing the Fourier transformation, H_0 is decomposed into a sum for different $\mathbf{k}$'s. This allows us to diagonalize each $H_\mathbf{k}$ separately. In order to proceed, we choose the vector potential $\mathbf{A}_l$ to be $\frac{1}{2}\mathbf{B} \times \mathbf{u}_l$ and then the Fourier transformed vector potential is $\mathbf{A_k} = \frac{1}{2}\mathbf{B} \times \mathbf{u_k}$, which, with the relation $\mathbf{\Pi_k} = \mathbf{p_k} - \frac{q}{c}\mathbf{A_k}$, leads

to the following specific form of H_0

$$H_0(\mathbf{k}) = \frac{p_x^2+p_y^2+p_z^2}{2m} + \frac{1}{2}[m(\frac{\Omega_c}{2})^2 + G_{xx}]x_\mathbf{k}^2 + \frac{1}{2}[m(\frac{\Omega_c}{2})^2 + G_{yy}]y_\mathbf{k}^2 + \frac{1}{2}G_{zz}z_\mathbf{k}^2$$

$$+\frac{\Omega_c}{2}(y_\mathbf{k}p_x - x_\mathbf{k}p_y) + G_{xy}x_\mathbf{k}y_\mathbf{k} + G_{xz}x_\mathbf{k}z_\mathbf{k} + G_{yz}y_\mathbf{k}z_\mathbf{k} \tag{4.7}$$

where $(x_\mathbf{k}, y_\mathbf{k}, z_\mathbf{k}) = \mathbf{u}_\mathbf{k}$ and $(p_x, p_y, p_z) = \mathbf{p}_\mathbf{k}$ and in Eq.(4.7) the subscripts $\mathbf{k}$ for (p_x, p_y, p_z) have been suppressed in order to save space.

In order to derive the phonon modes from $H_0(\mathbf{k})$, we need to find a canonical transformation from $(x_\mathbf{k}, y_\mathbf{k}, z_\mathbf{k}, p_x, p_y, p_z)$ to new canonical variables $(Q_{1,\mathbf{k}}, Q_{2,\mathbf{k}}, Q_{3,\mathbf{k}}$, $P_{1,\mathbf{k}}, P_{2,\mathbf{k}}, P_{3,\mathbf{k}})$ such that $H_0(\mathbf{k})$ is diagonalized into the the Hamiltonian of three independent harmonic oscillators:

$$H_0(\mathbf{k}) = \sum_{j=1,2,3} \frac{\mathbf{P}_{j,\mathbf{k}}^2}{2m} + \frac{1}{2}m\omega_j(\mathbf{k})^2\mathbf{Q}_{j,\mathbf{k}}^2 \tag{4.8}$$

Then we may identify $(Q_{j,\mathbf{k}}, P_{j,\mathbf{k}})$ to be the canonical variables describing the jth normal mode and $\omega_j(\mathbf{k})$ is the mode frequency. Obviously $(Q_{j,\mathbf{k}}(t), P_{j,\mathbf{k}}(t))$ evolve according to the trajectory of a harmonic oscillator and are given by

$$Q_{j,\mathbf{k}}(t) = Q_{j,\mathbf{k}}(0)\cos(\omega_j(\mathbf{k})t) + \frac{P_{j,\mathbf{k}}(0)}{m\omega_j(\mathbf{k})}\sin(\omega_j(\mathbf{k})t)$$

$$P_{j,\mathbf{k}}(t) = P_{j,\mathbf{k}}(0)\cos(\omega_j(\mathbf{k})t) - m\ Q_{j,\mathbf{k}}(0)\sin(\omega_j(\mathbf{k})t) \tag{4.9}$$

and furthermore through the canonical transformation we may write the particle's orbit $(x_\mathbf{k}(t), y_\mathbf{k}(t), z_\mathbf{k}(t))$ in terms of $(Q_{j,\mathbf{k}}(t), P_{j,\mathbf{k}}(t))$.

As shown by Eq.(2.5), the coordinate variables and the momentum variables are mixed due to the existence of the magnetic field. Therefore, although the Hamiltonian is harmonic, the usual point transformation approach, which only transforms the coordinate variables, can not diagonalize $H_0(\mathbf{k})$. In order to diagonalize $H_0(\mathbf{k})$, a

full canonical transformation must transform both the coordinate variables and the momentum variables simultaneously. As a consequence, the new canonical variables $(Q_{j,\mathbf{k}}, P_{j,\mathbf{k}})$ are generally linear combinations of both $(x_{\mathbf{k}}, y_{\mathbf{k}}, z_{\mathbf{k}})$ and (p_x, p_y, p_z).

The procedure to find such a canonical transformation is nontrivial. In fact, as far as we know, the general transformation for a 3-D crystal in a magnetic field has never been written down previously. In appendix D, we discuss this transformation by using the Bosonic Bogoluibov formalism. We define the following variables in order to put $H_0(\mathbf{k})$ in a symmetrized form.

$$\begin{aligned} c_1 &= \frac{\sqrt{m\Omega_c}}{2} x_{\mathbf{k}} + \frac{ip_x}{\sqrt{m\Omega_c}} \\ c_2 &= \frac{\sqrt{m\Omega_c}}{2} y_{\mathbf{k}} + \frac{ip_y}{\sqrt{m\Omega_c}} \\ c_3 &= \sqrt{\frac{m\omega_z}{2}} z_{\mathbf{k}} + \frac{ip_z}{\sqrt{2m\omega_z}} \end{aligned} \tag{4.10}$$

where $\omega_z = \sqrt{G_{zz}/m}$.

Furthermore, in order to simplify the algebra we introduce a dimensionless dynamical matrix $\mathbf{g} = \mathbf{G}/m{\omega_p}^2$ and dimensionless frequency $\bar{\omega_z} = \sqrt{g_{zz}} = \omega_z/\omega_p$. In terms of the base vector $\mathbf{c}$ defined by

$$\mathbf{c} = \begin{pmatrix} c_1 \\ c_2 \\ c_3 \end{pmatrix}.$$

We may write $H_0(\mathbf{k})$ as

$$H_0(\mathbf{k}) = \frac{1}{2}(\mathbf{c}^*, \mathbf{c})^{tr} \cdot \mathbf{h} \cdot \begin{pmatrix} \mathbf{c} \\ \mathbf{c}^* \end{pmatrix},$$

where the Hamiltonian matrix $\mathbf{h}$ is given by

$$\mathbf{h} = \begin{bmatrix} \mathbf{N} & \mathbf{M} \\ \mathbf{M}^* & \mathbf{N}^* \end{bmatrix}$$

and

$$\mathbf{M} = \Omega_c \begin{bmatrix} \varepsilon^2 g_{xx} & \varepsilon^2 g_{xy} & \varepsilon\sqrt{\varepsilon}\tilde{g}_{xz} \\ \varepsilon^2 g_{xy} & \varepsilon^2 g_{yy} & \varepsilon\sqrt{\varepsilon}\tilde{g}_{yz} \\ \varepsilon\sqrt{\varepsilon}\tilde{g}_{xz} & \varepsilon\sqrt{\varepsilon}\tilde{g}_{yz} & 0 \end{bmatrix}$$

$$\mathbf{N} = \Omega_c \begin{bmatrix} \frac{1}{2} + \varepsilon^2 g_{xx} & \frac{i}{2} + \varepsilon^2 g_{xy} & \varepsilon\sqrt{\varepsilon}\tilde{g}_{xz} \\ -\frac{i}{2} + \varepsilon^2 g_{xy} & \frac{1}{2} + \varepsilon^2 g_{yy} & \varepsilon\sqrt{\varepsilon}\tilde{g}_{yz} \\ \varepsilon\sqrt{\varepsilon}\tilde{g}_{xz} & \varepsilon\sqrt{\varepsilon}\tilde{g}_{yz} & \varepsilon\bar{\omega}_z \end{bmatrix}$$

where $\tilde{g}_{xz} = g_{xz}/\sqrt{2\bar{\omega}_z}$ and $\tilde{g}_{yz} = g_{yz}/\sqrt{2\bar{\omega}_z}$.

In what follows, we proceed to find a linear canonical transformation described by

$$\begin{pmatrix} \mathbf{c} \\ \mathbf{c}^* \end{pmatrix} = \mathbf{S} \cdot \begin{pmatrix} \mathbf{e} \\ \mathbf{e}^* \end{pmatrix} \tag{4.11}$$

such that in the representation of the new variables $(\mathbf{e}, \mathbf{e}^*)$ the Hamiltonian matrix $\mathbf{h}$ is diagonalized, i.e., $\mathbf{S}^\dagger\mathbf{h}\mathbf{S}$ is diagonal. Furthermore, according to Eq.(3.6) and Eq.(3.7) of Appendix 4B, in order to ensure the transformation is canonical, matrix

$\mathbf{S}$ must be of the form

$$\mathbf{S} = \begin{bmatrix} \mathbf{A} & \mathbf{B}^* \\ \mathbf{B} & \mathbf{A}^* \end{bmatrix}$$

and $\mathbf{S}$ must satisfy

$$\mathbf{S}^{-1} = \mathbf{\Lambda}\mathbf{S}^{\dagger}\mathbf{\Lambda} \tag{4.12}$$

where $\mathbf{A}$ and $\mathbf{B}$ are 3×3 matrices and $\mathbf{\Lambda} = \begin{bmatrix} \mathbf{1} & 0 \\ 0 & -\mathbf{1} \end{bmatrix}$, where $\mathbf{1}$ denotes the 3×3 unit matrix. As a conclusion of Appendix 4B, such a transformation matrix $\mathbf{S}$ can be constructed in terms of the eigenvectors of a 6×6 matrix $\mathbf{K} = \mathbf{\Lambda h}$:

$$\mathbf{S} = (\eta_1, \eta_2, \eta_3, (\mathbf{\Sigma}\eta_1)^*, (\mathbf{\Sigma}\eta_2)^*, (\mathbf{\Sigma}\eta_3)^*) \tag{4.13}$$

with normalization condition:

$$\eta_j^{\dagger}\mathbf{\Lambda}\eta_j = 1 \tag{4.14}$$

for $j = 1, 2, 3$, where $\mathbf{\Sigma} = \begin{bmatrix} 0 & \mathbf{1} \\ \mathbf{1} & 0 \end{bmatrix}$, $\mathbf{\Lambda} = \begin{bmatrix} \mathbf{1} & \mathbf{0} \\ \mathbf{0} & -\mathbf{1} \end{bmatrix}$, and $\eta_j (j = 1, 2, 3)$ are the eigenvectors corresponding to the three positive eigenvalues of $\mathbf{K}$. Furthermore, we show in Appendix 4B that these positive eigenvalues correspond to the ω_j's (j=1,2,3) in Eq.(4.8), which are the frequencies of the normal modes.

After some algebra we find that the eigenvalue ω of matrix $\mathbf{K}$ is determined by

$$\omega^6 - (1 + \varepsilon^2)\omega^4 + \varepsilon^2[\bar{\omega_z}^2 + \varepsilon^2\sigma)]\omega^2 - \varepsilon^6 \det(\mathbf{g}) = 0$$

where

$$\sigma = g_{xy}^2 + g_{xz}^2 + g_{yz}^2 - g_{xx}g_{yy} - g_{xx}\bar{\omega_z}^2 - g_{yy}\bar{\omega_z}^2$$

Evidently, the solutions for ω appear in pairs with opposite signs. As we have mentioned, the calculation of the exact eigenvalue problem for matrix $\mathbf{K}$ is rather tedious, however, because ε is small, it would be useful to do expansions about ε so that the calculation can be simplified. After conventional, but rather complicated computations for the eigenvalue problem of matrix $\mathbf{K}$, we obtain the following results for the eigenvalues $\omega_i\,(i = 1, 2, 3)$ and the corresponding eigenvectors η_i :

$$\eta_i = \begin{pmatrix} \eta_i^{(1)} \\ \eta_i^{(2)} \\ \eta_i^{(3)} \\ \eta_i^{(4)} \\ \eta_i^{(5)} \\ \eta_i^{(6)} \end{pmatrix}$$

as following, where only terms up to the second order in ε are kept:

$$\omega_1 = \Omega_c[1 + \frac{1 - \bar{\omega_z}^2}{2}\varepsilon^2];$$

$$\eta_1^{(1)} = [1 + \frac{\varepsilon^2}{2}(g_{xx} - g_{yy})]/\sqrt{2}$$

$$\eta_1^{(2)} = [-i + \varepsilon^2(2g_{xy} + \frac{i}{2}(g_{xx} - g_{yy})]/\sqrt{2}$$

$$\eta_1^{(3)} = \varepsilon^{3/2}(\tilde{g}_{xz} - i\tilde{g}_{yz})/\sqrt{2}$$

$$\eta_1^{(4)} = \varepsilon^2(-\frac{3}{4}g_{xx} - \frac{g_{yy}}{4} + \frac{i}{2}g_{xy})/\sqrt{2}$$

$$\eta_1^{(5)} = \frac{\varepsilon^2}{2}(\frac{i}{2}g_{xx} + i\frac{3}{2}g_{yy} - g_{xy})/\sqrt{2}$$

$$\eta_1^{(6)} = -\eta_1^{(3)} \tag{4.15}$$

and

$$\omega_2 = \omega_p\bar{\omega}_z[1 + \frac{\varepsilon^2}{2}(\bar{\omega_z}^2 - 1 + \frac{\sigma}{\bar{\omega_z}^2} - \frac{det(\mathbf{g})}{\bar{\omega_z}^4})]$$

$$\eta_2^{(1)} = \sqrt{\varepsilon}s_1\mu_1^* + \varepsilon^{3/2}s_2(\mu_1\mu_2 + \mu_3)$$

$$\eta_2^{(2)} = i\sqrt{\varepsilon}s_1\mu_1^* + i\varepsilon^{3/2}s_2(-\mu_1\mu_2^* + \mu_3)$$

$$\eta_2^{(3)} = 1 - \frac{\varepsilon^2\Delta_2}{2\bar{\omega_z}^4}$$

$$\eta_2^{(4)} = -\sqrt{\varepsilon}s_1\mu_1 + \varepsilon^{3/2}s_2(\mu_1^*\mu_2^* + \mu_3^*)$$

$$\eta_2^{(5)} = i\sqrt{\varepsilon}s_1\mu_1 - i\varepsilon^{3/2}s_2(-\mu_1^*\mu_2 + \mu_3^*)$$

$$\eta_2^{(6)} = 0$$

and

$$\omega_3 = \varepsilon\omega_p\frac{\sqrt{\det(\mathbf{g})}}{\bar{\omega}_z}[1 + \frac{\varepsilon^2}{2\bar{\omega_z}^2}(\frac{det(\mathbf{g})}{\bar{\omega_z}^2} - \sigma)]$$

$$\eta_3^{(1)} = \bar{\omega}_z s_3\Delta_0$$

$$\eta_3^{(2)} = (i\bar{\omega}_z s_3 + 2i\epsilon^2 \Delta_1 \bar{\omega}_z{}^2 s_4)\Delta_0$$

$$\eta_3^{(3)} = (-\sqrt{\epsilon} s_3 - \epsilon^{3/2} \Delta_0 s_4)\Delta_2$$

$$\eta_3^{(4)} = -\bar{\omega}_z s_3 \Delta_1 - 2\epsilon^2 \bar{\omega}_z{}^2 s_4 \Delta_3$$

$$\eta_3^{(5)} = i\bar{\omega}_z s_3 \Delta_1 - 2\epsilon^2 \bar{\omega}_z{}^2 s_4 \Delta_4$$

$$\eta_3^{(6)} = (-\sqrt{\epsilon} s_3 + \epsilon^{3/2} \Delta_0 s_4)\Delta_2$$

where

$$\mu_1 = \tilde{g}_{xz} + i\tilde{g}_{yz}$$

$$\mu_2 = -\bar{\omega}_z{}^2 + i g_{xy}$$

$$\mu_3 = g_{yy}\tilde{g}_{xz} - i g_{xx}\tilde{g}_{yz}$$

$$s_1 = (2\bar{\omega}_z)^{-1}$$

$$s_2 = (2\bar{\omega}_z{}^2)^{-3/2}$$

$$s_3 = 1/(\Delta_0 \bar{\omega}_z D)$$

$$s_4 = \sqrt{det(\mathbf{g})}/(\Delta_0^2 \bar{\omega}_z{}^3 D)$$

$$\Delta_0 = \sqrt{det(\mathbf{g})}\mu_1^* + \bar{\omega_z}(ig_{xy}\mu_1 + \mu_3)$$

$$\Delta_1 = \sqrt{det(\mathbf{g})}\mu_1 + \bar{\omega_z}(ig_{xy}\mu_1^* - \mu_3^*)$$

$$\Delta_2 = 2\tilde{g}_{xz}^2 g_{yy}\bar{\omega_z} - 4g_{xy}\tilde{g}_{xz}\tilde{g}_{yz}\bar{\omega_z} + 2g_{xx}\tilde{g}_{yz}^2\bar{\omega_z}$$

$$\Delta_3 = det(\mathbf{g})(\tilde{g}_{xz}^2 - \tilde{g}_{yz}^2) + i\sqrt{det(\mathbf{g})}\bar{\omega_z}[\tilde{g}_{xz}(g_{xy}\tilde{g}_{xz} - g_{xx}\tilde{g}_{yz}) +$$

$$+3\tilde{g}_{yz}(g_{xy}\tilde{g}_{yz} - \tilde{g}_{xz}g_{yy})] + 2\bar{\omega_z}^2(g_{xy}\tilde{g}_{yz} - \tilde{g}_{xz}g_{yy})^2$$

$$\Delta_4 = 2det(\mathbf{g})\tilde{g}_{xz}\tilde{g}_{yz} + \sqrt{det(\mathbf{g})}\bar{\omega_z}[\tilde{g}_{xz}\tilde{g}_{yz}(g_{xx} - g_{yy}) + g_{xy}(\tilde{g}_{yz}^2 - \tilde{g}_{xz}^2) +$$

$$2i(\tilde{g}_{xz}^2 g_{yy} - \tilde{g}_{yz}^2 g_{xx})]$$

$$+\bar{\omega_z}^2[2(g_{xy}^2\tilde{g}_{xz}\tilde{g}_{yz} - g_{xy}\tilde{g}_{xz}^2 g_{yy} + g_{xx}\tilde{g}_{xz}g_{yy}\tilde{g}_{yz} - g_{xx}g_{xy}\tilde{g}_{yz}^2)$$

$$-i(g_{xy}^2\tilde{g}_{xz}^2 + \tilde{g}_{xz}^2 g_{yy}^2 + g_{xx}^2\tilde{g}_{yz}^2 + g_{xy}^2\tilde{g}_{yz}^2) + 2ig_{xy}\tilde{g}_{yz}\tilde{g}_{xz}(g_{xx} + g_{yy})] \quad (4.16)$$

Where η_j's have been normalized according to Eq.(4.14) and D is determined by the normalization condition of Eq. (4.14):

$$|\eta_3^{(1)}|^2 + |\eta_3^{(2)}|^2 + |\eta_3^{(3)}|^2 - |\eta_3^{(4)}|^2 - |\eta_3^{(5)}|^2 - |\eta_3^{(6)}|^2 = 1$$

To lowest order in ϵ,

$$D = \sqrt{2(|\Delta_0|^2 - |\Delta_1|^2)}/\Delta_0. \quad (4.17)$$

One may easily identify ω_1, ω_2 and ω_3 to be the frequencies of the cyclotron

mode, the plasma compression mode and the $\mathbf{E} \times \mathbf{B}$ guiding center drifting mode respectively. In terms of the $(\mathbf{e}, \mathbf{e}^*)$, the Hamiltonian takes a diagonalized form as

$$H_0(\mathbf{k}) = \omega_1(\mathbf{k}) e_1^* e_1 + \omega_2(\mathbf{k}) e_2^* e_2 + \omega_3(\mathbf{k}) e_3^* e_3 \tag{4.18}$$

and furthermore we may define the final new canonical variables $(Q_{j,\mathbf{k}}, P_{j,\mathbf{k}})(j = 1, 2, 3)$ through

$$e_j = \sqrt{\frac{m\omega_j(\mathbf{k})}{2}} Q_{j,\mathbf{k}} + \frac{iP_{j,\mathbf{k}}}{\sqrt{2m\omega_j(\mathbf{k})}} \tag{4.19}$$

In fact, substituting the above form for $(\mathbf{e}, \mathbf{e}^*)$ into Eq.(4.23), we find that $H_0(\mathbf{k})$ then takes the form given by Eq.(4.8).

Finally, combining Eq.(4.10),Eq.(4.11) and Eq.(4.13), we can write down the harmonic trajectory $(x_{\mathbf{k}}(t), y_{\mathbf{k}}(t), z_{\mathbf{k}}(t))$ as

$$\begin{aligned}
x_{\mathbf{k}}(t) &= \frac{c_1(t) + c_1^*(t)}{\sqrt{m\Omega_c}} \\
&= \frac{1}{\sqrt{m\Omega_c}} \sum_{j=1}^{3} [(\eta_j^{(1)} + \eta_j^{(4)}) e_j(t) + c.c] \\
y_{\mathbf{k}}(t) &= \frac{c_2(t) + c_2^*(t)}{\sqrt{m\Omega_c}} \\
&= \frac{1}{\sqrt{m\Omega_c}} \sum_{j=1}^{3} [(\eta_j^{(2)} + \eta_j^{(5)}) e_j(t) + c.c] \\
z_{\mathbf{k}}(t) &= \frac{c_3(t) + c_3^*(t)}{\sqrt{2m\omega_z}} \\
&= \frac{1}{\sqrt{2m\omega_z}} \sum_{j=1}^{3} [(\eta_j^{(3)} + \eta_j^{(6)}) e_j(t) + c.c]
\end{aligned} \tag{4.20}$$

where according to Eq. (4.19) and Eq. (4.9), $e_j(t)$ is given by

$$e_j(t) = \sqrt{\frac{m\omega_j(\mathbf{k})}{2}} Q_{j,\mathbf{k}}(0) e^{-i\omega_j(\mathbf{k})t} + \frac{iP_{j,\mathbf{k}}(0)}{\sqrt{2m\omega_j(\mathbf{k})}} e^{i\omega_j(\mathbf{k})t} \tag{4.21}$$

We notice that the expressions for ω_j's and η_j's are quite complicated, and so we'd better examine them before making further progress. One of the useful methods to check these results is to evaluate the mean square of the particle's displacements $< x_{\mathbf{k}}^2 >, < y_{\mathbf{k}}^2 >$ and $< z_{\mathbf{k}}^2 >$ for a thermal equilibration system. We may write the distribution function as $\prod_{\mathbf{k}} f_{\mathbf{k}}$ with $f_{\mathbf{k}} = exp[-H_0(\mathbf{k})/kT]$. The statistical average can be obtained by two approaches, namely, using the old canonical variables and using the new transformed canonical variables. These two approaches must yield the same results.

We first evaluate $< x_{\mathbf{k}}^2 >$ in terms of the old canonical variables ($x_{\mathbf{k}}$, $y_{\mathbf{k}}$, $z_{\mathbf{k}}$, p_x, p_y, p_z). Substituting Eq. (4.5) and Eq. (4.6) for $H_0(\mathbf{k})$ into $f_{\mathbf{k}}$, we have

$$\begin{aligned} < x_{\mathbf{k}}^2 > &= \frac{\int x_{\mathbf{k}}^2 e^{-\frac{m\omega_p^2}{2kT}\mathbf{u}_k \cdot \mathbf{g} \cdot \mathbf{u}_k} d^3\mathbf{u}_k}{\int e^{-\frac{m\omega_p^2}{2kT}\mathbf{u}_k \cdot \mathbf{g} \cdot \mathbf{u}_k} d^3\mathbf{u}_k} \\ &= -\frac{2kT}{m\omega_p^2} \frac{\frac{\partial}{\partial \mathbf{g}_{xx}} [\int e^{-\frac{m\omega_p^2}{2kT}\mathbf{u}_k \cdot \mathbf{g} \cdot \mathbf{u}_k} d^3\mathbf{u}_k]}{\int e^{-\frac{m\omega_p^2}{2kT}\mathbf{u}_k \cdot \mathbf{g} \cdot \mathbf{u}_k} d^3\mathbf{u}_k} \\ &= \lambda^2 \frac{\mathbf{g}_{yy}\mathbf{g}_{zz} - \mathbf{g}_{yz}^2}{det(\mathbf{g})} \end{aligned} \tag{4.22}$$

where $\lambda = \sqrt{kT/m\omega_p^2}$ and we have used formula

$$\int e^{-\frac{m\omega_p^2}{2kT}\mathbf{u}_k \cdot \mathbf{g} \cdot \mathbf{u}_k} d^3\mathbf{u}_k = \frac{1}{\sqrt{det(\mathbf{g})}} [\frac{2\pi kT}{m\omega_p^2}]^{3/2}$$

An important observation is that $< x_{\mathbf{k}}^2 >$ is independent of the magnetic field though the plasma is magnetized. This is because that the magnetic field does not alter the

particle's energy and it only enters the Hamiltonian in the velocity term, so the magnetic field dependence vanishes after the averaging.

We now proceed to evaluate $< x_{\mathbf{k}}^2 >$ through the second approach, that is, by using the new transformed canonical variables. In order to make the algebra simpler, we introduce the action-angle variables $(I_{\mathbf{k}}^{(i)}, \Psi_{\mathbf{k}}^{(i)})$, which are defined by

$$e_i(\mathbf{k}) = \sqrt{I_{\mathbf{k}}^{(i)}} e^{i\Psi_{\mathbf{k}}^{(i)}}$$

Then Eq.(4.18) becomes

$$H_0(\mathbf{k}) = \sum_{i=1}^{3} \omega_i(\mathbf{k}) I_{\mathbf{k}}^{(i)} \tag{4.23}$$

Inserting this form of $H_0(\mathbf{k})$ into $f_{\mathbf{k}}$ and using Eq.(4.20) for $x_{\mathbf{k}}$, we obtain

$$< x_{\mathbf{k}}^2 > = \frac{1}{m\Omega_c} \frac{\prod_{i=1}^{3} \int_0^{2\pi} d\Psi_{\mathbf{k}}^{(i)} \int_0^{\infty} dI_{\mathbf{k}}^{(i)} \sum_{j=1}^{3} [(\eta_j^{(1)} + \eta_j^{(4)}) e_j(t) + c.c]^2 e^{-\frac{\omega_i(\mathbf{k}) I_{\mathbf{k}}^{(i)}}{kT}}}{\prod_{i=1}^{3} \int_0^{2\pi} d\Psi_{\mathbf{k}}^{(i)} \int_0^{\infty} dI_{\mathbf{k}}^{(i)} e^{-\frac{\omega_i(\mathbf{k}) I_{\mathbf{k}}^{(i)}}{kT}}}$$

$$= \sum_{j=1}^{3} < (x_{\mathbf{k}}^{(j)})^2 > \tag{4.24}$$

where $< (x_{\mathbf{k}}^{(j)})^2 >= \frac{2kT}{m\Omega_c \omega_j} |\eta_j^{(1)} + \eta_j^{(4)}|^2$ is the mean square x-displacement due to the jth mode. Making use of our results for ω_j and η_j, we have

$$< (x_{\mathbf{k}}^{(1)})^2 > = \lambda^2 \varepsilon^2$$

$$< (x_{\mathbf{k}}^{(2)})^2 > = \lambda^2 \varepsilon^2 \frac{4\tilde{g}_{yz}^2}{\bar{\omega}_z^3}$$

$$< (x_{\mathbf{k}}^{(3)})^2 > = \frac{2\bar{\omega}_z}{\sqrt{det(\mathbf{g})}} \lambda^2 |\bar{\omega}_z s_3 (\Delta_0 - \Delta_1)$$

$$- \quad \varepsilon^2[2\bar{\omega}_z^2 s_4\Delta_3 + \frac{s_3}{4\bar{\omega_z}^2}(\frac{det(\mathbf{g})}{\bar{\omega_z}^2} - \sigma)(\Delta_0 - \Delta_1)]|^2$$

where only terms up to the second order of ε have been kept. We note that because $\lambda \ll a_{ws}$ for a strongly correlated system, $< (x_{\mathbf{k}}^{(j)})^2 >$ are small compared with the inter-particle spacing for all the three modes($j = 1, 2, 3$). In particular, the lowest order term in ε arises from the guiding center drifting mode and is given by

$$\begin{aligned} < x_{\mathbf{k}}^2 > &= \frac{2\bar{\omega}_z}{\sqrt{det(\mathbf{g})}}\lambda^2|\frac{\Delta_0 - \Delta_1}{\Delta_0 D}|^2 + O(\varepsilon^2) \\ &= \frac{\bar{\omega}_z}{\sqrt{det(\mathbf{g})}}\lambda^2\frac{|\Delta_0 - \Delta_1|^2}{|\Delta_0|^2 - |\Delta_1|^2} + O(\varepsilon^2) \end{aligned} \tag{4.25}$$

where we have made use of Eq.(4.17). Furthermore, Eq.(4.16) allows us to simplify $|\Delta_0|^2 - |\Delta_1|^2$ as $\sqrt{det(\mathbf{g})}\Delta_2/\bar{\omega}_z$ and to rewrite $|\Delta_0 - \Delta_1|^2$ as $(g_{yy}g_{zz} - g_{yz}^2)\Delta_2/\bar{\omega}_z$. Using these relations in Eq.(4.25) leads us to Eq.(4.22) for $< x_{\mathbf{k}}^2 >$. However, since our results of ω_j and η_j are valid up to the second order of ε, $< x_{\mathbf{k}}^2 >$ given by Eq.(4.24) must agree to that given by Eq.(4.22) up to the second order of ε, rather than just the zeroth order. We have performed the tedious calculation for $< x_{\mathbf{k}}^2 >$ with the help of the symbolic algebra package MATHEMATICA and as a result, we indeed found that the term on the order of ε^2 vanishes.

In addition, we have also performed the similar calculations for $< y_{\mathbf{k}}^2 >$ and $< z_{\mathbf{k}}^2 >$. As expected, the $< y_{\mathbf{k}}^2 >$ displacements is similar to that of $< x_{\mathbf{k}}^2 >$, while the $< z_{\mathbf{k}}^2 >$ displacements is determined to the lowest order in ε by the parallel phonons.

4.3 Many-Particle Adiabatic Invariant

As we have seen, there exists a large frequency separation between the three branches of the phonon modes: $\omega_1 \gg \omega_2, \omega_3$ and we thus expect an adiabatic invariant associated with the high frequency cyclotron modes to exist. In particular, from Eq.(4.23) we see that the angle variables $\Psi_{\mathbf{k}_n}(n = 0, 1, 2, \cdot, \cdot, \cdot, N)$ corresponding to the action variable $I_{\mathbf{k}}^{(1)}$ are rapidly varying compared to the other variables and so there must exist an adiabatic invariant due to the presence of this fast time scale. Indeed, after we introduce the final canonical transformation

$$\theta_0 = \Psi_0^{(1)}, \theta_n = \Psi_{\mathbf{k}_n}^{(1)}(n \neq 0), J_0 = \sum_{n=0}^{N-1} I_{\mathbf{k}_n}, J_n = I_{\mathbf{k}_n}^{(1)}(n \neq 0),$$

θ_0 is the only rapidly varying variable and so the total action of the cyclotron modes J_0 is the adiabatic invariant.

In order to gain a physical insight into the adiabatic invariant J_0, we note that according to Eq.(4.5) and Eq.(4.6), the Hamiltonian $H_0(\mathbf{k})$ is exactly the same as that of a single particle confined in an anisotropic electrostatic potential well Φ_H. We thus expect that $I_{\mathbf{k}_n}$ must take the same conventional form of the cyclotron action of a single particle, which equals the cyclotron kinetic energy divided by the cyclotron frequency Ω_c. To prove this, we recall that in terms of $(\mathbf{e}, \mathbf{e}^*)$, $I_{\mathbf{k}_n} = e_1^* e_1$ according to Eq.(4.23), where according to Eq.(4.11) and Eq.(4.12), (e_1, e_1^*) are related to $(\mathbf{c}, \mathbf{c}^*)$ via

$$\begin{pmatrix} \mathbf{e} \\ \mathbf{e}^* \end{pmatrix} = \mathbf{S}^{-1} \begin{pmatrix} \mathbf{c} \\ \mathbf{c}^* \end{pmatrix}$$

$$= (\mathbf{\Lambda S^{\dagger} \Lambda}) \begin{pmatrix} \mathbf{c} \\ \mathbf{c^*} \end{pmatrix}.$$

Substitution of Eq.(4.13) for $\mathbf{S}$ yields

$$e_1^* = \eta_1^{(1)} c_1^* + \eta_1^{(2)} c_2^* + \eta_1^{(3)} c_3^* - \eta_1^{(4)} c_1 - \eta_1^{(5)} c_2 - \eta_1^{(6)} c_3 \tag{4.26}$$

where $\eta_1^{(j)}$ are given by Eq.(4.15), which leads to

$$e_1^* = \frac{c_1^* - i c_2^*}{\sqrt{2}} + \varepsilon^{3/2} \frac{c_3 + c_3^*}{2\sqrt{\tilde{\omega}_z}} (g_{xz} - i g_{yz}) + \frac{\varepsilon^2}{\sqrt{2}} g_{xx} (\frac{c_1^*}{2} + \frac{i}{2} c_2^* + \frac{3}{4} c_1 - \frac{i}{4} c_2)$$

$$+ \frac{\varepsilon^2}{\sqrt{2}} g_{yy} (-\frac{c_1^*}{2} - \frac{i}{2} c_2^* - \frac{3}{4} i c_2 + \frac{1}{4} c_1) + \frac{\varepsilon^2}{\sqrt{2}} g_{xy} (2 c_2^* - \frac{i}{2} c_1 + \frac{c_2}{2}).$$

We next express c_j and c_j^* in terms of particles' displacement $(x_{\mathbf{k}}, y_{\mathbf{k}}, z_{\mathbf{k}})$ and velocity (v_x, v_y, v_z). Noticing that the canonical momentum $m\mathbf{v_k} = \mathbf{p_k} - \frac{q}{c}\mathbf{A_k}$ with vector potential $\mathbf{A_k} = (-\frac{\mathbf{B}}{2} y_{\mathbf{k}}, \frac{\mathbf{B}}{2} x_{\mathbf{k}}, 0)$, we can rewrite Eq.(4.10) as

$$c_1 = \frac{\sqrt{m\Omega_c}}{2} (x_{\mathbf{k}} - i y_{\mathbf{k}}) + \frac{i m v_x}{\sqrt{m\Omega_c}}$$

$$c_2 = \frac{\sqrt{m\Omega_c}}{2} (y_{\mathbf{k}} + i x_{\mathbf{k}}) + \frac{i m v_y}{\sqrt{m\Omega_c}}$$

$$c_3 = \sqrt{\frac{m\omega_z}{2}} z_{\mathbf{k}} + \frac{i m v_z}{\sqrt{2 m \omega_z}}$$

and consequently Eq.(4.26) becomes

$$e_1^* = -\frac{m(v_y + i v_x)}{\sqrt{2 m \Omega_c}} + \varepsilon^2 \sqrt{\frac{m\Omega_c}{2}} z_{\mathbf{k}} (g_{xz} - i g_{yz}) + \varepsilon^2 \sqrt{\frac{m\Omega_c}{2}} x_{\mathbf{k}} (g_{xx} - i g_{xy})$$

$$-i\varepsilon^2 \sqrt{\frac{m\Omega_c}{2}} y_{\mathbf{k}} (g_{yy} + i g_{xy}) + \varepsilon^2 \frac{m v_x}{2 m \Omega_c} (\frac{i}{4} g_{xx} + i \frac{3}{4} g_{yy} + \frac{g_{xy}}{2})$$

$$+\varepsilon^2 \frac{m v_y}{2m\Omega_c}\left(\frac{g_{yy}}{4}+\frac{3}{4}g_{xx}-i\frac{3}{2}g_{xy}\right)$$

with this form for e_1^*, up to the second order in ε, the action variable $I_{\mathbf{k}}$ takes the form

$$I_{\mathbf{k}} = e_1^* e_1 = \frac{m(v_x^2+v_y^2)}{2\Omega_c} + \varepsilon^2 m[v_x(z_{\mathbf{k}}g_{yz}+y_{\mathbf{k}}g_{yy}+x_{\mathbf{k}}g_{xy}) - v_y(z_{\mathbf{k}}g_{xz}+y_{\mathbf{k}}g_{xy}+x_{\mathbf{k}}g_{xx})] \tag{4.27}$$

Recalling the physical meaning of the dynamical matrix, we write the Fourier component of the electrostatic restoring force $q\mathbf{E}_{\mathbf{k}} = -\partial\Phi_H/\partial\mathbf{u}_{\mathbf{k}} = -\mathbf{G}\cdot\mathbf{u}_{\mathbf{k}} = -m{\omega_p}^2\mathbf{g}\cdot\mathbf{u}_{\mathbf{k}}$, where Φ_H is given by Eq.(4.6). $\mathbf{E}_{\mathbf{k}}$ can be understood as the Fourier component of the electric field induced by the Fourier component of the particle displacement, $\mathbf{u}_{\mathbf{k}}$, from the equilibrium position. Using Eq.(4.6) we can relate the second term in Eq.(4.27) to $\mathbf{E}_{\mathbf{k}}$:

$$\begin{aligned} & v_x \quad (z_{\mathbf{k}}g_{yz}+y_{\mathbf{k}}g_{yy}+x_{\mathbf{k}}g_{xy}) - v_y(z_{\mathbf{k}}g_{xz}+y_{\mathbf{k}}g_{xy}+x_{\mathbf{k}}g_{xx}) \\ &= -v_x\frac{qE_{\mathbf{k}y}}{m{\omega_p}^2} + v_y\frac{qE_{\mathbf{k}x}}{m{\omega_p}^2} \\ &= -\frac{qE_{\mathbf{k}y}}{m{\omega_p}^2}(\mathbf{v}_\perp \times \mathbf{E}_{\mathbf{k}\perp})\cdot\hat{\mathbf{b}} \\ &= -\frac{\mathbf{v}_d\cdot\mathbf{v}_\perp}{\varepsilon^2\Omega_c} \end{aligned}$$

where $\mathbf{v}_d = c\mathbf{E}_{\mathbf{k}}\times\mathbf{B}/|\mathbf{B}|^2$ is the guiding center drift velocity, $\mathbf{v}_\perp = \mathbf{v} - (\hat{\mathbf{b}}\cdot\mathbf{v})\hat{\mathbf{b}}$ is the perpendicular velocity and $\mathbf{E}_{\mathbf{k}\perp} = \mathbf{E}_{\mathbf{k}} - (\hat{\mathbf{b}}\cdot\mathbf{E}_{\mathbf{k}})\hat{\mathbf{b}}$ is the perpendicular electric field. Substituting the above results into Eq.(4.27) yields

$$I_{\mathbf{k}} = \frac{m(\mathbf{v}_\perp - 2\mathbf{v}_d\cdot\mathbf{v}_\perp)}{2\Omega_c} \simeq \frac{m[(\mathbf{v}_\perp-\mathbf{v}_{\mathbf{d}})^2+O(\varepsilon^2)]}{2\Omega_c}$$

which equals the cyclotron energy divided by the the cyclotron frequency Ω_c. Finally, we note that since $\mathbf{E_k}$ is the Fourier component of the harmonic electric field at wavevector $\mathbf{k}$, one may easily check that to the first order of ϵ, the adiabatic invariant J_0, $J_0 = \sum_{\mathbf{k}} I_{\mathbf{k}}$, is also equal to the sum of the cyclotron actions of each single particle.

4.4 The Guiding Center Limit

Here and in following sections, we will focus on the $\epsilon \to 0$ limit, specifically, we will only keep the leading order terms in ϵ in the guiding center approximation in order to simplify the problem and also to make the guiding center picture more clear. In this case, the results of the eigenvalues and the eigenvalues of matrix $\mathbf{K}$ is reduced to

$$\omega_1 = \Omega_c;\ \omega_2 = \omega_p\bar{\omega}_z;\ \omega_3 = \epsilon\omega_p\frac{\sqrt{\det(\mathbf{g})}}{\bar{\omega}_z};$$

$$\eta_1 = \frac{1}{\sqrt{2}}\begin{pmatrix}1\\-i\\0\\0\\0\\0\end{pmatrix};\eta_2 = \begin{pmatrix}0\\0\\1\\0\\0\\0\end{pmatrix};\eta_3 = \frac{1}{\sqrt{2(|\Delta_0|^2-|\Delta_1|^2)}}\begin{pmatrix}\Delta_0\\i\Delta_0\\0\\-\Delta_1\\i\Delta_1\\0\end{pmatrix},$$

In this guiding center limit, as we have discussed, the adiabatic invariant J_0 simply becomes the particle's total perpendicular kinetic energy divided by the cyclotron frequency Ω_c. Also, in this limit, the particle's harmonic trajectory becomes simple. It consists of the rapid cyclotron motion perpendicular to the magnetic

field **B**, a slow oscillation along **B** and a very slow guiding center drifting motion. Since the guiding center drifting motion has much smaller frequency than the other motions and its amplitude is small compared with the inter-particle distance (see Eq.(4.25)), it has negligible contribution to the breaking of the adiabatic invariant and so will be ignored in our calculation.

The trajectory of $\mathbf{u_k}(t) = (x_\mathbf{k}(t), y_\mathbf{k}(t), z_\mathbf{k}(t))$ can be obtained by substituting the above expression for ω_j and $\eta_j (j = 1, 2, 3)$ into Eq.(4.20) and Eq.(4.21), which yields

$$\begin{aligned} x_\mathbf{k}(t) &= r_\mathbf{k} \sin(\Omega_c t + \Psi_\mathbf{k}) \\ y_\mathbf{k}(t) &= -r_\mathbf{k} \cos(\Omega_c t + \Psi_\mathbf{k}) \\ z_\mathbf{k}(t) &= Q_{2,\mathbf{k}} \cos \omega_z(\mathbf{k}) t + \frac{P_{2,\mathbf{k}}}{m\omega_z(\mathbf{k})} \sin \omega_z(\mathbf{k}) t \end{aligned} \tag{4.28}$$

where $r_\mathbf{k} = \sqrt{2I_\mathbf{k}/m\Omega_c}$, $\Psi_\mathbf{k}$ is the initial cyclotron phase. Having obtained the expression for the harmonic trajectory $\mathbf{u_k}(t)$, we now proceed to evaluation $d < J_0 > /dt$.

4.4.1 Integral Expression for the Breaking of the Adiabatic Invariant

In this section, we will derive an integral expression for the rate of the breaking of the adiabatic invariant $d < J_0 > /dt$. In Appendix 3A, we have derived a general formula for $d < J_0 > /dt$, which can be written as the following time integral (see Eq. (3.16) of Appendix 3A):

$$\frac{d < J_0 >}{dt} = (\frac{1}{T_\perp} - \frac{1}{T_\parallel}) \frac{1}{2\varepsilon} \int_{-\infty}^{\infty} d\tau < \frac{\partial \Phi(t)}{\partial \theta_0} \frac{\partial \Phi(0)}{\partial \theta_0} > \tag{4.29}$$

where $\tau = \omega_p t$ and the statistical average is performed by using distribution function $D_0(H, J_0)$:

$$D_0(H, J_0) = Z^{-1} \exp[-\frac{\omega_0 J_0}{T_\perp} - \frac{H - \omega_0 J_0}{T_\parallel}]$$

In order to evaluate the time integral, we follow the standard practice of substituting approximate trajectories determined by the harmonic Hamiltonian H_0, and we also replace $D_0(H, J_0)$ by $D_0(H_0, J_0)$. That is, we approximate the system by an ideal phonon gas. As we have mentioned in Chapter 3, this approximation is only expected to be valid for a strongly correlated system, i.e., Γ must be large. Moreover, despite the fact that the approximation of integration along the unperturbed orbits works well for a weakly correlated system, the validity of using the harmonic phonon orbits needs to be tested for a strongly correlated system.

To calculate the time integral in $d < J_0 > /dt$, we start with Φ given by Eq.(4.3), where $\mathbf{r}_l = \mathbf{R}_l + \mathbf{u}_l$, and the displacement $\mathbf{u}_l$ is related to the Fourier components $\mathbf{u_k}$ through the transformation given by Eq.(4.4) with $\mathbf{u_k} = (x_\mathbf{k}(t), y_\mathbf{k}(t), z_\mathbf{k}(t))$ determined by Eq.(4.28). As we expect, the process involving the creation and annihilation of one cyclotron phonon will dominate the equilibration rate so we Taylor expand $\partial\Phi(t)/\partial\theta_0$ in x and y keeping only the lowest order nonzero terms:

$$\frac{\partial\Phi(t)}{\partial\theta_0} = -\frac{q^2}{2}\sum_l \sum_{n\neq l} \frac{X_{ln}\frac{\partial x_{ln}(t)}{\partial\theta_0} + Y_{ln}\frac{\partial y_{ln}(t)}{\partial\theta_0}}{[(Z_{ln} + z_{ln})^2 + X_{ln}^2 + Y_{ln}^2]^{3/2}}$$

The correlation function appearing in Eq. (4.29) splits into parallel and perpendicular parts:

$$< \frac{\partial\Phi(t)}{\partial\theta_0}\frac{\partial\Phi(0)}{\partial\theta_0} > \;=\; \frac{q^4}{4a_0^6}\sum_l\sum_{n\neq l}\sum_{l'}\sum_{n'\neq l'} < h_{ln}(t)h_{l'n'}(0) >$$

$$< [X_{ln}\frac{\partial x_{ln}(t)}{\partial\theta_0} + Y_{ln}\frac{\partial y_{ln}(t)}{\partial\theta_0}][X_{l'n'}\frac{\partial x_{l'n'}(0)}{\partial\theta_0} + Y_{l'n'}\frac{\partial y_{l'n'}(0)}{\partial\theta_0}] >$$

where we have used the notation

$$h_{ln}(t) = \frac{a_0^3}{[(Z_{ln} + z_{ln}(t))^2 + X_{ln}^2 + Y_{ln}^2]^{3/2}}. \tag{4.30}$$

Here $a_0 \equiv a/2$ is half of the lattice constant, $\tau = \omega_p t$, $X_{ln} = \hat{\mathbf{x}} \cdot \mathbf{R}_{ln}$; $Y_{ln} = \hat{\mathbf{y}} \cdot \mathbf{R}_{ln}$; $Z_{ln} = \hat{\mathbf{b}} \cdot \mathbf{R}_{ln}$, $\mathbf{R}_{ln} \equiv \mathbf{R}_n - \mathbf{R}_l$ and

$$\begin{aligned}
x_{ln}(t) &= \hat{\mathbf{x}} \cdot (\mathbf{u}_l - \mathbf{u}_n) \\
&= \sqrt{\frac{2}{N}} \sum_{\mathbf{k}>0} [r_{\mathbf{k}} c_{ln} \sin(\Omega_c t + \Psi_{\mathbf{k}}) + r_{-\mathbf{k}} s_{ln} \sin(\Omega_c t + \Psi_{-\mathbf{k}})] \\
y_{ln}(t) &= \hat{\mathbf{y}} \cdot (\mathbf{u}_l - \mathbf{u}_n) \\
&= \sqrt{\frac{2}{N}} \sum_{\mathbf{k}>0} [-r_{\mathbf{k}} c_{ln} \cos(\Omega_c t + \Psi_{\mathbf{k}}) - r_{-\mathbf{k}} s_{ln} \cos(\Omega_c t + \Psi_{-\mathbf{k}})] \\
z_{ln}(t) &= \hat{\mathbf{b}} \cdot (\mathbf{u}_l - \mathbf{u}_n) \\
&= \sqrt{\frac{2}{N}} \sum_{\mathbf{k}>0} [c_{ln}(z_{\mathbf{k}} \cos \omega_z(\mathbf{k}) t + \frac{\dot{z}_{\mathbf{k}}}{\omega_z(\mathbf{k})} \sin \omega_z(\mathbf{k}) t) \\
&\qquad s_{ln}(z_{-\mathbf{k}} \cos \omega_z(\mathbf{k}) t + \frac{\dot{z}_{-\mathbf{k}}}{\omega_z(\mathbf{k})} \sin \omega_z(\mathbf{k}) t)].
\end{aligned}$$

where notations c_{ln} and s_{ln} are defined as

$$\begin{aligned}
c_{ln} &= \cos \mathbf{k} \cdot \mathbf{R}_l - \cos \mathbf{k} \cdot \mathbf{R}_n \\
s_{ln} &= \sin \mathbf{k} \cdot \mathbf{R}_l - \sin \mathbf{k} \cdot \mathbf{R}_n.
\end{aligned}$$

In order to evaluate $< \frac{\partial\Phi(t)}{\partial\theta_0}\frac{\partial\Phi(0)}{\partial\theta_0} >$, we first simplify $< \frac{\partial x_{ln}(t)}{\partial\theta_0}\frac{\partial x_{l'n'}(0)}{\partial\theta_0} >$:

$$< \frac{\partial x_{ln}(t)}{\partial\theta_0}\frac{\partial x_{l'n'}(0)}{\partial\theta_0} >$$

$$= \frac{2}{N}\sum_{\mathbf{k}>0}\sum_{\mathbf{k}'>0}[< r_{\mathbf{k}}r_{\mathbf{k}'} >< \cos(\Omega_c t + \Psi_{\mathbf{k}})\cos\Psi_{\mathbf{k}'} > c_{ln}c_{l'n'}$$

$$+ < r_{-\mathbf{k}}r_{-\mathbf{k}'} >< \cos(\Omega_c t + \Psi_{-\mathbf{k}})\cos\Psi_{-\mathbf{k}'} > s_{ln}s_{l'n'}]$$

$$= (\delta_{ll'} + \delta_{nn'} - \delta_{ln'} - \delta_{nl'})\frac{T_\perp}{m{\Omega_c}^2}\cos\Omega_c t$$

where we have made use of the fact that $< \sin\Psi_{\mathbf{k}}\sin\Psi_{\mathbf{k}'} >= 0$; $< \cos\Psi_{\mathbf{k}}\cos\Psi_{\mathbf{k}'} >= \frac{1}{2}\delta_{\mathbf{k}\mathbf{k}'}$ and that $< r^2(\mathbf{k}) > \simeq \frac{T_\perp}{m{\Omega_c}^2}$, where as an approximation, $D_0(H_0, J_0)$ has been used for the statistical average of $r^2(\mathbf{k})$.

By the same argument, we also obtain

$$< \frac{\partial y_{ln}(t)}{\partial\theta_0}\frac{\partial y_{l'n'}(0)}{\partial\theta_0} >= (\delta_{ll'} + \delta_{nn'} - \delta_{ln'} - \delta_{nl'})\frac{T_\perp}{m{\Omega_c}^2}\cos\Omega_c t;$$

$$< \frac{\partial x_{ln}(t)}{\partial\theta_0}\frac{\partial y_{l'n'}(0)}{\partial\theta_0} >= -(\delta_{ll'} + \delta_{nn'} - \delta_{ln'} - \delta_{nl'})\frac{T_\perp}{m{\Omega_c}^2}\sin\Omega_c t$$

We then have

$$< \frac{\partial\Phi(t)}{\partial\theta_0}\frac{\partial\Phi(0)}{\partial\theta_0} >$$

$$= \frac{T_\perp q^4}{4m{\Omega_c}^2 a_0^6}\sum_l\sum_{n\neq l}\sum_{l'}\sum_{n'\neq l'}(\delta_{ll'} + \delta_{nn'} - \delta_{ln'} - \delta_{nl'}) < h_{ln}(t)h_{l'n'}(0) >$$

$$[(X_{ln}X_{l'n'} + Y_{ln}Y_{l'n'})\cos\Omega_c t - (X_{ln}Y_{l'n'} - Y_{ln}X_{l'n'})\sin\Omega_c t]$$

Furthermore, as we will see soon in the following section, the correlation function

$< h_{ln}(t)h_{ln'}(0) >$ is symmetric under exchange $(ln) \leftrightarrow (ln')$ and so the sum of the terms proportional to $\sin \Omega_c t$ vanishes because these terms are antisymmetric under the exchange of the dummy indices. Finally, substituting $< \frac{\partial \Phi(t)}{\partial \theta_0} \frac{\partial \Phi}{\partial \theta_0} >$ into Eq.(4.29) for $\frac{d<J_0>}{dt}$ we obtain

$$\frac{d < J_0 >}{dt} = \frac{1}{\pi}(\frac{3}{\pi})^{1/3}(1 - \frac{T_\perp}{T_\parallel})T_\perp \varepsilon \Gamma_\perp \sum_l \sum_{n>l} \sum_{n' \neq l} (\bar{X}_{ln}\bar{X}_{ln'} + \bar{Y}_{ln}\bar{Y}_{ln'})$$

$$\int_{-\infty}^{\infty} d\tau \cos(\tau/\varepsilon) < h_{ln}(t)h_{ln'}(0) >$$

where $\bar{X} \equiv X/a_0, \bar{Y} \equiv Y/a_0$, and we have used the relation between the density n and $a_0 : 4a_0^3 n = 1$ for a bcc lattice. Here we define $\sum_{n>l}$ to be the sum over lattice sites n with $\bar{Z}_{ln} = \bar{Z}_n - \bar{Z}_l > 0$ and define $\sum_{n' \neq l}$ to be the sum over all the lattice sites except l.

We note that it appears that the time integral in $\frac{d<J_0>}{dt}$ is not convergent because as $\tau \to \infty$, $< h_{ln}(t)h_{ln'}(0) > \to < h_{ln}(t) >< h_{ln'}(0) >$, which does not vanish (see Eq.(4.30)). However, when summing over the lattice, for every (l, n) there exists a point $(l, \bar{n})$ for which $X_{l\bar{n}} = -X_{ln}$ (i.e. a reflection) but $< h_{l\bar{n}} >=< h_{ln} >$, so the sum is antisymmetric and vanishes as $\tau \to \infty$.

Physically this can be understood from the picture in Fig.4.1. From Fig.4.1 we see that the adiabatic invariant is broken by the perpendicular component of the slowly varying electrostatic force $\delta \mathbf{f}_{ln\perp}$, which has the form of $q^2(X_{ln}, Y_{ln})h_{ln}$. Obviously while $< \delta \mathbf{f}_{ln\perp} > \neq 0$ since $< h_{ln} > \neq 0$, the total averaged perpendicular force $\sum_{ln} < \delta \mathbf{f}_{ln\perp} >$ does vanish because the system is in equilibrium.

However, we will evaluate the time integral before we perform the lattice sums, so it proves useful to write down a form for $\frac{d<J_0>}{dt}$ where each term is explicitly

convergent. This can be done by integrating by parts:

$$\int_{-\infty}^{+\infty} d\tau \cos\frac{\tau}{\varepsilon} < h_{ln}(t)h_{ln'}(0) >= \varepsilon \sin\frac{\tau}{\varepsilon} < h_{ln}(t)h_{ln'}(0) > |_{-\infty}^{+\infty}$$

$$-\varepsilon \int_{-\infty}^{+\infty} d\tau \sin\frac{\tau}{\varepsilon}\frac{d}{d\tau} < h_{ln}(t)h_{ln'}(0) >$$

We neglect the first term because it's contribution to $\frac{d<J_0>}{dt}$ vanishes after performing the lattice sum, since $< h_{ln}(\infty)h_{ln'}(0) >=< h_{ln}(\infty) >< h_{ln'}(0) >$. However, we will soon see that the second term is a convergent integral and it gives the rate of the breaking of the adiabatic invariant. We can now write the rate of temperature equilibration $\nu = \dot{T_\perp}/T_\perp$ as

$$\nu = \sum_{n>l}\sum_{n'\neq l} \nu_{lnn'} \tag{4.31}$$

$$\nu_{lnn'} = -\frac{\Omega_c}{\pi}(\frac{3}{\pi})^{1/3}(1-\frac{T_\perp}{T_\parallel})\varepsilon^2\Gamma_\perp\bar{\rho}_{ln}\bar{\rho}_{ln'}\cos(\phi_{ln}-\phi_{ln'})$$

$$\int_{-\infty}^{\infty} d\tau \sin(\tau/\varepsilon)\frac{d}{d\tau} < h_{ln}(t)h_{ln'}(0) >$$

where we have used the approximation $< J_0 >\simeq NT_\perp/\Omega_c$ and where $\bar{\rho}_{ln} = \sqrt{\bar{X}_{ln}^2 + \bar{Y}_{ln}^2}$ and ϕ_{ln} is the azimuthal angle of $\mathbf{R}_{ln}$ with respect to the magnetic field: $\phi_{ln} \equiv \tan^{-1}[\bar{Y}_{ln}/\bar{X}_{ln}]$ (see Fig.4.1). Note that since $\nu_{lnn'}$ only depends on l, n and n' through the relative positions, we have changed $\sum_l \sum_{n>l} \sum_{n'\neq l}$ to $N\sum_{n>l}\sum_{n'\neq l}$.

4.4.2 Asymptotic Expression for ν in the Limit $\varepsilon \ll 1$

In this section, we derive an asymptotic expression for ν given by Eq.(4.31) in the $\varepsilon \ll 1$ limit. We first derive an asymptotic expression for $\nu_{lnn'}$. Since $\varepsilon \ll 1$, the integrand of the time integral in $\nu_{lnn'}$ consists of a rapidly oscillating func-

tion $\cos(\tau/\epsilon)$ associated with the cyclotron motion and a slowly varying function $\frac{d}{d\tau} < h_{ln}(t)h_{ln'}(0) >$ associated with the parallel oscillation. This behavior of the integrand leads to an exponentially small result of the rate ν.

As discussed in section 4.1, the equilibration rate of the amorphous systems in the experiments is determined by averaging ν over the randomly varying crystal axes orientation. Since the result of such an average is dominated by the peak values of $\nu_{lnn'}$, which occur at small but nonzero $\bar{\rho}/\bar{Z}$, we will therefore focus on the $\tan\theta_{ln} = \bar{\rho}_{ln}/\bar{Z}_{ln} \leq 1$ and $\tan\theta_{ln'} = \bar{\rho}_{ln'}/\bar{Z}_{ln'} \leq 1$ case. Here θ_{ln} ($\theta_{ln'}$) is the angle between $\mathbf{R}_{ln}$ ($\mathbf{R}_{ln'}$) and $\mathbf{B}$.

In order to evaluate the correlation function $< h_{ln}(t)h_{ln'}(0) >$, we note the following identity:

$$h_{ln} = \frac{1}{\bar{\rho}_{ln}^3}\int_0^\infty dx x J_1(x) e^{-x|\bar{Z}_{ln}+\bar{z}_{ln}|/\rho_{ln}} \tag{4.32}$$

When θ_{ln} is small, $|\bar{Z}_{ln}| \sim O(\bar{R}_{ln}) \gg |\bar{z}_{ln}|$ in the harmonic approximation. In this case we can make the approximation:

$$|\bar{Z}_{ln} + \bar{z}_{ln}| \simeq |\bar{Z}_{ln}| + sgn(\bar{Z}_{ln})\bar{z}_{ln}, \tag{4.33}$$

which yields tractable Gaussian integrals when $< h_{ln}(t)h_{ln'}(0) >$ is evaluated. However, in the harmonic approximation there is an exponentially small but nevertheless finite probability for $|\bar{Z}_{ln}| + sgn(\bar{Z}_{ln})\bar{z}_{ln} < 0$. In this case, substitution of Eq.(4.33) into Eq.(4.32) yields a singular result. In order to remove the singularity, but still use Eq.(4.33), we introduce a cutoff β to the integral:

$$h_{ln} = \frac{1}{\bar{\rho}_{ln}^3}\int_0^\beta dx x J_1(x) e^{-x(|\bar{Z}_{ln}|+sgn(\bar{Z}_{ln})\bar{z}_{ln})/\rho_{ln}}. \tag{4.34}$$

The expression for the rate will be dominated by values of $|\bar{z}_{ln}| < |\bar{Z}_{ln}|$ so use of approximation Eq.(4.33) is justified. The small measure of conditions for which

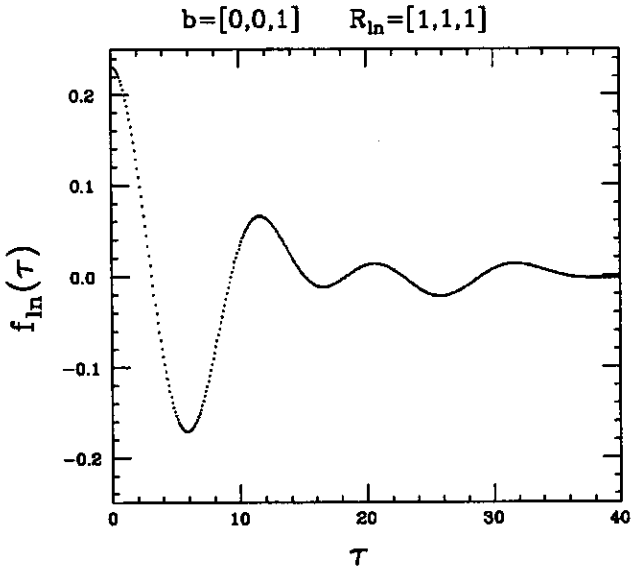

Figure 4.2: Plot of the parallel correlation function $f_{ln}(\tau)$ for a 3D magnetized plasma

$|\bar{Z}_{ln}| + sgn(\bar{Z}_{ln})\bar{z}_{ln} < 0$ is suppressed by β. We will find that there is a range of large but finite β values for which the rate is independent of β, provided that $\epsilon\Gamma_{||} > 1$.

With the form of $h_{ln}(t)$ and $h_{ln'}(0)$ given by Eq. (4.34), we can easily perform the statistical average for $< h_{ln}(t)h_{ln'}(0) >$ by using the results derived in Appendix 3C, which allows us to rewrite $\nu_{lnn'}$ in the following form

$$\nu_{lnn'} = \frac{\Omega_c}{\pi}(\frac{3}{\pi})^{1/3}(1 - \frac{T_\perp}{T_{||}})\epsilon\Gamma_\perp\rho_{ln}^{-2}\rho_{ln'}^{-2}\cos(\phi_{ln} - \phi_{ln'})\int_0^\beta\int_0^\beta dx_1dx_2$$

$$J_1(x_1)J_1(x_2)e^{-x_1|\cot\theta_{ln}| - x_2|\cot\theta_{ln'}| + \frac{2}{3\Gamma_{||}}(\frac{3}{\pi})^{2/3}[f_{l-n}(0)\frac{x_1^2}{\bar{\rho}_{ln}^2} + f_{l-n'}(0)\frac{x_2^2}{\bar{\rho}_{ln'}^2}]}$$

$$\cdot I_{lnn'}(\epsilon, sgn(\bar{Z}_{ln}\bar{Z}_{ln'})\frac{2x_1x_2}{3\Gamma_{||}\bar{\rho}_{ln}\bar{\rho}_{ln'}}(\frac{3}{\pi})^{2/3}) \qquad (4.35)$$

Here, the correlation function $f_{l-n}(\tau) = \frac{m\omega_p^2}{4T_{||}} < z_{ln}(t)z_{ln}(0) >$ is an integral over the

Brillouin zone (see Fig. 4.2):

$$f_{l-n}(\tau) = \frac{1}{2}\int_{B.Z}\frac{vd^3\mathbf{k}}{(2\pi)^3}\frac{1-\cos\mathbf{k}\cdot\mathbf{R}_{ln}}{\bar{\omega}_z(\mathbf{k})^2}\cos(\bar{\omega}_z(\mathbf{k})\tau).$$

The function $I_{lnn'}(\epsilon,\alpha)$ is defined as

$$\begin{aligned} I_{lnn'}(\epsilon,\alpha) &= -\varepsilon\alpha\int_{-\infty}^{\infty}d\tau\sin(\frac{\tau}{\epsilon})\frac{d}{d\tau}[f_{l-n}(\tau)+f_{l-n'}(\tau)-f_{n-n'}(\tau)] \\ & e^{\alpha[f_{l-n}(\tau)+f_{l-n'}(\tau)-f_{n-n'}(\tau)]} \end{aligned} \tag{4.36}$$

Asymptotic Formula for $I_{lnn'}(\epsilon,\alpha)$ in the $\epsilon \ll 1$ Limit

To evaluate $\nu_{lnn'}$, we first need to calculate the time integral $I_{lnn'}(\epsilon,\alpha)$. We note that $I_{lnn'}(\epsilon,\alpha)$ is a convergent integral because the envelope of f_{l-n} approaches zero like $1/\tau^{7/2}$ as $\tau\to\infty$ (see Appendix 4A).

For $\epsilon \ll 1$, the integral can evaluated using the saddle point method by deforming the integration contour into the complex τ plane. By changing the variable τ to $\bar{t} = -i\tau$, Eq.(4.36) becomes

$$I_{lnn'}(\epsilon,\alpha) = \alpha\, Im\int_{-i\infty}^{i\infty}d\bar{t}\, e^{\alpha[f_{l-n}(i\bar{t})+f_{l-n'}(i\bar{t})-f_{n-n'}(i\bar{t})]}\frac{d}{d\bar{t}}[f_{l-n}(i\bar{t})+f_{l-n'}(i\bar{t})-f_{n-n'}(i\bar{t})] \tag{4.37}$$

Since the integrand is an entire function of $\bar{t}$, we can deform the contour through the saddle points. The saddle point positions are the solutions of the saddle point equation:

$$\frac{d}{d\bar{t}}[f_{l-n}(i\bar{t})+f_{l-n'}(i\bar{t})-f_{n-n'}(i\bar{t})] = \frac{1}{\epsilon\alpha} \tag{4.38}$$

As we will see, the integrand of $\nu_{lnn'}$ given by Eq.(4.35) is peaked at $(x_1,x_2)\sim(\frac{1}{\varepsilon|\cot\theta_{ln}|},\frac{1}{\varepsilon|\cot\theta_{ln'}|})$, where θ_{ln} is the angle between $\mathbf{R}_{ln}$ and the magnetic field

(see Fig.4.1). Using the α value given by Eq.(4.35), this peak corresponds to $\epsilon\alpha = \epsilon \cdot \frac{2x_1x_2}{3\Gamma_{\|}\bar{\rho}_{ln}\bar{\rho}_{ln'}}(\frac{3}{\pi})^{2/3} \sim \frac{1}{\epsilon\Gamma_{\|}|\bar{Z}_{ln}\bar{Z}_{ln'}|}$. Furthermore we will also see that in order for Eq.(4.35) to be valid, we must require $1/\sqrt{\epsilon\Gamma_{\|}} \ll \bar{Z}_{ln}, \bar{Z}_{ln'}$, which yields $\epsilon\alpha \ll 1$. We thus expect that the solutions of the saddle point equation satisfy $|\bar{t}| \gg 1$, which allows us to use the asymptotic expressions for $f_{l-n}(i\bar{t}), f_{l-n'}(i\bar{t})$ and $f_{n-n'}(i\bar{t})$ derived in Appendix 4A, for example,

$$f_{l-n}(i\bar{t}) \simeq \frac{3\sqrt{2\pi}}{8\pi^2}\frac{\bar{Z}_{ln}^2}{c_0^{5/2}}\frac{e^{\bar{t}}}{\bar{t}^{7/2}}, \tag{4.39}$$

where only the lowest order term in $1/\bar{t}$ has been kept and the parameter c_0 is equal to $1.583 \times 10^{-2} + 0.102(b_x^4 + b_y^4 + b_z^4)$. Then to the lowest order in $1/\bar{t}$ and using the form for α from Eq.(4.35), the saddle point equation becomes

$$\frac{e^{\bar{t}}}{\bar{t}^{7/2}} = p_0(\epsilon x_1 x_2) \tag{4.40}$$

where

$$p_0(x) = \pi\sqrt{2\pi}(\frac{\pi}{3})^{2/3}c_0^{5/2}\frac{\Gamma_{\|}}{x}|\tan\theta_{ln}||\tan\theta_{ln'}|$$

and where we have used the identity $\bar{Z}_{ln}^2 + \bar{Z}_{ln'}^2 - \bar{Z}_{nn'}^2 = 2\bar{Z}_{ln}\bar{Z}_{ln'}$. There are an infinite number of saddle points distributed symmetrically on each side of the real $\bar{t}$ axis as well as a pure real solution (see Fig.4.3). However, for small ϵ, as we show in the following, only the real saddle point gives the dominant contribution.

For large $p_0(\epsilon x_1 x_2)$, Eq. (4.40) has an iterative solution

$$\bar{t}_j \simeq \ln p_0 + i2\pi j + \frac{7}{2}\ln[\ln p_0 + i2\pi j] \tag{4.41}$$

where $j = 0, \pm1, \pm2, \cdots, p_0 \equiv p_0(\epsilon x_1 x_2)$. By employing the saddle point equation and using the approximation $f'_{l-n}(i\bar{t}) \simeq f_{l-n}(i\bar{t})$ for large $|\bar{t}|$, we can rewrite the exponent

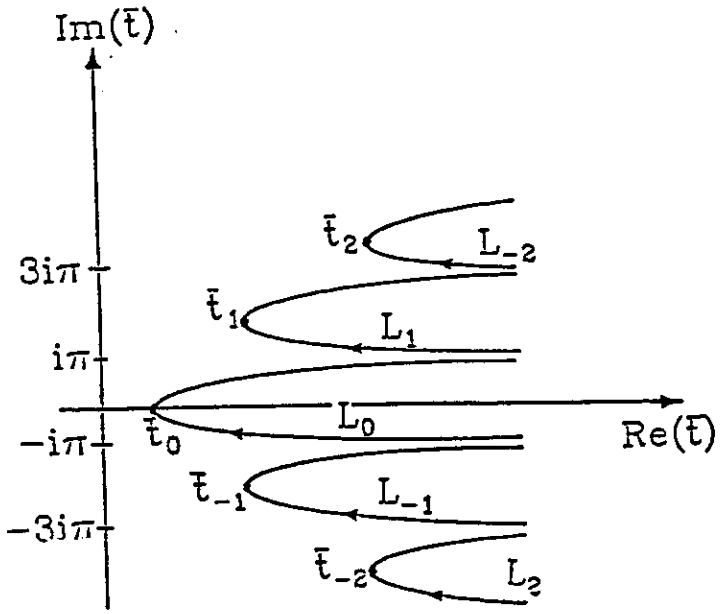

Figure 4.3: Plot of the steepest decent contour in the complex $\bar{t}$ plane for the saddle point calculation of $I_{\mathbf{m}^*}(\epsilon, \alpha)$

in Eq. (4.37) at $\bar{t} = \bar{t}_j$ as

$$h_j = -\frac{\bar{t}_j}{\epsilon} + \alpha[f_{l-n}(i\bar{t}_j) + f_{l-n'}(i\bar{t}_j) - f_{n-n'}(i\bar{t}_j)]$$

$$\simeq -\frac{1}{\epsilon}(\bar{t}_j - 1)$$

According to the saddle point method , the magnitude of $I_{lnn'}(\epsilon, \alpha)$ is dominated by the exponential factor $\exp[Re(h_j)]$, which is given by

$$e^{Re(h_j)} \simeq e^{-\frac{7}{4\epsilon}\ln[4\pi^2 j^2 + \ln^2 p_0]} e^{-\frac{1}{\epsilon}(\ln p_0 - 1)}$$

$$\simeq [1 + (\frac{2\pi j}{\ln p_0})^2]^{-7/4\epsilon}$$

Obviously $e^{Re(h_j)} \ll e^{Re(h_0)}$ for $j \neq 0$ and this allows us to neglect the $j \neq 0$ terms.

Making use of the approximation $f''_{l-n}(i\bar{t}_0) \simeq f'_{l-n}(i\bar{t}_0)$ for large $\bar{t}_0$, we obtain

$$I_{lnn'}(\epsilon, \alpha) \simeq \sqrt{\frac{2\pi}{\epsilon}} e^{-\frac{1}{\epsilon}(\bar{t}_0 - 1)} \tag{4.42}$$

We note that the largest $I_{lnn'}$ comes from the smallest $\bar{t}_0$. According to Eq. (4.40), $\bar{t}_0$ is the smallest only when p_0 is the smallest, which occurs when $\tan\theta_{ln}$ and $\tan\theta_{ln'}$ are small. Therefore, we expect that $\nu_{lnn'}$ is dominated by the contributions from the terms with small θ_{ln} and small $\theta_{ln'}$. However, at $\theta_{ln} = 0$ and $\theta_{ln'} = 0$, ρ_{ln} and $\rho_{ln'}$ vanish and thus $\nu_{lnn'}$ vanish. Therefore, as we discussed at the beginning of this chapter, the maximum rate occurs at small but nonzero θ_{ln} and $\theta_{ln'}$. In this case, the sum in Eq.(4.31) can effectively be replaced by the sum over lattice sites with small θ_{ln} and $\theta_{ln'}$.

Sum Over Lattice Sites

For a bcc lattice, for each lattice site n', there always exists another lattice site $\bar{n}'$ which is the reflection point of n' with respect to l (see Fig.4.4). Because $|\tan\theta_{ln'}| = |\tan\theta_{l\bar{n}'}|$ and $\phi_{l\bar{n}'} = \pi - \phi_{ln'}$, we can easily show by using Eq. (4.42) that $\nu_{lnn'} = -\nu_{ln\bar{n}'}$ for each n', which leads to $\nu = 0$. However, this conclusion is actually not correct. In fact, $\nu_{lnn'}$ and $\nu_{ln\bar{n}'}$ are not equal and one is much smaller than the other. In order to see this, we must keep the next order term in the asymptotic expression of $f_{l-n}(i\tau)$. This next order term $\delta f_{l-n}(i\tau)$ is given by Eq.(4.65) derived in Appendix 4A. By taking $\delta f_{l-n}(i\tau)$ into account, we can rewrite the saddle point equation as

$$\frac{e^{\tau}}{\tau^{7/2}} = p_0[1 + \frac{5}{24}\frac{1}{c_0\tau}(\frac{\bar{Z}^4_{ln} + \bar{Z}^4_{ln'} - \bar{Z}^4_{nn'}}{\bar{Z}_{ln}\bar{Z}_{ln'}}) - 10\frac{c_3}{c_0\tau}(\frac{\mu_{l-n} + \mu_{l-n'} - \mu_{n-n'}}{\bar{Z}_{ln}\bar{Z}_{ln'}})] \tag{4.43}$$

In order to focus on the difference between $I_{lnn'}$ and $I_{ln\bar{n}'}$, terms on the order of $1/\tau$ which only depend on R_{ln} or $R_{ln'}$ through $\bar{Z}^2_{ln}$ or $\bar{Z}^2_{ln'}$ have been ignored because

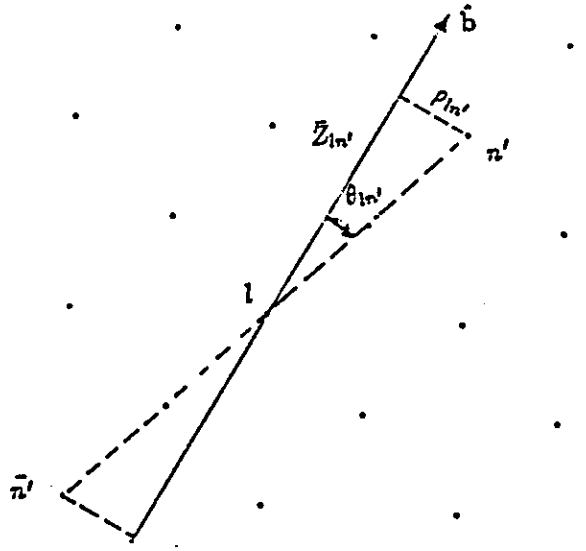

Figure 4.4: Schematic picture for a lattice site n and its reflection point $\bar{n}$.

they cause no difference between $I_{lnn'}$ and $I_{ln\bar{n}'}$. In Eq. (4.43), $c_3 \simeq 0.102$ and μ_{l-n} is defined by Eq.(4.67) of Appendix 4A as:

$$\mu_{l-n} = \bar{Z}_{ln}\rho_{ln}[b_x^3\sqrt{1-b_x^2}\cos(\phi_{ln}-\phi_x)+b_y^3\sqrt{1-b_y^2}\cos(\phi_{ln}-\phi_y)+b_z^3\sqrt{1-b_z^2}\cos(\phi_{ln}-\phi_z)]$$

Here (b_x, b_y, b_z) are the components of $\hat{\mathbf{b}} \equiv \mathbf{B}/B$ projected on the crystal axes $(\hat{x}, \hat{y}, \hat{z})$. (ϕ_x, ϕ_y, ϕ_z) are the azimuthal angles of $(\hat{x}, \hat{y}, \hat{z})$ with respect to $\hat{\mathbf{b}}$ separately (see Fig.4.19 in Appendix 4A). As we expected, only the relative azimuthal angles appear in μ_{l-n}, etc.

We note that for small θ_{ln} and $\theta_{ln'}$, we have $\bar{Z}_{ln} \gg \rho_{ln}$ and $\bar{Z}_{ln'} \gg \rho_{ln'}$ and therefore we expect that the third term in the bracket of Eq. (4.43) is small compared with the second term. We may therefore write the saddle point solution as

$$\bar{t} \simeq \bar{t}_s + \frac{5}{24}\frac{g_{lnn'}}{c_0\bar{t}_s} \tag{4.44}$$

where $\bar{t}_s$ is the solution to Eq. (4.40) and $g_{lnn'} \equiv 4(\bar{Z}_{ln}^2 + \bar{Z}_{ln'}^2) - 6\bar{Z}_{ln}\bar{Z}_{ln'}$. Obviously $g_{ln\bar{n}'} - g_{lnn'} = 12\bar{Z}_{ln}\bar{Z}_{ln'}$, which shows that for $\bar{Z}_{ln} \cdot \bar{Z}_{ln'} > 0$, $I_{ln\bar{n}'}$ is smaller than

$I_{lnn'}$ by a factor $\gamma \equiv exp[-5\bar{Z}_{ln}\bar{Z}_{ln'}/(2\epsilon c_0 \bar{t}_s)]$. Furthermore, as $\epsilon \to 0$, Eq.(4.41) implies $\epsilon \bar{t}_s \to 0$ and so γ is exponentially small for $\epsilon \ll 1$. Because $\gamma \ll 1$, $\nu_{lnn'} \simeq O(\gamma)\nu_{lnn'} \ll \nu_{lnn'}$ for $\bar{Z}_{ln} \cdot \bar{Z}_{ln'} > 0$ and $\epsilon \ll 1$.

Another important observation for Eq. (4.44) is that when $\bar{Z}_{ln}$ and $\bar{Z}_{ln'}$ become larger, $\bar{t}$ becomes larger. We therefore expect that $\nu_{lnn'}$ is only dominated by the contributions from the nearest neighbors. We will see this in our numerical analysis in the next section.

We have seen that the rate is dominated by small θ_{ln} and $\theta_{ln'}$. Counting only nearest neighbors, for a bcc lattice, θ_{ln} and $\theta_{ln'}$ can both be small only when $n = n'$. Therefore, as a conclusion of our discussion, we rewrite Eq.(4.31) as a sum over the nearest neighbors:

$$\nu = \sum_{n>l} \nu_{lnn} \tag{4.45}$$

To calculate ν_{lnn}, we substitute the leading order term in Eq. (4.41) for the pure real saddle point $\bar{t}_0 \simeq \ln p_0$ into ν_{lnn} given by Eq. (4.35) and obtain

$$\nu_{lnn} = \frac{\Omega_c}{\pi}(\frac{3}{\pi})^{1/3}(1 - \frac{T_\perp}{T_\parallel})\epsilon\sqrt{\frac{2\pi}{\epsilon}}\Gamma_\perp \bar{\rho}_{ln}^{-4} e[1 - \ln p_0(\epsilon)]/\epsilon | \int_0^\beta dx A_{ln}(x)|^2 \tag{4.46}$$

where

$$A_{ln}(x) \equiv x^{1+1/\epsilon} J_1(x) e^{-x|\cot\theta_{ln}| + \frac{2}{3\Gamma_\parallel}(\frac{3}{\pi})^{2/3} f_{l-n}(0)\frac{x^2}{\bar{\rho}_{ln}^2}}. \tag{4.47}$$

$A_{ln}(x)$ is a oscillatory function with the envelope sharply peaked at $x_a \simeq (\frac{1}{2} + 1/\epsilon)/|\cot\theta_{ln}|$, before starting to grow at $x_b \simeq \frac{3}{4}(\frac{\pi}{3})^{2/3}\rho_{ln}\bar{Z}_{ln}\Gamma_\parallel/f_{l-n}(0)$ (see Fig.4.5). This growth is due to the aforementioned unphysical singularity arising from the approximation for the absolute value in the integral transform for h_{ln} (see Eq.(4.32) and Eq.(4.34)). However, we find that the integral $\int_0^\beta dx A_{ln}(x)$ is independent of the choice of β provided that $x_a \ll \beta \ll x_b$, which implies that $\epsilon\Gamma_\parallel \gg 1/\bar{Z}_{ln}^2$

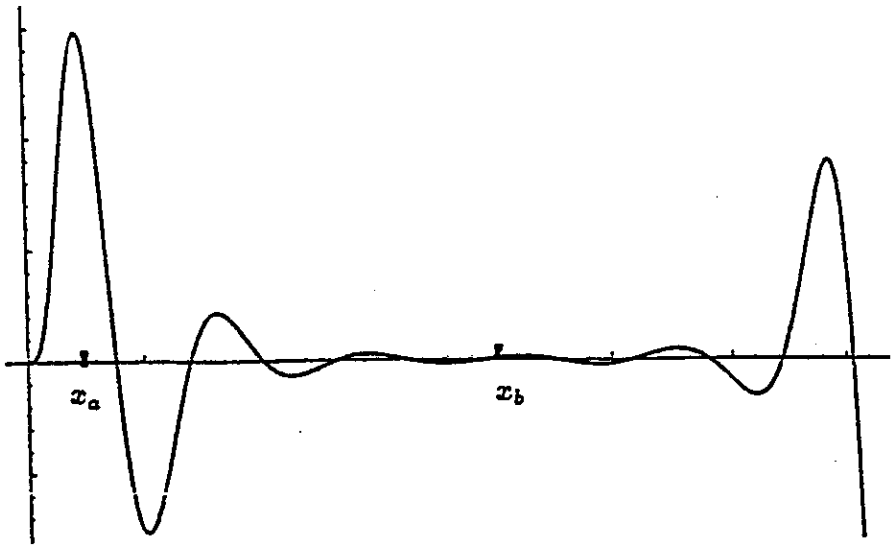

Figure 4.5: A schematic plot of $A_{ln}(x)$

for $\epsilon \ll 1$. The physical meaning for this inequality is clear. According to our crude estimate based on the phonon collision picture, the equilibration is dominated by the displacement δz with a peak at $\delta \bar{z}_m \sim 1/\sqrt{\epsilon\Gamma_{||}}$ and thus in order to use Eq.(4.33) we must require $\delta \bar{z}_m < \bar{Z}_{ln}$, which leads to inequality $\epsilon\Gamma_{||} > 1/\bar{Z}_{ln}^2$. This is a validity condition for the use of the integral transform Eq.(4.34) under the harmonic approximation. In particular, for nearest neighbors l and n with $\theta_{ln} < 1$, this validity condition is reduced to the validity condition of the harmonic approximation: $\epsilon\Gamma_{||} > 1$, which was derived at the beginning of this chapter (see section 4.1).

When condition $\epsilon\Gamma_{||} \gg 1$ is satisfied, we may ignore the $O(x^2)$ term in the exponent of Eq. (4.47) and take the $\beta \to \infty$ limit, we obtain[8]

$$\int_0^\beta dx A_{ln}(x) \simeq \int_0^\infty dx x^{1+1/\epsilon} J_1(x) e^{-x|\cot\theta_{ln}|}$$

$$= (-1)^{1+1/\epsilon} C(\theta_{ln}, 1/\epsilon) \bar{\rho}_{ln}^{2+1/\epsilon} / \bar{R}_{ln}$$

where

$$C(\theta_{ln}, 1/\epsilon) = \bar{R}_{ln} \frac{\partial}{\partial \bar{\rho}_{ln}} \frac{\partial^{1/\epsilon}}{\partial \bar{Z}_{ln}^{1/\epsilon}} \frac{1}{\sqrt{\bar{\rho}_{ln}^2 + \bar{Z}_{ln}^2}} \tag{4.48}$$

$$= (-\bar{R}_{ln})^{-1-1/\epsilon} \Gamma(3 + 1/\epsilon) P_{1+1/\epsilon}^{-1}(\cos\theta_{ln}) \tag{4.49}$$

where $P_{1+1/\epsilon}^{-1}(x)$ is the associated Legendre function of the first kind. By comparing Eq. (4.49) with Eq.(4.2) one may easily identify $C(\theta_{ln}, 1/\epsilon)$ defined here as exactly equal to that defined by Eq.(4.2).

We now substitute Eq. (4.49) into Eq. (4.46) and obtain

$$\nu_{lnn} = \Omega_c 4\sqrt{2\pi} (\frac{3}{\pi})^{1/3} (1 - \frac{T_\perp}{T_\parallel}) \Gamma_\perp \epsilon^{-9/2} e^{-\tilde{\Phi}/\epsilon} \bar{R}_{ln}^{-4} [(\cos\theta_{ln})^{1/\epsilon} P_{1+1/\epsilon}^{-1}(\cos\theta_{ln})]^2 \tag{4.50}$$

where

$$\tilde{\Phi} \equiv \ln[\frac{\pi^2}{\sqrt{2\pi}} (\frac{\pi}{3})^{2/3} c_0^{5/2} \epsilon \Gamma_\parallel] + 1 \tag{4.51}$$

and we have used the approximation $\Gamma(x) \simeq \sqrt{2\pi/x}\, exp[-x + xln(x)]$ for $x \gg 1$.

From Eq. (4.50) we obtain the final equilibration rate: $\nu = \sum_{n>l} \nu_{lnn}$. We find that ν_{lnn} given by Eq. (4.50) does show several important characteristics verified by the numerical results of the next section. For example, ν_{lnn} decreases like $\bar{R}_{ln}^{-4}$ as $\bar{R}_{ln}$ increases, which implies that the dominant contributions are from the nearest neighbor interactions. As we have already discussed, next order terms in the saddle point position $\bar{t}_0$ reduce the effect of distant ions even further.

We also find that the factor $(\cos\theta_{ln})^{1/\epsilon}$ shows an exponential decrease in ν_{lnn} as θ_{ln} increases for $\epsilon \ll 1$. As an extreme case, $\nu_{lnn} = 0$ for $\theta_{ln} = \frac{\pi}{2}$ because in this case $\delta z_{ln}(t)$ vanishes for those modes with $\mathbf{k} \parallel \mathbf{B}$, by which the equilibration process is dominated.

Moreover, the Legendre function exhibits a rapid oscillation in θ_{ln} associated

with the Taylor coefficient $C(\tan\theta_{ln}, 1/\epsilon)$ of the interaction potential energy. Furthermore, as in the crude estimate of Eq. (4.1), smaller ϵ corresponds to a higher order Taylor expansion and thus is expected to lead to more rapid oscillations. In fact, for small θ_{ln} we may approximate $P^{-1}_{1+1/\epsilon}(\cos\theta_{ln})$ by $J_1((3+2/\epsilon)\sin\frac{\theta_{ln}}{2})/(3+2/\epsilon)$, which oscillates faster in θ_{ln} for smaller ϵ.

In order for our calculation to yield a quantitatively good result, the validity condition for the asymptotic expression of $f_{l-n}(i\tau)$, $c_0\bar{t}_0 \gg 1$, i.e., $c_0 \ln p_0(\epsilon x_a^2) \gg 1$, must be also satisfied (see Appendix 4A). This condition, for the largest possible value of c_0, becomes $\epsilon\Gamma_{\|} \gg 1.25 \times 10^5$. Notice that this is a very strong condition which is not satisfied by current experiments and therefore the asymptotic approximation can only be expected to provide us with qualitative information for ν. In the next section we will calculate the rate numerically.

As we have discussed, Eq.(4.34) is only valid for the $\theta_{ln} < 1$ case. In order to be complete, in what follows we consider the $\theta_{ln} \geq 1$ case. When $\theta_{ln} \geq 1$, we use another type of integral transform:

$$h_{ln}(t) = \frac{1}{\pi\rho_{ln}^3}\int_{-\infty}^{\infty} dx x K_1(x) e^{ix(\bar{Z}_{ln}+\bar{z}_{ln}(t))/\bar{\rho}_{ln}} \tag{4.52}$$

For this case, we will see that a singularity occurs when $\rho_{ln} \to 0$ due to the contribution from $\bar{Z}_{ln} + \bar{z}_{ln}(t) = 0$, which corresponds to the close collisions between the$l$th particle and the nth particle. After performing the statistical average for $< h_{ln}(t)h_{ln}(0) >$, we obtain the equilibration rate given by

$$\nu_{lnn} = 4\frac{\Omega_c}{\pi}(\frac{3}{\pi})^{1/3}(1-\frac{T_\perp}{T_{\|}})\epsilon\Gamma_\perp\rho_{ln}^{-4}$$

$$\int_0^\infty\int_0^\infty dx_1 dx_2 K_1(x_1)K_1(x_2)e^{-\frac{2}{3\Gamma_{\|}}(\frac{3}{\pi})^{2/3}f_{l-n}(0)\frac{x_1^2+x_2^2}{\bar{\rho}_{ln}^2}}$$

$$[\cos[(x_1 - x_2)\cot\theta_{ln}]I_{lnn}(\epsilon, \frac{2x_1x_2}{3\Gamma_{\|}\bar{\rho}_{ln}^2}(\frac{3}{\pi})^{2/3})$$

$$+ \cos[(x_1 + x_2)\cot\theta_{ln}]I_{lnn}(\epsilon, -\frac{2x_1x_2}{3\Gamma_{\|}\bar{\rho}_{ln}^2}(\frac{3}{\pi})^{2/3})] \tag{4.53}$$

We found that the saddle points of $I_{lnn}(\epsilon, -\frac{2x_1x_2}{3\Gamma_{\|}\bar{\rho}_{ln}^2}(\frac{3}{\pi})^{2/3})$ are all complex, and the imaginary parts of these saddle points make I_{lnn} oscillatory. On the other hand, we found that the first term in the bracket of Eq. (4.54) is nonoscillatory because of the existence of the pure real saddle point, which dominates the integral. Furthermore, as we will show, this nonoscillatory term gives the trend of the variation of ν_{lnn} as a function of θ_{ln}. This may provide a way to check our results for ν_{lnn} determined by Eq.(4.35). We therefore focus on this nonoscillatory term in the following discussion. By dropping the second term in the bracket in Eq.(4.53), we write

$$\tilde{\nu}_{lnn} \equiv 4\frac{\Omega_c}{\pi}(\frac{3}{\pi})^{1/3}(1 - \frac{T_\perp}{T_{\|}})\epsilon\Gamma_\perp\rho_{ln}^{-4}$$

$$\int_0^\infty \int_0^\infty dx_1dx_2K_1(x_1)K_1(x_2)e^{-\frac{2}{3\Gamma_{\|}}(\frac{3}{\pi})^{2/3}f_{l-n}(0)\frac{x_1^2+x_2^2}{\bar{\rho}_{ln}^2}}$$

$$\cos[(x_1 - x_2)\cot\theta_{ln}]I_{lnn}(\epsilon, \frac{2x_1x_2}{3\Gamma_{\|}\bar{\rho}_{ln}^2}(\frac{3}{\pi})^{2/3}). \tag{4.54}$$

By substituting Eq. (4.42) into Eq. (4.54), we obtain

$$\tilde{\nu}_{lnn} = 4\frac{\Omega_c}{\pi}(\frac{3}{\pi})^{1/3}(1 - \frac{T_\perp}{T_{\|}})\epsilon\Gamma_\perp\sqrt{\frac{2\pi}{\epsilon}}e^{[1 - \ln p_0(\epsilon)]/\epsilon}[C_{ln}^2 + S_{ln}^2] \tag{4.55}$$

where

$$C_{ln} = \frac{1}{\bar{\rho}_{ln}^{2+1/\epsilon}}\int_0^\infty \int_0^\infty dx K_1(x)\cos(x\cot\theta_{ln})e^{-\frac{2}{3\Gamma_{\|}}(\frac{3}{\pi})^{2/3}f_{l-n}(0)x_1^2/\bar{\rho}_{ln}^2}$$

$$S_{ln} = \frac{1}{\bar{\rho}_{ln}^{2+1/\epsilon}} \int_0^\infty \int_0^\infty dx K_1(x) \sin(x \cot\theta_{ln}) e^{-\frac{2}{3\Gamma_\parallel}(\frac{3}{\pi})^{2/3} f_{l-n}(0) x_1^2/\bar{\rho}_{ln}^2}$$

For large $\Gamma_\parallel$ we may neglect the exponentially decaying factors in C_{ln} and S_{ln} and we obtain

$$C_{ln} \simeq 2^{1/\epsilon} \bar{\rho}_{ln}^{-2-1/\epsilon} \Gamma(\frac{3}{2} + \frac{1}{2\epsilon}) \Gamma(\frac{1}{2} + \frac{1}{2\epsilon}) F(\frac{3}{2} + \frac{1}{2\epsilon}, \frac{1}{2} + \frac{1}{2\epsilon}; \frac{1}{2}; -(\cot\theta_{ln})^2) \qquad (4.56)$$

$$S_{ln} \simeq 2^{1+1/\epsilon} \bar{Z}_{ln} \bar{\rho}_{ln}^{-3-1/\epsilon} \Gamma(2 + \frac{1}{2\epsilon}) \Gamma(1 + \frac{1}{2\epsilon}) F(2 + \frac{1}{2\epsilon}, 1 + \frac{1}{2\epsilon}; \frac{3}{2}; -(\cot\theta_{ln})^2) \qquad (4.57)$$

where $F(\alpha, \beta; \gamma; x)$ is Gauss' hypergeometric function.

Some important features of $\tilde{\nu}_{lnn}$ given by Eq. (4.55) should be noted. In the limit of small $\tan\theta_{ln}$, the $\bar{\rho}_{ln}$ dependence of $F(\frac{3}{2} + \frac{1}{2\epsilon}, \frac{1}{2} + \frac{1}{2\epsilon}; \frac{1}{2}; -(\cot\theta_{ln})^2)$ is $(\tan\theta_{ln})^{1+1/\epsilon}$ and so $C_{ln} \sim \bar{\rho}_{ln}^{-1}$. Similarly, we have $S_{ln} \sim \bar{\rho}_{ln}^{-1}$ and therefore $\tilde{\nu}_{lnn} \sim \bar{\rho}_{ln}^{-2} \to \infty$ as $\bar{\rho}_{ln} \to 0$. As we have discussed, this singularity is due to the improper inclusion of the close collisions.

In order to make comparison between $\tilde{\nu}_{lnn}$ and ν_{lnn}, we employ the following asymptotic formula for the Gauss' hypergeometric function for $\epsilon \ll 1$:

$$F(\frac{3}{2} + \frac{1}{2\epsilon}, \frac{1}{2} + \frac{1}{2\epsilon}; \frac{1}{2}; -(\cot\theta_{ln})^2) \simeq \cos(\frac{\cot\theta_{ln}}{\epsilon})$$

$$F(2 + \frac{1}{2\epsilon}, 1 + \frac{1}{2\epsilon}; \frac{3}{2}; -(\cot\theta_{ln})^2) \simeq \epsilon \sin(\frac{\cot\theta_{ln}}{\epsilon}) / \cot\theta_{ln}$$

and then

$$(C_{ln}^2, S_{ln}^2) \simeq \frac{\pi^2}{\epsilon^2} \bar{\rho}_{ln}^{-4-2/\epsilon} e^{\frac{2}{\epsilon}(\ln\frac{1}{\epsilon} - 1)} (\cos^2(\frac{\cot\theta_{ln}}{\epsilon}), \sin^2(\frac{\cot\theta_{ln}}{\epsilon}))$$

Furthermore substitution of C_{ln} and S_{ln} into $\tilde{\nu}_{lnn}$ yields

$$\tilde{\nu}_{lnn} = 4\frac{\Omega_c}{\pi}(\frac{3}{\pi})^{1/3}(1 - \frac{T_\perp}{T_\parallel})\frac{\Gamma_\perp}{\epsilon}\sqrt{\frac{2\pi}{\epsilon}}\bar{\rho}_{ln}^{-4}(\cot\theta_{ln})^{2/\epsilon} e^{-\tilde{\Phi}/\epsilon} \qquad (4.58)$$

where $\tilde{\Phi}$ is defined by Eq.(4.51).

We now see that $\tilde{\nu}_{lnn}$ is nonoscillatory despite the fact that both C_{ln} and S_{ln} are oscillatory. In order to make a comparison between $\tilde{\nu}_{lnn}$ and ν_{lnn} given by Eq.(4.50) and Eq.(4.58), we substitute the asymptotic formula for the Legendre function for $\epsilon \ll 1$:

$$\begin{aligned} P^{-1}_{1+1/\epsilon}(\cos\theta_{ln}) &= \frac{\Gamma(1+1/\epsilon)}{\Gamma(3+1/\epsilon)} P^{1}_{1+1/\epsilon}(\cos\theta_{ln}) \\ &= \frac{-1}{2+1/\epsilon}\sqrt{\frac{2}{(1+1/\epsilon)\pi\sin\theta_{ln}}}\cos[(3/2+1/\epsilon)\theta_{ln}+\pi/4]+O(\epsilon^{5/2}) \end{aligned}$$

into Eq. (4.50) and obtain

$$\nu_{lnn} = \tilde{\nu}_{lnn}(\sin\theta_{ln})^{-3-2/\epsilon}[1-\sin(3+2/\epsilon)\theta_{ln}](1+O(\epsilon))$$

which shows that $\tilde{\nu}_{lnn}$ represents the trend of the oscillation in θ_{ln} of ν_{lnn}. This full oscillatory behavior is expected to be recovered when we take into account the second term in the bracket of Eq. (4.53).

4.4.3 Numerical Calculation of ν and Discussions

Though we have derived the asymptotic expression for the rate in the $\varepsilon \ll 1$ and $\varepsilon\Gamma_{\|} \gg 1$ limit, for a general parameter regime of ε and $\Gamma_{\|}$, the asymptotic expression only gives the qualitative behavior of ν and the rate must be determined numerically.

To perform the numerical evaluation of ν using either Eq. (4.35) or Eq. (4.54), we must first calculate the time integral $I_{lnn'}(\varepsilon,\alpha)$, where $\alpha = \pm\frac{2x_1x_2}{3\Gamma_{\|}}(\frac{3}{\pi})^{2/3}$. Furthermore, in order to calculate $I_{lnn'}(\varepsilon,\alpha)$, we must obtain function $f_{l-n}(i\bar{t})$. As a first step, we calculate the frequency $\omega_z(\mathbf{k})$. In our calculation, we write $\mathbf{k}$ as

$\mathbf{k} = x_1\mathbf{b}_1 + x_2\mathbf{b}_2 + x_3\mathbf{b}_3$, where $\mathbf{b}_1$, $\mathbf{b}_2$ and $\mathbf{b}_3$ are the reciprocal lattice vectors:

$$\mathbf{b}_1 = \pi(0,1,1); \mathbf{b}_2 = \pi(1,0,1); \mathbf{b}_3 = \pi(1,1,0).$$

where the lengths are scaled by a_0 and the wavenumbers are scaled by $1/a_0$. We tabulate the dynamical matrix elements $G_{xy}(\mathbf{k})$ and $G_{zz}(\mathbf{k})$ given by Eq.(4.62) in Appendix 4A on a $31 \times 31 \times 31$ grid, where on each grid point (l, m, n),

$$x_1(l) = \frac{l-16}{31}; x_2(m) = \frac{m-16}{31}; x_3(n) = \frac{n-16}{31}.$$

The other matrix elements can then be obtained through the permutational symmetries:

$$G_{xy}(l,m,n) = G_{xz}(l,n,m) = G_{yz}(n,m,l)$$

and

$$G_{zz}(l,m,n) = G_{xx}(n,m,l) = G_{yy}(l,n,m).$$

With these matrix elements, we thus obtain the frequency given by $\bar{\omega_z} = \hat{\mathbf{b}} \cdot \mathbf{G} \cdot \hat{\mathbf{b}}$, where $\hat{\mathbf{b}}$ is the unit vector of the magnetic field. In Fig.4.6, we plot the numerical results of ${\bar{\omega_z}}^2$, where the solid lines represent ${\bar{\omega_z}}^2(\mathbf{k})$ with $\mathbf{k}$ along [001] and [111] respectively.

After obtaining $\bar{\omega_z}$, we may furthermore calculate the value of the integrand of $f_{l-n}(i\bar{t})$ on each grid point (l, m, n), where $f_{l-n}(i\bar{t})$ is given by

$$\begin{aligned} f_{l-n}(i\bar{t}) &= \frac{1}{2}\int_{B.Z} \frac{v d^3\mathbf{k}}{(2\pi)^3} \frac{1-\cos\mathbf{k}\cdot\mathbf{R}_{ln}}{\bar{\omega}_z(\mathbf{k})^2} \cosh(\bar{\omega}_z(\mathbf{k})\bar{t}) \\ &= \int_{-1/2}^{1/2} dx_1 \int_{-1/2}^{1/2} dx_2 \int_{-1/2}^{1/2} dx_3 \frac{1-\cos\mathbf{k}\cdot\mathbf{R}_{ln}}{2\bar{\omega}_z(\mathbf{k})^2} \cosh(\bar{\omega}_z(\mathbf{k})\bar{t}) \quad (4.59) \end{aligned}$$

Here we have taken $v = 4$ for a bcc crystal and we have changed $d^3\mathbf{k}$ to $dx_1 dx_2 dx_3$

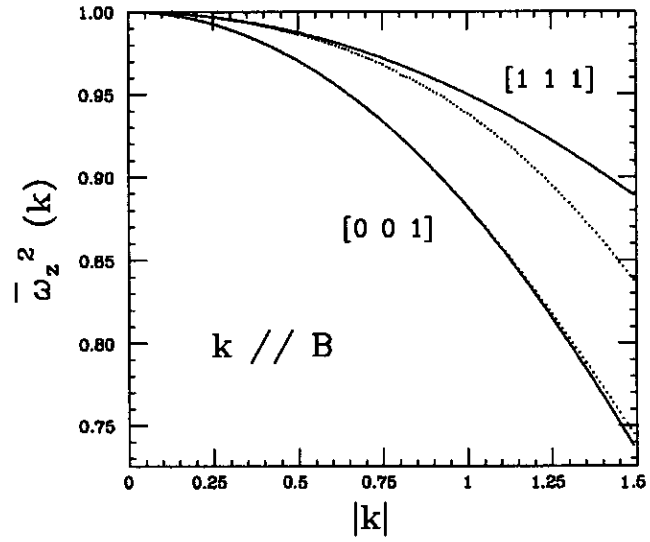

Figure 4.6: Plot of the parallel dispersion relation $\bar{\omega_z}^2(\mathbf{k})$ for a 3D strongly magnetized crystallized plasma, with **k** // **b** // [1,1,1] and [0,0,1] respectively. Here frequency $\bar{\omega_z}$ is scaled by plasma frequency ω_p, wavevector **k** is scaled by $1/a_0$, where a_0 is half of the bcc lattice constant. The solid lines represent the numerical results and the dotted lines representate the approximate analytical results given by Eq.(4.54).

with Jacobian $\partial^3\mathbf{k}/(\partial x_1 \partial x_2 \partial x_3) = 2\pi^3$. The three dimensional integral is performed in the following way. We first evaluate the x_3 integral by applying the extended Simpson's integral rule to the grid points $x_3(n)(n = 1, 2, \cdots, 31)$ while treating $x_1 = x_1(l), x_2 = x_2(m)(1 \leq l, m \leq 31)$ as parameters. The estimated relative error for the Extended Simpson's Integral Rule is on the order of[9] $1/31^4$ which is small. After performing the x_3 integral, we are left with the integrand of the x_1, x_2 integral in a form of a 2D array $(l, m)(1 \leq l, m \leq 31)$. We repeat the same technique used for the x_3 integral holding x_1 fixed, the resulting 1D array is also integrated via Simpson's rule. We also evaluate the derivatives $\frac{d}{d\bar{t}} f_{l-n}(i\bar{t})$ and $\frac{d^2}{d^2\bar{t}} f_{l-n}(i\bar{t})$, by taking derivatives of Eq.(4.59) analytically and then numerically integrating through the same procedure.

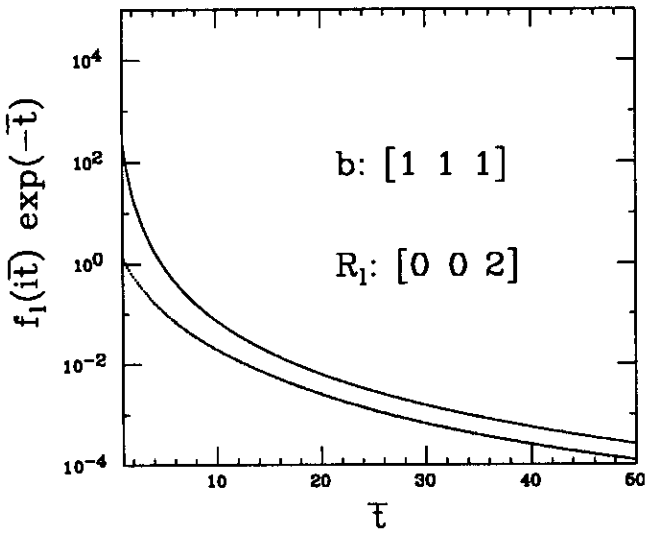

Figure 4.7: Plot of $f_{l-n}(i\bar{t})$ for **B**// [111], $\mathbf{R}_{ln}$ =[0,0,2], where $\bar{t}$ is scaled by $1/\omega_p$. Solid lines: asymptotic results (Eq.(4.65); dotted lines: numerical results.

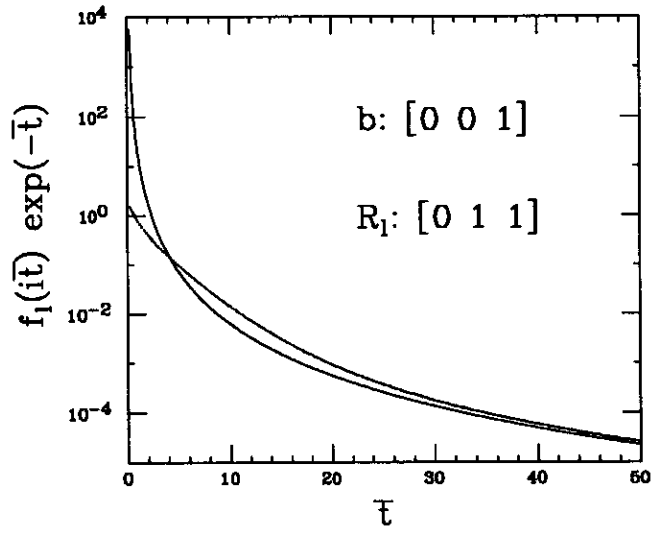

Figure 4.8: Plot of $f_{l-n}(i\bar{t})$ for **B**// [0 0 1], $\mathbf{R}_{ln}$ = [0,1,1]. Solid lines: asymptotic results (Eq.(4.65); dotted lines: numerical results.

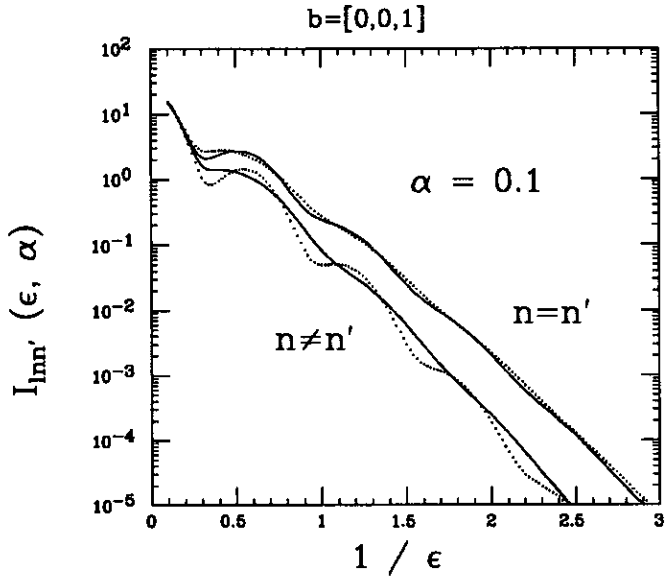

Figure 4.9: A comparison between $I_{lnn}(\varepsilon,\alpha)$ and $I_{lnn'}(\varepsilon,\alpha)$, where $I_{lnn}(\varepsilon,\alpha)$ and $I_{lnn'}(\varepsilon,\alpha)$ are evaluated by direct numerical integration (see Eq.(4.36)). The upper solid line is for $\mathbf{R}_{ln} = \mathbf{R}_{ln'}$ =[1,1,1], the upper dotted line is for $\mathbf{R}_{ln} = \mathbf{R}_{ln'}$ =[2,0,2], the lower solid line is for $\mathbf{R}_{ln}$ = [1, 1, 1], $\mathbf{R}_{ln'}$ =[2,0,2] and the lower dotted line is for $\mathbf{R}_{ln}$ =[1,1,1], $\mathbf{R}_{ln'}$ = [1,-1,1].

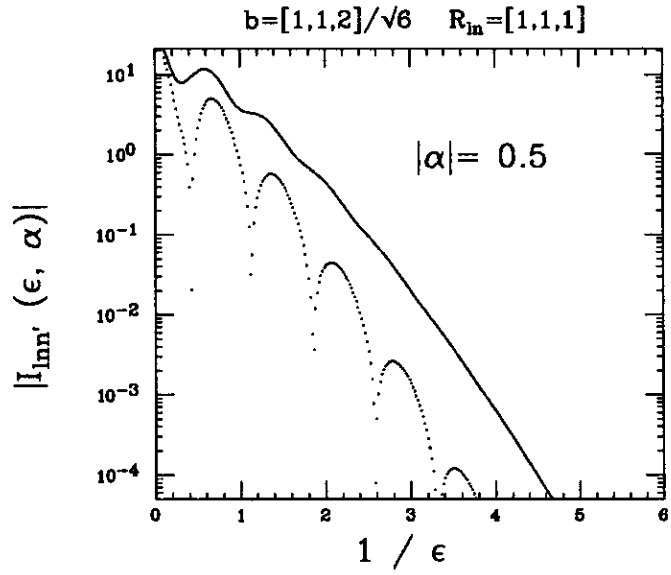

Figure 4.10: A comparison between $|I_{lnn}(\varepsilon,\alpha)|$ and $|I_{ln\bar{n}}(\varepsilon,\alpha)|$, where $\mathbf{R}_{ln}$ =[1,1,1] and $\mathbf{R}_{l\bar{n}}$ =[-1,-1,-1]. Her we plot the absolute value of I_{lnn} and $I_{ln\bar{n}}$ because $I_{ln\bar{n}}$ is oscillatory and can be negative.

The numerical results of $f_{l-n}(i\bar{t})$ for $\mathbf{k}$ along [001] and [111] are plotted in Fig.4.7 and Fig.4.8, where dotted lines and the solid lines represent the numerical and asymptotic results respectively.

After obtaining $f_{l-n}(i\bar{t})$ and its derivatives, we may now evaluate the time integral $I_{lnn'}(\epsilon, \alpha)$. We first compare the numerical result of $I_{lnn'}(\epsilon, \alpha)$ for different l, n and n' and as we found in the asymptotic analysis, the nondiagonal term, $n \neq n'$, is much smaller than the diagonal term, $n = n'$ (see Fig.4.9).

Furthermore, we calculate $I_{ln\bar{n}}$ and I_{lnn} numerically, where $\bar{n}$ is the reflection point of n with respect to n (see Fig.4.4). We find that, $I_{ln\bar{n}}$ is much smaller than I_{lnn} (see Fig.4.10), as we discussed in our asymptotic analysis.

The fact that $|I_{lnn'}| \ll |I_{lnn}| (n \neq n')$ allows us to focus on the $n = n'$ case. We then proceed to calculate the time integral I_{lnn} using both the saddle point method and direct numerical integration. First we discuss the saddle point method. As we discussed in the asymptotic analysis, we only need to keep the saddle point on the real axis, which is the root of the saddle point equation

$$\frac{d}{d\bar{t}} f_{l-n}(i\bar{t}) = \frac{1}{\epsilon\alpha}$$

In order to evaluate I_{lnn}, we first tabulate $f_{l-n}(i\bar{t})$, $\frac{d}{d\bar{t}} f_{l-n}(i\bar{t})$ and $\frac{d^2}{d^2\bar{t}} f_{l-n}(i\bar{t})$ for $\bar{t}$ varying from 0 to 20 with steps $\Delta\bar{t} = 0.1$ for $\bar{t} \leq 10$ and $\Delta\bar{t} = 0.5$ for $\bar{t} > 10$. Here we take nonuniform steps because $f_{l-n}(i\bar{t})$ and its derivatives vary faster for smaller $\bar{t}$'s. Using these discrete values at different $\bar{t}$'s, we make the cubic spline approximation for $f_{l-n}(i\bar{t})$, $\frac{d}{d\bar{t}} f_{l-n}(i\bar{t})$ and $\frac{d^2}{d^2\bar{t}} f_{l-n}(i\bar{t})$, and we can then solve the saddle point equation numerically. In our calculation, the saddle point equation is solved by using the SLATEC subroutine DZERO.F. Having obtained the saddle point position $\bar{t} = \bar{t}_s$,

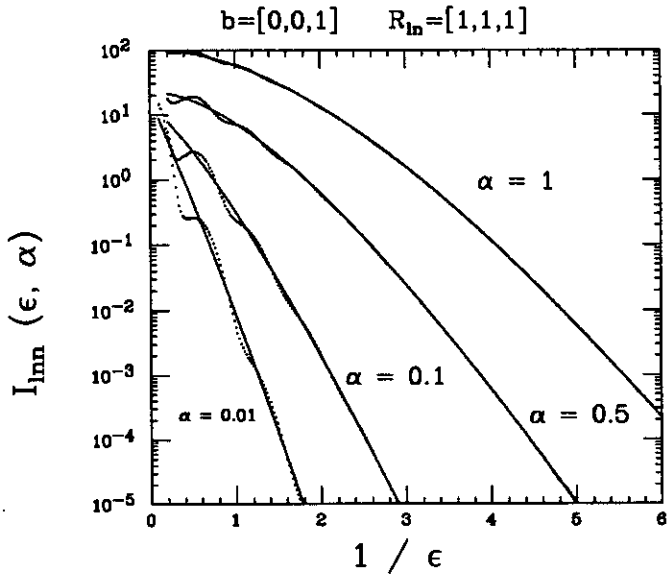

Figure 4.11: Plot of the time integral $I_{lnn}(\epsilon, \alpha)$ with $\mathbf{B}$// [0 0 1], R_{ln} =[1,1,1]. Solid lines: the results from the saddle point calculation keeping only the pure real saddle point; Dotted lines: the results from direct numerical integration.

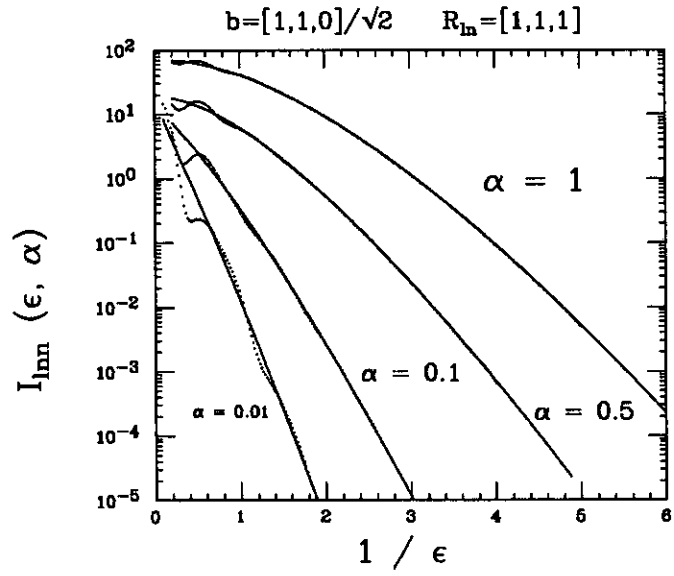

Figure 4.12: Plot of the time integral $I_{lnn}(\epsilon, \alpha)$ with $\mathbf{B}$//[1 1 0], R_{ln} =[1,1,1]. Solid lines: the results from the saddle point calculation keeping only the pure real saddle point; Dotted lines: the results from direct numerical integration.

the time integral is then evaluated by the saddle point method:

$$I_{lnn}(\epsilon,\alpha) \simeq \frac{1}{\varepsilon}\sqrt{\frac{2\pi}{\alpha f''_{l-n}(i\bar{t}_s)}}e^{-\frac{\bar{t}_s}{\varepsilon}+\alpha f_{l-n}(i\bar{t}_s}.$$

In order to compare our result of saddle point calculation with the direct numerical integration result, in Fig.4.11 and Fig.4.12 we plot $I_{lnn}(\epsilon,\alpha)$ as a function $1/\varepsilon$ for different α, $\bar{R}_{ln}$ and $\hat{\mathbf{b}}$'s. From these figures, we see a good agreement between the saddle point calculation and the numerical integration. Furthermore, as we expected, we see that I_{lnn} decreases exponentially for small ε.

An important feature shown in Fig.4.11 and Fig.4.12 is that, in contrast to Fig.3.3 for the 1D Coulomb chain case, the steps in I_{lnn} as a function of ε is strongly suppressed for large $1/\varepsilon$. From the point of view of the saddle point method, the oscillations are due to the contribution of the complex saddle points. They play important roles for the 1D case but are negligible for the 3D case. As a result, the abrupt steps appeared in I_{lnn} for the 1D case are suppressed for the 3D case.

This can also understood through the following physical argument. According to Eq.(4.36), the integral I_{lnn} is

$$I_{lnn} = -2\varepsilon\alpha\int \frac{d}{dt}f_{ln}(\tau)e^{2\alpha f_{ln}(\tau)}\sin(\Omega_c t)dt,$$

which can be written as

$$I_{lnn} = -2\varepsilon\alpha\int dt\frac{d}{dt}f_{ln}(\tau)\sum_{j=0}^{\infty}\frac{(2\alpha)^j}{j!}[f_{ln}(\tau)]^j\sin(\Omega_c t),$$

where $\tau \equiv \omega_p t$. Thus I_{lnn} is the $\omega = \Omega_c$ Fourier component of a sum over products of f_{ln} and it's derivative. This can be written as a convolution of the products of the Fourier transform of f_{ln}.

As shown in Fig.3.4, the Fourier transform of $f_{ln}(\tau)$ for the 1D case has a sharp cutoff at the largest parallel frequency and this sharp cutoff causes the abrupt

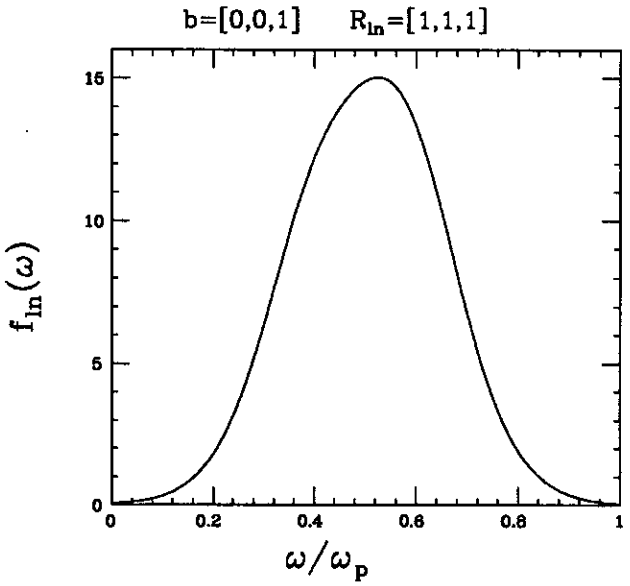

Figure 4.13: Plot of the Fourier transform of the correlation function $f_{ln}(\tau)$

steps in I_{lnn}. However, for the present 3D case, as shown in Figure 4.13, instead of the sharp cutoff, there only exists a gentle bump near half of the maximum frequency. This gentle bump only causes smooth oscillations in I_{lnn} for small $1/\epsilon$ as shown in Fig.4.11 and Fig.4.12. For large $1/\epsilon$, these oscillations disappear because I_{lnn} is then determined by many high order terms, each of which has a small effect when taken individually.

We evaluate the x_1, x_2 integral to complete the rate calculation. Recall that we have two versions of the rate calculations, one is given by Eq.(4.34) valid for small θ_{ln}, the other given by Eq.(4.54) valid for $\theta_{ln} > 1$. We first calculate the rate for small θ_{ln} by performing the x_1, x_2 integral in Eq. (4.35). As we discussed in section 4.4.2, we must choose the upper integration limit β such that $x_a \ll \beta \ll x_b$, where the integrand is peaked at $(x_1, x_2) = (x_a, x_a)$ and the integrand starts to grow along the $x_1 = x_2$ direction when $x_{1,2} > x_b$. Here $x_a \sim (1 + 1/\epsilon)/\bar{Z}_{ln}$ and $x_b \sim \bar{Z}_{ln}\Gamma_{||}/f_{l-n}(0)$. In our calculation, we find that the rate is independent of the choice of β provided that $\epsilon\Gamma_{||} \gg 1$.

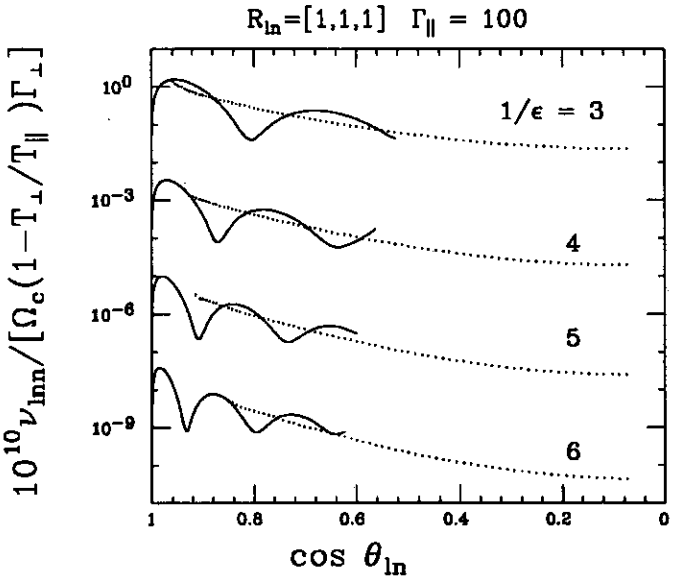

Figure 4.14: Plot of ν_{lnn} as a function of $\cos\theta_{ln}$, where $\bar{R}_{ln}$ =[1,1,1] and $\hat{\mathbf{b}}$ varies in the plane spanned by lattice vectors [111], [002]. The solid lines represent the results of Eq. (4.35), which is valid for small θ_{ln}, and the dotted lines represent the results of Eq. (4.54).

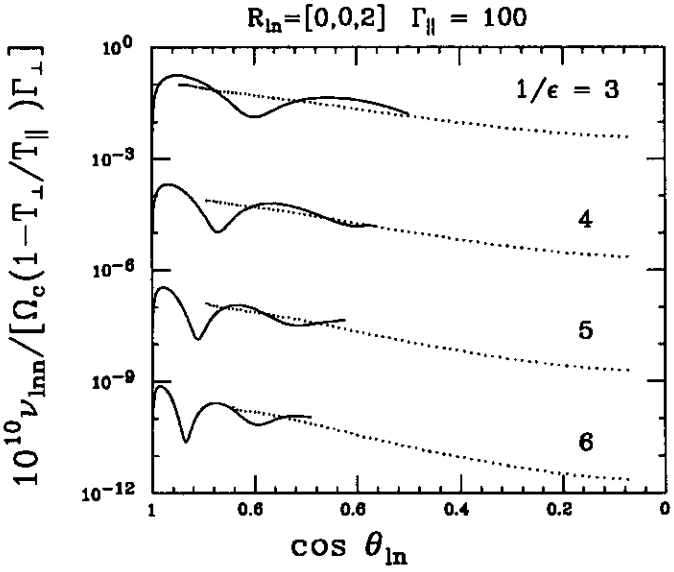

Figure 4.15: Plot of ν_{lnn} as a function of $\cos\theta_{ln}$, where $\bar{R}_{ln}$ =[0,0,2] and $\hat{\mathbf{b}}$ varies in the plane spanned by lattice vectors [200], [002]. The solid lines represent the results of Eq. (4.35), which is valid for small θ_{ln}, and the dotted lines represent the results of Eq. (4.54).

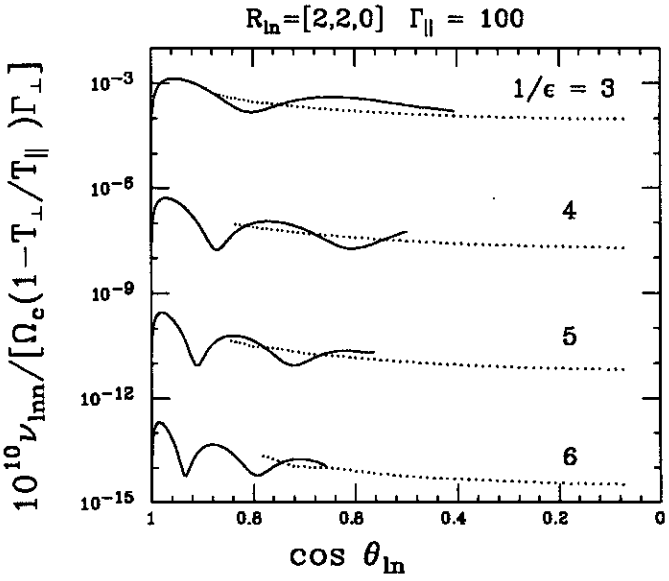

Figure 4.16: Plot of ν_{lnn} as a function of $\cos\theta_{ln}$, where $\bar{R}_{ln}$ =[2,2,0] and $\hat{\mathbf{b}}$ varies in the plane spanned by lattice vectors [200], [220].The solid lines represent the results of Eq. (4.35), which is valid for small θ_{ln}, and the dotted lines represent the results of Eq. (4.54).

For $\theta_{ln} > 1$, the rate is given by Eq. (4.53). In this case, as we did in the asymptotic analysis, we performed the x_1, x_2 integral for $\tilde{\nu}_{lnn}$ given by Eq. (4.54). The numerical integration is straightforward since the behavior of the integrand is regular.

The results for our numerical calculations for ν_{lnn} are plotted in Fig.4.14 and Fig.4.15 and Fig.4.16 as a function of $\cos\theta_{ln}$, where the solid lines represent the results given by Eq. (4.35), and the dotted lines represent the results of Eq. (4.54). We can see that the numerical results do exhibit the qualitative features predicted by the asymptotic analysis. For example, the dotted lines give the trend of the oscillatory solid lines. The rate ν_{lnn} is an oscillatory function of the angle θ_{ln} with a rapidly decaying amplitude. And as ϵ decreases, these oscillations in θ_{ln} becomes faster. Also, recall that in our order of magnitude estimate (see section 4.1), we found that the maximum rate occurs roughly at $\theta_{ln} \sim 1/\sqrt{2M} = \sqrt{\epsilon/2}$. Here from these

figures, we see that the angle θ_{ln} at which the maximum ν_{lnn} occurs does decrease slowly as $1/\varepsilon$ increases. Moreover, we see that ν_{lnn} decreases as $|\bar{\mathbf{R}}_{ln}|$ increases, but it decreases much more rapidly than $|\bar{\mathbf{R}}_{ln}|^{-4}$, which is predicted in our asymptotic analysis if we had kept higher order terms in $1/\tau$.

Finally, by summing ν_{lnn} over different lattice sites (ln), we obtain the equilibration rate ν of the crystal as a function of the magnetic field orientation (θ, ϕ) with respect to the crystal axis. Since the rate decreases rapidly when $|\bar{\mathbf{R}}_{ln}|$ increases, we only sum ν_{lnn} over nearest neighbor points $\bar{R}_{ln} = [\pm 1, \pm 1, \pm 1]$, $[0, 0, \pm 2]$, $[0, \pm 2, 0]$, $[0, 0, \pm 2]$, $[\pm 2, \pm 2, 0]$,$[0, \pm 2, \pm 2]$ and $[\pm 2, 0, \pm 2]$.

The variation of ν with θ and ϕ is presented in Fig.4.17. From Fig.4.17 we find that the rate is strongly dominated by the contribution from the nearest neighbor lattice site $\bar{R}_{ln} = [1, 1, 1]$ and is highly peaked when the magnetic field makes a small but nonzero angle with the $[1, 1, 1,]$ direction. As we have mentioned, in practice, the system is not a perfect bcc crystal and the overall temperature equilibration rate may be approximated by averaging $\nu(\theta, \phi)$ over randomly varying angles (θ, ϕ).

One may have noticed that the rate obtained is physically relevant to the experiments only for $1/\varepsilon \sim 3 - 5$. For larger $1/\varepsilon$, the rate may become so small that it would make an experimental test quite difficult. On the other hand, for $1/\varepsilon \sim 3 - 5$, corrections to our guiding center approximation, for example, the terms in ω_z of higher orders in ε, may be important. Nevertheless, the present calculation as a preliminary investigation for the temperature equilibration process in a strongly correlated plasma is expected to provide the zeroth order result for the temperature equilibration rate.

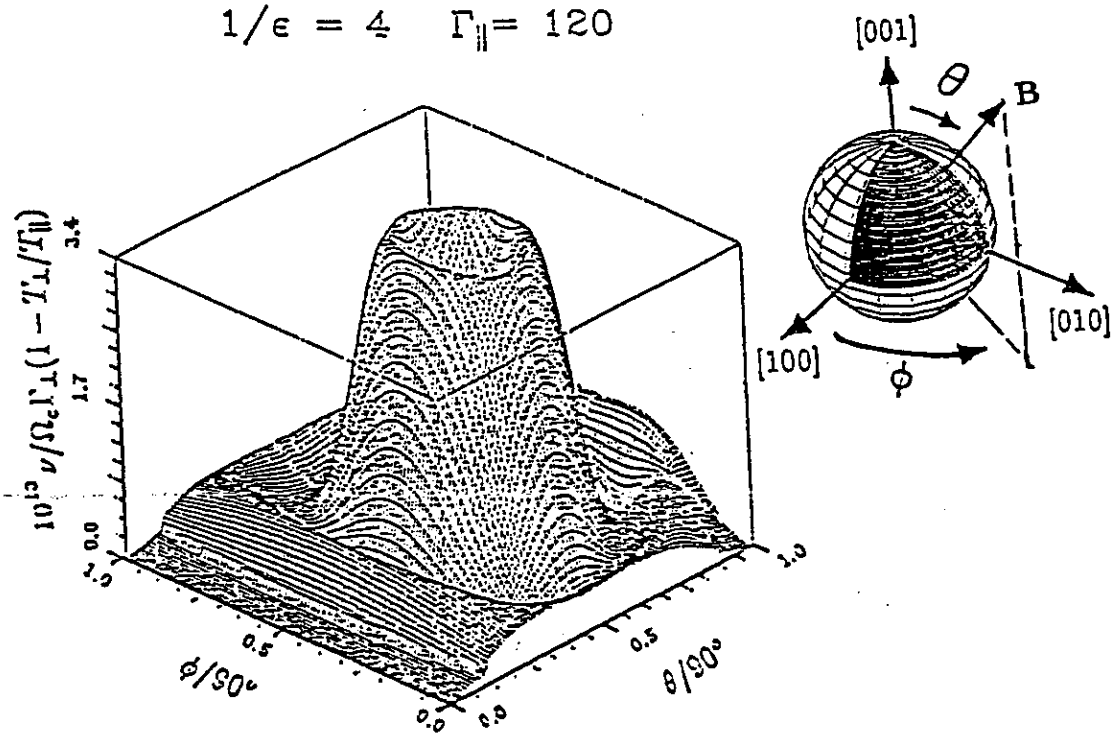

Figure 4.17: Plot of $\nu(\theta, \phi)$ for different magnetic field direction (θ, ϕ), where θ and ϕ are defined with respect to the crystal axes and run over the shaded region of the inset. This figure repeats for (θ, ϕ) in other quadrants of the sphere.

4.5 Appendix 4A: Asymptotic Expression for $f_l(i\bar{t})$ in the $|\bar{t}| \gg 1$ Limit

In this appendix, we derive an asymptotic formula for the correlation function $f_l(i\bar{t})$ in the $|\bar{t}| \gg 1$ Limit, where $f_l(i\bar{t})$ is defined by equation (3.25) for a three dimensional crystallized and strongly magnetized plasma.

For a 3D system, $f_l(i\bar{t})$ can be written as a 3D integral in the Brillouin zone:

$$f_l(i\bar{t}) = \frac{1}{2}\int_{B.Z} \frac{v d^3\mathbf{k}}{(2\pi)^3} \frac{1-\cos \mathbf{k}\cdot\mathbf{R}_l}{\bar{\omega}_z(\mathbf{k})^2} \cosh(\bar{\omega}_z(\mathbf{k})\bar{t}) \tag{4.60}$$

Here $v = 4a_0^3, \bar{t} = \omega_p t$ and $\mathbf{k}$ and $\mathbf{R}_l$ are normalized by $1/a_0$ and a_0 respectively, where a_0 is half of the lattice constant.

For $\bar{t} \gg 1, f_l(i\bar{t})$ is dominated by the contribution from the largest frequency

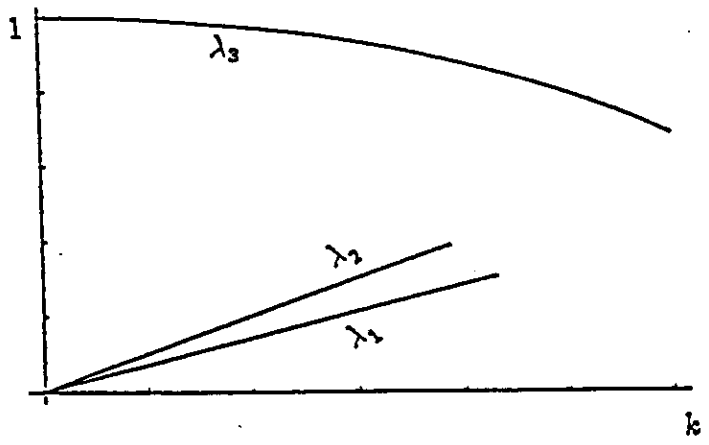

Figure 4.18: A schematic picture for the eigenmodes for a unmagnetized bcc Coulomb crystal

$\bar{\omega}_z(\mathbf{k})$. In the guiding center limit, $\bar{\omega}_z$ is given by

$$\bar{\omega}_z^2 = \hat{\mathbf{b}} \cdot \bar{\mathbf{G}} \cdot \hat{\mathbf{b}}$$

where $\hat{\mathbf{b}}$ is the unit vector along the magnetic field and $\bar{\mathbf{G}}$ is the dynamical matrix normalized by $m\omega_p{}^2$. The condition for the largest $\bar{\omega}_z$ can be found by maximizing the Lagrange target function $F(\hat{\mathbf{b}}) \equiv \hat{\mathbf{b}} \cdot \bar{\mathbf{G}} \cdot \hat{\mathbf{b}} - \lambda^2 |\hat{\mathbf{b}}|^2$ subject to the constraint $|\hat{\mathbf{b}}|^2 = 1$, where λ is the Lagrange multiplier. $\partial F(\hat{\mathbf{b}})/\partial \hat{\mathbf{b}} = 0$ yields

$$\bar{\mathbf{G}} \cdot \hat{\mathbf{b}} = \lambda^2 \hat{\mathbf{b}}$$

which means that the maxima of $\bar{\omega}_z$ occurs when $\hat{\mathbf{b}}$ is a polarization vector of $\bar{\mathbf{G}}$ with eigenfrquency λ. The eigenmodes of $\bar{\mathbf{G}}$ was found to be one longitudinal mode and two transverse modes[10], as shown schematically in Fig.4.18. From the figure we see that the maximum frequency comes from the long wavelength longitudinal mode. At $k = 0$, the frequencies of the the transverse modes, λ_1 and λ_2, vanish and

λ_3 reaches its maximum value :$\lambda_3 = 1$. Furthermore, this frequency must be the largest possible frequency of the modes because of the Kohn rule: $\lambda_1^2 + \lambda_2^2 + \lambda_3^2 = 1$.

Before proceeding to derive the asymptotic formula of $f_l(i\bar{t})$, we first need to obtain an expression for $\bar{\omega}_z(\mathbf{k})$ in the small k limit. We start with a formula for $\bar{\mathbf{G}}$ derived by Dubin[11] using the Ewald sum technique:

$$\bar{\mathbf{G}}(\mathbf{k}) = \mathbf{G}(0) - \mathbf{G}(\mathbf{k}) \tag{4.61}$$

with the matrix $\mathbf{G}(\mathbf{k})$ given by

$$G_{ij} = \frac{v}{4\pi}[\frac{\delta_{ij}}{6\sqrt{\pi}R^2} + \sum_{\mathbf{p}}{}'(-\frac{\delta_{ij}}{p^3}F_1 + \frac{p_i p_j}{p^5}F_2]\cos\mathbf{k}\cdot\mathbf{p} -$$

$$\sum_{\mathbf{g}\neq\mathbf{k}} \frac{(\mathbf{g}-\mathbf{k})_i(\mathbf{g}-\mathbf{k})_j}{|\mathbf{g}-\mathbf{k}|^2} e^{-|\mathbf{g}-\mathbf{k}|^2R^2} - \frac{\partial^2}{\partial x_i \partial x_j}[\phi(\mathbf{x}) - \frac{e^2}{|\mathbf{x}|}]_{x=0} \tag{4.62}$$

and F_1 and F_2 are given by

$$F_1 = erfc(\frac{p}{2R}) + \frac{p}{\sqrt{\pi}R}e^{-(\frac{p}{\sqrt{\pi}R})^2}$$

$$F_2 = 3erfc(\frac{p}{2R}) + (3 + \frac{p^2}{2R^2})\frac{p}{\sqrt{\pi}R}e^{-(\frac{p}{\sqrt{\pi}R})^2}.$$

Here R is the parameter introduced to break the Ewald sum into two terms; in fact, G_{ij} is independent of the choice of R. $\sum_{\mathbf{p}}{}'$ is the sum over all the lattice sites except $\mathbf{p} = 0$ and $\sum_{\mathbf{g}\neq\mathbf{k}}$ is the sum over the reciprocal lattice points. The last term in Eq. (4.62) is added to remove the singularity at $x = 0$.

Expansion of G_{ij} up to the second order in $\mathbf{k}$ yields

$$\bar{\omega}_z(\mathbf{k})^2 = \hat{\mathbf{b}}\cdot(\mathbf{G}(0) - \mathbf{G}(\mathbf{k}))\cdot\hat{\mathbf{b}}$$

$$= \frac{(\mathbf{k}\cdot\hat{\mathbf{b}})^2}{k^2} - c_1(\mathbf{k}\cdot\hat{\mathbf{b}})^2 + c_2k^2 - c_3(k_x^2b_x^2 + k_y^2b_y^2 + k_z^2b_z^2) \tag{4.63}$$

where (k_x, k_y, k_z) are the components of $\mathbf{k}$ along the crystal axes, (b_x, b_y, b_z) are the components of $\hat{\mathbf{b}}$ along the crystal axes, and where the coefficients c_1, c_2 and c_3 are given by

$$c_1 = R^2 - \frac{v}{4\pi}\sum_{\mathbf{p}}{}' \frac{p_x^2 p_y^2}{p^5} F_2 - \sum_{\mathbf{g}}{}' \frac{e^{-R^2 g^2}}{g^2} \cdot$$

$$\left(1 - \frac{2(g_x^2+g_y^2)}{g^2}(1-R^2 g_z^2) - \frac{2R^2}{g^2}(g_x^4+g_y^4) + \frac{4g_x^2 g_y^2 R^2}{g^4}(1+g^2R^2) + \frac{8g_x^2 g_y^2}{g^4}\right)$$

$$c_2 = \frac{v}{8\pi}\sum_{\mathbf{p}}{}' \left(-\frac{p_x^2}{p^3}F_1 + \frac{p_x^2 p_y^2}{p^5}F_2\right) + \sum_{\mathbf{g}}{}' \frac{e^{-R^2 g^2}}{g^2} \cdot$$

$$\left(-\frac{g_y^2}{g^2}(1+g^2R^2) + \frac{4g_x^2 g_y^2}{g^4} + \frac{2g_x^2 g_y^2 R^2}{g^2}(2+g^2R^2)\right)$$

$$c_3 = \frac{v}{8\pi}\sum_{\mathbf{p}}{}' \frac{3p_x^2 p_y^2 - p_x^4}{p^5} F_2 + \sum_{\mathbf{g}}{}' \frac{e^{-R^2 g^2}}{g^2} \cdot$$

$$\left(2R^4 g_x^2(3g_y^2 - g_x^2) + (3+g^2R^2+2g_z^2R^2)\frac{g_x^2-g_y^2}{g^2} - \frac{2R^2}{g^2}(g_x^4+g_y^4) - \frac{12g_x^2g_y^2R^2}{g^2}\right)$$

The numerical values of c_1, c_2 and c_3 for a bcc lattice are calculated and are found to be:

$$c_1 \simeq 7.491 \times 10^{-2}; c_2 \simeq 5.908 \times 10^{-2}; c_3 \simeq 0.102$$

We have tested our results by choosing different values of parameter R and we find that the results are indeed independent of the choice of R. In Fig.4.6 $\bar{\omega}_z(\mathbf{k})^2$ given by Eq. (4.63) is compared with the numerical result given by Eq. (4.61) and Eq. (4.62) for $\mathbf{k}$ along [001] direction and [111] directions. We can see that for small k these two results are in good agreement.

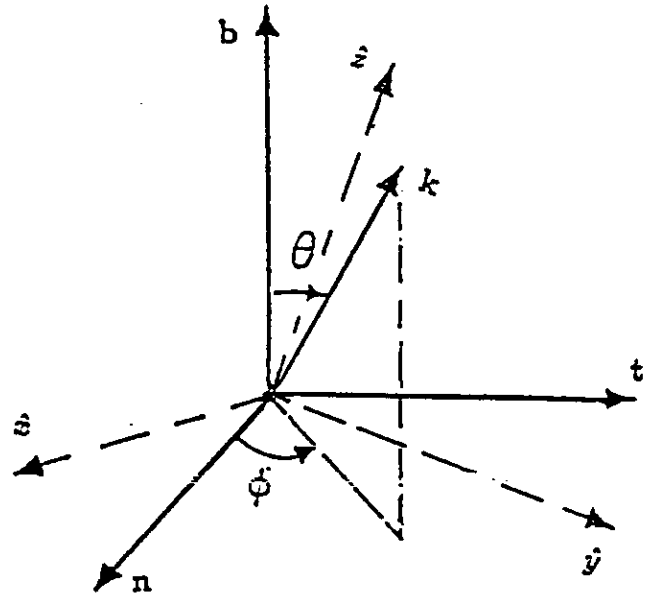

Figure 4.19: A schematic picture for the Frenet coordinate system $(\mathbf{n}, \mathbf{t}, \mathbf{b})$, where $\mathbf{b} \equiv \mathbf{B}/B$ and $(\mathbf{n}, \mathbf{t})$ are two orthogonal unit vectors in the plane perpendicular to $\mathbf{b}$. (θ, ϕ) are the polar and azimuthal angle for the wavevector $\mathbf{k}$ with respect to $(\mathbf{n}, \mathbf{t}, \mathbf{b})$. $(\hat{x}, \hat{y}, \hat{z})$ are the crystal axes.

We now proceed to calculate $f_l(i\bar{t})$. It proves useful to use the Frenet coordinate system which is described by three orthogonal base vectors: $(\mathbf{n}, \mathbf{t}, \mathbf{b})$ (see Fig.4.19). Here $\mathbf{b} \equiv \mathbf{B}/B$ and $(\mathbf{n}, \mathbf{t})$ are two orthogonal unit vectors in the plane perpendicular to $\mathbf{b}$. In this coordinate system, the direction of any vector, e.g., $\mathbf{k}$, can be described by the the polar and azimuthal angle (θ, ϕ) with respect to $\hat{\mathbf{b}}$. Though the choice of $(\mathbf{n}, \mathbf{t})$ is arbitrary, we will see that our results only depend on the relative azimuthal angle between two vectors, which is independent of the choice of $(\mathbf{n}, \mathbf{t})$.

We rewrite Eq. (4.63) as

$$\bar{\omega}_z(\mathbf{k})^2 \simeq \cos^2\theta - s(\theta, \phi)k^2 \tag{4.64}$$

where (θ, ϕ) are the polar and azimuthal angles of $\mathbf{k}$.

$$s(\theta, \phi) = c_1 \cos^2\theta - c_2 + c_3(k_x^2 b_x^2 + k_y^2 b_y^2 + k_z^2 b_z^2)/k^2.$$

Here $(k_x, k_y, k_z)/k$ and (b_x, b_y, b_z) are the components of $\hat{\mathbf{k}}$ and $\hat{\mathbf{b}}$ along the crystal axes $(\hat{x}, \hat{y}, \hat{z})$. In the following calculation, we will write these components as functions of the polar and azimuthal angles in the Frenet coordinate system.

From Eq. (4.64) we see that the maximum $\bar{\omega}_z(\mathbf{k})^2$ occurs for $k = 0$ and $\theta = 0$ or π. We also see that for small θ, where the maximum $\bar{\omega}_z(\mathbf{k})$ occurs, $s(\theta, \phi)$ is always positive.

We now substitute Eq. (4.64) into Eq. (4.60) and assume $\bar{t}$ is large. Then by expanding the integrand for small k, and for θ near 0 or π, we obtain

$$\begin{aligned} f_l(i\bar{t}) &\simeq \frac{v}{4(2\pi)^3}\int_0^{2\pi} d\phi \int_0^{\pi} d\theta \sin\theta \int_0^{\infty} dk k^2 \frac{(\mathbf{k}\cdot\bar{\mathbf{R}}_l)^2}{2(\cos\theta)^2} e^{\bar{t}|\cos\theta| - \frac{k^2 s(\theta,\phi)}{2|\cos\theta|}\bar{t}}[1 + O(1/\bar{t})] \\ &\simeq \frac{3\sqrt{2\pi}}{8\pi^2}\frac{\bar{Z}_l^2}{c_0^{5/2}}\frac{e^{\bar{t}}}{\bar{t}^{7/2}}[1 + O(1/\bar{t})] \end{aligned} \tag{4.65}$$

where $c_0 \equiv s(0, \phi) = c_1 - c_2 + c_3(b_x^4 + b_y^4 + b_z^4)$, $\bar{Z}_l \equiv \hat{\mathbf{b}} \cdot \bar{\mathbf{R}}_l$.

The asymptotic formula given by Eq. (4.65), which is to the lowest order in $1/\bar{t}$, is proportional to $\bar{Z}_l^2$. However, in our asymptotic analysis for the temperature equilibration rate , we will see that keeping only terms proportional to $\bar{Z}_l^2$ will make the contribution from $\mathbf{R}_l$ cancel the contribution from $-\mathbf{R}_l$, causing a zero rate, which is obviously not correct. In order to obtain a sensible result in our asymptotic analysis for the rate, we must include the $O(1/\bar{t})$ term, particularly those terms not in the form of $\bar{Z}_l^2$.

In order to find the $O(1/\bar{t})$ term, we make use of the following formula:

$$\mathbf{k}\cdot\bar{\mathbf{R}}_l = k\bar{R}_l[\cos\theta\cos\theta_l + \sin\theta\sin\theta_l + \cos(\phi - \phi_l)]$$

$$k_x = b_x \cos\theta + \sin\theta\sqrt{1-b_x^2}\cos(\phi-\phi_x)$$

$$k_y = b_y \cos\theta + \sin\theta\sqrt{1-b_y^2}\cos(\phi-\phi_y)$$

$$k_z = b_z \cos\theta + \sin\theta\sqrt{1-b_z^2}\cos(\phi-\phi_z)$$

where (θ_l, ϕ_l) is the polar and azimuthal angle of $\bar{\mathbf{R}}_l$ and (ϕ_x, ϕ_y, ϕ_z) are the azimuthal angles of the three orthogonal crystal axis in the Frenet coordinate system. Substituting the above formulas into Eq. (4.60) and expanding the integrand to higher orders in $O(1/\bar{t})$, we obtain the next order correction to Eq. (4.65):

$$\delta f_l(i\bar{t}) = -\frac{5\sqrt{2\pi}}{32\pi^2 c_0^{7/2}}\frac{e^{\bar{t}}}{\bar{t}^{9/2}}\bar{Z}_l^4 + \frac{15\sqrt{2\pi}c_3}{2\pi^2 c_0^{7/2}}\frac{e^{\bar{t}}}{\bar{t}^{9/2}}\mu_l \tag{4.66}$$

where

$$\mu_l \equiv \bar{\rho}_l \bar{Z}_l[b_x^3\sqrt{1-b_x^2}\cos(\phi_l-\phi_x) + [b_y^3\sqrt{1-b_y^2}\cos(\phi_l-\phi_y) + [b_z^3\sqrt{1-b_z^2}\cos(\phi_l-\phi_z)] \tag{4.67}$$

where terms which depend on $\bar{R}_l$ only through $\bar{Z}_l^2$ have been ignored.

Fig.4.7 and Fig.4.8 show the comparisons between the direct numerical integration results and the asymptotic analysis results given by Eq. (4.65). We find that the numerical and analytical results agree with each other only for sufficiently large $\bar{t}$. This is because that in order for the asymptotic formula to be valid, we must require $\bar{t}f(0,0) \gg 1$, i.e., $\bar{t} \gg 1/c_0 \sim 10/(0.16+b_x^4+b_y^4+b_z^4)$, otherwise the boundary of the Brillouin zone may play an important role. Notice that this is a rather strong condition for $\bar{t}$. Furthermore, from this condition we see that the numerical and analytical results would converge faster for a larger $b_x^4+b_y^4+b_z^4$. In the figures, we do see a faster convergence for the $\hat{\mathbf{b}} = [0,0,1]$ case compared with the $\hat{\mathbf{b}} = [1,1,1]/\sqrt{3}$ case. In fact, from Fig.4.6, we find that $\bar{\omega}_z(\mathbf{k})$ given by Eq. (4.64) is a much better

approximation for the $\hat{\mathbf{b}} = [0,0,1]$ case than the $\hat{\mathbf{b}} = [1,1,1]/\sqrt{3}$ case, this fact also makes the numerical and analytical results converge faster for the $\hat{\mathbf{b}} = [0,0,1]$ case.

In addition, in Fig.4.7 (Fig.4.8) we see that the asymptotic result is larger (smaller) than the numerical result for $\hat{\mathbf{b}}$ along $[1,1,1]$ ($[0,0,1]$). This is because, as shown in Fig.4.6, that the analytical approximation for $\bar{\omega}_z(\mathbf{k})$ is larger (smaller) than the exact numerical result for $\hat{\mathbf{b}}$ along $[1,1,1]$ ($[0,0,1]$).

4.6 Appendix 4B: Formalism for the Canonical Transformation to Diagonalize a General Quadratic Hamiltonian

In this appendix we derive a canonical transformation $\mathbf{L}$ which transforms the canonical variables $(\mathbf{q},\mathbf{p})$ to new canonical variables $(\mathbf{Q},\mathbf{P})$ via

$$\begin{bmatrix} \mathbf{q} \\ \mathbf{p} \end{bmatrix} = \mathbf{L} \begin{bmatrix} \mathbf{Q} \\ \mathbf{P} \end{bmatrix} \tag{4.68}$$

so that the Hamiltonian, which is generally in the form of

$$H = (\mathbf{q},\mathbf{p}) \begin{bmatrix} \mathbf{A}_q & \mathbf{B} \\ \mathbf{B}^{tr} & \mathbf{A}_p \end{bmatrix} \begin{pmatrix} \mathbf{q} \\ \mathbf{p} \end{pmatrix}$$

is diagonalized in the representation of the new canonical variables:

$$H = \sum_{j=1}^{n} [\frac{P_j^2}{2m} + \frac{1}{2} m\omega_i^2 Q_j^2] \tag{4.69}$$

where

$$\mathbf{q} = \begin{pmatrix} q_1 \\ q_2 \\ . \\ . \\ . \\ q_n \end{pmatrix} ; \mathbf{p} = \begin{pmatrix} p_1 \\ p_2 \\ . \\ . \\ . \\ p_n \end{pmatrix} ; \mathbf{Q} = \begin{pmatrix} Q_1 \\ Q_2 \\ . \\ . \\ . \\ Q_n \end{pmatrix} ; \mathbf{P} = \begin{pmatrix} P_1 \\ P_2 \\ . \\ . \\ . \\ P_n \end{pmatrix}$$

and where $\mathbf{A}_q$ and $\mathbf{A}_p$ are $n \times n$ real matrices satisfying $\mathbf{A}_q^{tr} = \mathbf{A}_q$, and $\mathbf{A}_p^{tr} = \mathbf{A}_p$.

In quantum many-body theory there exists the well-known Bogoliubov transformation to diagonalize a quadratic Hamiltonian in the creation and annihilation operator representation. In classical mechanics, such a canonical transformation also exists if one notices that the creation and annihilation operators can be written as linear combinations of the coordinate and momentum operators. In this appendix, by closely following the quantum formalism we derive a classical canonical transformation which diagonalizes the Hamiltonian H. In order to manipulate the symmetry of H and thereby simplify our argument, we define auxiliary variables c_j through

$$q_j = \frac{c_j + c_j^*}{\sqrt{2m\bar{\omega}_j}}$$

$$p_j = -i\sqrt{\frac{m\bar{\omega}_j}{2}}(c_j - c_j^*) \tag{4.70}$$

where $\bar{\omega}_j$ is a properly chosen positive frequency from the coefficients $A_{q,ij}$ and $A_{p,ij}$. In principle, we can choose any positive numbers for $\bar{\omega}_j$ and the result for matrix $\mathbf{L}$ is independent of the artificially constructed variables (c_j, c_j^*). However, in practice, we find that suitably chosen $\bar{\omega}_j$'s can simplify the algebra. We find that using (c_j, c_j^*)

formalism is advantageous because (q_j, p_j) appear in pairs in c_j's, the Hamiltonian H is symmetrized :

$$H = (\mathbf{c}^+, \mathbf{c}^{tr})\mathbf{h}\begin{pmatrix} \mathbf{c} \\ \mathbf{c}^* \end{pmatrix} \tag{4.71}$$

where

$$\mathbf{c} = \begin{pmatrix} c_1 \\ c_2 \\ . \\ . \\ . \\ c_n \end{pmatrix}$$

$$\mathbf{h} = \begin{bmatrix} \mathbf{N} & \mathbf{M} \\ \mathbf{M}^* & \mathbf{N}^* \end{bmatrix}$$

where $\mathbf{M}$ and $\mathbf{N}$ are $n \times n$ matrices which are related to the matrices $\mathbf{A}_q$, $\mathbf{A}_p$ and $\mathbf{B}$ by

$$M_{ij} = \frac{A_{q,ij}}{2m\sqrt{\bar{\omega}_i\bar{\omega}_j}} - \frac{m}{2}\bar{\omega}_i\bar{\omega}_j A_{p,ij} - \frac{i}{2}(\sqrt{\frac{\bar{\omega}_j}{\bar{\omega}_i}}B_{ij} + \sqrt{\frac{\bar{\omega}_i}{\bar{\omega}_j}}B_{ji})$$

$$N_{ij} = \frac{A_{q,ij}}{2m\sqrt{\bar{\omega}_i\bar{\omega}_j}} - \frac{m}{2}\bar{\omega}_i\bar{\omega}_j A_{p,ij} + \frac{i}{2}(\sqrt{\frac{\bar{\omega}_j}{\bar{\omega}_i}}B_{ij} - \sqrt{\frac{\bar{\omega}_i}{\bar{\omega}_j}}B_{ji})$$

Obviously M and N satisfies $\mathbf{M}^{tr} = \mathbf{M}$, $\mathbf{N}^+ = \mathbf{N}$, and hence $\mathbf{h}^+ = \mathbf{h}$.

In this appendix we derive a canonical transformation which diagonalize the matrix $\mathbf{h}$. Specifically, we need to find a $2n \times 2n$ matrix $\mathbf{S}$ to generate a transformation

from $(\mathbf{c}, \mathbf{c}^*)$ to $(\mathbf{e}, \mathbf{e}^*)$ through

$$\begin{bmatrix} \mathbf{c} \\ \mathbf{c}^* \end{bmatrix} = \mathbf{S} \begin{bmatrix} \mathbf{e} \\ \mathbf{e}^* \end{bmatrix} \tag{4.72}$$

such that in the new representation,

$$H = \frac{\omega_c}{2}(\mathbf{e}^+, \mathbf{e}^{tr})\mathbf{S}^+\mathbf{h}\mathbf{S} \begin{pmatrix} \mathbf{e} \\ \mathbf{e}^* \end{pmatrix}$$

is diagonalized i.e.

$$\mathbf{S}^+\mathbf{h}\mathbf{S} = \textit{diagonal} \tag{4.73}$$

In order to ensure the transformation to be canonical, we require that all the Poisson brackets must be be invariant under the transformation. Specifically, because (q_j, p_j) are canonical, we have

$$[\mathbf{c}, \mathbf{c}] = 0; \ [\mathbf{c}, \mathbf{c}^*] = -i\mathbf{1}; \ [\mathbf{c}^*, \mathbf{c}^*] = 0. \tag{4.74}$$

Since the Poisson bracket is invariant, we require that the same commutation relations hold for $(\mathbf{e}, \mathbf{e}^*)$:

$$[\mathbf{e}, \mathbf{e}] = 0; \ [\mathbf{e}, \mathbf{e}^*] = -i\mathbf{1}; \ [\mathbf{e}^*, \mathbf{e}^*] = 0 \tag{4.75}$$

Combining Eq.(4.75) with Eq.(4.72), we have

$$\mathbf{S} = \begin{bmatrix} \mathbf{A} & \mathbf{B}^* \\ \mathbf{B} & \mathbf{A}^* \end{bmatrix}, \tag{4.76}$$

where $n \times n$ matrices A and B are defined by

$$A_{jk} = i[c_j, e_k^*]$$

$$B_{jk} = i[c_j^*, e_k^*]$$

Moreover,because $(\mathbf{e}, \mathbf{e}^*)$ has the same commutation relations as $(\mathbf{c}, \mathbf{c}^*)$, the matrix $\mathbf{S}^{-1}$ which generates the inverse transformation must have the same form as shown in Eq.(4.76) with c and e exchanged:

$$\mathbf{S}^{-1} = \begin{bmatrix} \mathbf{A}^\dagger & -\mathbf{B}^\dagger \\ -\mathbf{B}^{tr} & \mathbf{A}^{tr} \end{bmatrix}$$

$$= \mathbf{\Lambda S}^\dagger \mathbf{\Lambda}$$

which, in turn, yields the condition for $\mathbf{S}$:

$$\mathbf{S}^\dagger \mathbf{\Lambda S} = \mathbf{\Lambda}; or, \mathbf{S \Lambda S}^\dagger = \mathbf{\Lambda} \tag{4.77}$$

where $\mathbf{\Lambda}$ is a $n \times n$ matrix defined as

$$\mathbf{\Lambda} = \begin{bmatrix} \mathbf{1} & \mathbf{0} \\ \mathbf{0} & -\mathbf{1} \end{bmatrix}$$

and we have used the identity $\mathbf{\Lambda\Lambda} = \mathbf{1}$ to derive Eq.(4.77).

Here we must note that Eq.(4.77) does not look the same as the conventional symplectic condition[12]. In order to show its equivalence to the usual symplectic condition, in what follows, we prove that Eq.(4.77) combined with Eq.(4.75) lead to the usual symplectic condition for the transformation matrix $\mathbf{L}$. We begin with the definition of (c_j, c_j^*) and write

$$\begin{bmatrix} \mathbf{c} \\ \mathbf{c}^* \end{bmatrix} = \mathbf{T}_1 \begin{bmatrix} \mathbf{q} \\ \mathbf{p} \end{bmatrix}$$

where

$$\mathbf{T}_1 = \begin{bmatrix} \mathbf{U}_1 & \frac{i}{2}\mathbf{U}_1^{-1} \\ \mathbf{U}_1 & -\frac{i}{2}\mathbf{U}_1^{-1} \end{bmatrix} \tag{4.78}$$

$$\mathbf{U}_1 = \begin{bmatrix} \sqrt{\frac{m\bar{\omega}_1}{2}} & 0 & 0 \\ 0 & \sqrt{\frac{m\bar{\omega}_2}{2}} & 0 \\ 0 & 0 & \sqrt{\frac{m\bar{\omega}_3}{2}} \end{bmatrix}$$

Similarly, the new variables are related by

$$\begin{bmatrix} \mathbf{e} \\ \mathbf{e}^* \end{bmatrix} = \mathbf{T}_2 \begin{bmatrix} \mathbf{Q} \\ \mathbf{P} \end{bmatrix}$$

where

$$\mathbf{T}_2 = \begin{bmatrix} \mathbf{U}_2 & \frac{i}{2}\mathbf{U}_2^{-1} \\ \mathbf{U}_2 & -\frac{i}{2}\mathbf{U}_2^{-1} \end{bmatrix} \tag{4.79}$$

where matrix $\mathbf{U}_2$ has the same form as $\mathbf{U}_1$ except that $\bar{\omega}_i$ is replaced by ω_i, the frequency appearing in Eq.(4.69). With the aid of Eq.(4.78) and Eq.(4.79), we find that

$$\mathbf{T}_{1,2}^* = \Sigma \mathbf{T}_{1,2} \tag{4.80}$$

$$\mathbf{T}_{1,2}^+ \Lambda \mathbf{T}_{1,2} = i\mathbf{J} \tag{4.81}$$

where

$$\Sigma = \begin{bmatrix} 0 & 1 \\ 1 & 0 \end{bmatrix}; \mathbf{J} = \begin{bmatrix} 0 & 1 \\ -1 & 0 \end{bmatrix}$$

Due to the definition of the transformation matrices, $\mathbf{L}$ is found to be related to $\mathbf{S}$ through

$$\mathbf{L} = \mathbf{T}_1^{-1}\mathbf{S}\mathbf{T}_2 \tag{4.82}$$

or, equivalently, $\mathbf{S} = \mathbf{T}_1\mathbf{L}\mathbf{T}_2^{-1}$. In what follows, we first show that $\mathbf{L}$ is real. By taking the complex conjugate of the Eq.(4.82), we have $\mathbf{L}^* = (\mathbf{T}_1^*)^{-1}\mathbf{S}^*\mathbf{T}_2^* = \mathbf{T}_1^{-1}\Sigma\mathbf{S}\Sigma\mathbf{T}_2 = \mathbf{L}$, which means that $\mathbf{L}$ is real. Here we have used Eq.(4.80) and we have also used the fact that $\Sigma\mathbf{S}\Sigma = \mathbf{S}$ due to Eq.(4.76). We next prove that $\mathbf{L}$ satisfies the symplectic condition if Eq.(4.77) is satisfied by $\mathbf{S}$. To show this, we substitute $\mathbf{S} = \mathbf{T}_1\mathbf{L}\mathbf{T}_2^{-1}$ into Eq.(4.77), and then obtain $\mathbf{L}^{tr}\mathbf{T}_1^{\dagger}\Lambda\mathbf{T}_1\mathbf{L} = \mathbf{T}_2^{\dagger}\Lambda\mathbf{T}_2$, which leads to the symplectic condition $\mathbf{L}^{tr}\mathbf{J}\mathbf{L} = \mathbf{J}$ due to Eq.(4.81).

In summary, Eq.(4.73), Eq.(4.76) and Eq.(4.77) are the three conditions which must be satisfied by $\mathbf{S}$. In what follows, we will derive $\mathbf{S}$ according to these three equations. However, before proceeding we first examine the number of the equations and the number of the unknown variables. According to Eq.(4.76), we have a total of $4n^2$ unknown variables that need to be solved from Eq.(4.73) and Eq.(4.77). In order to see how many equations are implied by Eq.(4.73), we make use of the $\mathbf{S}$ given by Eq.(4.76), and find that

$$\mathbf{S}^{+}\mathbf{h}\mathbf{S} = \begin{bmatrix} \tilde{\mathbf{N}} & \tilde{\mathbf{M}} \\ \tilde{\mathbf{M}}^* & \tilde{\mathbf{N}}^* \end{bmatrix}$$

Here $\tilde{\mathbf{M}}$ and $\tilde{\mathbf{N}}$ are $n \times n$ matrices:

$$\tilde{\mathbf{M}} = \mathbf{A}^{+}\mathbf{N}\mathbf{B}^{*} + \mathbf{B}^{+}\mathbf{M}^{*}\mathbf{A}^{*}$$

$$\tilde{\mathbf{N}} = \mathbf{A}^{+}\mathbf{N}\mathbf{A} + \mathbf{B}^{+}\mathbf{M}^{*}\mathbf{B}.$$

One may easily check that $\tilde{\mathbf{M}}^{tr} = \tilde{\mathbf{M}}$ and $\tilde{\mathbf{N}}^{+} = \tilde{\mathbf{N}}$. Since $\mathbf{S}^{+}\mathbf{h}\mathbf{S}$ must be diagonal, we have $n^2 - n$ equations from matrix $\tilde{\mathbf{N}}$ and $n^2 + n$ equations from matrix $\tilde{\mathbf{M}}$. For equation (4.77), again we make use of the $\mathbf{S}$ given by Eq.(4.76),and find that

$$\mathbf{S}\mathbf{\Lambda}\mathbf{S}^{\dagger} = \begin{bmatrix} \mathbf{A}\mathbf{A}^{+} - \mathbf{B}^{*}\mathbf{B}^{+} & \mathbf{A}\mathbf{B}^{+} - \mathbf{B}^{*}\mathbf{A}^{tr} \\ \mathbf{B}\mathbf{A}^{+} - \mathbf{A}^{*}\mathbf{B}^{tr} & \mathbf{B}\mathbf{B}^{+} - \mathbf{A}^{*}\mathbf{A}^{tr} \end{bmatrix}$$

Notice that the matrix on the right hand side is hermitian and we have n^2 equations from condition $\mathbf{A}\mathbf{A}^{+} - \mathbf{B}^{*}\mathbf{B}^{+} = 1$ and we have $n^2 - n$ equations from condition $\mathbf{A}\mathbf{B}^{+} - \mathbf{B}^{*}\mathbf{A}^{tr}$. So, totally we have $(n^2 - n) + (n^2 + n) + n^2 + (n^2 - n) = 4n^2 - n$ equations and we have $4n^2$ unknowns, which means that we have n free choices left over. As we will see, these n free choices corresponds to the n phases of the eigenvectors of matrix $\mathbf{K} = \mathbf{\Lambda}\mathbf{h}$.

We now proceed to calculate $\mathbf{S}$ according to Eq.(4.73), Eq.(4.76) and Eq.(4.77). We start with the following observation. From Eq.(4.77) we have $\mathbf{S}^{\dagger} = (\mathbf{S}\mathbf{\Lambda})^{-1}\mathbf{\Lambda} = \mathbf{\Lambda}\mathbf{S}^{-1}\mathbf{\Lambda}$. Substitution of this result into Eq.(4.73) yields a diagonal matrix $\mathbf{\Lambda}\mathbf{S}^{-1}\mathbf{\Lambda}\mathbf{h}\mathbf{S}$. This shows that matrix $\mathbf{K} = \mathbf{\Lambda}\mathbf{h}$ is diagonalized by $\mathbf{S}$ since $\mathbf{\Lambda}$ is diagonal. Note that strictly speaking $\mathbf{h}$ is not diagonalized by $\mathbf{S}$ because η_i's are not the eigenvectors of $\mathbf{h}$. This observation proves that matrix $\mathbf{S}$ may be constructed by the eigenvectors of matrix $\mathbf{K}$:

$$\mathbf{S} = (\eta_1, \eta_2, \eta_3, \cdots, \eta_n, \eta_{n+1}, \cdots \eta_{2n}) \tag{4.83}$$

where $\eta_l (l = 1, 2, \cdots, 2n)$ are the eigenvectors of $\mathbf{K}$. In order to confirm this conclusion, we proceed to show that such $\mathbf{S}$ also satisfies Eq.(4.76) and Eq.(4.77).

We first show that the eigenvalues of $\mathbf{K}$ are real. We begin with the eigenvalue equation

$$\mathbf{K}\eta_l = \omega_l \eta_l \tag{4.84}$$

Multiplying the both sides of above equation by $\eta_l^\dagger \mathbf{\Lambda}$ yields

$$\eta_l^\dagger \mathbf{h} \eta_l = \omega_l \eta_l^\dagger \mathbf{\Lambda} \eta_l$$

which shows that the eigenvalue ω_l is real because both $\eta_l^\dagger \mathbf{h} \eta_l$ and $\eta_l^+ \mathbf{\Lambda} \eta_l$ are real due to the Hermitean property of matrix $\mathbf{h}$ and $\mathbf{\Lambda}$.

We next show that the eigenvalues occur in pairs. We notice that the form of $\mathbf{h}$ given in Eq.(4.76) is special and satisfies

$$\mathbf{\Sigma h \Sigma} = \mathbf{h}^*; \ \mathbf{\Sigma} = \begin{bmatrix} \mathbf{0} & \mathbf{1} \\ \mathbf{1} & \mathbf{0} \end{bmatrix}$$

which yields

$$\mathbf{K} = -\mathbf{\Sigma K^* \Sigma}$$

Substituting this equation in Eq.(4.84), then after taking the complex conjugate on both sides , we are left with

$$\mathbf{K}(\mathbf{\Sigma}\eta_l)^* = -\omega_l (\mathbf{\Sigma}\eta_l)^* \tag{4.85}$$

where identity $\mathbf{\Sigma\Sigma} = 1$ has been used. Thus $-\omega_l$ is also a eigenvalue with eigenvector $(\mathbf{\Sigma}\eta_l)^*$. To be specific, we set $\omega_{l+n} = -\omega_l$ and $\eta_{l+n} = \mathbf{\Sigma}\eta_l^*$ for $l = 1, 2, 3, \cdots, n$. Then

Eq.(4.83) becomes

$$\mathbf{S} = (\eta_1, \eta_2, \cdots, \eta_n, \boldsymbol{\Sigma}\eta_1^*, \boldsymbol{\Sigma}\eta_2^*, \cdots, \boldsymbol{\Sigma}\eta_n^*) \tag{4.86}$$

which obviously satisfies Eq.(4.76). According to Eq.(4.86), we have $S_{ij} = \eta_j^{(i)}$, where $\eta_j^{(i)}$ is the ith component of the jth eigenvector. Finally, we show that $\mathbf{S}$ given by Eq.(4.86) satisfies Eq.(4.77). We take the Hermitian conjugate of Eq.(4.84), yielding:

$$\eta_l^\dagger \mathbf{h}\boldsymbol{\Lambda} = \omega_l \eta_l^\dagger$$

where we have used the fact that $\mathbf{h}^+ = \mathbf{h}$. Furthermore, multiplying above equation by $\boldsymbol{\Lambda}\eta_{l'}$ and inserting $\mathbf{1} = \Lambda\Lambda$ between $\eta_l^\dagger$ and $\mathbf{h}$, we have:

$$(\omega_l - \omega_{l'})(\eta_l^\dagger \boldsymbol{\Lambda} \eta_{l'}) = 0 \tag{4.87}$$

where the eigenvalue equation for $\eta_{l'}$: $\mathbf{K}\eta_{l'} = \omega_{l'}\eta_{l'}$ has been used. We assume that matrix $\mathbf{K}$ is nondegenerate, then Eq.(4.87) implies that

$$\eta_l^\dagger \boldsymbol{\Lambda} \eta_{l'} = \eta_l^\dagger \boldsymbol{\Lambda} \eta_l \delta_{ll'}$$

which leads to Eq.(4.77) provided that the normalization condition

$$\eta_l^\dagger \boldsymbol{\Lambda} \eta_{l'} = \boldsymbol{\Lambda}_{ll'}$$

is satisfied.

Finally, in the $(\mathbf{e}, \mathbf{e}^*)$ representation, $\mathbf{S}^{-1}\mathbf{K}\mathbf{S}$ is diagonal with the diagonal elements ω_1,ω_2, $\cdots$,ω_n, $-\omega_1$, $-\omega_2$,$\cdot$,$\cdot$,$\cdot$,$-\omega_n$, and $\mathbf{h}$ becomes $\mathbf{S}^\dagger\mathbf{h}\mathbf{S} = \boldsymbol{\Lambda}(\mathbf{S}^{-1}\mathbf{K}\mathbf{S})$, which is also diagonal with the diagonal elements ω_1,ω_2, $\cdots$,ω_n, ω_1, ω_2,$\cdot$,$\cdot$,$\cdot$,ω_n and then the

Hamiltonian take the following form.

$$H = \sum_{j=1}^{n} \omega_j e_j^* e_j \tag{4.88}$$

The final new canonical variable can be constructed in terms of $(\mathbf{e}, \mathbf{e}^*)$ through Eq.(4.70) with (q_j, p_j) replaced by (Q_j, P_j) and $\bar{\omega}_j$ replaced by ω_j. Also, by writing $(\mathbf{e}, \mathbf{e}^*)$ in terms of (Q_j, P_j), we find that Eq.(4.88) becomes Eq.(4.69). Evidently, the time evolution of $(Q_j(t), P_j(t))$ is a linear superpositions of the three simple harmonic oscillators determined by Eq.(4.69). The particle's trajectory $(q_j(t), p_j(t))$ can thus be obtained from Eq.(4.68) with $\mathbf{L}$ given by Eq.(4.82) and the particle's motion is then completely solved.

4.7 References

1. S. Gilbert, J. Bollinger and D. Wineland, Phys. Rev. Lett. **60**, 2022 (1988)

2. E. Pollock and J. Hansen, Phys. Rev. A **8**, 3110 (1973)

3. T. M. O'Neil and P. Hjorth, Phys. Fluids **28**, 3241 (1985)

4. Beck, B.R., J. Fajans and J.H. Malmberg, Phys. Rev. Lett. **68**, 317(1992).

5. D. Dubin and T. M. O'Neil, Phys. Rev. Lett. **60**, 511 (1988)

6. S. Ichimaru, Rev. Mod. Phys. **54**, 1017 (1982)

7. F. P. Ulinich and N. A. Usov, Sov. Phys. JETP **49**, 147 (1979)

8. I.S. Gradshteyn and I.M. Ryzhik, *Tables of Integrals, Series, and Products* (Academic Press, Inc., 1980)

9. W.H. Press, B.P. Flannery, S.A. Teukolsky and W.T. Vetterling, Numerical Recipes (Cambridge Univ. Press, 1989). p. 108.

10. J. -P. Hansen, I. R. McDonald and E. L. Pollock, Phys. Rev. A **11**, 1025 (1975)

11. Daniel H. E. Dubin, Phys. Rev. A **42**, 4972 (1990)

12. Herbert Goldstein, Classical mechanics, Reading, Mass. : Addison-Wesley Pub. Co., 1980.